3.0 UNIT 2 REACTOR

3.1 SUMMARY DESCRIPTION

This chapter describes 1) the mechanical components of the reactor and reactor core including the fuel rods and fuel assemblies, reactor internals, and the control rod drive mechanism (CRDMs), 2) the nuclear design, and 3) the thermal-hydraulic design.

The fresh fuel for the initial core through Cycle 3 was supplied by Westinghouse Electric Company LLC. Fresh fuel for Cycles 4 through 7 were supplied by Exxon Nuclear Company. Commencing in Cycle 8, Westinghouse Electric Corporation has been supplying fuel assemblies of the VANTAGE 5 design.

The reactor core is comprised of an array of 17 x 17 fuel assemblies that are similar in mechanical design. Different fuel assembly enrichments are selected for a particular refueling scheme. The core may consist of any combination of Westinghouse VANTAGE 5 fuel assemblies, with or without certain cycle-specific enhancements. All cycle-specific enhancements are licensed on a cycle-by-cycle basis.

The significant new mechanical features of the VANTAGE 5 design relative to the previous Optimized Fuel Assembly (OFA) design include the following:

1. Integral Fuel Burnable Absorber (IFBA),
2. Intermediate Flow Mixer (IFM) Grids,
3. Westinghouse Integral Nozzle (WIN) Top Nozzle,
4. Debris Filter Bottom Nozzle (DFBN), and
5. Axial Blankets.

The above design features are described and evaluated in Reference 1.

In addition, the fuel assemblies contain debris mitigating features. These features are described in Section 3.2.1

The information contained in this chapter is principally concerned with the nuclear fuel and reactor internals design. It does not necessarily reflect the same information as that used in the safety analysis. For information concerning the safety analysis, Chapter 14 should be consulted.

The core is cooled and moderated by light water at a pressure of 2250 psia in the reactor coolant system. The moderator coolant contains boron as a neutron poison. The concentration of boron in the coolant is varied as required to control relatively slow reactivity changes including the

effects of fuel burnup. Additional boron, in the form of integral fuel burnable absorber (IFBA), is employed in the reload core to establish the desired initial reactivity.

Two hundred and sixty-four fuel rods are mechanically joined in a square array to form a fuel assembly (see Figure 3.2-1). The fuel rods are supported at intervals along their length by grid assemblies, including IFM grids, which maintain the lateral spacing between the rods throughout the design life of the assembly. The grid assembly consists of an "egg-crate" arrangement of interlocked straps. The straps contain spring fingers and dimples for fuel rod support as well as coolant mixing vanes. The fuel rods consist of slightly enriched uranium dioxide ceramic cylindrical pellets contained in slightly cold worked Zircaloy-4/ZIRLO™ or partially annealed **Optimized ZIRLO™** tubing which is plugged and seal welded at the ends to encapsulate the fuel. An axial blanket of natural or enriched UO_2 fuel pellets may be placed at each end of the enriched fuel pellet stack to reduce the neutron leakage and to improve fuel utilization. All fuel rods are pressurized with helium during fabrication to reduce stresses, strains, and to increase fatigue life.

The center position in the assembly is reserved for the incore instrumentation, while the remaining 24 positions in the array are equipped with guide thimbles joined to the grids and the top and bottom nozzles. Depending upon the position of the assembly in the core, the guide thimbles are used as core locations for rod cluster control assemblies (RCCAs), neutron source assemblies, and burnable absorber assemblies. Otherwise, the guide thimbles may be fitted with plugging devices to limit bypass flow.

The bottom nozzle is a box-like structure, which serves as a bottom structural element of the fuel assembly and directs the coolant flow distribution to the assembly.

The top nozzle assembly functions as the upper structural element of the fuel assembly in addition to providing a partial protective housing for the RCCA or other components.

The RCCAs each consist of a group of individual absorber rods fastened at the top end to a common hub or spider assembly. These assemblies contain full-length absorber material to control the reactivity of the core under operating conditions.

The CRDMs for the full length RCCAs are of the magnetic jack type. Control rods are positioned by electro-mechanical (solenoid) action utilizing gripper latches, which engage grooved drive rods, which in turn are coupled to the RCCAs. The CRDMs for the full-length rods are so designed that upon a loss of electrical power to the coils, the RCCA is released and falls by gravity to shutdown the reactor.

The components of the reactor internals are divided into three parts consisting of the lower core support structure (including the entire core barrel and thermal shield assembly), the upper core support structure and the incore instrumentation support structure. The reactor internals support the core, maintain fuel alignment, limit fuel assembly movement, maintain alignment between fuel assemblies and CRDMs, direct coolant flow past the fuel elements and to the pressure vessel head, provide gamma and neutron shielding, and provide guides for the incore instrumentation.

For each cycle, the nuclear design analyses and evaluation establish physical locations for IFBAs, and burnable absorbers and physical parameters such as fuel enrichments and boron concentration in the coolant. The nuclear design evaluation also establishes that the reactor core has inherent characteristics, which together with corrective actions of the reactor control and protective systems, provide adequate reactivity control even if the highest reactivity worth RCCA is stuck in the fully withdrawn position.

The design also provides for inherent stability against diametral and azimuthal power oscillations and for control of induced axial power oscillations through the use of the control rods.

The thermal-hydraulic design analyses and evaluations use established coolant flow parameters to assure that adequate heat transfer is provided between the fuel clad and the reactor coolant. The thermal design takes into account local variations in dimensions, power generation, flow distribution and mixing. The mixing vanes incorporated in the fuel assembly spacer grid design and the IFM grids induces additional flow mixing between the various flow channels within a fuel assembly as well as between adjacent assemblies. Beginning with Cycle 21, these mixing vanes are now balanced to mitigate the risk of fuel assembly self-excitation, which is a primary contributor to the grid to rod fretting leaking mechanism. The design of the balanced vanes does not result in any loss of the heat transfer capabilities.

Instrumentation is provided in and out of the core to monitor the nuclear, thermal-hydraulic and mechanical performance of the reactor and to provide inputs to automatic control functions.

Table 3.1-1 presents a comparison of the typical nuclear, thermal-hydraulic and mechanical design parameters between the initial cycle of Cook Nuclear Plant Unit 2 and the Cook Nuclear Plant Unit 2 parameters for a typical cycle with the Westinghouse VANTAGE 5 design.

The analysis techniques employed in the core design are tabulated in Table 3.1-2. The loading conditions considered in general for the core internals and components are tabulated in Table 3.1-3. Specific or limiting loads considered for design purposes of the various components are listed as follows: fuel assemblies in Section 3.2.1.1.2; reactor internals in Section 3.2.2.3; neutron absorber rods, burnable absorber rods, neutron source rods and thimble plug assemblies

in Section 3.2.3.1.3; full CRDMs in Section 3.2.3.1.4. This information is supplemented by further analyses discussed in Section 14.3.3.

3.1.1 References For Section 3.1

1. Davidson, S. L. and Kramer, W. R.; (Ed.) "Reference Core Report VANTAGE 5 Fuel Assembly," WCAP-10444-P-A, September 1985.
2. Chelemer, H., Boman, L. H. and Sharp, D. R., "Improved Thermal Design Procedure," WCAP-8567-P, July, 1975 (Proprietary) and WCAP-8568, July, 1975 (Non-Proprietary).
3. Friedland, A. J., and Ray, S., "Revised Thermal Design Procedure," WCAP-11397-P-A, April 1989.

3.2 MECHANICAL DESIGN

The plant conditions for design are divided into four categories in accordance with their anticipated frequency of occurrence and risk to the public: Condition I - Normal Operation; Condition II - Incidents of Moderate Frequency; Condition III - Infrequent Incidents; Condition IV - Limiting Faults.

The reactor is designed so that its components meet the following performance and safety criteria:

1. The mechanical design of the reactor core components and their physical arrangement, together with corrective actions of the reactor control, protection and emergency cooling systems (when applicable) assure that:
   a. Fuel damage* is not expected during Condition I and Condition II events. It is not possible, however, to preclude a very small number of rod failures. These are within the capability of the plant cleanup system and are consistent with plant design bases.
   b. The reactor can be brought to a safe state following a Condition III event with only a small fraction of fuel rods damaged* although sufficient fuel damage might occur to preclude resumption of operation without considerable outage time.
   c. The reactor can be brought to a safe state and the core can be kept subcritical with acceptable heat transfer geometry following transients arising from Condition IV events.
2. The fuel assemblies are designed to withstand, without exceeding the criteria of Section 3.2.l.l.2, loads induced during shipping, handling and core loading.
3. The fuel assemblies are designed to accept control rod insertions in order to provide the required reactivity control for power operations and reactivity shutdown conditions.
4. All fuel assemblies have provisions for the insertion of incore instrumentation necessary for plant operation.
5. The reactor internals, in conjunction with the fuel assemblies, direct reactor coolant through the core to achieve acceptable flow distribution and to restrict

* Fuel damage as used here is defined as penetration of the fission product barrier (i.e., the fuel rod clad).

bypass flow so that the heat transfer performance requirements can be met for all modes of operation. In addition, the internals provide core support and distribute coolant flow to the pressure vessel head so that the temperature differences between the vessel flange and head do not result in leakage from the flange during the Condition I and II modes of operation. Required inservice inspection can be carried out as the internals are removable and provide access to the inside of the pressure vessel.

3.2.1 Fuel

3.2.1.1 Design Bases

The fuel rod and fuel assembly design bases are established to satisfy the general performance and safety criteria presented in Section 3.2 and specific criteria noted below.

3.2.1.1.1 Fuel Rods

The integrity of the fuel rods is ensured by designing to prevent excessive fuel temperatures, excessive internal rod gas pressures due to fission gas releases, and excessive cladding stresses and strains.

This is achieved by designing the fuel rods so that the conservative design bases in the following subsections are satisfied during Condition I and Condition II events over the fuel lifetime. For each design basis, the performance of the limiting fuel rod must not exceed the limits specified by the design basis.

1. Fuel Pellet Temperatures

   The center line temperature of the hottest pellet is to be below the melting temperature of UO_2 (melting point of 5080°F (Reference 1) unirradiated and decreasing by 58°F per 10,000 MWD/MTU). While a limited amount of center melting can be tolerated, the design conservatively precludes center melting. A calculated fuel centerline temperature of 4700°F has been selected as an overpower limit to assure no fuel melting. This provides sufficient margin for uncertainties as described in Sections 3.4.1.2 and 3.4.2.10.1.

2. Internal Gas Pressure

   The rod internal gas pressure shall remain below the value, which causes the fuel-clad diametral gap to increase due to outward cladding creep during steady-state operation. Rod pressure is also limited so that extensive departure from nucleate

boiling (DNB) propagation does not occur during normal operation and any accident event as discussed in References 24 and 25.

3. Clad Stress

   The von Mises criterion is used to calculate the effective stresses. The cladding stresses under Condition I and II events are less than the Zircaloy/ZIRLO™ 0.2% yield stress, with due consideration of temperature and irradiation effects, as discussed in References 24, 25 and 33. While the clad has some capability for accommodating plastic strain, the yield stress has been accepted as a conservative design basis.

4. Clad Tensile Strain

   The total plastic tensile creep strain due to uniform clad creep and uniform cylindrical fuel pellet expansion associated with fuel swelling and thermal expansion is less than 1% from the unirradiated condition (Reference 19). The acceptance limit for fuel rod clad strain during Condition II events is that the total tensile strain due to uniform cylindrical pellet thermal expansion is less than 1% from the pre-transient value. These limits are consistent with proven practice.

5. Strain Fatigue

   The fatigue life usage factor is less than 1.0 (Reference 19). That is, for a given strain range, the number of strain fatigue cycles are less than those required for failure, considering a minimum safety factor of 2 on the stress amplitude or a minimum safety factor of 20 on the number of cycles, whichever is more conservative.

The peak fuel rod average burnup is cycle-specific. The fuel rod average burnup limit is 62,000 MWD/MTU (Reference 32), provided the evaluation of the fuel design performance is performed with PAD 4.0 (Reference 30).

Manufacturing tolerances on the prestated parameters are considered in the design evaluation. The design also considers effects such as fuel density changes, fission gas release, clad creep, and other physical properties, which vary with burnup.

Extensive irradiation testing and fuel surveillance operational experience program are conducted to verify the adequacy of the fuel performance and design bases, such as the program discussed in References (2) and (19). Fuel surveillance and testing results, as they became available, are used to improve fuel rod design and manufacturing processes and assure that the design bases and safety criteria are satisfied.

3.2.1.1.2 Fuel Assembly Structure

Structural integrity of the fuel assemblies is assured by setting limits on stresses and deformations due to various loads and by determining that the assemblies do not interfere with the functioning of other components. Three types of loads are considered.

1. Non-operational loads such as those due to shipping and handling.
2. Normal and abnormal loads which are defined for Conditions I and II.
3. Abnormal loads which are defined for Conditions III and IV.

These criteria are applied to the design and evaluation of the top and bottom nozzles, the guide thimbles, the grids and the thimble joints.

The design bases for evaluating the structural integrity of the fuel assemblies are:

1. Non-operational - 4 g axial loading and 6 g lateral loading with dimensional stability (Reference 27).
2. For the normal operating and upset conditions, the fuel assembly component structural design criteria are classified into two material categories, namely austenitic steels and Zircaloy/ZIRLO™. The stress categories and strength theory presented in the ASME Boiler and Pressure Vessel Code (ASME Code), Section III, are used as a general guide. The maximum shear-theory (Tresca Criterion) for combined stresses is used to determine the stress intensities for the austenitic steel components. The stress intensity is defined as the numerically largest difference between the various principal stresses in a three dimensional field. The allowable stress intensity value for austenitic steels, such as nickel-chromium-iron alloys, is given by the lowest of the following:
   a. 1/3 of the specified minimum tensile strength or 2/3 of the specified minimum yield strength at room temperature.
   b. 1/3 of the tensile strength or 90 percent of the yield strength at operating temperature but not to exceed 2/3 of the specified minimum yield strength at room temperature.

   The stress limits for the austenitic steel components are given below. All stress nomenclature is per the ASME Code, Section III: e.g. Sm, ASME Code Design Stress Intensity; Su, Material Tensile Strength; and Sy, Material Yield Strength.

Stress Intensity Limits

Categories	Limit
General Primary Membrane Stress Intensity	Sm
Local Primary Membrane Stress Intensity	1.5 Sm
Primary Membrane plus Bending Stress Intensity	1.5 Sm
Total Primary plus Secondary Stress Intensity	3.0 Sm

The Zircaloy/ZIRLO/**Optimized ZIRLO™** structural components, which consist of guide thimbles and fuel tubes, are in turn subdivided into two categories because of material differences and functional requirements. The fuel tube design criteria is covered separately in Section 3.2.1.3.1. The maximum shear theory is used to evaluate the guide thimble design. For conservative purposes, the Zircaloy/ZIRLO™ unirradiated properties are used to define the stress limits.

3. Abnormal loads during Conditions III or IV - worst cases represented by combined seismic and blowdown loads.

   a. Deflections or failures of components cannot interfere with the reactor shutdown or emergency cooling of the fuel rods.

   b. The fuel assembly structural component stresses under faulted conditions are evaluated using primarily the methods outlined in Appendix F of the ASME Code, Section III. Since the current analytical methods utilize elastic analysis, the stress allowables are defined as the smaller value of 2.4 Sm or 0.70 Su for primary membrane and 3.6 Sm or 1.05 Su for primary membrane plus primary bending. For the austenitic steel fuel assembly components, the stress intensity is defined in accordance with the rules described in the previous section for normal operating conditions. For the Zircaloy/ZIRLO™ components the stress intensity limits are set at two-thirds of the material yield strength, Sy, at reactor operating temperature. This results in Zircaloy/ZIRLO™ stress limits being the smaller of 1.6 Sy or 0.70 Su for primary membrane and 2.4 Sy or 1.05 Su for primary membrane plus bending. For conservative purposes, the Zircaloy/ZIRLO™ unirradiated properties are used to define the stress limits.

The grid component strength criteria are based on experimental tests. Tests have been performed at an elevated temperature of 600oF. The dynamic crush test strength value is established on the 95% confidence level of the true mean crush strength for the grid.

3.2.1.2 Design Description

The VANTAGE 5 fuel assembly and fuel rod design data are given in Table 3.3-1.

Two hundred and sixty-four fuel rods, twenty-four guide thimble tubes and one instrumentation thimble tube are arranged within a supporting structure to form a fuel assembly. The instrumentation thimble is located in the center position and provides a channel for insertion of an incore neutron detector, if the fuel assembly is located in an instrumented core position. The guide thimbles provide channels for insertion of either a rod cluster control assembly, a neutron source assembly, a burnable poison assembly or a plugging device, depending on the position of the particular fuel assembly in the core and core design requirements. Figure 3.2-1 shows a cross section of the fuel assembly array, and Figure 3.2-2 shows a fuel assembly full-length view. The fuel rods are loaded into the fuel assembly structure so that there is clearance between the fuel rod ends and the top and bottom nozzles. All VANTAGE 5 fuel assemblies in the core are similar in mechanical construction.

Each fuel assembly is installed vertically in the reactor vessel and stands upright on the lower core plate, which is fitted with alignment pins to locate and orient the assembly. After all fuel assemblies are set in place, the upper support structure is installed. Alignment pins, built into the upper core plate, engage and locate the upper ends of the fuel assemblies. The upper core plate then bears downward against the fuel assembly top nozzle via the holddown springs to hold the fuel assemblies in place.

3.2.1.2.1 Fuel Rods

The fuel rod consists of uranium dioxide ceramic pellets contained in a cold worked Zircaloy-4/ZIRLO or partially annealed **Optimized ZIRLO™** tubing which is plugged and seal welded at the ends to encapsulate the fuel. Beginning with Cycle 21, the fuel rod tubing is **Optimized ZIRLO™.** The lower portion of the Zircaloy-4, ZIRLO, or **Optimized ZIRLO™** cladding has a protective oxide coating that helps mitigate the detrimental effects of potential debris. A schematic of the fuel rod is shown in Figure 3.2-3. The fuel pellets are right circular cylinders consisting of slightly enriched uranium dioxide powder, which has been compacted by cold pressing and then sintered to the required density. The ends of each pellet are dished slightly to allow for greater axial expansion at the center of the pellets and have a small chamfer at the outer

cylindrical surface, which improves manufacturability. The fuel rods also contain axial blanket pellets, and an Integral Fuel Burnable Absorber (IFBA) coating on some of the enriched fuel pellets.

Axial blankets of a nominal six inches in length of unenriched or enriched fuel pellets may be located at each end of the fuel rod pellet stack. Axial blankets reduce neutron leakage and improve fuel utilization. The axial blankets may utilize solid or annular pellets, which are physically different than the enriched pellets to help prevent accidental mixing during manufacturing. The physical difference includes a longer pellet length for the axial blanket pellets (see Table 3.1-1).

A limited number of fuel rods may be replaced with substitutions of zirconium alloy, zircaloy-4, ZIRLO^{TM}, or stainless steel filler rods, in accordance with the NRC approved methodology in Reference 34.

IFBA coated fuel pellets are identical to the enriched uranium dioxide pellets except for the addition of a thin zirconium diboride (ZrB2) on the pellet cylindrical surface. Coated pellets occupy the central portion of the fuel stack. The number and pattern of IFBA rods within an assembly may vary depending on specific application. The ends of the enriched-coated pellets are dished to allow for greater axial expansion at the pellet centerline. The effect of this is to increase the void volume for fission gas release.

To avoid overstressing of the clad or seal welds, void volume and clearances are provided within the rods to accommodate fission gases released from the fuel, differential thermal expansion between the clad and the fuel, and fuel density changes during irradiation. Shifting of the fuel within the clad during handling or shipping prior to core loading is prevented by a stainless steel helical spring which bears on top of the fuel. At assembly the pellets are stacked in the clad to the required fuel height, the spring is then inserted into the top end of the fuel tube and the end plugs pressed into the ends of the tube and welded. All fuel rods are internally pressurized with helium during the welding process in order to minimize compressive clad stresses and prevent clad flattening due to coolant operating pressures.

The fuel rods are presently being pre-pressurized and designed so that:

1. the internal gas pressure will not exceed the value which causes the fuel-clad diametral gap to increase due to outward cladding creep during steady-state operation,
2. the cladding stress-strain limits (Section 3.2.1.1.1) are not exceeded for Condition I and II events, and
3. clad flattening will not occur during the fuel core life.

Calculations performed for VANTAGE 5 fuel show that predicted clad flattening time exceeds residence times expected for extended burnup fuel management using the model given in Reference 3. The evaluations reported in Reference 26 concluded that clad flattening will not occur for current Westinghouse fuel.

3.2.1.2.2 Fuel Assembly Structure

The fuel assembly structure consists of a bottom nozzle, top nozzle, guide thimbles and grids, as shown in Figure 3.2-2.

Bottom Nozzle

The bottom nozzle is a box-like structure, which serves as a bottom structural element of the fuel assembly and directs the coolant flow distribution to the assembly. The VANTAGE 5 fuel assembly included a two piece composite Debris Filtering Bottom Nozzle (DFBN) design incorporating a highly machined stainless steel adaptor plate welded to a low cobalt investment casing as shown in Figure 3.2-2. The plate itself acts to prevent a downward ejection of the fuel rods from their fuel assembly. The DFBN is fastened to the fuel assembly guide tubes by crimped-locked screws which penetrate through the nozzle and mate with an inside fitting in each guide tube.

The DFBN was designed to reduce the possibility of fuel rod damage due to debris-induced fretting. The relatively large flow holes in a conventional nozzle were replaced with a pattern of smaller flow holes. The holes are sized to minimize the passage of debris particles large enough to cause damage while providing sufficient flow area, comparable pressure drop and continued structural integrity of the nozzle. A skirt was added to the nozzle to improve the structural integrity. In addition, five holes were placed on each face of the skirt to allow flow communication.

Cycle 20 implements the Westinghouse Standardized Debris Filter Bottom Nozzle (SDFBN) which Westinghouse has developed for 17x17 fuel and is designed to have a loss coefficient that is the same, independent of supplier. The SDFBN has eliminated the side skirt communication

flow holes as a means of improving the debris mitigation performance of the bottom nozzle. This nozzle has been extensively evaluated and analyzed and it was demonstrated that it meets all of the applicable mechanical design criteria. In addition, specific testing was performed to demonstrate that there is no adverse affect on the thermal hydraulic performance of the SDFBN either with respect to the pressure drop or with respect to DNB.

Coolant flow through the fuel assembly is directed from the plenum in the bottom nozzle upward through the penetrations in the plate to the channels between the fuel rods. The penetrations in the plate are positioned between the rows of the fuel rods.

Axial loads (holddown) imposed on the fuel assembly and the weight of the fuel assembly are transmitted through the bottom nozzle to the lower core plate. Indexing and positioning of the fuel assembly is controlled by alignment holes in two diagonally opposite bearing plates, which mate with locating pins in the lower core plate. Any lateral loads on the fuel assembly are transmitted to the lower core plate through the locating pins.

Top Nozzle

The top nozzle functions as the upper structural element of the fuel assembly in addition to providing a partial protective housing for the rod cluster control assembly or other components. The Westinghouse Integral Nozzle (WIN) top nozzle design is a direct replacement for the reconstitutable top nozzle (RTN) design. The WIN design incorporates design and manufacturing improvements to eliminate the Alloy 718 spring screw for attachment of the holddown springs. The springs are assembled into the nozzle pad and pinned in place. The WIN design provides a wedged rather than a clamped (bolted) joint for transfer of the fuel assembly holddown forces into the top nozzle structure. The flow plate, thermal characteristics, and method of attachment of the nozzle are all unchanged from the RTN top nozzle design. The RTN top nozzle consists of an adapter plate, enclosure, top plate, and pads. The nozzle assembly comprises holddown springs, and screws and clamps mounted on the top plate. The springs and spring screws are made of Inconel-718 whereas other components are made of Type 304 stainless steel. The RTN design differs from the previous, standard nozzle design in two ways: 1) a groove is provided in each thimble thru-hole in the nozzle plate to facilitate attachment and removal, and 2) the nozzle plate thickness is reduced to provide additional axial space for fuel rod growth. The sleeves are mechanically fitted to the top nozzle using a finger arrangement and a lock tube.

The square adapter plate is provided with round penetrations and semicircular ended slots to permit the flow of coolant upward through the top nozzle. Other round holes are provided to accept inserts which are swaged to the adapter plate and mechanically attached to the thimble

tubes. The ligaments in the plate cover the tops of the fuel rods and prevent their upward ejection from the fuel assembly. The enclosure is a box-like structure, which sets the distance between the adapter plate and the top plate. The top plate has a large square hole in the center to permit access for the control rods and the control rod spiders. Holddown springs are mounted on the top plate and are retained by spring screws and clamps located at two diagonally opposite corners. On the other two corners integral pads are positioned which contain alignment holes for locating the upper end of the fuel assembly.

To remove the top nozzle, a tool is first inserted through a lock tube and expanded radially to engage the bottom edge of the tube. An axial force is then exerted on the tool which overrides local lock tube deformations and withdraws the lock tube from the insert. After the lock tubes have been withdrawn, the nozzle is removed by raising it off the upper slotted ends of the nozzle inserts, which deflect inwardly under the axial lift load. With the top nozzle removed, direct access is provided for fuel rod examinations or replacement. Reconstitution is completed by the remounting of the nozzle and the insertion of lock tubes.

Guide and Instrument Thimbles

The guide thimbles are structural members, which also provide channels for the neutron absorber rods, burnable poison rods or neutron source assemblies. Each one is fabricated from Zircaloy-4/ZIRLO™ tubing having two different diameters. The larger diameter at the top section provides a relatively large annular area necessary to permit rapid control rod insertion during a reactor trip as well as to accommodate the flow of coolant during normal operation. Four holes are provided on the thimble tube above the dashpot to reduce the rod drop time. The lower portion of each guide thimble is swaged to a smaller diameter to reduce diametral clearances and produce a dashpot action near the end of the control rod travel during normal operation and to accommodate the outflow of water from the dashpot during a reactor trip. The dashpot is closed at the bottom by means of an end plug, which is provided with a small flow port to avoid fluid stagnation in the dashpot volume during normal operation. The top end of the guide thimble is fastened to a tubular insert by three expansion swages. The inserts have a formed section that mates with the top nozzle adapter plate and is secured with lock tubes. The lower end of the guide thimble is fitted with an end plug, which is then fastened into the bottom nozzle by a shoulder screw with a locking cup.

Each grid is fastened to the guide thimble assemblies to create an integrated structure. For the top and mid-grids in a fuel assembly, Westinghouse has chosen the fastening technique depicted in Figures 3.2-4, 3.2-5, 3.2-5A and 3.2-6A.

An expanding tool is inserted into the inner diameter of the Zircaloy/ZIRLO™ thimble tube at the elevation of the stainless steel sleeves that have been brazed into the Inconel top grid assembly on the Zircaloy/ZIRLO™ sleeve that has been welded into the mid-grid assembly. The four lobed tool forces the thimble and sleeve outward to a predetermined diameter, thus joining the two components.

The guide thimble to top nozzle attachment is shown in Figures 3.2-6 and 3.2-6A. The stainless steel top nozzle inserts are mechanically connected to the top nozzle adapter plate by means of a pre-formed bulge near the top of the insert. The insert engages a mating groove in the wall of the adapter plate/thimble tube thru-hole. The insert has four equally spaced axial slots, which allow the insert to deflect inwardly at the elevation of the bulge thus permitting the installation or removal of the nozzle. The insert bulge is positively held in the adapter plate-mating groove by placing a lock tube, with a uniform inside diameter identical to that of the thimble tube, into the insert.

The bottom non-mixing vane grid assembly is joined to the assembly as shown in Figure 3.2-7. The stainless steel insert is spotwelded to the bottom grid and later captured between the guide thimble end plug and the bottom nozzle by means of a stainless steel thimble screw.

The central instrumentation thimble of each fuel assembly is constrained by seating in counterbores in each nozzle. This tube is of constant diameter and guides the incore neutron detectors. This tube is expanded at the top and mid grids in the same manner as the previously discussed expansion of the guide thimbles to the grids.

The Intermediate Flow Mixer (IFM) grids employ a single bulge connection to the sleeve and thimble just as is used in the intermediate grids.

The Protective Grid is assembled with the bottom grid by four bottom grid inserts that are positioned and welded in the four corner positions.

Grid Assemblies

The fuel rods, as shown in Figure 3.2-2, are supported at intervals along their length by grid assemblies, which maintain the lateral spacing between the rods. Each fuel rod is supported within each grid by the combination of support dimples and springs. The grid assembly consists of individual slotted straps interlocked and brazed in an "egg-crate" arrangement to join the straps permanently at their points of intersection. The straps contain spring fingers, support dimples and mixing vanes.

The grid material for the top and bottom grids is Inconel-718, chosen because of its corrosion resistance and high strength. The grid material for the mid-grids is Zircaloy/ZIRLO™, chosen

because of its low neutron absorption characteristic and its extensive successful in-reactor use. The magnitude of the grid restraining force on the fuel rod is set high enough to minimize possible fretting, without overstressing the cladding at the points of contact between the grids and fuel rods. The grid assemblies also allow axial thermal expansion of the fuel rods without imposing restraint sufficient to develop buckling or distortion of the fuel rods.

The intermediate flow mixer (IFM) grids shown in Figure 3.2-2 are located in the three uppermost spans between the Zircaloy-4/ZIRLO™, mixing vane structural grids and incorporate a similar mixing vane array. The primary function of the IFM grid is to provide mid-span flow mixing in the hottest fuel assembly spans. Each IFM grid cell contains four dimples, which are designed to prevent mid-span channel closure in the spans containing IFMs and fuel rod contact with the IFM mixing vanes. This simplified cell arrangement allows for short grid cells so that the IFM grid can accomplish its flow-mixing objective with minimal pressure drop.

The outer strap configuration was designed similar to current fuel designs to preclude grid hang-up and damage during fuel handling. Additionally, the grid envelope is smaller which further minimizes the potential for damage and reduces calculated forces during seismic/LOCA events. A coolable geometry is, therefore, assured at the IFM grid elevation, as well as at the structural grid elevation.

Westinghouse has developed the balanced vane mid and IFM grids to balance hydraulic forces on the grids to provide more design margin to fuel assembly self-excitation (FASE). The grids' flow mixing vane pattern has been modified to provide 90 degree symmetry and direct the vanes along grid diagonals. The hydraulically balanced pattern was achieved by flipping the bend angle of selected vanes, so the number of vanes and individual vane geometry remain the same. Therefore, the DNB correlation applicability is not impacted by the new mixing vane pattern. The mid grid inner strap dimple profile has also been modified for improved manufacturability. Thermal hydraulic and mechanical testing has been performed to confirm that design criteria are satisfied.

The most recent fuel assembly designs incorporate a Protective Grid and modifications to the bottom fuel rod end plug. The Protective Grid is a partial height grid similar in configuration to the IFM grid, but fabricated of Inconel without mixing vanes. It is positioned on the top plate of the bottom nozzle. The fuel rod bottom end plug positioned within the protective grid is an elongated version of the previous fuel rod bottom end plug design. The Protective Grid and elongated end plug together provide a zone below the active fuel in which debris can be entrapped.

Cycle 20 implements the Westinghouse Robust Protective Grid (RPG) which was developed as a result of observed failures in the field as noted in Post Irradiation Exams (PIE) performed at several different plants. It was determined that observed failures were the result of two primary issues;

1. fatigue failure within the protective grid itself at the top of the end strap and
2. stress corrosion cracking (SCC) primarily within the rod support dimples.

The RPG implements design changes such as increasing the maximum nominal height of the grid, increasing the ligament length and the radii of the ligament cutouts, and the use of four additional spaces for a total of 8 spacers to help strengthen the grid. The nominal height of the grid was increased to allow "V-notch" window cutouts to be added to help minimize flow-induced vibration caused by vortex shedding at the trailing edge of the inner grid straps. These design changes incorporated into the RPG design help address the issues of fatigue failures and failures due to SCC. It was demonstrated that the above changes do not impact the thermal hydraulic performance of the RPG as there is no change to the pressure loss coefficient. In addition, the RPG retains the original protective grid function as a debris mitigation feature.

As part of the addition of the Protective Grid, a bottom Inconel grid with longer inserts and a bottom grid span reduction were also incorporated. The bottom Inconel grid was raised and the first mixing vane grid was lowered to reduce the lower most span length in the fuel assembly. This change increases the resistance of the fuel assembly to flow induced fuel rod vibration to preclude excessive clad wear.

A core coolable geometry must be maintained during a seismic or LOCA event. For the Westinghouse 17X17 VANTAGE 5 fuel assemblies, a seismic and LOCA analysis for a mixed Westinghouse and ANF fueled core showed that the VANTAGE 5 assemblies maintain a coolable geometry.

The structural adequacy of the 17X17 VANTAGE 5 fuel assembly design under the Design Basis Earthquake (DBE) and the accumulator line pipe break for Donald C. Cook Nuclear Plant Unit 2 was evaluated. The Reference 21 analysis methodology, requirements, and acceptance criteria were used for the fuel assembly structural integrity evaluation. The structural adequacy of the 17X17 VANTAGE 5 assembly was assessed using US NRC requirements for combined seismic and LOCA loads per Appendix A to the NRC Standard Review Plan 4.2. The methodology and analysis procedures including the fuel assembly modeling, grid strength determination and computer code have been reviewed and approved by the NRC, References 22 and 23. The grid load was combined using the square-root-sum-of-squares (SRSS) method from the maximum loads obtained from seismic and loss-of-coolant accident analyses.

The time history method was used to obtain the maximum assembly deflections and grid loads. The synthesized time history was generated based on actual earthquake records. The acceleration response spectrum of the synthesized time history envelops the acceleration spectra of the Design Basis Earthquake for the Cook Nuclear Plant Unit 2 site. The core plate motions were obtained from the analysis of the reactor pressure vessel/internals system model (Section 14.3.3). The reactor cores were evaluated using a discrete lumped mass, linear spring-viscous damper, and gaps finite element model. The displacement motions of the core plates are the input forcing functions to the reactor core model. The results of the seismic analysis for the VANTAGE 5 core indicate the maximum grid impact forces are less than the allowable strength. The allowable grid strength is established as the lower 95 percent confidence level on true mean from the distribution of experimentally determined grid crush strength data at temperature. Therefore, the core coolability requirements were met.

The asymmetric LOCA analyses were performed to obtain the grid impact forces and fuel assembly deflection resulting from accumulator line pipe break. The LOCA grid results indicated that the maximum grid impact forces are less than the allowable grid and IFM strengths.

The maximum fuel assembly deflection is well below that obtained from seismic analysis. The fuel assembly component stress resulting from LOCA transients would indicate substantial margins in maintaining fuel assembly structural integrity.

The maximum grid responses obtained from two accident analyses are combined, using the SRSS method. The maximum grid loads were calculated at all the grid elevations. There will be no permanent set of grid spacer deformation. Under the combined earthquake and LOCA loading conditions, the reactor can be safety shut down.

3.2.1.3 Design Evaluation

3.2.1.3.1 Fuel Rods

The IFBA and non-IFBA fuel rods are designed to assure that the design bases are satisfied for Condition I and II events. This assures that the fuel performance and safety criteria (Section 3.2) are satisfied.

3.2.1.3.1.1 Materials - Fuel Cladding

The desired fuel rod clad is a material which has a superior combination of neutron economy (low absorption cross section), high strength (to resist deformation due to differential pressures and mechanical interaction between fuel and clad), high corrosion resistance (to coolant, fuel and fission products), and high reliability. Zircaloy-4, ZIRLO, or **Optimized ZIRLO™** cladding has

this desired combination of clad properties. As shown in References (4 and 33), there is considerable PWR operating experience on the capability of Zircaloy/ZIRLO™ as a clad material. The use of **Optimized ZIRLO™** cladding has been approved in Reference 33. Clad hydriding has not been a significant cause of clad perforation since current controls on levels of fuel contained moisture were instituted (References 4 and 33).

3.2.1.3.1.2 Materials - Fuel Pellets

Sintered, high-density uranium dioxide fuel reacts only slightly with the clad at core operating temperatures and pressures. In the event of clad defects, the high resistance of uranium dioxide to attack by water protects against fuel deterioration although limited fuel erosion can occur. As has been shown by operating experience and extensive experimental work, the thermal design parameters conservatively account for changes in the thermal performance of the fuel elements due to pellet fracture, which may occur during power operation. The consequences of defects in the clad are greatly reduced by the ability of uranium dioxide to retain fission products including those, which are gaseous or highly volatile. Observations from several operating Westinghouse PWR's (References 2 and 4) has shown that fuel pellets can densify under irradiation to a density higher than the manufactured values. Fuel densification and subsequent settling of the fuel pellets could result in local and distributed gaps in the fuel rods.

An extensive analytical and experimental effort has been conducted by Westinghouse (References 2 and 4) to characterize the fuel densification phenomenon. Fuel densification is cycle specific. The effects of fuel densification have been taken into account in the nuclear and thermal hydraulic design of the reactor described in Sections 3.3 and 3.4, respectively.

Metallographic examination of irradiated commercial fuel rods have shown occurrences of fuel/clad chemical interaction. Reaction layers of < 1 mil in thickness have been observed between fuel and clad at limited points around the circumference. Westinghouse metallographic data indicates that this interface layer remains very thin even at high burnup. Thus, there is no indication of propagation of the layer and eventual clad penetration.

Stress corrosion cracking is another postulated phenomenon related to fuel/clad chemical interaction. Out of pile tests have shown that in the presence of high clad tensile stresses, large concentrations of iodine can chemically attack the Zircaloy/ZIRLO/**Optimized ZIRLO™** tubing and can lead to eventual clad cracking. Westinghouse has no inpile evidence that this mechanism is operative in commercial fuel.

3.2.1.3.1.3 Materials - Strength Considerations

One factor in fuel element duty is potential mechanical interaction of fuel and clad. This fuel/clad interaction produces cyclic stresses and strains in the clad, and these in turn consume clad fatigue lifetime.

The reduction of fuel/clad interaction is therefore a goal of design. In order to achieve this goal and to enhance the cyclic operational capability of the fuel rod, the technology for using pre-pressurized fuel rods in Westinghouse PWR's has been developed.

Initially the gap between the fuel and clad is sufficient to prevent hard contact between the two. However, during power operation a gradual compressive creep of the clad onto the fuel pellet occurs due to the external pressure exerted on the rod by the coolant. Clad compressive creep eventually results in the fuel/clad contact. During this period of fuel/clad contact, changes in power level could result in changes in clad stresses and strains. By using pre-pressurized fuel rods to partially offset the effect of the coolant external pressure, the rate of clad creep toward the surface of the fuel is reduced. Fuel rod pre-pressurization delays the time at which fuel/clad interaction and contact occur and hence significantly reduces the number and extent of cyclic stresses and strains experienced by the clad both before and after fuel/clad contact. These factors result in an increase in the fatigue life margin of the clad and lead to greater clad reliability. If gaps should form in the fuel stacks, clad flattening will be prevented by the rod pre-pressurization so that the flattening time will be greater than the fuel's core life.

A two dimensional (r,h) finite element model has been established to investigate the effects of radial pellet cracks on stress concentrations in the clad. Stress concentration, herein, is defined as the difference between the maximum clad stress in the h-direction and the mean clad stress. The first case has the fuel and clad in mechanical equilibrium and as a result the stress in the clad are close to zero. In subsequent cases the pellet power is increased in steps and the resultant fuel thermal expansion imposes tensile stresses in the clad. In addition to uniform clad stresses, stress concentrations develop in the clad adjacent to radial cracks in the pellet. These radial cracks have a tendency to open during a power increase but the frictional forces between fuel and clad oppose the opening of these cracks and result in localized increases in clad stress. As the power is further increased, large tensile stresses exceed the ultimate tensile strength of UO_2, additional cracks in the fuel are created which limits the magnitude of the stress concentration in the clad.

As part of the standard fuel rod design analysis, the maximum stress concentration evaluated from finite element calculations is added to the volume averaged effective stress in the clad as determined from one-dimensional stress/strain calculations. The resultant clad stress is then

compared to the temperature dependent Zircaloy/ZIRLO/**Optimized ZIRLO™** yield stress in order to assure that the stress criterion is satisfied. Analysis of **Optimized ZIRLO™** cladding must account for a reduction yield strength, per Reference 33.

3.2.1.3.1.4 Steady-State Performance Evaluation

In the calculation of the cycle specific steady-state performance of a nuclear fuel rod, the following interacting factors must be considered:

1. Clad creep and elastic deflection.
2. Pellet density changes, thermal expansion, gas release and thermal properties as a function of temperature and fuel burnup.
3. Internal pressure as a function of fission gas release, rod geometry and temperature distribution.

These effects are evaluated using models, References 5, 6, 20, 30 and 31, which include appropriate fuel rod design models for time dependent fuel densification. With these interacting factors considered, the model determines the fuel rod performance characteristics for a given rod geometry, power history and axial power shape. In particular, internal gas pressure, fuel and clad temperatures, and clad deflections are calculated. The fuel rod is divided into several axial sections and radially into a number of annular zones. Fuel density changes, clad stresses, strains and deformations, and fission gas releases are calculated separately for each segment. The effects are integrated to obtain the internal rod pressure.

The initial rod internal pressure is selected to delay fuel/clad mechanical interaction to avoid the potential for flattened rod formation, to prevent fuel-clad diametral gap increases due to outward cladding creep during steady state operation and to limit extensive DNB propagation during Condition I and II operation. It is limited, however, by the design criteria for the rod internal pressure, which includes the helium released from the IFBA coating on the pellets of the IFBA rods.

The gap conductance between the pellet surface and the clad inner diameter is calculated as a function of the composition, temperature, and pressure of the gas mixture, and the gap size or contact pressure between clad and pellet. After computing the fuel temperature for each pellet annular zone, the fractional fission gas release is assessed using an empirical model derived from experimental data (References 20 and 30). The total amount of gas released is based on the average fractional release within each axial and radial zone and the gas generation rate, which in turn is a function of burnup. Finally, the gas released is summed over all zones and the pressure is calculated.

This model shows good agreement in fit for a variety of published and proprietary data on fission gas release, fuel temperatures and clad deflections (References 20, 30 and 31). Included in this spectrum are variations in power, time, fuel density and geometry.

The fission gas release model given in References 20 and 30 are used in determining the internal gas pressures as a function of irradiation time. The plenum region of the fuel rod provides void volume in the rod to help minimize the effects of fission gas release on rod internal pressure.

The clad stresses at a constant local fuel rod power are low. Compressive stresses are created by the pressure differential between the coolant pressure and the rod internal gas pressure. Because of the prepressurization with helium, the volume average effective stresses are typically less than approximately 15,000 psi at the pressurization level used in typical fuel rod design. Stresses due to the temperature gradient are not included in this average effective stress because thermal stresses are, in general, negative at the clad inside diameter and positive at the clad outside diameter and their contribution to the clad volume average stress is small. Furthermore, the thermal stress decreases with time during steady-state operation due to stress relaxation. The stress due to pressure differential is highest in the minimum power rod at the beginning-of-life (due to low internal gas pressure) and the thermal stress is highest in the maximum power rod (due to the steep temperature gradient).

The internal gas pressure throughout life for the lead burnup rod, the total tangential stresses at the clad inside diameter throughout life and volume average effective stresses throughout life are calculated every cycle. These stresses are below the yield stress of the material.

Tensile stresses could be created once the clad has come in contact with the pellet. These stresses would be induced by the fuel pellet swelling during irradiation. Fuel swelling can result in small clad strains (< 1 percent) for expected discharge burnups but the associated clad stresses are very low because of clad creep (thermal and irradiation-induced creep). Furthermore, the 1 percent strain criterion is extremely conservative for clad strain due to fuel swelling because the strain rate associated with solid fission products swelling is very slow.

3.2.1.3.1.5 Transient Evaluation Method

Pellet thermal expansion due to power increases is considered the only mechanism by which significant stresses and strains can be imposed on the clad. Power increases in commercial reactors can result from fuel shuffling, reactor power escalation, and full length control rod movement. In the mechanical design model, lead rods are depleted using best estimate power histories as determined by core physics calculations. During the depletion, the amount of diametral gap closure is evaluated based upon the pellet expansion-cracking model, clad creep model, and fuel-swelling model. At various times during the depletion of the core, the power is

increased locally on the rod to the burnup attainable power density as determined by core physics calculations during the transient (Condition I or II) event simulation. The radial, tangential, and axial clad stresses resulting from the power increase are combined into a volume average effective clad stress.

The Von Mises criterion is used to determine if the clad yield stress has been exceeded. This criterion states that an isotropic material in multi-axial stress will begin to yield plastically when the effective stress exceeds the yield as determined by a uniaxial tensile test. The yield stress correlation is that for irradiated cladding since fuel/clad interaction occurs at high burnup. Furthermore, the effective stress is increased by an allowance, which accounts for stress concentrations in the clad adjacent to radial cracks in the pellet, prior to the comparison with the yield stress. This allowance was evaluated using a two-dimensional (r,ϕ) finite element model.

Slow transient power increases can result in large clad strains without exceeding the clad yield stress because of clad creep and stress relaxation. Therefore, in addition to the yield stress criterion, a criterion on allowable clad positive strain is necessary.

Based upon high strain rate burst and tensile test data on irradiated tubing, 1 percent strain was determined to be the lower limit on irradiated clad ductility and thus adopted as a design criterion.

A comprehensive review of the available strain-fatigue models was conducted by Westinghouse as early as 1968.

This included the Langer-O'Donnel model (Reference 7), the Yao-Munse model and the Manson-Halford model. Upon completion of this review and using the results of the Westinghouse experimental programs discussed below, it was concluded that the approach defined by Langer-O'Donnel would be retained and the empirical factors of their correlation modified in order to conservatively bound the results of the Westinghouse testing program.

The Langer-O'Donnel empirical correlation has the following form:

$$S_a = \frac{E}{4\sqrt{N_f}} \ln \frac{100}{100 - RA} + S_e$$

Where:

S_a = $(1/2)E\Delta\varepsilon_t$=pseudo – stress amplitude which cause failure in Nf cycles (lb/in2).

$\Delta\varepsilon_t$ = total strain range (in/in).

E = Young's Modulus (lb/in^2).

N_f = number of cycles to failure.

RA = reduction in area at fracture in a uniaxial tensile test (%).

S_e = endurance limit (lb/in^2).

Both RA and S_e are empirical constants, which depend on the type of material, the temperature and irradiation. The Westinghouse testing program was subdivided into the following subprograms:

1. A rotating bend fatigue experiment on unirradiated Zircaloy-4 specimens at room temperature and at 725°F. Both hydrided and non-hydrided Zircaloy-4 cladding were tested.
2. A biaxial fatigue experiment in gas autoclave on unirradiated Zircaloy-4 cladding both hydrided and non-hydrided.
3. A fatigue test program on irradiated cladding from the CVS and Yankee Core V conducted at Battelle Memorial Institute.

The results of these test programs provided information on different cladding conditions including the effects of irradiation, of hydrogen level, and of temperature.

The Westinghouse design equations followed the concept for the fatigue design criterion according to the ASME Code, Section III. Namely,

1. The calculated pseudo-stress amplitude (S_a) has to be multiplied by a factor of 2 in order to obtain the allowable number of cycles (N_f).
2. The allowable cycles for a given S_a is 5 percent of N_f, or a safety factor of 20 on cycles.

The lesser of the two allowable number of cycles is selected. The cumulative fatigue life fraction is then computed as:

$$\frac{kn_k}{\sum_1 N_{fk}} \geq 1$$

Where:

n_k = number of diurnal cycles of mode k.

It is recognized that a possible limitation to the satisfactory behavior of the fuel rods in a reactor which is subjected to daily load follow is the failure of the clad by low cycle strain fatigue. During their normal residence time in the reactor, the fuel rods may be subjected to 1000 or more cycles with typical changes in power level from 50 to 100 percent of their steady-state values.

The assessment of the fatigue life of the fuel rod clad is subjected to a considerable uncertainty due to the difficulty of evaluating the strain range, which results from the cyclic interaction of the fuel pellets and clad. This difficulty arises for example from such highly unpredictable phenomena as pellet cracking, fragmentation, and relocation. Nevertheless, since early 1968, Westinghouse has been investigating this particular phenomenon both analytically and experimentally. Strain fatigue tests on irradiated and nonirradiated hydrided Zircaloy- 4 claddings were performed which permitted a definition of a conservative fatigue life limit and recommendation of a methodology to treat the strain fatigue evaluation of the Westinghouse reference fuel rod designs.

However, Westinghouse is convinced that the final proof of the adequacy of a given fuel rod design to meet the load follow requirements can only come from incore experiments performed on actual reactors. Westinghouse has significant experience in load follow operation dating back to early 1970 with the load follow operation of the Saxton reactor. There has been no significant coolant activity increase that could be associated with the load follow mode of operation.

The potential effects of operation with waterlogged fuel are discussed in Section 3.4.3.6. Waterlogging is not considered to be a concern during operational transients.

3.2.1.3.1.6 Rod Bowing

Reference (8) presents the model used for evaluation of fuel rod bowing. To the present time this model has been used for bow assessment in 14 x 14, 15 x 15, and 17 x 17 type cores.

3.2.1.3.2 Fuel Assembly Structure

3.2.1.3.2.1 Stresses and Deflections

The fuel assembly component stress levels are limited by the design. For example, stresses in the fuel rod due to thermal expansion and Zircaloy/ZIRLO/**Optimized ZIRLO™** irradiation growth are limited by the relative motion of the rod as it slips over the grid spring and dimple surfaces. Clearances between the fuel rod ends and nozzles are provided so that Zircaloy/ZIRLO/**Optimized ZIRLO™** irradiation growth does not result in rod end interferences. Stresses in the fuel assembly caused by tripping of the rod cluster control assembly have little influence on fatigue because of the small number of events during the life on an assembly. Assembly components and prototype fuel assemblies made from production parts are subjected to structural tests to verify that the design bases requirements are met.

The fuel assembly design loads for shipping have been established at 4 g axial and 6 g lateral. Accelerometers are permanently placed into the shipping cask to monitor and detect fuel assembly accelerations that would exceed the criteria. Past history and experience has indicated that loads, which exceed the allowable limits rarely, occur. Exceeding the limits requires reinspection of the fuel assembly for damage. Tests on various fuel assembly components such as the grid assembly, sleeves, inserts and structure joints have been performed to assure that the shipping design limits do not result in impairment of fuel assembly function.

3.2.1.3.2.2 Dimensional Stability

The basis for fuel assembly structural integrity considering the effect of faulted condition is discussed in Reference (23).

The coolant flow channels are established and maintained by the structure composed of grids and guide thimbles. The lateral spacing between fuel rods is provided and controlled by the support dimples of adjacent grid cells. Contact of the fuel rods on the dimples is maintained through the clamping force of the grid springs. Lateral motion of the fuel rods is opposed by the spring force and the internal moments generated between the spring and the support dimples.

No interference with control rod insertion into thimble tubes will occur during a postulated loss of coolant accident transient due to fuel rod swelling, thermal expansion, or bowing. In the early phase of the transient following the coolant break, the high axial loads, which potentially could be generated by the difference in thermal expansion between fuel clad and thimbles, are relieved by slippage of the fuel rods through the grids. The relatively low drag force restraint on the fuel rods will induce only minor thermal bowing, which is sufficient to close the fuel rod-to-thimble tube gap. This rod-to-grid slip mechanism occurs simultaneously with control rod drop.

Subsequent to the control rod insertion the transient temperature increase of the fuel rod clad can result in swelling sufficient to contact the thimbles. Grid crush strength tests and seismic and LOCA evaluations show that the grids will maintain a geometry capable of being cooled under the worst case accident Condition IV event.

3.2.1.3.2.3 Vibration and Wear

Fuel rod vibrations are flow induced. The effect of the vibration on the fuel assembly and individual fuel rods is minimal. The cyclic stress range associated with deflections of such small magnitude is insignificant and has no effect on the structural integrity of the fuel rod.

The grid spring force on the rod early in the fuel's life sufficient to preclude wears of the fuel cladding. By the time a grid-rod gap has formed (due to clad creepdown and spring relaxation), the clad has developed an oxide thickness that under normal operating conditions, precludes significant wear of the clad through end of life. No significant wear of the clad or grid supports is expected during the life of the fuel assembly. Clad fretting and fuel rod vibration has been experimentally investigated as discussed in Reference (10).

3.2.1.3.3 Operational Experience

A discussion of fuel operating experience is given in Reference (4).

3.2.1.3.4 High Power Fuel Rod Development

A high power fuel test program had as its objective the defining of failure limits for the combined effects of linear heat generation rate and burnup, providing increased assurance that current plants have an adequate performance and design margin to failure threshold, and verifying the adequacy of design methods and computer codes. This program is described in Reference (2).

3.2.1.4 Tests and Inspections

3.2.1.4.1 Quality Assurance Program

The Westinghouse Electric Company 'Quality Management System' (QMS) , as summarized in Reference (11), has been developed in conjunction with the Nuclear Fuel Business Unit (NFBU) to serve the division in planning and monitoring its activities for the design and manufacture of nuclear fuel assemblies and associated components.

The NRC-approved QMS program provides for control over all activities affecting product quality, commencing with design and development and continuing through procurement, materials handling, fabrication, testing and inspection.

3.2.1.4.2 Quality Control

The Westinghouse QMS is fully implemented within NFBU by lower level internal procedures such as

1. Manufacturing Operating Procedures,
2. Chemical Operating Procedures, and
3. Quality Control Instructions.

Taken collectively, these procedures are fully responsive to 10CFR50 Appendix B, as well as ISO 9001 requirements. These procedures cover all areas of manufacturing including, but not limited to, fuel system components and parts, pellets, rod inspection, non-fuel core components, fuel assemblies, and components. With respect to supplier quality control, Westinghouse reviews and approves process outlines and inspection procedures by suppliers to ensure that applicable design and specification requirements are met.

3.2.1.4.3 Tests and Inspections by Others

If any tests and inspections are to be performed on behalf of Westinghouse or other fuel supplier, the fuel supplier will review and approve the quality control procedures, inspection plans, etc. to be utilized to ensure that they are equivalent to the description provided above and are performed properly to meet all fuel vender's requirements.

3.2.1.4.4 Onsite Inspection

Onsite inspection programs for fuel, control rods and internals are based on the NSSS supplier's detailed procedures. In the event reloads or other components are supplied by other suppliers additional programs will be developed based on that supplier's procedures.

Loaded fuel containers, when received on site, are externally inspected to ensure that labels and markings are intact and seals are unbroken. After the containers are opened, the accelerometers are inspected to determine if movement during transit exceeded design limitations.

Following removal of the fuel assembly from the container in accordance with detailed procedures, which contain guidance from the fuel fabricator, the polyethylene wrapper is removed and a visual inspection of the entire bundle is performed.

Control rod assemblies are typically shipped in fuel assemblies and are inspected during fuel receipt operations. The RCCA's and core components must be handled in the vertical position unless completely inserted in a fuel assembly or shipping container. Surveillance of fuel and reactor performance is routinely conducted by operating personnel. Coolant activity and chemistry are followed to permit early detection of any fuel-clad defects.

Visual fuel inspection is routinely conducted during refueling. Additional fuel inspections are dependent on the results of the operational monitoring and the visual inspections.

Irradiated Fuel Tests and Inspections

Should they be determined to be desirable or necessary, tests and/or inspections of irradiated fuel may be elected to be performed. These tests and/or inspections are usually performed during refueling outages, but not necessarily so. Inspections are performed to determine the status of the integrity of the fuel rod cladding, to observe any other types of mechanical fuel damage or failure, or to obtain information as to the cause of fuel damage or failure. Various inspection methods may be used to accomplish these goals. These methods include: non-intrusive visually-aided inspections, eddy current inspection, ultrasonic testing, and in-mast fuel sipping. A description of each of these activities follows below:

3.2.1.4.4.1 Non-Intrusive Visually-Aided Inspections

Non-intrusive inspections of fuel, meaning that the fuel assembly is not disassembled during the inspection, for indications of fuel damage or failure, or to verify fuel assembly identification, are performed using visual aids. These aids could be binoculars or could be underwater cameras. These underwater cameras could either be fixed in position on the fuel racks, or hang from the spent fuel pool bridge crane or side of the transfer canal or spent fuel pool through use of cables or poles. No safety concerns are identified with this process provided that the fuel being inspected is handled in accordance with technical specifications and plant procedures.

A special version of this type of inspection is a "lift-and-rotate" inspection, which is performed to obtain information as to fuel failure mechanism. During a "lift-and-rotate" inspection, special tooling is used to manipulate fuel rods that reside within the fuel assembly envelope. The tooling can be used to raise, lower, and rotate each fuel rod so that a large percentage of the surface area of the fuel rod can be exposed to the outside of the fuel assembly to be observed by a camera. A fuel assembly that has been inspected using the "lift-and-rotate" inspection technique may not be reloaded into the reactor due to the inability to control lateral forces on the fuel rod being manipulated by the tooling that may cause unacceptable deformation of the spring in the lower grid strap for that fuel rod location.

3.2.1.4.4.2 In-Mast Fuel Sipping

When handling fuel with the manipulator crane, it may be desired to test the irradiated fuel for leaks using the in-mast fuel sipping system. The inspection is typically performed during core unload. When a fuel assembly is raised from the core and is in the full up position in the manipulator crane mast, the inspection of a fuel assembly may proceed. Air bubbles are pumped

to the bottom of the mast such that they enter the mast and raise past the fuel assembly. The air bubbles up to above the surface of the water inside the mast, where it can be suctioned past a detector to measure its radioactivity. Should the fuel assembly contain failed fuel, radioactive fission gases that will be escaping the failed fuel rod(s) due to the chance in rod pressure corresponding to the change in surrounding water pressure with elevation will be stripped by the air bubbles as they traverse upward through the mast. A change in the measurement of radioactivity from the background level will indicate the presence of failed fuel.

An evaluation was performed to assess the effects of voiding due to the presence of air bubbles in the mast on heat transfer and criticality. No concerns were identified. Two air regulators are required in series on the supply air to the mast to provide double failure protection to prevent an excessive amount of air being supplied to the mast above the 1 gpm required for the inspection.

3.2.1.4.4.3 Ultrasonic Testing

Ultrasonic testing (UT) is another method used to detect the presence of fuel failures. This inspection is typically performed in the spent fuel pool. An inspection station is mounted on top of a spent fuel pool storage rack, one, which does not contain irradiated fuel. Administrative controls are in place during set up and removal of the equipment on the spent fuel pool storage rack such that impact energy limits would not be exceeded should the inspection station inadvertently be dropped. The inspection station is set up such that when a fuel assembly is lowered into the inspection station, no interaction will be encountered between the fuel and the spent fuel pool storage rack.

During UT, fuel assemblies are positioned one at a time in the UT inspection station through use of the spent fuel bridge crane. The fuel assembly being tested is lowered into the inspection station such that the lowest grid is below the level of the probe. A probe is inserted between the fuel rods to send and receive ultrasonic signals through each fuel rod. The return signal will be different depending upon the condition inside the fuel rod. If the fuel rod is not failed, the inside surface should contain helium gas. The return signal will be nearly identical to the sent signal. However, if the fuel rod is failed, water present on the inside of the fuel rod will dampen the spent signal, returning a signal different than what was sent. In this manner, failed fuel rods are detected. No safety concerns are identified since procedural and technical specifications requirements for fuel handling are adhered to.

3.2.1.4.4.4 Rod Cluster Control Assembly Wear Inspections

Mechanical damage has been known to occur on rod cluster control assemblies (RCCAs). Flow induced vibration of the RCCAs while in operation cause the RCCAs to come in contact with the guide support structure, potentially causing wear rings to form on the RCCAs. Also, axial

cracking has been observed at the tips of the RCCAs at other nuclear facilities. Examinations have been occurring on a periodic basis to assess the rate and extent of wear and cracking of the RCCAs.

Similar to UT, an inspection station is set upon a spent fuel pool rack. Administrative controls are in place during set up and removal of the equipment on the spent fuel pool storage rack such that impact energy limits would not be exceeded should the inspection station inadvertently be dropped.

RCCAs are handled using the RCCA handling tool connected to the spent fuel pool bridge crane. RCCAs are taken to the inspection station one at a time for inspection. The inspection station consists of the appropriate number of eddy current encircling coils to assess the amount of wall loss from each RCCA rodlet at any axial location. No safety concerns are identified since procedural and technical specifications requirements for fuel handling are adhered to. Evaluation of the data determines whether reuse of the RCCA is appropriate and when the next inspection should be performed.

3.2.1.4.4.5 Bottom Mounted Instrumentation Thimble Tube Wear Inspections

Mechanical wear on thimble tubes has been observed at axial locations corresponding to the lower core plate and the bottom fuel nozzle, as well as in the lower internals area. This wear has been attributed to flow induced vibration.

In an effort to eliminate the concerns of flow induced wear, all 58 of the bottom mounted instrumentation (BMI) flux thimble tubes were replaced with new thimble tubes. The replacement thimble tubes, beginning 12 feet from the bullet end, are chrome plated over 14-foot length of the outside circumference. Chrome plating of flux thimble tubes has been determined to be an effective engineering solution to wear due to flow induced vibration.

Monitoring of the extent and rate of wear is necessary to ensure the integrity of thimble tubes, so that they may be replaced or repositioned whenever possible, and so that the reactor core may have at least the minimum number of required instrumented locations for flux map surveillances.

Wear is observed using eddy current techniques. This inspection is performed with the reactor in Mode 5 or 6 and at atmospheric pressure. An eddy current probe is pushed into and pulled from each of the thimble tubes at the seal table to determine wall loss at each axial location.

3.2.2 Reactor Vessel Internals

3.2.2.1 Design Bases

The design bases for the mechanical design of the reactor vessel internals components are as follows:

1. The reactor internals in conjunction with the fuel assemblies shall direct reactor coolant flow through the core to achieve acceptable flow distribution and to restrict bypass flow so that the heat transfer performance requirements are met for all modes of operation. In addition, required cooling for the pressure vessel head shall be provided so that the temperature differences between the vessel flange and head do not result in leakage from the flange during reactor operation.
2. In addition to neutron shielding provided by the reactor coolant, a separate thermal shield is provided to limit the neutron exposure of the pressure vessel material in order to maintain the required ductility of the material for all modes of operation.
3. Provisions shall be made for installing incore instrumentation useful for the plant operation and vessel material test specimens required for a pressure vessel irradiation surveillance program.
4. The reactor internals shall be designed to withstand mechanical loads arising from operating basis earthquake, safe shutdown earthquake and pipe ruptures and meet the requirement of Item 5 below.
5. The reactor shall have mechanical provisions, which are sufficient to adequately support the core and internals, and to assure that the core is intact with acceptable heat transfer geometry following transients arising from abnormal operating conditions.
6. Following the design basis accident, the plant shall be capable of being shutdown and cooled in an orderly fashion so that fuel-cladding temperature is kept within specified limits. This implies that the deformation of certain critical reactor internals must be kept sufficiently small to prevent overstressing of fuel elements to failure plus allow adequate core cooling.

The functional limitations for the core structures during the design basis accident are shown in Table 3.2-1. To ensure no column loading of rod cluster control guide tubes, the upper core plate deflection is limited to not exceed the value shown in Table 3.2-1.

Details of the dynamic analyses, input forcing functions, and response loadings are presented in Section 14.3.3.

3.2.2.2 Description and Drawings

The reactor vessel internals are described as follows:

The components of the reactor internals are divided into three parts consisting of the lower core support structure (including the entire core barrel and thermal shield), the upper core support structure and the incore instrumentation support structure. The reactor internals support the core, maintain fuel alignment, limit fuel assembly movement, maintain alignment between fuel assemblies and control rod drive mechanisms, direct coolant flow past the fuel elements, direct coolant flow to the pressure vessel head, provide gamma and neutron shielding, and guides for the incore instrumentation. The coolant flows from the vessel inlet nozzles down the annulus between the core barrel and the vessel wall and then into a plenum at the bottom of the vessel. It then reverses and flows up through the core support and through the lower core plate. The lower core plate is sized to provide the desired inlet flow distribution to the core. After passing through the core, the coolant enters the region of the upper support structure and then flows radially to the core barrel outlet nozzles and directly through the vessel outlet nozzles. A small portion of the coolant flows between the baffle plates and the core barrel to provide additional cooling of the barrel. Similarly, a small amount of the entering flow is directed into the vessel head plenum and exits through the vessel outlet nozzles.

All the major material for the reactor internals is Type 304 stainless steel. Parts not fabricated from Type 304 stainless steel include bolts and dowel pins which are fabricated from Type 316 stainless steel and radial support key bolts which are fabricated of Inconel. Originally installed baffle-former bolts are Type 347 Stainless Steel. Replacement baffle-former bolts are Type 316 Stainless Steel. There are no other materials used in the reactor internals or core support structures which are not otherwise included in the ASME Code, Section III, Appendix I.

Austenitic stainless steel is used for the majority of reactor internals structures, and this material is not subject to brittle fracture. The core hold down spring, however, is made of ASTM A 182 Type F304 stainless steel. Significant crack growth was found to be impossible for this component considering the stress state and possible flaw size. The core hold down spring is the only stainless steel material in the reactor core support structure with a yield strength greater than 90,000 psi and is acceptable based upon ASME Code Case 1337.

All reactor internals are removable from the vessel for the purpose of their inspection as well as the inspection of the vessel internal surface.

3.2.2.2.1 Lower Core Support Structure

The major containment and support member of the reactor internals is the lower core support structure, shown in Figure 3.2-8. This support structure assembly consists of the core barrel, the core baffle, the lower core plate and support columns, the thermal shield and the core support which is welded to the core barrel. All the major material for this structure is Type 304 stainless steel. The lower core support structure is supported at its upper flange from a ledge in the reactor vessel head flange and its lower end is restrained in its transverse movement by a radial support system attached to the vessel wall. Within the core barrel are an axial baffle and a lower core plate, both of which are attached to the core barrel wall and form the enclosure periphery of the assembled core. The lower core support structure and principally the core barrel serve to provide passageways and control for the coolant flow. The lower core plate is positioned at the bottom level of the core below the baffle plates and provides support and orientation for the fuel assemblies.

The lower core plate is a member through which the necessary flow distribution holes for each fuel assembly are machined. Fuel assembly locating pins (two for each assembly) are also inserted into this plate. Columns are placed between this plate and the core support of the core barrel in order to provide stiffness and to transmit the core load to the core support. Adequate coolant distribution is obtained through the use of the lower core plate and core support.

The top of the one-piece thermal shield is rigidly attached to the core barrel. The bottom of the thermal shield is connected to the core barrel with axial flexures. This bottom support allows for differential axial growth of the shield/core barrel but restricts radial or horizontal movement of the bottom of the shield. Rectangular tubing in which reactor vessel material samples can be inserted and irradiated during reactor operation are welded to the thermal shield. These samples are held in the rectangular tubing by a preloaded spring device.

Vertically downward loads from weight, fuel assembly preload forces, control rod dynamic loading, hydraulic loads and earthquake acceleration are carried by the lower core plate partially into the lower core plate support flange on the core barrel shell and partially through the lower support columns to the core support and then through the core barrel shell to the core barrel flange supported by the vessel ledge. Transverse loads from earthquake acceleration, coolant cross flow and vibration are carried by the core barrel shell and distributed between the lower radial support to the vessel wall and to the vessel ledge. Transverse loads of the fuel assemblies are transmitted to the core barrel shell by direct connection of the lower core plate to the barrel wall and by upper core plate alignment pins, which are welded into the core barrel.

The main radial support system of the lower end of the core barrel is accomplished by "key" and "keyway" joints to the reactor vessel wall. At equally spaced points around the circumference, an Inconel clevis block is welded to the vessel inner diameter. Another Inconel insert block is bolted to each of these blocks and has a "keyway" geometry. Opposite each of these is a "key" which is attached to the internals. At assembly, as the internals are lowered into the vessel, the keys engage the keyways in the axial direction. With this design, the internals are provided with a support at the furthest extremity, and may be viewed as a beam fixed at the top and simply supported at the bottom.

Radial and axial expansions of the core barrel are accommodated but transverse movement of the core barrel is restricted by this design. With this system, cyclic stresses in the internal structures are within the ASME Code, Section III limits. In the event of an abnormal downward vertical displacement of the internals following a hypothetical failure of the core barrel, energy-absorbing devices limit the displacement after contacting the vessel bottom head. The load is then transferred through the energy absorbing devices of the internals to the vessel.

The energy absorbers, cylindrical in shape, are contoured on their bottom surface to the reactor vessel bottom head geometry. Assuming a downward vertical displacement the kinetic energy of the system is absorbed mostly by the strain energy of the energy absorbing devices.

3.2.2.2.2 Upper Internals Assembly

The upper internals assembly, shown in Figures 3.2-9 and 3.2-10 consists of the upper support plate, deep beam sections, and the upper core plate between which are contained support columns and guide tube assemblies. The support columns establish the spacing between the upper support plate and the upper core plate and are fastened at top and bottom to these plates. The support columns transmit the mechanical loadings between the two plates and serve the supplementary function of supporting thermocouple guide tubes. The guide tube assemblies sheath and guide the control rod drive shafts and control rods. They are fastened to the upper support and are restrained by pins in the upper core plate for proper orientation and support. Additional guidance for the control rod drive shafts is provided by the upper guide tube which is attached to the upper support plate and guide tube. Flow restrictors are installed in the guide tubes at core locations D6, D10, F4, F12, K4, M6, and M10. The part length CRDM drive shafts were eliminated at these locations.

The upper internals assembly is positioned in its proper orientation with respect to the lower support structure by flat-sided pins pressed into the core barrel which in turn engage in slots in the upper core plate. At an elevation in the core barrel where the upper core plate is positioned, the flat-sided pins are located at angular positions of 90^{o} from each other. Four slots are milled

into the core plate at the same positions. As the upper internals structure is lowered into the barrel, the slots in the upper plate engage the flat-sided pins in the axial direction. Lateral displacement of the core plate is restricted by this design. Fuel assembly locating pins protrude from the bottom of the upper core plate and engage the fuel assemblies as the upper internals assembly is lowered into place. Proper alignment of the lower core support structure, the upper internals assembly, the fuel assemblies and control rods is thereby assured by this system of locating pins and guidance features. The upper internals assembly is restrained from any axial movements by a large circumferential spring, which rests between the upper barrel flange and the upper support flange and is compressed when the reactor vessel head is installed on the pressure vessel.

Vertical loads from weight, earthquake acceleration, hydraulic loads and fuel assembly preload are transmitted through the upper core plate via the support columns to the upper support flange and then the reactor vessel head. Transverse loads from coolant cross flow, earthquake acceleration, and possible vibrations are distributed by the support columns to the upper support plate and upper core plate. The upper support plate is particularly stiff to minimize deflection.

3.2.2.2.3 Incore Instrumentation Support Structures

The incore instrumentation support structures consist of an upper system to convey and support thermocouples penetrating the vessel through the head and a lower system to convey and support flux thimbles penetrating the vessel through the bottom.

The upper system utilizes the reactor vessel head penetrations. Instrumentation port columns are slip-connected to inline columns that are in turn fastened to the upper support plate. These port columns protrude through the head penetrations. The thermocouples are carried through these port columns and the upper support plate at positions above their readout locations. The thermocouple conduits are supported from the columns of the upper core support system. The thermocouple conduits are sealed stainless steel tubes.

In addition to the upper incore instrumentation, there are reactor vessel bottom penetration tubes (see Figure 3.2-8) which admit the retractable, partially chrome plated, cold worked stainless steel flux thimbles that are pushed upward into the reactor core. Conduits extend from the bottom of the reactor vessel down through the concrete shield area and up to a thimble seal line. The minimum bend radii are about 120 inches and the trailing ends of the thimbles (at the seal table) are extracted approximately 15 feet during refueling of the reactor in order to avoid interference within the core. The thimbles are closed at the leading ends and serve as the pressure barrier between the reactor pressurized water and the containment atmosphere.

Mechanical seals between the retractable thimbles and conduits are provided at the seal table. During normal operation, the retractable thimbles are stationary and are moved only during refueling or for maintenance, at which time a space of approximately 15 feet above the seal table is cleared for the retraction operation.

The incore instrumentation support structure is designed for adequate support of instrumentation during reactor operation and is rugged enough to resist damage or distortion under the conditions imposed by handling during the refueling sequence. These are the only conditions, which affect the incore instrumentation support structure.

3.2.2.3 Design Loading Conditions

The design loading conditions that provide the basis for the design of the reactor internals are:

1. Fuel assembly weight.
2. Fuel assembly spring forces.
3. Internals weight.
4. Control rod trip (equivalent static load).
5. Differential pressure.
6. Spring preloads.
7. Coolant flow forces (static).
8. Temperature gradients.
9. Differences in thermal expansion.
    a. Due to temperature differences.
    b. Due to expansion of different materials.
10. Interference between components.
11. Vibration (mechanically or hydraulically induced).
12. One or more loops out of service.
13. Operational transients.
14. Pump overspeed.
15. Seismic loads (operating basis earthquake and safe shutdown earthquake).
16. Blowdown forces (due to cold or hot leg break).

The main objective of the design analysis is to satisfy allowable stress limits, to assure an adequate design margin, and to establish deformation limits, which are concerned primarily with

the functioning of the components. The stress limits are established not only to assure that peak stresses will not reach unacceptable values, but also limit the amplitude of the oscillatory stress component in consideration of fatigue characteristics of the materials. Both low and high cycle fatigue stresses are considered when the allowable amplitude of oscillation is established. Dynamic analysis on the reactor internals are provided in Section 14.3.3.

As part of the evaluation of design loading conditions, extensive testing and inspections are performed from the initial selection of raw materials up to and including component installation and plant operation. Among these tests and inspections are those performed during component fabrication, plant construction, startup and checkout, and during plant operation.

3.2.2.4 Design Loading Categories

The combination of design loadings fit into either the normal, upset, emergency or faulted conditions as defined in the ASME Code, Section III.

Loads and deflections imposed on components due to shock and vibration are determined analytically and experimentally in both scaled models and operating reactors. The cyclic stresses due to these dynamic loads and deflections are combined with the stresses imposed by loads from component weights, hydraulic forces and thermal gradients for the determination of the total stresses of the internals. The reactor internals are designed to withstand stresses originating from various operating conditions. The scope of the stress analysis problem is very large requiring many different techniques and methods, both static and dynamic. The analysis performed depends on the mode of operation under consideration.

Allowable Deflections

For normal operating conditions, downward vertical deflection of the lower core support plate is negligible.

For the loss of coolant accident plus the safe shutdown earthquake condition, the deflection criteria of critical internal structures are the limiting values given in Table 3.2-1. The corresponding no loss of function limits are included in Table 3.2-1 for comparison purposes with the allowed criteria.

The criteria for the core drop accident is based upon analyses which have to determine the total downward displacement of the internal structures following a hypothesized core drop resulting from loss of the normal core barrel supports. The initial clearance between the secondary core support structures and the reactor vessel lower head in the hot condition is approximately one half inch. An additional displacement of approximately 3/4 inch would occur due to strain of the energy absorbing devices of the secondary core support; thus the total drop distance is about 1-

1/4 inches which is insufficient to permit the tips of the rod cluster control assembly to come out of the guide thimble in the fuel assemblies.

Specifically, the secondary core support is a device which will never be used, except during a hypothetical accident of the core support (core barrel, barrel flange, etc.). There are 4 supports in each reactor. This device limits the fall of the core and absorbs much of the energy of the fall which otherwise would be imparted to the vessel. The energy of the fall is calculated assuming a complete and instantaneous failure of the primary core support and is absorbed during the plastic deformation of the controlled volume of stainless steel, loaded in tension. The maximum deformation of this austenitic stainless piece is limited to approximately 23 percent, after which a positive stop is provided to ensure support.

3.2.2.5 Design Criteria Basis

The basis for the design stress and deflection criteria is identified below:

Allowable Stresses

For normal operating conditions Section III of the ASME Code is used as a basis for evaluating acceptability of calculated stresses. Both static and alternating stress intensities are considered. It should be noted that the allowable stresses in Section III of the ASME Code are based on unirradiated material properties. In view of the fact that irradiation increases the strength of the Type 304 stainless steel used for the internals, although decreasing its elongation, it is considered that use of the allowable stresses in Section III is appropriate and conservative for irradiated internal structures.

3.2.2.6 Reactor Internals Vibration Considerations

The vibration characteristics and behavior due to flow induced excitation are very complex and not readily ascertained by analytical means alone. Reactor components are excited by the flowing coolant, which causes oscillatory pressures on the surfaces. The integration of these pressures over the applied area should provide the forcing functions to be used in the dynamic analysis of the structures. In view of the complexity of the geometries and the random character of the pressure oscillations, a closed form solution of the vibratory problem by integration of the differential equation of motion is not always practical and realistic. The determination of the forcing functions as a direct correlation of pressure oscillations can not be practically performed independently of the dynamic characteristics of the structure. The main objective is to establish the characteristics of the forcing functions that essentially determine the response of the structures. By studying the dynamic properties of the structure from previous analytical and

experimental work, the characteristics of the forcing function can be deduced. These studies indicate that the most important forcing functions are flow turbulence and pump-related excitation. The relevance of such excitations depends on many factor such as type and location of component and flow conditions. The effects of these forcing functions have been studied from test runs on components, models and prototype plants.

The Indian Point Unit 2 plant has been established as the prototype for a 4-loop plant internals verification program. The vibration program performed at Indian Point Unit 2 during hot functional testing is presented in Reference (12).

The Donald C. Cook Unit 2 internals design is similar to that of Indian Point Unit 2; the only significant differences are the structural ranges in the internals resulting from the design change from the 15 x 15 to the 17 x 17 fuel assembly, which affect the guide tube and control drive line. The fuel assembly itself is relatively unchanged in mass and spring rate, and thus no significant deviation is expected from the 15 x 15 fuel assembly vibration characteristics. The 17 x 17 guide tubes are stronger and more rigid, hence flow induced vibration levels are lower. It was verified during the Trojan Unit 1 hot functional testing that this design change has no adverse effect on the internals vibratory response. The Trojan Unit 1 program results are presented in Reference (13).

3.2.3 Reactivity Control System

3.2.3.1 Design Bases

Bases for temperature, stress on structural members, and material compatibility are imposed on the design of the reactivity control components.

3.2.3.1.1 Design Stresses

The reactivity control system is designed to withstand stresses originating from various operating conditions.

1. Allowable Stresses

   For normal operating conditions Section III of the ASME Code is used. All pressure boundary components are analyzed as Class I components under Article NB-3000.

2. Dynamic Analysis

The cyclic stresses due to dynamic loads and deflections are combined with the stresses imposed by loads from component weights, hydraulic forces and thermal gradients for the determination of the total stresses of the reactivity control system.

3.2.3.1.2 Material Compatibility

Materials are selected for compatibility in a PWR environment, for adequate mechanical properties at room and operating temperature, for resistance to adverse property changes in a radioactive environment, and for compatibility with interfacing components.

3.2.3.1.3 Reactivity Control Components

The reactivity control components are subdivided into two categories:

1. Permanent devices used to control or monitor the core.
2. Temporary devices used to control or monitor the core.

The permanent type components are the full-length rod cluster control assemblies, control rod drive mechanisms, neutron source assemblies, and thimble plug assemblies. Although the thimble plug assembly does not directly contribute to the reactivity control of the reactor, it is presented as a reactivity control system component in this document because it may be present to restrict bypass flow through those thimbles not occupied by absorber, source or burnable absorber rods.

The temporary component is the absorber assembly. The design bases for each of the mentioned components are in the following paragraphs.

Absorber Rods

The following are considered design conditions under Article NB-3000 of the ASME Code, Section III.

1. The external pressure equal to the reactor coolant system operating pressure.
2. The wear allowance equivalent to 1,000 reactor trips.
3. Bending of the rod due to a misalignment in the guide tube.
4. Forces imposed on the rods during rod drop.
5. Loads caused by accelerations imposed by the control rod drive mechanism.
6. Radiation exposure for maximum core life.

The control rod, which is cold, rolled Type 304 stainless steel is the only non-code material used in the control rod assembly. The stress intensity limit Sm for this material is defined at 2/3 of the 0.2 percent offset yield stress.

The absorber material temperature shall not exceed its melting temperature (1454^{o}F for Ag-In-Cd absorber material) (Reference 14)*.

* The melting point is determined by the nominal material melting point minus uncertainty.

Burnable Absorber Rods

The burnable absorber rod clad is designed as a Class I component under Article NB-3000 of the ASME Code, Section III, 1973 for Conditions I and II. For abnormal loads during Conditions III and IV code stresses are not considered limiting. Failures of the burnable absorber rods during these conditions must not interfere with reactor shutdown or cooling of the fuel rods.

The burnable absorber material is non-structural. The structural elements of the burnable absorber rod are designed to maintain the absorber geometry even if the absorber material is fractured. The standard burnable absorber material is borosilicate glass and is designed so that the absorber material is below its softening temperature (1220°F for 12.5 w/o and 1040°F for 18 w/o B_2O_3 Pyrex rods**). In addition, the structural elements are designed to prevent excessive slumping.

The Westinghouse designed wet annular burnable absorber (WABA) may be used in reload cores. The WABA material is B4C contained in an alumina matrix. Thermalphysical and gas release properties of AL2O3-B4C are described in References 28 and 29. Wet annular burnable absorber rods are designed so that the absorber temperature does not exceed 1200°□F during normal operation or an overpower transient. The 1200°□F maximum temperature Helium gas release in a WABA rod will not exceed 30 percent (Reference 29).

Neutron Source Rods

The neutron source rods are designed to withstand the following:

1. The external pressure equal to the reactor coolant system operating pressure.
2. An internal pressure equal to the pressure generated by released gases over the source rod life.

Thimble Plug Assembly

The thimble plug assemblies satisfy the following:

1. Accommodate the differential thermal expansion between the fuel assembly and the core internals.
2. Maintain positive contact with the fuel assembly and the core internals.
3. Be inserted into or withdrawn from the fuel assembly by a force not exceeding that specified in vendor's specification.

3.2.3.1.4 Control Rod Drive Mechanisms

The control rod drive mechanisms (CRDMs) pressure housings are Class I components designed to meet the stress requirements for normal operating conditions of Section III of the ASME

Code. Both static and alternating stress intensities are considered. The stresses originating from the required design transients are included in the analysis.

A dynamic seismic analysis is required on the CRDMs when a seismic disturbance has been postulated to confirm the ability of the pressure housing to meet ASME Code, Section III allowable stresses and to confirm its ability to trip when subjected to the seismic disturbance.

Full Length Control Rod Drive Mechanism Operational Requirements

The basic operational requirements for the full length CRDM's are:

1. 5/8 inch step.
2. 144.024 inch travel.
3. 360 pound maximum load.
4. Step in or out at 45 inches/minute (72 steps/minute).
5. Electrical power interruption shall initiate release of drive rod assembly.
6. Trip delay time of less than 150 milliseconds - Free fall of drive rod assembly shall begin less than 150 milliseconds after power interruption no matter what holding or stepping action is being executed with any load and coolant temperature of 100°F to 550°F.
7. 40 year design life with normal refurbishment.

3.2.3.2 Design Description

Reactivity control is provided by neutron absorbing rods and a soluble chemical neutron absorber (boric acid). The boric acid concentration is varied to control long term reactivity changes such as:

1. Fuel depletion and fission product buildup.
2. Cold to hot, zero power reactivity change.
3. Reactivity change produced by intermediate term fission products such as xenon and samarium.
4. Burnable poison depletion.

The rod cluster control assemblies provide reactivity control for:

1. Shutdown.
2. Reactivity changes due to coolant temperature changes in the power range.
3. Reactivity changes associated with the power coefficient of reactivity.
4. Reactivity changes due to void formation.

The first fuel cycle contains more excess reactivity than subsequent cycles due to the loading of all fresh (unburned) fuel. If soluble boron were the sole means of control, the moderator temperature coefficient would be positive. It is desirable to have a negative moderator temperature coefficient throughout the entire cycle in order to reduce possible deleterious effects caused by a positive coefficient during loss of coolant or loss of flow accidents. This is accomplished by installation of burnable poison assemblies.

The neutron source assemblies provide a means of monitoring the core during periods of low neutron activity.

The most effective reactivity control components are the full-length rod cluster control assemblies and their corresponding CRDMs. Figure 3.2-11 identifies the full-length rod cluster control and CRDM assembly, in addition to the arrangement of these components in the reactor relative to the interfacing fuel assembly and guide tubes. In the following paragraphs, each reactivity control component is described in detail except for the IFBA rods which are discussed in Section 3.3.2.5.3.

The guidance system for the full-length control rod cluster is provided by the guide tube as shown in Figure 3.2-11. The guide tube provides two regimes of guidance: 1) In the lower section a continuous guidance system provides support immediately above the core. This system protects the rod against excessive deformation and wear due to hydraulic loading. 2) The region above the continuous section provides support and guidance at uniformly spaced intervals.

The envelope of support is determined by the pattern of the control rod cluster as shown in Figure 3.2-12. The guide tube assures alignment and support of the control rods, spider body, and drive rod while maintaining trip times at or below required limits.

3.2.3.2.1 Reactivity Control Components

Full Length Rod Cluster Control Assembly

The full length rod cluster control assemblies are divided into two categories: control and shutdown. The control groups compensate for reactivity changes due to variations in operating conditions of the reactor, i.e., power and temperature variations. Two nuclear design criteria

have been employed for selection of the control group. First, the total reactivity worth must be adequate to meet the nuclear requirements of the reactor. Second, in view of the fact that these rods may be partially inserted at power operation, the total power peaking factor should be low enough to ensure that the power capability is met. The control and shutdown group provides adequate shutdown margin which is defined as the amount by which the core would be subcritical at hot shutdown if all rod cluster control assemblies are tripped assuming that the highest worth assembly remains fully withdrawn and assuming no changes in xenon or boron concentration.

A rod cluster control assembly comprises a group of individual neutron absorber rods fastened at the top end to a common spider assembly, as illustrated in Figure 3.2-12.

The absorber material used in the control rods is silver-indium-cadmium alloy, which is essentially "black" to thermal neutrons and has sufficient additional resonance absorption to significantly increase its worth. The alloy is in the form of extruded rods, which are sealed in cold worked stainless steel tubes to prevent the rods from coming in direct contact with the coolant (Figure 3.2-13). Sufficient diametral end clearance is provided to accommodate relative thermal expansions. The bottom plugs are made bullet-nosed to reduce the hydraulic drag during reactor trip and to guide smoothly into the dashpot section of the fuel assembly guide thimbles.

The material used in the absorber rod end plugs is Type 308 stainless steel. The design stresses used for the Type 308 material are the same as those defined in the ASME Code, Section III, for Type 304 stainless steel. At room temperature the yield and ultimate stresses per ASTM-580 are exactly the same for the two alloys. In view of the similarity of the alloy composition, the temperature dependence of strength for the two materials is also assumed to be the same.

The allowable stresses used as a function of temperature are listed in Table 1-1.2 of Section III of the ASME Code. The fatigue strength for the Type 308 material is based on the S-N curve for austenitic stainless steels in Figure 1-9.2 of Section III.

The spider assembly is in the form of a central hub with radial vanes containing cylindrical fingers from which the absorber rods are suspended. Handling detents and detents for connection to the drive rod assembly are machined into the upper end of the hub. A coil spring inside the spider body absorbs the impact energy at the end of a trip insertion. The radial vanes are joined to the hub by tack weld and braze and the fingers are joined to the vanes by brazing. A centerpost, which holds the spring and its retainer, is threaded into the hub within the skirt and welded to prevent loosening in service. All components of the spider assembly are made from Types 304 and 308 stainless steel except for the retainer which is of 17-4 pH material and the springs which are Inconel-718 alloy.

The absorber rods are fastened securely to the spider to assure trouble free service. The rods are first threaded into the spider fingers and then pinned to maintain joint tightness, after which the pins are welded in place. The end plug below the pin position is designed with a reduced section to permit flexing of the rods to correct for small operating or assembly misalignments.

The overall length is such that when the assembly is withdrawn through its full travel the tips of the absorber rods remain engaged in the guide thimbles so that alignment between rods and thimbles is always maintained. Since the rods are long and slender, they are relatively free to conform to any small misalignments with the guide thimble.

Part Length Rod Cluster Control Assembly

Part Length Control Rods are not installed in Unit 2 of the Donald C. Cook Nuclear Plant for the following reasons:

a. No credit is taken for their presence in the safety analysis performed by the vendor. Therefore, the decision not to mount them does not constitute a safety issue,

b. The reactor's Operating License and Technical Specifications preempt their use,

c. Unit 1 of the Donald C. Cook Nuclear Plant has successfully load followed and controlled artificially created large xenon oscillations without the use of these rods, and

d. The storage of these rods outside the reactor vessel will prevent their irradiation and subsequent radioactivity.

Burnable Absorber Assembly

Each burnable absorber assembly consists of borosilicate or wet annular burnable absorber rods attached to a hold down assembly. Borosilicate glass, wet annular, and integral fuel burnable absorbers may be used in any combination as supported on a cycle- by -cycle basis by core design and accident analysis.

The standard absorber rods, (Figure 3.2-15), have consisted of borosilicate glass tubes contained within Type 304 stainless steel tubular cladding which is plugged and seal welded at the ends to encapsulate the glass. The glass is also supported along the length of its inside diameter by a thin wall tubular inner liner. The top end of the liner is open to permit the diffused helium to pass into the void volume and the liner overhangs the glass. The liner has an outward flange at the bottom end to maintain the position of the liner with the glass. A typical borosilicate burnable absorber rod is shown in longitudinal and transverse cross sections in Figure 3.2-16. The absorber rods have also consisted of Al_2O_3 - B_4C pellets encapsulated with zircaloy.

Wet annular burnable absorber rods consist of annular pellets of alumina-boron carbide (AL_2O_3-B_4C) burnable absorber material contained within two concentric Zircaloy tubes. These Zircaloy tubes which form the inner and the outer clad for the WABA rod are plugged, pressurized with helium, and seal-welded at each end to encapsulate the annular stack of absorber material. The absorber stack length (Figure 3.2-15B) is positioned axially within the WABA rods by the use of Zircaloy bottom-end spacers.

An annular plenum is provided within the rod to accommodate the helium gas released from the absorber material as it depletes during irradiation. The reactor coolant flows inside the inner tube and outside the outer tube of the annular rod. A Typical WABA rod is shown in longitude and cross-section in figure 3.2-16B. Additional design details are given in Section 3.0 of reference 29.

The absorber rods in each fuel assembly are grouped and attached together at the top end of the rods to a hold down assembly by a flat, perforated retaining plate which fits within the fuel assembly top nozzle and rests on the adaptor plate. The retaining plate (and the poison rods) is held down and restrained against vertical motion through a spring pack, which is attached to the plate and is compressed by the upper core plate when the reactor upper internals assembly is lowered into the reactor. This arrangement ensures that the absorber rods cannot be ejected from the core by flow forces. Each rod is permanently attached to the base plate by a nut, which is lock welded into place.

Neutron Source Assembly

The purpose of the neutron source assembly is to provide base neutron level to ensure that the detectors are operational and responding to core multiplication neutrons. Since there is very little neutron activity during loading, refueling, shutdown and approach to criticality, a neutron source is placed in the reactor during approach to criticality to provide a minimum neutron count of at least 2 counts per second on the source range detectors attributable to core neutrons. The detectors, called source range detectors, are used primarily when the core is subcritical and during special subcritical modes of operations. When count rate decreases below 2 counts per second due to neutron source decay, the detectors may provide indication through the use of the scaler-timer in accordance with appropriate procedural control.

The source assembly also permits detection of changes in the core multiplication factor during core loading, refueling and approach to criticality. This can be done since the multiplication factor is related to an inverse function of the detector count rate. Therefore, a change in the multiplication factor can be detected during addition of fuel assemblies while loading the core, a change in control rod positions and changes in boron concentration.

Both primary and secondary neutron source rods can be used. The primary source rod, containing a radioactive material, spontaneously emits neutrons during initial core loading and the associated reactor startup. After the primary source rod decays beyond the desired neutron flux level, neutrons are then supplied by the secondary source rod. The secondary source rod contains a stable material, which must be activated by neutron bombardment during reactor operation. The activation results in the subsequent release of neutrons. This becomes a source of neutrons during periods of low neutron flux, such as during refueling and the subsequent startups.

The initial reactor core employed four source assemblies; two primary source assemblies and two secondary source assemblies. Each primary source assembly contains one primary source rod and between zero and twenty-three burnable poison rods. Each secondary source assembly contains a symmetrical grouping of four secondary source rods and between zero and twenty burnable poison rods. Locations not filled with a source or burnable poison rod contain a thimble plug. Conceptual source assemblies are shown in Figures 3.2-17 and 3.2-18.

Neutron source assemblies are employed at diametrically opposite sides of the core. The assemblies are inserted into the rod cluster control guide thimbles in fuel assemblies at selected unrodded locations.

The primary and secondary source rods both utilize the same cladding material as the absorber rods. The secondary source rods contain Sb-Be pellets stacked to a height of approximately 88 inches. The primary source rods contain capsules of Californium (Pu-Be possible alternate) source material and alumina spacer rods to position the source material within the cladding. The rods in each assembly are permanently fastened at the top end to a holddown assembly, which is identical to that of the burnable poison assemblies.

The other structural members are constructed of Type 304 stainless steel except for the springs. The springs exposed to the reactor coolant are constructed of Inconel-718.

Thimble Plug Assembly

Thimble plug assemblies may be used to limit bypass flow through the rod cluster control guide thimbles in fuel assemblies, which do not contain either control rods, source rods, or burnable poison rods.

The thimble plug assemblies as shown in Figure 3.2-19 consist of a flat base plate with short rods suspended from the bottom surface and a spring pack assembly. The twenty-four short rods, called thimble plugs, project into the upper ends of the guide thimbles to reduce the bypass flow. Each thimble plug is permanently attached to the base plate by a nut, which is locked to the

threaded end of the plug by a small lock bar welded to the nut. Similar short rods are also used on the source assemblies and burnable poison assemblies to plug the ends of all vacant fuel assembly guide thimbles. At installation in the core, the thimble plug assemblies interface with both the upper core plate and with the fuel assembly top nozzles by resting on the adaptor plate. The spring pack is compressed by the upper core plate when the upper internals assembly is lowered into place.

All components in the thimble plug assembly, except for the springs, are constructed from Type 304 stainless steel. The springs are constructed of Inconel-718.

3.2.3.2.2 Control Rod Drive Mechanism

All parts exposed to reactor coolant are fabricated of metals, which resist the corrosive action of the primary coolant. Three types of metals are used exclusively: stainless steels, nickel-chrome-iron alloy and cobalt based alloys. In the case of stainless steels, only austenitic and martensitic stainless steels are used, the martensitic stainless steels for pressure boundary components are not used in the heat transfer conditions which cause susceptibility to stress corrosion cracking or accelerated corrosion in the Westinghouse PWR chemistry. These martensitic stainless steels are procured in accordance with ASME Code Case 1337 wherein the minimum tempering temperature is 1125^{o}F.

Wherever magnetic flux is carried by parts exposed to the main coolant, 400 series stainless steel is used. Cobalt based alloys are used for the pins and latch tips. Nickel-chrome-iron alloy is used for the springs of full length latch assemblies and Type 304 stainless steel is used for all pressure containing parts.

Hard chrome plating provides wear surfaces on the sliding parts and prevents galling between mating parts.

Full Length Control Rod Drive Mechanism

Control rod drive mechanisms are located on the dome of the reactor vessel. They are coupled to rod control clusters, which have absorber material over the entire length of the control rods and derive their name from this feature. The full-length control rod drive mechanism is shown in Figure 3.2-20 and schematically in Figure 3.2-21.

The primary function of the full-length control rod drive mechanism is to insert or withdraw rod cluster control assemblies within the core to control average core temperature and to shutdown the reactor.

The full-length control rod drive mechanism is a magnetically operated jack. A magnetic jack is an arrangement of three electromagnets which are energized in a controlled sequence by a power

cycler to insert or withdraw rod cluster control assemblies in the reactor core in discrete steps. Rapid insertion of the rod cluster control assemblies occurs when electrical power is interrupted.

The control rod drive mechanism consists of four separate subassemblies. They are the pressure vessel, coil stack assembly, latch assembly and the drive rod assembly.

1. The pressure vessel includes a latch housing and a rod travel housing which are connected by a threaded, seal welded, maintenance joint which facilitates replacement of the latch assembly. The closure at the top of the rod travel housing is a threaded plug with an omega seal weld for pressure integrity. This closure contains a threaded plug used for venting.

   The latch housing is the lower portion of the vessel and contains the latch assembly. The rod travel housing is the upper portion of the vessel and provides space for the drive rod during its upward movement as the control rods are withdrawn from the core.

2. The coil stack assembly includes the coil housings, an electrical conduit and connector, and three operating coils: 1) the stationary gripper coil, 2) the moveable gripper coil and 3) the lift coil.

   The coil stack assembly is a separate unit, which is installed on the drive mechanism by sliding it over the outside of the latch housing. It rests on the base of the latch housing without mechanical attachment.

   Energizing the operating coils causes movement of the pole pieces and latches in the latch assembly.

3. The latch assembly includes the guide tube, stationary pole pieces, moveable pole pieces, and two sets of latches: 1) the moveable gripper latches and 2) the stationary gripper latches.

   The latches engage grooves in the drive rod assembly. The moveable gripper latches are moved up or down in 5/8 inch steps by the lift pole to raise or lower the drive rod. The stationary gripper latches hold the drive rod assembly while the moveable gripper latches are repositioned for the next 5/8 inch step.

4. The drive rod assembly includes a flexible coupling, a drive rod, a disconnect button, a disconnect rod, a locking button and locking springs.

   The drive rod has 5/8 inch grooves which receive the latches during holding or moving of the drive rod. The flexible coupling is attached to the drive rod and provides the means for coupling to the rod cluster control assembly.

   The disconnect button, disconnect rod and locking button provide positive locking of the coupling to the rod cluster control assembly and permits remote disconnection of the drive rod.

The control rod drive mechanism is a trip design. Tripping can occur during any part of the power cycler sequencing if electrical power to the coils is interrupted.

The control rod drive mechanism is threaded and seal welded to an adaptor on top of the reactor vessel and is coupled to the rod cluster control assembly directly below.

The mechanism is capable of raising or lowering a 360 pound load, (which includes the drive rod weight) at a rate of 45 inches/minute. Withdrawal of the rod cluster control assembly is accomplished by magnetic forces while insertion is by gravity.

The mechanism internals are designed to operate in 650°F reactor coolant. The pressure vessel is designed to contain reactor coolant at 650°F and 2500 psia. The three operating coils are designed to operate at 392°F with forced air cooling required to maintain that temperature.

The full length control rod drive mechanism shown schematically in Figure 3.2-21 withdraws and inserts a rod cluster control assembly as shaped electrical pulses are received by the operating coils. An ON or OFF sequence, repeated by silicon controlled rectifiers in the power programmer, causes either withdrawal or insertion of the control rod.

During plant operation the stationary gripper coil of the drive mechanism holds the rod cluster control assembly in a static position until a stepping sequence is initiated at which time the moveable gripper coil and lift coil is energized sequentially.

Rod Cluster Control Assembly Withdrawal

The rod cluster control assembly is withdrawn by repetition of the following sequence of events (refer to Figure 3.2-21):

1. Movable Gripper Coil (B) - ON

   The latch-locking plunger raises and swings the movable gripper latches into the drive rod assembly groove. A nominal 0.047 inch axial clearance exists between the latch teeth and the drive rod.

2. Stationary Gripper Coil (A) - OFF

   The force of gravity, acting upon the drive rod assembly and attached control rod, causes the stationary gripper latches and plunger to move downward 0.047 inch until the load of the drive rod assembly and attached control rod is transferred to the movable gripper latches. The plunger continues to move downward and swings the stationary gripper latches out of the drive rod assembly groove.

3. Lift Coil (C) - ON

   The 5/8 inch gap between the movable gripper pole and the lift pole closes and the drive rod assembly raises one step length (5/8 inch).

4. Stationary Gripper Coil (A) - ON

   The plunger raises and closes the gap below the stationary gripper pole. The three links, pinned to the plunger, swing and the stationary gripper latches into a drive rod assembly groove. The latches contact the drive rod assembly and lift it (and the attached control rod) 0.047 inch. The 0.047 inch vertical drive rod assembly movement transfers the drive rod assembly load from the movable gripper latches to the stationary gripper latches.

5. Movable Gripper Coil (B) - OFF

   The latch-locking plunger separates from the movable gripper pole under the force of a spring and gravity. Three links, pinned to the plunger, swing the three movable gripper latches out of the drive rod assembly groove.

6. Lift Coil (C) - OFF

   The gap between the movable gripper pole and lift pole opens. The movable gripper latches drop 5/8 inch to a position adjacent to a drive rod assembly groove.

7. Repeat Step 1

The sequence described above (Items 1 through 6) is termed as one step or one cycle. The rod cluster control assembly moves 5/8 inch for each step or cycle. The sequence is repeated at a rate of up to 72 steps per minute and the drive rod assembly (which has 5/8 inch groove pitch) is raised 72 grooves per minute. The rod cluster control assembly is thus withdrawn at a rate up to 45 inches per minute.

Rod Cluster Control Assembly Insertion

The sequence for rod cluster control assembly insertion is similar to that for control rod withdrawal, except the timing of lift coil (C) ON and OFF is changed to permit lowering the control assembly.

1. Lift Coil (C) - ON

   The 5/8 inch gap between the movable gripper and lift pole closes. The movable gripper latches are raised to a position adjacent to a drive rod assembly groove.

2. Movable Gripper Coil (B) - ON

   The latch locking plunger raises and swings the movable gripper latches into a drive rod assembly groove. A 0.047 inch axial clearance exists between the latch teeth and the drive rod assembly.

3. Stationary Gripper Coil (A) - OFF

   The force of gravity, acting upon the drive rod assembly and attached rod cluster control assembly, causes the stationary gripper latches and plunger to move downward 0.047 inch until the load of the drive rod assembly and attached rod cluster control assembly is transferred to the movable gripper latches. The plunger continues to move downward and swings the stationary gripper latches out of the drive rod assembly groove.

4. Lift Coil (C) - OFF

   The force of gravity and spring force separates the movable gripper pole from the lift pole and the drive rod assembly and attached rod cluster control drop down 5/8 inch.

5. Stationary Gripper (A) - ON

   The plunger raises and closes the gap below the stationary gripper pole. The three links, pinned to the plunger, swing the three stationary gripper latches into a drive rod assembly groove. The latches contact the drive rod assembly and lift it (and

the attached control rod) 0.047 inch. The 0.047 inch vertical drive rod assembly movement transfers the drive rod assembly load from the movable gripper latches to the stationary gripper latches.

6. Movable Gripper Coil (B) - OFF

   The latch-locking plunger separates from the movable gripper pole under the force of a spring and gravity. Three links, pinned to the plunger, swing the three movable gripper latches out of the drive rod assembly groove.

7. Repeat Step 1

   The sequence is repeated, as for rod cluster control assembly withdrawal, up to 72 times per minute which gives an insertion rate of 45 inches per minute.

Holding and Tripping of the Control Rods

During most of the plant operating time, the control rod drive mechanisms hold the rod cluster control assemblies withdrawn from the core in a static position. In the holding mode, only one coil, the stationary gripper coil (A), is energized on each mechanism. The drive rod assembly and attached rod cluster control assemblies hang suspended from the three latches.

If power to the stationary gripper coil is cut off, the combined weight of the drive rod assembly and the rod cluster control assembly plus the stationary gripper return spring is sufficient to move latches out of the drive rod assembly groove. The control rod falls by gravity into the core. The trip occurs as the magnetic field, holding the stationary gripper plunger half against the stationary gripper pole, collapses and the stationary gripper plunger half is forced down by the stationary gripper return spring and the weight acting upon the latches. After the rod cluster control assembly is released by the mechanism, it falls freely until the control rods enter the dashpot section of the thimble tubes in the fuel assembly.

3.2.3.3 Design Evaluation

3.2.3.3.1 Reactivity Control Components

The components are analyzed for loads corresponding to normal, upset, emergency and faulted conditions. The analysis performed depends on the mode of operation under consideration.

The scope of the analysis requires many different techniques and methods, both static and dynamic.

Some of the loads that are considered on each component where applicable are as follows:

1. Control rod trip (equivalent static load).
2. Differential pressure.
3. Spring preloads.
4. Coolant flow forces (static).
5. Temperature gradients.
6. Differences in thermal expansion.
    a. Due to temperature differences.
    b. Due to expansion of different materials.
7. Interference between components.
8. Vibration (mechanically or hydraulically induced).
9. Operational transients.
10. Pump overspeed.
11. Seismic loads (operating basis earthquake and safe shutdown earthquake).
12. Blowdown forces (due to cold or hot leg break).
13. Material swelling and gas generation pressure.

The main objective of the analysis is to satisfy allowable stress limits, to assure an adequate design margin, and to establish deformation limits, which are concerned primarily with the functioning of the components. The stress limits are established not only to assure that peak stresses will not reach unacceptable values, but also limit the amplitude of the oscillatory stress component in consideration of fatigue characteristics of the materials. Standard methods of strength of materials are used to establish the stresses and deflections of these components. The dynamic behavior of the reactivity control components has been studied using experimental test data and experience from operating reactors.

The design of incore component rods provides a sufficient cold void volume within the burnable absorber and source rods to limit the internal pressures to a value, which satisfies the criteria in Section 3.2.3.1. The void volume for the helium in the burnable absorber rods is obtained through the use of absorber material in tubular form, which provides a central void along the length of the rods. Helium gas is not released by the neutron absorber rod material, thus the absorber rod only sustains an external pressure during operating conditions. The internal

pressure of source rods continues to increase from ambient until end of life. The stress analysis of reactivity component rods assumes 100 percent gas release to the rod void volume.

Based on available data for properties of the borosilicate glass and on nuclear and thermal calculations for the burnable absorber rods, gross swelling or cracking of the glass tubing is not expected during operation. Some minor creep of the glass at the hot spot on the inner surface of the tube could occur but would continue only until the glass came in contact with the inner liner. The wall thickness of the inner liner is sized to provide adequate support in the event of slumping and to collapse locally before rupture of the exterior cladding if unexpected large volume changes due to swelling or cracking should occur. The top of the inner liner is open to allow communication to the central void by the helium, which diffuses out of the glass.

Sufficient diametral and end clearances have been provided in the neutron absorber, burnable poison and source rods to accommodate the relative thermal expansions between the enclosed material and the surrounding clad and end plugs. There is no bending or warping induced in the rods although the clearance offered by the guide thimble would permit a postulated warpage to occur if there were no restraint on the rods. Bending, therefore, is not considered in the analysis of the rods. The radial and axial temperature profiles have been determined by considering gap conductance, thermal expansion and neutron and/or gamma heating of the contained material as well as gamma heating of the clad. The maximum neutron absorber material temperature was found to be less than 850°F, which occurs axially at only the highest flux region. The maximum borosilicate glass temperature was calculated to be about 1200°F and takes place following the initial rise to power. The glass temperature then decreases rapidly for the following reasons: 1) reduction in power generation due to B_{10} depletion; 2) better gap conductance as the helium produced diffuses to the gap; and 3) external gap reduction due to borosilicate glass creep. Rod, guide thimble and dashpot flow analysis performed indicates that the flow is sufficient to prevent coolant boiling and maintain clad temperatures at which the clad material has adequate strength to resist coolant operating pressures and rod internal pressures.

Coolant temperatures for thimbles at the bottom of the fuel assemblies range from approximately 530°F to 553°F. Mid-assembly temperatures reach a high of about 593°F while the maximum temperatures at the top of the assemblies are about 641°F.

Analysis on the full length rod cluster control spider indicates the spider is structurally adequate to withstand the various operating loads including the higher loads which occur during the drive mechanism stepping action and rod drop. Experimental verification of the spider structural capability has been completed.

The materials selected are considered to be the best available from the standpoint of resistance to irradiation damage and compatibility to the reactor environment. The materials selected partially dictate the reactor environment (e.g., $C1^-$ control in the coolant). The current design type reactivity controls have been in service for more than six years with no unanticipated degradation of construction materials.

With regard to the materials of construction exhibiting satisfactory resistance to adverse property changes in a radioactive environment, it should be noted that work on breeder reactors in current design, similar materials are being applied. At high fluences the austenitic materials increase in strength with a corresponding decreased ductility (as measured by tensile tests) but energy absorption (as measured by impact tests) remain quite high. Corrosion of the materials exposed to the coolant is quite low and proper control of $C1^-$ and O_2 in the coolant will prevent the occurrence of stress corrosion. All of the austenitic stainless steel base materials used are processed and fabricated to preclude sensitization. Although the control rod spiders are fabricated by furnace brazing, the procedure used requires that the pieces be rapidly cooled so that the time-at-temperature is minimized. The time that is spent by the control rod spiders in the sensitization range, 800 - 1500°F, during fabrication is controlled to preclude sensitization. The 17-4 pH parts are all aged at the highest standard aging temperature of 1100°F to avoid stress corrosion problems exhibited by aging at lower temperatures.

Based on the following considerations, it is judged that the potential for interference with rod cluster control movement due to unusual local corrosion phenomena of the Zircaloy guide thimbles is very low. Operational experience to date and limited PIE data on irradiated thimbles are in support of this conclusion.

1. Gap Considerations

   The minimum hot diametral gap in the reduced dashpot area of the thimble is smaller than the minimum hot diametral gap in the upper thimble area. Thus, the dashpot area constitutes the region of maximum interest relative to any possible effects of localized corrosion.

2. Intrinsic Corrosion

   Using conservative calculations of corrosion kinetics in the dashpot area of the thimble (T coolant = 600°F and t = 1500 calendar days) it was determined that approximately 0.44 mils of oxide would be found on the Zircaloy. Taking the Pilling-Bedworth ratio at 1.56, then:

$$\text{mils metal} = \frac{0.44 \text{ mils}}{1.56} = 0.28 \text{ mils}$$

   and the decrease in tube inside diameter is:

$$2 \times (0.44 - 0.28) = 0.32 \text{ mils or } 0.00032 \text{ inches.}$$

   This latter value is considered to be very small compared to the minimum hot gap and the risk of interference with rod movement due to inherent corrosion is considered negligibly low.

   Corrosion of the stainless steel control rod clad is also considered negligible relative to potential for annulus blockage.

3. Deformation Enhanced Corrosion and Hydriding

   Maximum deformation in the expanded area of the thimble is taken to be less than 60 percent. Studies of the effect of cold work on Zircaloy alloys under both steam and water conditions show no significant effects attributable to residual cold work on corrosion or hydriding behavior (References 15 and 16). Preliminary examinations of thimbles taken from the Point Beach reactor indicate essentially equivalent corrosion rates in both bulged and unbulged areas. Thus, it is judged appropriate to estimate maximum corrosion effects by utilization of normal

corrosion and hydriding models for the nominal metallurgical condition of the thimble.

4. Crevice Corrosion

   Under certain conditions, the Zircaloy alloys are susceptible to serious caustic assisted corrosion. Since LiOH is used for pH control in the primary coolant, the potential for such corrosion exists in the Westinghouse design. Studies show that caustic assisted attack can occur in crevices with low LiOH concentrations, but only under conditions of nucleate boiling (References 17 and 18). Other work where crud, $C1^{-}$, Fe^{++}, and F^{-} were tested under conditions with no heat transfer, indicated no specific attack in crevices although in 0.01 M LiF, a general overall attack of the Zircaloy was noted.

   Since the Westinghouse system is conservatively designed to preclude nucleate boiling in the annulus of the sleeve and thimble, and the overall Li^{+}, $C1^{-}$, F^{-}, etc., concentrations are controlled by the primary coolant specification, it is judged that crevice corrosion will not occur. Observations to date on irradiated thimbles support this expectation.

5. Effects of Surface Contamination

   The use of any materials containing compounds of elements, which are suspected to be detrimental, if permitted to contact a fuel assembly component is subjected to control by specification. Materials considered particularly detrimental to Zircaloy are not used in the bulging operation. After the bulging operation, the completed skeleton is subjected to an aqueous cleaning operation. Tooling development studies, tests made to determine localized thinning, hydriding orientation studies relating to effects of plastic deformation, and limited post irradiation examination studies of expanded joints indicate no cases of significant surface contamination. These tests have not been formally documented. Taking all of these factors into account, and also the fact that the as-received surface condition of the thimble tubing is controlled by purchase specification, it is judged that the risk of significant corrosion due to surface contamination is quite low.

Analysis of the full length rod cluster control assemblies show that if the drive mechanism housing ruptures the rod cluster control assembly will be ejected from the core by the pressure differential of the operating pressure and ambient pressure across the drive rod assembly. The ejection is also predicated on the failure of the drive mechanism to retain the drive rod/rod

cluster control assembly position. It should be pointed out that a drive mechanism housing rupture will cause the ejection of only one rod cluster control assembly with the other assemblies remaining in the core. Analysis also showed that a pressure drop in excess of 4000 psi must occur across a two-fingered vane to break the vane/spider body joint causing ejection of two neutron absorber rods from the core. Since the greatest pressure drop in the system is only 2250 psi, a pressure drop in excess of 4000 psi is incredible. Thus, the ejection of the neutron absorber rods is not possible.

Ejection of a burnable absorber or thimble plug assembly is conceivable based on the postulation that the hold down bar fails and that the base plate and burnable absorber rods are severely deformed. In the unlikely event that failure of the hold down bar occurs, the upward displacement of the burnable absorber assembly only permits the base plate to contact the upper core plate. Since this displacement is small, the major portion of the borosilicate glass tubing remains positioned within the core. In the case of the thimble plug assembly, the thimble plugs will partially remain in the fuel assembly guide thimbles thus maintaining a majority of the desired flow impedance. Further displacement or complete ejection would necessitate the square base plate and burnable absorber rods be forced, thus plastically deformed, to fit up through a smaller diameter hole. It is expected that this condition requires a substantially higher force or pressure drop than that of the hold down bar failure.

Experience with control rods, burnable absorber rods and source rods are discussed in Reference (4).

The mechanical design of the reactivity control components provides for the protection of the active elements to prevent the loss of control capability and functional failure of critical components. The components have been reviewed for potential failure and consequences of a functional failure of critical parts. The results of the review are summarized below.

Full Rod Cluster Control Assembly

1. The basic absorbing material is sealed from contact with the primary coolant and the fuel assembly and guidance surfaces by a high quality stainless steel clad. Potential loss of absorber mass or reduction in reactivity control material due to mechanical or chemical erosion or wear is therefore reliably prevented.
2. A breach of the cladding for any postulated reason does not result in serious consequences. The silver-indium-cadmium absorber material is relatively inert and would still remain remote from high coolant velocity regions. Rapid loss of material resulting in significant loss of reactivity control material would not occur.

3. The individually clad absorber rods are doubly secured to the retaining spider vane by a threaded joint and a welded lock pin. This joint has been qualified by functional testing and actual service in operating plants. It should also be noted that in several instances of control rod jamming caused by foreign particles, the individual rods at the site of the jam have borne the full capacity of the control rod drive mechanism and higher impact loads to dislodge the jam without failure. The conclusion to be drawn from this experience is that this joint is extremely insensitive to potential mechanical damage. A failure of the joint would result in the almost complete insertion of the individual rod into the core during normal operating conditions.

4. The spider finger braze joint by which the individual rods are fastened to the vanes has also experienced the service described above and been subjected to the same jam freeing procedures also without failure. A failure of this joint would also result in the almost complete insertion of the individual rod into the core during normal operating conditions.

5. The radial vanes are attached to the spider body, again by a welded and brazed joint. The joints are designed to a theoretical strength in excess of that of the components joined. It is a feature of the design that the guidance of the rod cluster control is accomplished by the inner fingers of these vanes. They are therefore the most susceptible to mechanical damage. Since these vanes carry two rods, failure of the vane-to-hub joint does not prevent the free insertion of the rod pair. Neither does such a failure interfere with the continuous free operation of the drive line.

   Failure of the vane-to-hub joint of a single rod vane could potentially result in failure of the separated vane and rod to insert. This could occur only at withdrawal elevations where the spider is above the continuous guidance section of the guide tube (in the upper internals). A rotation of the disconnected vane could cause it to hang on one of the guide cards in the intermediate guide tube. Such an occurrence would be evident from the failure of the rod cluster control to insert below a certain elevation but with free motion above this point.

   This possibility is considered extremely remote because the single rod vanes are subjected to only vertical loads and very light lateral reactions from the rods. The consequences of such a failure are not considered critical since only one drive line

of the reactivity control system would be involved. This condition is readily observed and can be corrected at shutdown.

6. The spider hub being of single unit cylindrical construction is very rugged and of extremely low potential for damage. It is difficult to postulate any condition to cause failure. Should some unforeseen event cause fracture of the hub above the vanes, the lower portion with the vanes and rods attached would insert by gravity into the core causing a reactivity decrease. The rod could then not be removed by the drive line. Fracture below the vanes cannot be postulated since all loads, including scram impact, are taken above the vane elevation.

7. The guide thimbles of the fuel assembly provide a clear channel for insertion of the rod cluster. Fuel rod failure due to postulated control rod contacts is not possible by providing this physical barrier between the fuel rod and the intended insertion channel. Distortion of the fuel rods by bending cannot apply sufficient force to damage or significantly distort the guide thimble. Fuel rod distortion by swelling, though precluded by design, would be terminated by fracture before contact with the guide thimble occurs. If such were not the case, it would be expected that a force reaction at the point of contact would cause a slight deflection of the guide thimble. The radius of curvature of the deflected shape for the guide thimbles would be sufficiently large to have a negligible influence on rod cluster control insertion.

Burnable Absorber Assemblies

The burnable absorber assemblies are static temporary reactivity control elements. The axial position is assured by the hold down assembly, which bears against the upper core plate. Their lateral position is maintained by the guide thimbles of the fuel assemblies.

The individual rods are shouldered against the underside of the retainer plate and securely fastened at the top by a threaded nut, which is then locked in place by a welded pin. The square dimension of the retainer plate is larger than the diameter of the flow holes through the core plate. Failure of the hold down bar or spring pack therefore does not result in ejection of the burnable absorber rods from the core.

The only incident that could potentially result in ejection of the burnable absorber rods is a multiple fracture of the retainer plate. This is not considered credible because of the light loads borne by this component. During normal operation the loads borne by the plate are distributed at the points of attachment. Even a multiple fracture of the retainer plate would result in jamming

of the plate segments against the upper core plate, again preventing ejection. Excessive reactivity increase due to burnable absorber ejection is therefore prevented.

Drive Rod Assemblies

All postulated failures of the full length drive rod assemblies either by fracture or uncoupling lead to a decrease in reactivity. If the drive rod assembly fractures at any elevation, that portion remaining coupled falls with, and is guided by the rod cluster control assembly. This always results in reactivity decrease for full-length control rods.

3.2.3.3.2 Control Rod Drive Mechanism

Material Selection

All pressure-containing materials comply with Section III of the ASME Code, and are fabricated from austenitic (Type 304) stainless steel or martensitic (Type 403) stainless steel.

Magnetic pole pieces are fabricated from Type 410 stainless steel. All non-magnetic parts, except pins and springs, are fabricated from Type 304 stainless steel. Haynes 25 is used to fabricate link pins. Springs are made from nickel-chrome-iron alloy. Latch arm tips are clad with Stellite-6 to provide improved wearability. Hard chrome plate and Stellite-6 are used selectively for bearing and wear surfaces.

At the start of the development program, a survey was made to determine whether a material better than Type 410 stainless steel was available for the magnetic pole pieces. Ideal material requirements are as follows:

1. High magnetic saturation value.
2. High permeability.
3. Low coercive force.
4. High resistivity.
5. High curie temperature.
6. Corrosion resistant.
7. High impact strength.
8. Non-oriented.
9. High machinability.
10. Low susceptibility to radiation damage.

After a comprehensive material trade-off study was made it was decided that the Type 410 stainless steel was satisfactory for this application.

The cast coil housings require a magnetic material. Both low-carbon cast steel and ductile iron have been successfully tested for this application. The choice, made on the basis of cost, indicates that ductile iron will be specified on the control rod drive mechanism. The finished housings are zinc plated or flame sprayed to provide corrosion resistance.

Coils are wound on bobbins of molded Dow Corning 302 material, with double glass-insulated copper wire. Coils are then vacuum impregnated with silicon varnish. A wrapping of mica sheet is secured to the coil outside diameter. The result is a well-insulated coil capable of sustained operation at 200 degrees centigrade.

The drive rod assembly utilizes a Type 410 stainless steel drive rod. The coupling is machined from Type 403 stainless steel. Other parts are Type 304 stainless steel with the exception of the springs which are nickel-chrome-iron alloy and the locking button which is Haynes 25.

Radiation Damage

As required by the equipment specification, the control rod drive mechanisms are designed to meet a radiation requirement of 10 Rads/hour. Materials have been selected to meet this requirement. The above radiation level which amounts to 1.753×10^6 Rads in twenty years will not limit control rod drive mechanism life. Control rod drive mechanisms at Yankee Rowe which have been in operation since 1960 have not experienced problems due to radiation.

Positioning Requirements

The full length mechanism has a step length of 5/8 inches which determines the positioning capabilities of the control rod drive mechanism. (Note: Positioning requirements are determined by reactor physics.)

Evaluation of Material's Adequacy

The ability of the pressure housing components to perform throughout the design lifetime as defined in the equipment specification is confirmed by the stress analysis report required by the ASME Code, Section III. Internal components subjected to wear will withstand a minimum of 3,000,000 steps without refurbishment as confirmed by life tests. Latch assembly inspection is recommended after 2.5×10^6 steps have been accumulated on a single control rod drive mechanism.

Results of Dimensional and Tolerance Analysis

With respect to the control rod drive mechanism system as a whole, critical clearances are present in the following areas:

1. Latch assembly (diametral clearances).
2. Latch arm-drive rod clearances.
3. Coil stack assembly-thermal clearances.
4. Coil fit in coil housing.

The following write-up defines clearances that are designed to provide reliable operation in the control rod drive mechanism in these four critical areas. These clearances have been proven by life tests and actual field performance at operating plants.

Latch Assembly - Thermal Clearances

The magnetic jack has several clearances where parts made of Type 410 stainless steel fit over parts made from Type 304 stainless steel. Differential thermal expansion is therefore important. Minimum clearances of these parts at 68°F is 0.011 inches. At the maximum design temperature of 650°F minimum clearance is 0.0045 inches and at the maximum expected operating temperatures of 550°F is 0.0057 inches.

Latch Arm - Drive Rod Clearances

The control rod drive mechanism incorporates a load transfer action. The movable or stationary gripper latch are not under load during engagement, as previously explained, due to load transfer action.

Figure 3.2-23 shows latch clearance variation with the drive rod as a result of minimum and maximum temperatures. Figure 3.2-24 shows clearance variations over the design temperature range.

Coil Stack Assembly - Thermal Clearances

The assembly clearance of the coil stack assembly over the latch housing was selected so that the assembly could be removed under all anticipated conditions of thermal expansion.

At 70°F the inside diameter of the coil stack is 7.308/7.298 inches. The outside diameter of the latch housing is 7.260/7.270 inches.

Thermal expansion of the mechanism due to operating temperature of the control rod drive mechanism result in minimum inside diameter of the coil stack being 7.310 inches at 222°F and the maximum latch housing diameter being 7.302 inches at 532°F.

Under the extreme tolerance conditions listed above it is necessary to allow time for a 70°F coil housing to heat during a replacement operation.

Four coil stack assemblies were removed from four hot control rod drive mechanisms mounted on 11.035 inch centers on a 550°F test loop, allowed to cool, and then placed without incident as a test to prove the preceding.

Coil Fit in Coil Housing

Control rod drive mechanism and coil housing clearances are selected so that coil heat up results in a close to tight fit. This is done to facilitate thermal transfer and coil cooling in a hot control rod drive mechanism.

3.2.3.4 Tests, Verification and Inspections

3.2.3.4.1 Reactivity Control Components

Test and inspections are performed on reactivity control components consistent with the Westinghouse Electric Company "Quality Management System", as summarized in Reference 11. This program is described in more detail in UFSAR Section 3.2.1.4.1.

To assure proper fitup with the fuel assembly, the rod cluster control, burnable absorber and source assemblies are installed in the fuel assembly without restriction or binding in the dry condition with a force not to exceed 15 pounds. Also a straightness of 0.01 in./ft. is required on the entire inserted length of each rod assembly.

The full-length rod cluster control assemblies are functionally tested, following core loading but prior to criticality to demonstrate reliable operation of the assemblies. Each assembly is operated (and tripped) one time at no flow/cold conditions and one time at full flow/hot conditions. In addition, selected assemblies, amounting to about 15 to 20 percent of the total assemblies are operated at no flow/operating temperature conditions and full flow/ambient conditions. Also the slowest rod and the fastest rod are tripped 10 times at no flow/ambient conditions and at full flow/operating temperature conditions. Thus each assembly is tested a minimum of 2 times or up to 14 times maximum to ensure the assemblies are properly functioning.

3.2.3.4.2 Control Rod Drive Mechanisms

Quality assurance procedures during production of control rod drive mechanisms include material selection, process control, mechanism component tests and inspections during production and hydrotests.

After all manufacturing procedures had been developed, several prototype control rod drive mechanisms and drive rod assemblies were life tested with the entire drive line under

environmental conditions of temperature, pressure and flow. All acceptance tests confirm the 3 x 10^6 step life capability of the control rod drive mechanism and drive rod assembly.

These tests include verification that the trip time achieved by the full length control rod drive mechanisms meet the design requirement of 2.7 seconds from the beginning of decay of stationary gripper coil voltage to dashpot entry. This trip time requirement will be confirmed for each control rod drive mechanism prior to initial reactor operation and at periodic intervals after initial reactor operation. In addition, a Technical Specification has been set to ensure that the trip time requirement is met.

It is expected that all control rod drive mechanisms will meet specified operating requirements for the duration of plant life with normal refurbishment. However, a Technical Specification pertaining to an inoperable rod cluster control assembly has been set.

If a rod cluster control assembly cannot be moved by its mechanism, adjustments in the boron concentration ensure that adequate shutdown margin would be achieved following a trip. Thus, inability to move one rod cluster control assembly can be tolerated. More than one inoperable rod cluster control assembly could be tolerated, but would impose additional demands on the plant operator. Therefore, the number of inoperable rod cluster control assemblies has been limited to one.

In order to demonstrate proper operation of the control rod drive mechanism and to ensure acceptable core power distributions during operation partial rod cluster control assembly movement checks are performed on the full length rod cluster control assemblies as described in the Technical Specifications. In addition, periodic drop tests of the full length rod cluster control assemblies are performed at each refueling shutdown to demonstrate continued ability to meet trip time requirements, to ensure core subcriticality after reactor trip, and to limit potential reactivity insertions from a hypothetical rod cluster control assembly ejection. During these tests the acceptable drop time of each assembly is not greater than 2.7 seconds, at full flow and operating temperature, from beginning of decay of stationary gripper coil voltage to dashpot entry.

To confirm the mechanical adequacy of the fuel assembly, the control rod drive mechanism, and full-length rod cluster control assembly, functional test programs have been conducted on a full-scale 12 foot control rod. The 12-foot prototype assembly was tested under simulated conditions of reactor temperature, pressure and flow for approximately 1000 hours. A correlation was developed to predict the amplitude of flow excited vibration of individual fuel rods and fuel assemblies. Inspection of the drive line components did not reveal significant fretting.

There are no significant differences between the prototype control rod drive mechanisms and the production units. Design materials, tolerances and fabrication techniques (Section 3.2.3.3.2) are the same.

Actual experience in many operating Westinghouse plants indicates excellent performance of control rod drive mechanisms.

All units are production tested prior to shipment to confirm ability of control rod drive mechanisms to meet design specification-operational requirements.

Each production magnetic jack control rod drive mechanism undergoes a production test as listed below:

Test	Acceptance Criteria
Cold (ambient) hydrostatic	ASME Code, Section III
Confirm step length and load (stationary gripper to movable gripper or movable gripper to stationary gripper)	Step Length Transfer 5/8 ±0.015 inches axial movement Load Transfer 0.047 inches nominal axial movement
Cold (ambient) performance Test at design load -	Operating speed 45 inches/min
5 full travel excursions	Trip Delay Free fall of drive rod to begin within 150 milliseconds

3.2.3.5 Instrumentation Applications

Instrumentation for determining reactor coolant average temperature (T_{avg}) is provided to create demand signals for moving groups of full length rod cluster control assemblies to provide load follow (determined as a function of turbine impulse pressure) during normal operation and to counteract operational transients. The hot and cold leg resistance temperature detectors (RTDs) in the reactor coolant bypass loops are described in Chapter 7. The location of the RTDs in each

loop is shown on the flow diagrams in Chapter 4. The Reactor Control System, which controls the reactor coolant average temperature by regulation of control rod bank position, is described in Chapter 7.

Rod position indication instrumentation is provided to sense the actual position of each control rod so that the actual position of the individual rod may be displayed to the operator. Signals are also supplied by this system as input to the rod deviation comparator. The rod position indication system is described in Chapter 7.

The reactor makeup control system whose functions are to permit adjustment of the reactor coolant boron concentration for reactivity control (as well as to maintain the desired operating fluid inventory in the volume control tank), consists of a group of instruments arranged to provide a manually preselected makeup composition that is borated or diluted as required to the charging pump suction header or the volume control tank. This system, as well as other systems including boron sampling provisions that are part of the Chemical and Volume Control System, are described in Chapter 9.

When the reactor is critical, the normal indication of reactivity status in the core is the position of the control bank in relation to reactor power (as indicated by the Reactor Coolant System loop ΔT) and coolant average temperature. These parameters are used to calculate insertion limits for the control banks to give warning to the operator of excessive rod insertion. Monitoring of the neutron flux for various phases of reactor power operation as well as of core loading, shutdown, startup, and refueling is by means of the Nuclear Instrumentation System. The monitoring functions and readout and indication characteristics for the following means of monitoring reactivity are included in the discussion on safety-related display instrumentation in Chapter 7:

1. Nuclear Instrumentation System.
2. Temperature Indicators.
    a. T average (measured).
    b. ΔT (measured).
    c. Auctioneered T average.
    d. T reference.
3. Demand Position of Rod Cluster Control Assembly Group.
4. Actual Rod Position Indicator.

3.2.4 References For Section 3.2

1. Christensen, J. A., Allio, R. J. and Biancheria, A., "Melting Point of Irradiated UO_2," WCAP-6065, February, 1965.
2. Eggleston, F. T., "Safety-Related Research and Development for Westinghouse Pressurized Water Reactors, Program Summaries," WCAP-8768, Latest Revision.
3. Eng, G. H., George, R. A., and Lee, Y. C., "Revised Clad Flattening Model," WCAP-8377, July, 1974 (Proprietary) and WCAP-8381, July, 1974 (Non-Proprietary).
4. Slagle, W. H., "Operational Experience with Westinghouse Cores," WCAP-8183, Revision 23, January 1996.
5. Miller, J.W., (Ed.), "Improved Analytical Model Used in Westinghouse Fuel Rod Design Computations," WCAP-8720, October, 1976 (Proprietary) and WCAP-8785, October, 1976 (Non-Proprietary).
6. Hellman, J. M., (Ed.), "Fuel Densification Experimental Results and Model for Reactor Application," WCAP-8218-P-A, March, 1975 (Proprietary) and WCAP-8219-A, March, 1975 (Non-Proprietary).
7. O'Donnel, W. J. and Langer, B. F., "Fatigue Design for Zircaloy Components," Nuclear Science and Engineering, 20, 1-12, 1964.
8. Skaritka, J. (Ed.), "Fuel Rod Bow Evaluation," WCAP-8691, Revision 1, July 1979.
9. Davidson, S. L. (Ed.), et. al., "Westinghouse Reload Safety Evaluation Methodology," WCAP-9272-P-A, July, 1985.
10. WCAP-10444-P-A, “Reference Core Report – VANTAGE 5 Fuel Assembly,” Appendix A, September 1985.
11. “Westinghouse Electric Company Quality Management System (QMS),” Revision 3 (or latest revision).
12. Singleton, N. R. et. al., "Four-Loop PWR Internals Assurance and Test Program," WCAP-7879, August, 1972.
13. Bloyd, C. M., Singleton, N. R. and Ciaramitaro, W., Verification of Neutron Pad and 17 x 17 Guide Tube Designs by Preoperational Tests on the Trojan 1 Power Plant," WCAP-8780, May, 1976.

14. Cohen, J., "Development and Properties of Silver Base Alloys as Control Rod Materials for Pressurized Water Reactors," WAPD-214, December, 1959.

15. Carver, M. D. and Antrim, C. W., "Zirconium Progress Report for the Period June 15 - September 15," 1956, USBM-U-210.

16. Burns, W. A. and Maffei, H. P., ASTM Special Technical Publication No. 368.

17. Anderson, W. K. and McGoff, M. J., "Corrosion of Zircaloy in Crevices Under Nucleate Boiling Conditions," KAPL-2203, 1962.

18. Berry, W. E., White, E. L. and Fink, F. W., "Zircaloy-4 Corrosion in Halide Solutions and at Crevices in High Temperature Water," BMI-1571, 1962.

19. Davidson, S. L., (Ed.) et. al., "Extended Burnup Evaluation of Westinghouse Fuel," WCAP-10125-P-A, December, 1985.

20. Weiner, R. A., et. al., "Improved Fuel Performance Models for Westinghouse Fuel Rod Design and Safety Evaluations," WCAP-11873-A, August, 1988.

21. USNRC Standard Review Plan 4.2, "Fuel System Design," NUREG-0800, Rev. 2, July 1981. Appendix A, "Evaluation of Fuel Assembly Structural Response to Externally Applied Forces."

22. WCAP-9401-P-A, "Verification Testing and Analyses of the 17X17 Optimized Fuel Assembly, August, 1981.

23. WCAP-10444-P-A, "Reference Core Report - VANTAGE 5 Fuel Assembly," September, 1985.

24. WCAP-8963-P-A, “Safety Analysis for the Revised Fuel Rod Internal Pressure Design Basis.”

25. Davidson, S. L., et.al. (Ed.), WCAP-12488-A, “Westinghouse Fuel Criterion Evaluation Process,” October, 1994.

26. WCAP-13589-A, “Assessment of Clad Flattening and Densification Power Spikes Factor Elimination in Westinghouse Nuclear Fuel,” March, 1995.

27. Letter from E. P. Rahe (Westinghouse) to L. E. Phillips (NRC) dated April 12, 1984, NS-EPR-2893, Subject: Fuel Handling Load Criteria (6g vs. 4g).

28. Beaumont, M.D., et al., “Properties of Fuel and Core Component Materials,” WCAP-9179, Revision 1 (Proprietary), and WCAP-9224 (Nonproprietary), July 1978.

29. Skaritka, J., et al., "Westinghouse Wet Annular Burnable Absorber Evaluation Report," WCAP-10021-P-A, Revison 1 Proprietary), October 1983.

30. Slagle, W. H. (Ed.) et. al., "Westinghouse Improved Performance Analysis and Design Model (PAD 4.0)," WCAP-15063-P-A, Revision 1, July 2000.

31. Davidson, S.L. and Nuhfer, D. L. (Eds.), "VANTAGE + Fuel Assembly Reference Core Report," WCAP-12610-P-A, April 1995.

32. Letter from J.D. Peralta (USNRC) to B.F. Maurer (Westinghouse), "Approval for Increase in Licensing Burnup Limit to 62,000 MWD/MTU (TAC No. MD1486)," May25, 2006.

33. Shah, H. H., "**Optimized ZIRLO™**," WCAP-12610-P-A & CENPD-404-P-A Addendum 1-A, July, 2006.

34. Slagle, W. H. (ed.), "Westinghouse Fuel Assembly Reconstitution Evaluation Methodology," WCAP-13060-P-A, July 1993.

3.3 NUCLEAR DESIGN

This section is principally based on information presented for a typical cycle with the Westinghouse VANTAGE 5 design for Donald C. Cook Nuclear Plant Unit 2. The plant contained 17 x 17 fuel supplied solely by Westinghouse in Cycles 1 through 3. The fresh fuel for Cycles 4 through 7 was a 17 x 17 design supplied by Advanced Nuclear Fuels (ANF). Since Cycle 8, the fresh fuel has been the Westinghouse 17 x 17 VANTAGE 5 design.

3.3.1 Design Bases

This section describes the design bases and functional requirements used in the nuclear design of the fuel and reactivity control system and relates these design bases to the General Design Criteria (GDC) in 10 CFR 50, Appendix A. Where appropriate, supplemental criteria such as the Final Acceptance Criteria for Emergency Core Cooling Systems are addressed. Before discussing the nuclear design bases it is appropriate to briefly review the four major categories ascribed to conditions of plant operation.

The full spectrum of plant conditions is divided into four categories, in accordance with the anticipated frequency of occurrence and risk to the public:

1. Condition I - Normal Operation.
2. Condition II - Incidents of Moderate Frequency.
3. Condition III - Infrequent Faults.
4. Condition IV - Limiting Faults.

In general the Condition I occurrences are accommodated with margin between any plant parameter and the value of that parameter which would require either automatic or manual protective action. Condition II incidents are accommodated with, at most, a shutdown of the reactor with the plant capable of returning to operation after corrective action. Fuel damage (fuel damage as used here is defined as penetration of the fission product barrier, i.e., the fuel rod clad) is not expected during Condition I and Condition II events. It is not possible, however, to preclude a very small number of rod failures. These are within the capability of the plant cleanup system and are consistent with the plant design basis.

Condition III incidents shall not cause more than a small fraction of the fuel elements in the reactor to be damaged, although sufficient fuel element damage might occur to preclude immediate resumption of operation. The release of radioactive material due to Condition III incidents should not be sufficient to interrupt or restrict public use of these areas beyond the exclusion radius. Furthermore, a Condition III incident shall not, by itself generate a Condition

IV fault or result in a consequential loss of function of the reactor coolant or reactor containment barriers.

Condition IV occurrences are faults that are not expected to occur but are defined as limiting faults, which must be, designed against. Condition IV faults shall not cause a release of radioactive material that results in an undue risk to public health and safety.

The core design power distribution limits related to fuel integrity are met for Condition I occurrences through conservative design and maintained by the action of the control system. The requirements for Condition II occurrences are met by providing an adequate protection system which monitors reactor parameters. The control and protection systems are described in Chapter 7 and the consequences of Condition II, III and IV occurrences are given in Chapter 14.

3.3.1.1 Fuel Burnup

3.3.1.1.1 Basis

The fuel rod design basis is described in Section 3.2. The nuclear design basis is to install sufficient reactivity in the fuel to attain the desired region average discharge burnup subject to the limit on peck rod burnup reported in Section 3.2.1.1.1. The above along with the design basis in Section 3.3.1.3, Control of Power Distribution, satisfies GDC-10.

3.3.1.1.2 Discussion

Fuel burnup is a measure of fuel depletion, which represents the integrated energy output of the fuel (MWD/MTU) and is a convenient means for quantifying fuel exposure criteria.

The core design lifetime or design discharge burnup is achieved by installing sufficient initial excess reactivity in each fuel region and by following a fuel replacement program (such as that described in Section 3.3.2) that meets all safety-related criteria in each cycle of operation.

Initial excess reactivity installed in the fuel, although not a design basis, must be sufficient to maintain core criticality at full power operating conditions throughout cycle life with equilibrium xenon, samarium, and other fission products present. The end of design cycle life is defined to occur when the chemical shim concentration is essentially zero with control rods present to the degree necessary for operational requirements (e.g., the controlling band at the "bite" position). In terms of chemical shim boron concentration this represents approximately 10 ppm with no control rod insertion.

A limitation on initial installed excess reactivity is not required other than as is quantified in terms of other design bases such as core negative reactivity feedback and shutdown margin discussed below.

3.3.1.2 Negative Reactivity Feedbacks (Reactivity Coefficient)

3.3.1.2.1 Basis

The fuel temperature coefficient is negative and the moderator temperature coefficient of reactivity is non-positive for power operation at 100% RTP, thereby providing negative reactivity feedback characteristics. The design basis meets GDC-11.

3.3.1.2.2 Discussion

When compensation for a rapid increase in reactivity is considered, there are two major effects. These are the resonance absorption effects (Doppler) associated with changing fuel temperature and the spectrum effect resulting from changing moderator density. These basic physics characteristics are often identified by reactivity coefficients. The use of slightly enriched uranium ensures that the Doppler coefficient of reactivity is negative. This coefficient provides the most rapid reactivity compensation. The core is also designed to have an overall non-positive moderator temperature coefficient of reactivity at full power so that average coolant temperature or void content provides another, slower compensatory effect. Full power operation is permitted only in a range of overall non-positive moderator temperature coefficient. The non-positive moderator temperature coefficient can be achieved through use of fixed burnable absorber, integral fuel burnable absorbers and/or control rods by limiting the reactivity held down by soluble boron.

Burnable absorber content (quantity and distribution) is not stated as a design basis other than as it relates to accomplishment of a non-positive moderator temperature coefficient at full power operating conditions discussed above.

3.3.1.3 Control of Power Distribution

3.3.1.3.1 Basis

The nuclear design basis is that, with at least a 95 percent confidence level:

1. The fuel is not to be operated at greater than 13.0 Kw/ft under normal operating conditions (average thermal output at 3468 MWt is 5.54 Kw/ft and a maximum F_Q is 2.335) including an allowance of 0.34 percent for calorimetric error and not including power spike factor due to densification.
2. Under abnormal conditions including the maximum overpower condition, the fuel peak power does not cause melting as defined in Section 3.4.1.2.
3. The fuel does not operate with a power distribution that violates the departure from nucleate boiling (DNB) design basis as discussed in Section 3.4.1 under Condition I and II events including the maximum overpower condition.
4. Fuel management is such as to produce rod powers and burnups consistent with the assumptions in the fuel rod mechanical integrity analysis of Section 3.2.

The above basis meets GDC-10.

3.3.1.3.2 Discussion

Calculation of extreme power shapes, which affect fuel design limits, is performed with proven methods and verified frequently with measurements from operating reactors. The conditions under which limiting power shapes are assumed to occur are chosen conservatively with regard to any permissible operating state.

Even though there is good agreement between peak power calculations and measurements, a nuclear uncertainty margin (see Section 3.3.2.2) is applied to calculated peak local power. Such a margin is provided both for the analysis for normal operating states and for anticipated transients.

3.3.1.4 Maximum Controlled Reactivity Insertion Rate

3.3.1.4.1 Basis

The maximum reactivity insertion rate due to withdrawal of rod cluster control assemblies or by boron dilution is limited. During normal at power operation, the maximum controlled reactivity rate change is less than 38 pcm*/sec. A maximum reactivity change rate (63 pcm/sec for accidental withdrawal of two control banks from a subcritical condition and (110 pcm/sec) for

* 1 pcm = 10^{-5} $\Delta\rho$ (see the footnote to Table 3.3-2).

accidental withdrawal of control banks at power) is set such that peak heat generation rate and DNBR limits are met at overpower conditions. This satisfies GDC-25. The maximum reactivity worth of control rods and the maximum rates of reactivity insertion employing control rods are limited so as to preclude rupture of the coolant pressure boundary or disruption of the core internals to a degree which would impair core cooling capacity due to a RCCA bank withdrawal or RCCA ejection accident (see Chapter 14).

The current analyses consider a maximum control speed of 72 steps/minute (45 inches/minute). To accommodate a postulated failure of the control system, an increase in the maximum control rod speed of up to 77 steps/minute (48.125 inches/minute) has been evaluated and shown to be acceptable. In future cycles, the maximum allowed reactivity insertion rate will be maintained by reducing the maximum allowed differential rod worths accordingly to account for the increased maximum control rod speed.

Following any Condition IV event (rod ejection, steam line break, etc.) the reactor can be brought to the shutdown condition and the core can maintain acceptable heat transfer geometry. This satisfies GDC-28.

The reactivity change rates are conservatively calculated assuming unfavorable axial power and xenon distributions. The peak xenon burnout rate is 25 pcm/min, significantly lower than the analyzed maximum reactivity addition rate of 35 pcm/sec for normal operation and 63 pcm/sec for accidental withdrawal of two banks from a subcritical condition.

3.3.1.5 Shutdown Margins

Basis

Minimum shutdown margin as specified in the Technical Specifications is required at any power operating condition in the hot standby shutdown condition and in the cold shutdown condition.

In all analyses involving reactor trip, the single, highest worth rod cluster control assembly is postulated to remain untripped in its full-out position (stuck rod criterion). This satisfies GDC-26.

Discussion

Two independent reactivity control systems are provided, namely control rods and soluble boron in the coolant. The control rod system can compensate for the reactivity effects of the fuel and water temperature changes accompanying power level changes over the range from full-load to no-load. In addition, the control rod system provides the minimum shutdown margin under Condition I events and is capable of making the core subcritical rapidly enough to prevent

exceeding acceptable fuel damage limits assuming that the highest worth control rod is stuck out upon trip.

The boron system can compensate for all xenon burnout reactivity changes and will maintain the reactor in the cold shutdown condition. Thus, backup and emergency shutdown provisions are provided by a mechanical and a chemical shim control system which satisfies GDC-26.

Basis

When fuel assemblies are in the pressure vessel and the vessel head is not in place, K_{eff} is maintained at or below 0.95 with control rods and soluble boron. Further, the fuel will be maintained sufficiently subcritical such that removal of all rod cluster control assemblies will not result in criticality.

Discussion

ANSI Standard N18.2 specifies a K_{eff} not to exceed 0.95 in spent fuel storage racks and transfer equipment flooded with pure water and a K_{eff} not to exceed 0.98 in normally dry new fuel storage racks assuming optimum moderation. No criterion is given for the refueling operation, however a 5 percent margin, which is consistent with spent fuel storage and transfer and the new fuel storage, is adequate for the controlled and continuously monitored operations involved.

The boron concentration required to meet the refueling shutdown criteria is specified in the Technical Specifications. Verification that this shutdown criteria is met, including uncertainties, is achieved using standard Westinghouse design methods such as the PHOENIX-P and ANC codes (Reference 3). The subcriticality of the core is continuously monitored as described in the Technical Specifications.

3.3.1.6 Stability

3.3.1.6.1 Basis

The core is inherently stable to power oscillations at the fundamental mode. This satisfies GDC-12. Spatial power oscillations within the core with a constant core power output, should they occur can be reliably and readily detected and suppressed.

3.3.1.6.2 Discussion

Oscillations of the total power output of the core, from whatever cause, are readily detected by the loop temperature sensors and by the nuclear instrumentation. The core is protected by these systems and a reactor trip would occur if power increased unacceptably, preserving the design margins to fuel design limits. The stability of the turbine/steam generator/core systems and the reactor control system is such that total core power oscillations are not normally possible. The

redundancy of the protection circuits ensures an extremely low probability of exceeding design power levels.

The core is designed so that diametral and azimuthal oscillations due to spatial xenon effects are self-damping and no operator action or control action is required to suppress them. The stability to diametral oscillations is so great that this excitation is highly improbable. Convergent azimuthal oscillations can be excited by prohibited motion of individual control rods. Such oscillations are readily observable and alarmed, using the excore long ion chambers. Indications are also available from incore thermocouples and loop temperature measurements. Moveable incore detectors can be activated to provide more detailed information. In all presently proposed cores these horizontal plane oscillations are self-damping by virtue of reactivity feedback effects designed into the core.

However, axial xenon spatial power oscillations may occur late in core life. The control banks and excore detectors are provided for control and monitoring of axial power distributions. Assurance that fuel design limits are not exceeded is provided by reactor Overpower ΔT and Overtemperature ΔT trip functions, which use the measured axial power imbalance as an input.

3.3.1.7 Anticipated Transients Without Scram

In the Code of Federal Regulations, 10 CFR 50.62(c)(1) requires that each pressurized water reactor have equipment, from sensor output to final actuation device, that is diverse from the reactor trip system, to automatically initiate the auxiliary feedwater system and initiate a turbine trip under conditions indicative of an anticipated transient without scram (ATWS). Such a system has been installed at Cook Nuclear Plant, having been designed in accordance with Reference 1. This system is called "ATWS Mitigating System Actuation Circuitry" (AMSAC). This equipment will protect against reactor coolant system overpressurization in the event that a loss of normal feedwater or a loss of load transient is not accompanied by a reactor trip after having reached the reactor trip setpoint.

3.3.2 Description

Specific data presented within the text of this subsection refers to a typical Westinghouse VANTAGE 5 17 x 17 reload design. Referenced figures within this subsection present example information which is representative of the Westinghouse VANTAGE 5 17 x 17 fuel assembly design.

3.3.2.1 Nuclear Design Description

The reactor core consists of a specified number of fuel rods which are held in bundles by spacer grids attached to rod cluster control thimbles which are held in turn by top and bottom fittings. The fuel rods are constructed of Zircaloy/ZIRLO/**Optimized ZIRLO™** cylindrical tubes containing UO_2 fuel pellets. The bundles, known as fuel assemblies, are arranged in a pattern, which approximates a right circular cylinder.

Each fuel assembly contains a 17 x 17 rod array composed of 264 fuel rods, 24 rod cluster control thimbles and an incore instrumentation thimble. Figure 3.2-1 shows a cross sectional view of a 17 x 17 Westinghouse fuel assembly and the related rod cluster control locations. Further details of the fuel assembly are given in Section 3.2.1.

The fuel has axial zoning of uranium enrichment; however, the enrichment in the radial direction of an assembly is still maintained at a consistent enrichment. Generally, axial zoning consists of loading the top and bottom six (6) inches of the fuel with natural or enriched uranium. Blankets, as the natural uranium regions are referred to, reduce the axial neutron leakage, thereby contributing to better fuel utilization. Figure 3.3-1 shows the axial zoning of the fuel and the axial placement of the integral fuel burnable absorber (IFBA) coated fuel pellets. The reference reloading pattern is similar to the example in Figure 3.3-2. The loading of fresh fuel in the interior of the core decreases the radial neutron leakage by reducing the power produced on the core periphery. This type of reload pattern increases the fuel utilization and is referred to as a low leakage loading pattern.

The operating cycle length is determined according to energy requirements and mechanical design/assembly burnup limits. The exact reloading pattern, initial and final positions of assemblies and the number of fresh assemblies are dependent on the energy requirement for the cycle and power histories of the previous cycles.

The core average enrichment is determined by the amount of fissionable material required to provide the desired core lifetime and energy requirements. The physics of the burnup process are such that operation of the reactor depletes the amount of fuel available due to the absorption of neutrons by the U-235 atoms and their subsequent fission. The rate of U-235 depletion is directly proportional to the power level at which the reactor is operated. In addition, the fission process results in the formation of fission products, some of which readily absorb neutrons.

These effects, depletion and the buildup of fission products, are partially offset by the buildup of plutonium shown in Figure 3.3-3 for the 17 x 17 fuel assembly, which occurs due to the nonfission absorption of neutrons in U-238. Therefore, at the beginning of any cycle a reactivity

reserve equal to the depletion of the fissionable fuel and the buildup of fission product poisons over the specified cycle life must be "built" into the reactor. This excess reactivity is controlled by removable neutron absorbing material in the form of boron dissolved in the primary coolant and IFBA coating on fuel pellets.

The concentration of boric acid in the primary coolant is varied to provide control and to compensate for long-term reactivity requirements. The concentration of the soluble neutron absorber is varied to compensate for reactivity changes due to fuel burnup, fission product poisoning including xenon and samarium, burnable absorber depletion, and the cold-to-operating moderator temperature change. The normal and emergency boration paths of the chemical and volume control system (CVCS) are each capable of inserting negative reactivity at a rate in excess of the peak xenon burnout rate.

The amount of boric acid in the boric acid tank is sufficient to maintain the reactor subcritical by the necessary shutdown margin at hot conditions following a reactor trip from all credible operating conditions. The control rods provide the necessary shutdown margin immediately following a reactor trip from full power conditions, assuming that the most reactive RCCA is fully withdrawn. The boric acid tank contains sufficient borated water to compensate for subsequent xenon decay.

The flow rate of boric acid from the boric acid tank is sufficient to follow the highest burnout rate of xenon following reactor startup from peak xenon conditions.

As the boron concentration is increased, the moderator temperature coefficient becomes less negative. The use of a soluble poison alone could result in the MTC exceeding the Technical Specifications limit. Therefore, IFBA coated fuel pellets are used to reduce the soluble boron concentration sufficiently to ensure that the MTC is negative for full power operating conditions, and within safety limits for part power operating conditions. IFBA pins contain enriched uranium pellets with a thin coating of ZrB2 on the fuel pellet's cylindrical surface. During operation, the burnable absorber content in the IFBA coating is depleted thus adding positive reactivity to offset some of the negative reactivity from fuel depletion and fission product buildup. The depletion rate of the IFBA coating is not critical since chemical shim is always available and flexible enough to cover any possible deviations in the expected IFBA depletion rates. The IFBA coating is thin enough (approx. 0.6 mil) to not cause significant increases in resistance to heat conduction.

In addition to reactivity control and axial power shaping, the IFBA pins are strategically located to provide a favorable radial power distribution. Figure 3.3-4 shows example absorber distributions within a fuel assembly for several example IFBA configurations used in a 17 x 17

array. An example, IFBA core loading pattern is shown in Figure 3.3-5. Figure 3.3-6 is a graph of an example core depletion with IFBA coated fuel pellets.

Tables 3.3-1 through 3.3-3 contain a summary of the reactor core design parameters for an example fuel cycle, including reactivity coefficients, delayed neutron fraction and neutron lifetimes. Sufficient information is included to permit an independent calculation of the nuclear performance characteristics of the core.

3.3.2.2 Power Distributions

The accuracy of power distribution calculations has been confirmed through more than 1000 flux maps taken during over 20 plant years of operation under conditions very similar to those for the plant described herein. Details of this confirmation are given in Reference (2).

3.3.2.2.1 Definitions

Power distributions are quantified in terms of hot channel factors. These factors are a measure of the peak pellet power within the reactor core and the total energy produced in a coolant channel and are expressed in terms of quantities related to the nuclear or thermal design namely:

Power density	is the thermal power produced per unit volume of the core (kW/liter).
Linear power density	is the thermal power produced per unit length of active fuel (kW/ft). Since fuel assembly geometry is standardized this is the unit of power density most commonly used. For all practical purposes it differs from kW/liter by a constant factor which includes geometry and the fraction of the total thermal power which is generated in the fuel rod.
Average linear power density	is the total thermal power produced in the fuel rods divided by the total active fuel length of all rods in the core.
Local heat flux	is the heat flux at the surface of the cladding (BTU-ft^{-2}-hr^{-1}). For nominal rod parameters this differs from linear power density by a constant factor.
Rod power or rod integral power	is the length integrated linear power density in one rod (kW).
Average rod power	is the total thermal power produced in the fuel rods divided by the number of fuel rods (assuming all rods have equal length).

The hot channel factors used in the discussion of power distributions in this section are defined as follows:

F_Q (or F_q) Heat Flux Hot Channel Factor, is defined as the maximum local heat flux on the surface of a fuel rod divided by the average fuel rod heat flux, allowing for manufacturing tolerances on fuel pellets and rods.

F_Q^N Nuclear Heat Flux Hot Channel Factor, is defined as the measured maximum local fuel rod linear power density divided by the average fuel rod linear power density, assuming nominal fuel pellet and rod parameters.

The value of F_Q^N is calculated using data from the incore detectors according to:

$$F_Q^N = \frac{\text{MAX}\, q(x_0, y_0, z_0)}{\frac{1}{NH} \sum_{\text{all rods}} \int_0^H q(x, y, z) dz}$$

where *q(x,y,z)* is the local linear power density at a point *x,y,z* in the core with *N* fuel rods of height *H*.

F_Q^E Engineering Heat Flux Hot Channel Factor is the allowance on heat flux required for manufacturing tolerances. The engineering factor allows for local variations in enrichment, pellet density and diameter.

Combined statistically the net effect is a factor of 1.03 to be applied to fuel rod surface heat flux.

F_Q^M Measured Heat Flux Hot Channel Factor. These measurements, using the incore detector system, are generally taken with core at near equilibrium conditions.

F_Q^C Measured Heat Flux Hot Channel Factor times the flux map measurement uncertainty and factor that accounts for fuel manufacturing tolerances.

F_Q^W Transient Heat Flux Hot Channel Factor. Maximum anticipated value of F_Q obtained from equilibrium value of F_Q by adjusting by a factor that accounts for the calculated worst case transient conditions.

$F_{\Delta H}^N$ Nuclear Enthalpy Rise Hot Channel Factor is defined as the ratio of the integral of linear power along the rod with the highest integrated power to the average rod power.

Measured $F_{\Delta H}^N$ is also calculated using data from incore detectors according to:

$$F_{\Delta H}^N = \frac{\text{MAX} \int_0^H q(x_0, y_0, z) dz}{\frac{1}{N} \sum_{\text{all rods}} \int_0^H q(x, y, z) dz}$$

A measurement uncertainty factor of 1.04 is applied to the measured $F_{\Delta H}$ value derived from incore detector data.

Manufacturing tolerances, hot channel power distribution and surrounding channel power distributions are treated explicitly in the calculation of the DNBR described in Section 3.4.

It is convenient for the purposes of discussion to define subfactors of F_Q, however, design limits are set in terms of the total peaking factor.

F_Q = Total peaking factor or heat flux hot channel factor

$$= \frac{\text{Maximum kW/ft}}{\text{Average kW/ft}}$$

Without densification effects:

$$F_Q = F_Q^N \cdot F_Q^U = F_{XY}^N \cdot F_Z^N \cdot F_U^N \cdot F_Q^E$$

Where:

F_Q^N and F_Q^E are defined above.

F_U^N = factor of measurement, equal a to 1.05.

F_Q^U = total uncertainty on measured F_Q^N

F_{XY}^N = ratio of peak power density to average power density in the horizontal plane of peak local power.

F_Z^N = ratio of the power per unit core height in the horizontal plane of peak local power to the average value of power per unit core height. If the plane of peak local power coincides with the plane of maximum power per unit core height then is the core average axial peaking factor.

The independence of the individual uncertainties constituting the uncertainty factor on F_Q enables the uncertainty F_Q^U to be calculated statistically combining the individual uncertainties on the limiting rod. The standard deviation of the resultant distribution of F_Q^U is determined by taking the square root of the sum of the variances of each of the contributing distributions. Combining the values for F_Q^E and F_U^N (1.03 and 1.05, respectively) in this way provides margin for the accommodation of a further uncertainty term to account for rod bow effects.

3.3.2.2.2 Radial Power Distributions

The power shape in horizontal sections of the core at full power is a function of the fuel and burnable absorber loading patterns and the presence or absence of a single bank of full-length control rods. Thus, at any time in the cycle a horizontal section of the core can be characterized as either unrodded or with group D control rods. These two situations combined with burnup effects determine the radial power shapes, which can exist in the core at full power. Typical values of F_{XY}^{N} are given in Table 3.3-2. The effect on radial power shapes of power level, xenon, samarium and moderator density effects are considered also but these are quite small. The effect of non-uniform flow distribution is negligible. While radial power distributions in various planes of the core are often illustrated, the core radial enthalpy rise distribution as determined by the integral of power up each channel is of greater interest. Figures 3.3-7 through 3.3-11 show representative radial power distributions for 1/8 of the core for representative operating conditions. These conditions are 1) hot full power (HFP) near at beginning-of-life (NBOL) - unrodded - no xenon, 2) HFP at NBOL - unrodded - equilibrium xenon, 3) HFP at NBOL - Bank D at HFP insertion limit - equilibrium xenon, 4) HFP at middle-of-life (MOL) - unrodded - equilibrium xenon, and 5) HFP at end-of-life (EOL) - unrodded - equilibrium xenon.

Since the position of the hot channel varies from time to time a single reference radial design power distribution is selected for DNB calculations. This reference power distribution is chosen conservatively to concentrate power in one area of the core, minimizing the benefits of flow redistribution. Assembly powers are normalized to core average power.

The radial power distribution shown in Figure 3.3-9 involving the partial insertion of control rods is calculated by performing two group x-y-z calculations.

3.3.2.2.3 Axial Power Distributions

The shape of the power profile in the axial or vertical direction is largely under the control of the operator through manual and automatic motion of full-length rods and by responding to manual operation of the CVCS. Nuclear effects which cause variations in the axial power shape include moderator density, Doppler effect on resonance absorption, spatial xenon and burnup. Automatically controlled variations in total power output and full-length rod motion are also important in determining the axial power shape at any time. Signals are available to the operator from the excore ion chambers, which are long ion chambers outside the reactor vessel running parallel to the axis of the core. Separate signals are taken from the top and bottom halves of the chambers. The difference between top and bottom signals from each of four pairs of detectors is displayed on the control panel and called the flux difference, ΔI. Calculations of core average

peaking factor for many plants and measurements from operating plants under many operating situations are associated with either ΔI or axial offset in such a way that an upper bound can be placed on the peaking factor. For these correlations axial offset is defined as:

$$\text{axial offset} = \frac{\phi_t - \phi_b}{\phi_t + \phi_b}$$

and ϕ_t and ϕ_b are the top and bottom detector readings.

Representative axial power shapes during load follow operation for BOL, MOL, and EOL conditions for an example cycle are shown in Figures 3.3-14 through 3.3-16. These figures cover a wide range of axial offset including values not permitted at full power.

3.3.2.2.4 Fuel Rod Power Distributions

For the purpose of illustration, fuel rod power distributions from the BOL and EOL conditions corresponding to Figures 3.3-8 and 3.3-11, respectively, are given for the same assembly in Figures 3.3-12 and 3.3-13, respectively. Since the detailed power distribution surrounding the hot channel varies from time to time, a conservatively flat assembly power distribution is assumed in the DNB analysis, described in Section 3.4, with the rod of maximum integrated power artificially raised to the design value of $F_{\Delta H}^{N}$. Care is taken in the nuclear design of all fuel cycles and all operating conditions to ensure that a flatter assembly power distribution does not occur with limiting values of $F_{\Delta H}^{N}$.

3.3.2.2.5 Heat Flux Hot Channel Factor, F_Q

As stated previously, Condition I occurrences are those which are expected frequently or regularly in the course of power operation, maintenance, or maneuvering of the plant. As such, Condition I occurrences are accommodated with margin between any plant parameter and the value of that parameter which would require either automatic or manual protective action. Inasmuch as Condition I occurrences occur frequently or regularly, they must be considered from the point of view of affecting the consequences of fault conditions (Conditions II, III and IV). In this regard, analysis of each fault condition described is generally based on a conservative set of initial conditions corresponding to the most adverse set of conditions which can occur during Condition I operation.

Implicit in the definition of normal operation is proper and timely action by the reactor operator. That is, the operator follows recommended operating procedures for maintaining appropriate power distributions and takes any necessary remedial actions when alerted to do so by the plant instrumentation. Thus, as stated above, the worst or limiting power distribution which can occur

during normal operation is to be considered as the starting point for analysis of Condition II, III and IV events.

Improper procedural actions or error by the operator are assumed in the design as occurrences of moderate frequency (Condition II). Some of the consequences which might result are discussed in Chapter 14. Therefore, the limiting power shapes which result from such Condition II events, are those power shapes which deviate from the normal operating condition at the recommended axial offset band, e.g., due to lack of proper action by the operator during a xenon transient following a change in power level brought about by control rod motion. Power shapes which fall in this category are used for determination of the Reactor Protection System setpoints so as to maintain margin to overpower or DNB limits.

In previous analyses of power peaking factors for D.C. Cook Unit 2, it was necessary to apply a penalty on calculated overpower transient F_Q values to allow for interpellet gaps caused by pellet hang-ups and pellet shrinkage due to densification. This penalty is known as the densification spike factor. However, studies have shown (Reference 24) that this penalty can be eliminated from overpower transient calculations for the fuel type present in the D.C. Cook Unit 2 core.

Furthermore, results reported in Reference (5) show that such a power spike penalty should not be included in the LOCA evaluation.

The means for maintaining power distributions within the required hot channel factor limits are described in the Technical Specifications and associated bases. A complete discussion of power distribution control in Westinghouse PWRs is included in Reference (6). Detailed background information on the following: design constraints on local power density in a Westinghouse PWR, the defined operating procedures and the measures taken to preclude exceeding design limits; is presented in the Westinghouse Topical Report on power distribution control and load following procedures (Reference 7). The following paragraphs summarize these reports and describe the calculations used to establish the upper bound on peaking factors.

The calculations used to establish the upper bound on peaking factors, F_Q and $F_{\Delta H}$, include all of the nuclear effects which influence the radial and/or axial power distributions throughout core life for various modes of operation including load follow, reduced power operation, and axial xenon transients.

Radial power distributions are calculated for the full power condition and fuel and moderator temperature feedback effects are included for the average enthalpy plane of the reactor. The steady-state nuclear design calculations are done for normal flow with the same mass flow in each channel and flow redistribution effects neglected. The effect of flow redistribution is

calculated explicitly where it is important in the DNB analysis of accidents. The effect of xenon on radial power distribution is small (compare Figures 3.3-7 and 3.3-8) but is included as part of the normal design process.

Radial power distributions are relatively fixed and easily bounded with upper limits.

The core average axial profile, however, can experience significant changes, which can occur rapidly as a result of rod motion and load changes and more slowly due to xenon distribution. For the study of points of closest approach to axial power distribution limits, several thousand cases are examined. Since the properties of the nuclear design dictate what axial shapes can occur, boundaries on the limits of interest can be set in terms of the parameters which are readily observed on the plant. Specifically, the nuclear design parameters, which are significant to the axial power distribution analysis, are:

1. Core power level.
2. Core height.
3. Coolant temperature and flow.
4. Coolant temperature as a function of reactor power.
5. Fuel cycle lifetimes.
6. Rod bank worths.
7. Rod bank overlaps.

Normal operation of the plant assumes compliance with the following conditions:

1. Control rods in a single bank move together with no individual rod insertion differing by more than the following limits from the bank demand position.
   a. Below 85% RTP - 18 steps
   b. Above 85% RTP - between 12 to 18 steps dependent on $F_Q^W(z)$ and $F_{\Delta H}$ margins
2. Control banks are sequenced with overlapping banks.
3. The control full-length bank insertion limits are not violated.
4. Axial power distribution procedures, which are given in terms of flux difference control and control bank position, are observed.

The axial power distribution procedures referred to above are part of the required operating procedures, which are followed, in normal operation. Limits placed on the axial flux difference are designed to ensure that the total peaking factor of F_Q is maintained within acceptable limits,

which satisfy LOCA and local power requirements. The constant axial offset control (CAOC) operating procedures described in Reference (7) require control of the axial offset (flux difference divided by fractional power) at all power levels within a permissible operating band of a target value corresponding to the equilibrium full power value. In the typical cycle, the target value changes from about +2.0 to -2.5 percent through the life of the cycle. This minimizes xenon transient effects on the axial power distribution, since the procedures essentially keep the xenon distribution in phase with the power distribution.

Calculations are performed for normal operation of the reactor including load following maneuvers. Beginning, middle and end of cycle conditions are included in the calculations. Different histories of operation are assumed prior to calculating the effect of load follow transients on the axial power distribution. These different histories assume base load and load follow operation is maintained within the specified axial flux difference band. For a given plant and fuel cycle a finite number of maneuvers are studied to determine the general behavior of the local power density as a function of core elevation.

These cases represent many possible reactor states in the life of one fuel cycle and they have been chosen as sufficiently definitive of the cycle by comparison with much more exhaustive studies performed on some 20 or 30 different, but typical, plant and fuel cycle combinations. The cases are described in detail in Reference (7) and they are considered to be necessary and sufficient to generate a local power density limit which, when increased by 5 percent for conservatism, will not be exceeded with a 95 percent confidence level. Many of the numerous amounts of points do not approach the limiting envelope; however they are part of the time histories, which lead to the hundreds of, shapes, which do define the envelope. They also serve, as a check that the reactor studied is typical of those studied more exhaustively.

Thus it is not possible to single out any transient or steady-state condition which defines the most limiting case. It is not even possible to separate out a small number, which form an adequate analysis. The process of generating a myriad of shapes is essential to the philosophy that leads to the required level of confidence. A maneuver which provides a limiting case for one reactor fuel cycle (defined as approaching the bounding envelope of Figure 3.3-20) is not necessarily a limiting case for another reactor or fuel cycle with different control bank worths, enrichments, burnup, coefficient, etc. Each shape depends on the detailed history of operation up to that time and on the manner in which the operator conditioned xenon in the days immediately prior to the time at which the power distribution is calculated.

Each power shape generated is analyzed to determine if LOCA constraints are met or exceeded. The total peaking factor, F_Q is synthesized by combining the axial power profiles with cycle-specific radial factors appropriate for rodded and unrodded planes.

In these calculations the effects on the unrodded radial peak of xenon redistribution that occur following the withdrawal of a control bank (or banks) from a rodded region are obtained from three-dimensional X-Y-Z calculations. A factor, which may be height-dependent, to be applied on the unrodded radial peak is obtained from calculations in which xenon distribution was preconditioned by the presence of control rods and then allowed to redistribute for several hours. A detailed discussion of this effect may be found in References (7) and (8). The calculated values have been increased by a factor of 1.05 for calculational uncertainty, a factor of 1.03 for the engineering factor F_Q^E, and a factor of 1.014 to allow for the presence of the fuel grids.

The envelope in figure 3.3-20 represents an upper bound on local power density versus elevation in the core. (It should be noted that the allowed increase in the F_Q value at part power operation, as implied in this Figure, applies only to powers above 50% of rated power, as defined in the Technical Specifications.) It should be emphasized that this envelope is a conservative representation of the bounding values of local power density. Expected values are considerably smaller and, in fact, less conservative bounding values may be justified with additional analysis or surveillance requirements.

Finally, as previously discussed, this upper bound envelope is based on procedures of load follow which require operation within an allowed deviation from a target equilibrium value of axial flux difference. These procedures are predicated only upon excore surveillance supplemented by the normal monthly full core map requirement and by computer based alarms on deviation and time of deviation from the allowed flux difference band.

3.3.2.2.6 Limiting Power Distributions

Accident analyses for Cook Nuclear Plant Unit 2 are presented in Chapter 14 of the FSAR. The results of these analyses determined a limiting value of total peaking factor, F_Q, of 2.335, under normal operation, including load follow maneuvers. This value is derived from the conditions necessary to satisfy the limiting conditions specified in the LOCA analyses which meet 10 CFR 50.46 and Appendix K requirements. As noted previously on this section, an upper bound envelope of F_Q x power equal to 2.335 x K(z), as shown in Figure 3.3-20, results from operation in accordance with CAOC procedures using excore surveillance only. K(z) is defined simply as a multiplying factor which defines the shape of the F_Qx power limit curve as a function of core elevation, z. The maximum value of K(z) is unity.

The surveillance of the core hot channel factors in accordance with the above, is presented in the Cook Nuclear Plant Unit 2 Technical Specifications.

Allowing for fuel densification effects, the average kW/ft at 3468 MWt is 5.54 kW/ft. From Figure 3.3-20, the conservative upper bound value of normalized local power density, including uncertainty allowance, is 2.335 corresponding to peak local power density of 13.0 kW/ft at 100.34 percent power. Note that fuel densification leads to a slight shrinkage in the fuel stack, which is accounted for in the average kW/ft values quoted above. This is unaffected by the elimination of the densification spike factor in the overpower analysis (described earlier).

The Constant Axial Offset Control Procedure (CAOC) (Reference 7), enables Cook Nuclear Plant Unit 2 to manage core power distributions such that Technical Specification limits on F_Q are not violated during normal operation and limits on MDNBR are not violated during steady-state, load-follow, and anticipated transients.

The W(z) factor given in the Core Operating Limits Report (COLR) and applied by the Technical Specifications provides the means for predicting the maximum F_Q distribution anticipated during operation under the CAOC procedure taking into account the incore measured equilibrium power distribution. A comparison of this distribution with the Technical Specification limit curve determines the power level below which the Technical Specification limit can be protected by the CAOC procedure. If such protection can be confirmed for a given operating cycle interval, the excore monitored constant axial offset limits will protect the Technical Specification F_Q limits. Further details on this core surveillance procedure can be found in Reference 28.

The prediction of the maximum anticipated F_Q distribution, $F_Q^W(z)$ is made possible by controlling the distribution such that it does not increase by more than the factor W(z) times the equilibrium power distribution $F_Q^C(z)$. This is accomplished by maintaining the core axial offset within a specified range of values about a target value associated with the equilibrium power distribution. The value of the W(z) factor is determined from cycle-specific analysis of plant operation data during which the axial offset is maintained within a specified band about the equilibrium (target) axial offset. The core axial offset (AO) has been previously defined Sub-section 3.3.2.2.3.

A positive axial offset signifies a power shift toward the top half of the core, while a negative axial offset signifies a power shift toward the bottom half of the core.

The basic features of the CAOC procedures are as follows:

1. An $F_Q^C(z)$ distribution is determined along with an associated axial offset, denoted as the target axial offset (AO_T), at full power, equilibrium xenon conditions. The $F_Q^C(z)$ distribution is the measured $F_Q^M(z)$ distribution multiplied by the uncertainty factors 1.05 x 1.03, where 1.05 is the measurement uncertainty and 1.03 the engineering factor to account for manufacturing tolerances.

2. The $F_Q^C(z)$ distribution is multiplied by the W(z) factor to obtain the maximum anticipated $F_Q^W(z)$ which is compared to the Technical Specification limits, $F_Q^{Limit}(z)$. This limiting curve for $F_Q^{Limit}(z)$ is given by the product of $F_Q^{L/P}$ times K(z). If $F_Q^W(z)$ does not exceed the F_Q^{Limit} limit, then operation under the CAOC procedures will protect the F_Q Technical Specification limits and supplemental monitoring is not required. If the $F_Q^W(z)$ exceeds the $F_Q^{Limit}(z)$, then reactor core power must be reduced to meet the Technical Specification limits.

3. For each axial offset target value (AO_T), a target band (AO_{TB}) is allowed.

$$AO_{TB} = \frac{\pm S\%}{P/P_o}$$

where P = operating reactor power (MWth)

P_o = reactor rated power (MWth)

S = target band specified in the COLR; typically ± 3% or ± 5%

4. Below a relative power (P/P_o) of 0.9, or 0.9 x minimum value of [F_Q^L x K(z)/ $F_Q^W(z)$] (whichever is less) the axial offset is allowed to deviate from the target band for one hour out of each twenty-four consecutive hours, provided that the measured axial offset remains within a broader, axial offset band specified in the COLR. If this requirement is violated, the core relative power must be reduced below 0.5 of rated power where no restrictions on AO are imposed. Above a

relative power of 0.9 or 0.9 x minimum value of [F_Q^L x K(z)/ F_Q^W (z)] (whichever is less), the measured AO must remain within the allowable target band at all times.

3.3.2.2.7 Enthalpy Rise Hot Channel Factor, $F_{\Delta H}$

Analyses of possible operating power shapes for the reactor described herein show that the appropriate hot channel factors F_Q and $F_{\Delta H}^N$ for peak local power density and DNB analysis at full power are the values given in Table 3.3-2 and addressed in the Technical Specifications.

F_Q can be increased with decreasing power as shown in the Technical Specifications. Increasing $F_{\Delta H}^N$ with decreasing power is permitted by DNB protection setpoints and allows radial power shape changes with rod insertion to the insertion limits as described in Section 3.4.3.2. Also, the $F_{\Delta H}$ limit in combination with the F_Q limit ensures compliance with the ECCS acceptance criteria. The permitted allowance for increased $F_{\Delta H}^N$ is:

$$F_{\Delta H}^N = 1.61\left[1 + 0.3(1 - P)\right]$$

Where:

$$P = \frac{\text{Thermal Power}}{\text{Rated Thermal Power}}$$

This becomes a design basis criterion which is used for establishing acceptable control rod patterns and control bank sequencing. Likewise, fuel-loading patterns for each cycle are selected with consideration of this design criterion. The worst values of $F_{\Delta H}^N$ for possible rod configurations occurring in normal operation are used in verifying that this criterion is met. Typical radial factors are given in Table 3.3-2 and the radial power distributions are shown in Figures 3.3-7 through 3.3-11. The worst values generally occur when the rods are assumed to be at their insertion limits. Maintenance of constant axial offset control establishes rod positions, which are above the allowed rod insertion limits thus providing increased margin to the $F_{\Delta H}^N$ criterion. As discussed in Section 3.2 of Reference (9), it has been determined that provided the above conditions are observed, the Technical Specification limits, are met. These limits are taken as input to the thermal-hydraulic design basis as described in Section 3.4.

When a situation is possible in normal operation which could result in local power densities in excess of those assumed as the precondition for a subsequent hypothetical accident, but which would not itself cause fuel failure, administrative controls and alarms are provided for returning the core to a safe condition. These alarms are described in detail in Chapter 7.

3.3.2.2.8 Reactor Protection System Setpoints

To determine Reactor Protection System setpoints, with respect to power distributions, three categories of events are considered, namely rod control equipment malfunctions, operator errors of commission and operator errors of omission. In evaluating these three categories of events the core is assumed to be operating within four constraints for normal plant operation described before in Section 3.3.2.2.5.

The first category comprises uncontrolled rod withdrawal (with rods moving in the normal bank sequence) of full-length banks. Also included are motions of the full-length banks below their insertion limits, which would be caused, for example, by uncontrolled dilution with manual rod control or primary coolant cooldown. Power distributions were calculated throughout these occurrences assuming short-term corrective action, that is no transient xenon effects were considered to result from the malfunction. The event was assumed to occur from typical normal operating situations, which did include normal xenon transients. It was further assumed in determining the power distributions that total power level would be limited by reactor trip to below 118 percent. Since the study is to determine protection limits with respect to power and axial offset, no credit was taken for trip setpoint reduction due to flux difference. Typical results are given in Figure 3.3-21 in units of kW/ft. Assuming the reactor trip function limits the maximum core power to below 118 percent, results show that the peak power density that can be achieved will be considerably less than 22.0 kw/ft, including uncertainties and densification effects. The peak linear power for the prevention of fuel centerline melt is less than 22.0 kw/ft. The second category, also appearing in Figure 3.3-21, assumes that the operator mispositions the full length rod bank in violation of the insertion limits and creates short term conditions not included in normal operating conditions.

The third category assumes a flux difference violation can occur because of erroneous boration/dilutions with automatic rod control either due to a system malfunction or to an operator error. The peak power density results shown on Figure 3.3-22 include uncertainties, densification effects, and a 2 percent allowance for calorimetric error. (This original 2 percent allowance applied to Figure 3.3-22 remains preserved following the MUR power uprate, since the sum of a) the increase in Rated Thermal Power and b) the reduced calorimetric error allowance remains within 2 percent.) The figure shows that provided the assumed error in operation does not continue for a period which is long compared to the xenon time constant, the maximum local power does not exceed the centerline melt criteria of 22.0 kw/ft (see Section 3.4.1.2) including the above factors. Since the peak kW/ft is below the above limits, no flux difference penalties are required for overpower protection. It should be noted that a reactor

overpower accident is not assumed to occur coincident with an independent operator error. Additional detailed discussion of these analyses is presented in Reference (7).

3.3.2.2.9 Experimental Verification of Power Distribution Analysis

This subject is discussed in depth in Reference (2). A summary of this report is given here. It should be noted that power distribution-related measurements are incorporated into the evaluation of calculated power distribution information, using an incore instrumentation processing code described in Reference (25). The measured-versus-calculated comparison is normally performed periodically throughout the cycle lifetime of the core, as required by the Technical Specifications.

In a measurement of the heat flux hot channel factor, F_Q, with the movable detector system, the following uncertainties must be considered:

1. Reproducibility of the measured signal.
2. Errors in the calculated relationship between detector current and local flux.
3. Errors in the calculated relationship between detector flux and peak rod power some distance from the measurement thimble.

The appropriate allowance for category l above has been quantified by repetitive measurements made with several intercalibrated detectors by using the common thimble features of the incore detector system. This system allows more than one detector to access any thimble. Errors in category 2 above are quantified to the extent possible, by using the fluxes measured at one thimble location to predict fluxes at another location which is also measured. Local power distribution predictions are verified in critical experiments on arrays of rods with simulated guide thimbles, control rods, burnable poisons, etc. These critical experiments provide quantification of error of types 2 and 3 above.

Reference (2) describes critical experiments performed at the Westinghouse Reactor Evaluation Center and measurements taken on two Westinghouse plants with incore systems of the same type as used in the plant described herein. The report concludes that the uncertainty associated with the peak nuclear heat flux factor, F_Q is less than 5 percent at the 95 percent confidence level with only 5 percent of the measurements greater than the inferred value. This is the equivalent of a 1.645σ limit on a normal distribution and is the uncertainty to be associated with a full core flux map with movable detectors reduced with a reasonable set of input data incorporating the influence of burnup on the radial power distribution. The uncertainty is usually rounded up to 5 percent.

In comparing measured power distributions (or detector currents) against the calculations for the same situation, it is not possible to subtract out the detector reproducibility. Thus a comparison between measured and predicted power distributions has to include some measurement error. Such a comparison is given in Figure 3.3-23 for one of the maps used in Reference (2). Since the first publication of the report, hundreds of maps have been taken on these and other reactors. The results confirm the adequacy of the 5 percent uncertainty allowance on F_Q.

A similar analysis for the uncertainty in $F_{\Delta H}$ (rod integral power) measurements results in an allowance of less than 4 percent at the equivalent of a 1.645σ confidence level. For historical reasons an 8 percent uncertainty factor is allowed in the nuclear design basis; that is, the predicted rod integrals at full power must not exceed the design $F_{\Delta H}$ less 8 percent.

A measurement of the axial power distribution in the second cycle of a 121 assembly, 12 foot, core is compared with a simplified one dimensional core average axial calculation in Figure 3.3-24. This calculation does not give explicit representation to the fuel grids.

The accumulated data on power distributions in actual operation is basically of three types:

1. Much of the data is obtained in steady-state operation at constant power in the normal operating configuration.
2. Data with unusual values of axial offset are obtained as part of the excore detector calibration procedure which is performed quarterly.
3. Special tests have been performed in load follow and other transient xenon conditions which have yielded useful information on power distributions.

These data are presented in detail in Reference (7). Figure 3.3-25 contains a summary of measured values of F_Q as a function of axial offset for five plants from that report.

3.3.2.2.10 Testing

An extensive series of physics tests is performed at the start of each cycle prior to the power ascension. These tests and the criteria for satisfactory results are described in detail in Chapter 13. Since not all limiting situations can be created at beginning-of-life, the main purpose of the tests is to provide a check on the calculational methods used in the predictions for the conditions of the test.

3.3.2.2.11 Monitoring Instrumentation

The adequacy of instrument numbers, spatial deployment, required correlations between readings and peaking factors, calibration and errors are described in References (2), (6), and (9). The relevant conclusions are summarized here in Sections 3.3.2.2.9 and 3.4.5.

Provided the limitations given in Section 3.3.2.2.5 on rod insertion and flux difference are observed, the excore detector system provides adequate monitoring of power distributions.

Further details of specific limits on the observed rod positions and flux difference, as well as reactor trips, are given in the Technical Specifications and associated bases. Descriptions of the systems provided are given in Chapter 7.

3.3.2.3 Reactivity Coefficients

The kinetic characteristics of the reactor core determine the response of the core to changing plant conditions or to operator adjustments made during normal operation, as well as the core response during abnormal or accidental transients. These kinetic characteristics are quantified in reactivity coefficients. The reactivity coefficients reflect the changes in the neutron multiplication due to varying plant conditions such as power, moderator or fuel temperatures, or less significantly due to a change in pressure or void conditions. Since reactivity coefficients change during the life of the core, ranges of coefficients are employed in transient analysis to determine the response of the plant throughout life. The results of such simulations are presented in Chapter 14. The reactivity coefficients are calculated on a corewise basis by nodal analysis methods. The effect of radial and axial power distribution on core average reactivity coefficients is implicit in those calculations and is not significant under normal operating conditions. For example, a skewed xenon distribution which results in changing axial offset by 5 percent changes the moderator and Doppler temperature coefficients by less than 0.01 pcm/°F and 0.03 pcm/°F, respectively. An artificially skewed xenon distribution which results in changing the radial $F^N_{\Delta H}$ by 3 percent changes the moderator and Doppler temperature coefficients by less than 0.03 pcm/°F and 0.001 pcm/°F, respectively. The spatial effects are accentuated in some transient conditions; for example, in postulated rupture of the main steam line break and rupture of RCCA mechanism housing described in Chapter 14 and are included in these analyses.

The analytical methods and calculational models used in calculating the reactivity coefficients are described in Section 3.3.3. These models have been confirmed through extensive testing of more than 30 cores similar to the plant described herein; results of these tests are referenced in Section 3.3.3.

Quantitative information for calculated reactivity coefficients, including fuel-Doppler coefficient, moderator coefficients (density, temperature, pressure, void) and power coefficient is given in the following sections.

3.3.2.3.1 Fuel Temperature (Doppler) Coefficient

The fuel temperature (Doppler) coefficient is defined as the change in reactivity per degree change in effective fuel temperature and is primarily a measure of the Doppler broadening of U-238 and Pu-240 resonance absorption peaks. Doppler broadening of other isotopes such as U-236 and Np-237 is also considered but their contributions to the Doppler effect is small. An increase in fuel temperature increases the effective resonance absorption cross sections of the fuel and produces a corresponding reduction in reactivity.

The fuel temperature coefficient is calculated by performing two group x-y and x-y-z calculations using the ANC (Reference 3) Code. Moderator temperature is held constant and the power level is varied. Spatial variation of fuel temperature is taken into account by calculating the effective fuel temperature as a function of power density as discussed in Section 3.3.3.1.

An example Doppler temperature coefficient (which includes redistribution effects) is shown in Figure 3.3-26 as a function of the effective fuel temperature (at beginning-of-life and end-of-life conditions). The effective fuel temperature is lower than the volume averaged fuel temperature since the neutron flux distribution is non-uniform through the pellet and gives preferential weight to the surface temperature. An example Doppler-only contribution to the power coefficient, defined later, is shown in Figure 3.3-27 as a function of relative core power. The integral of the differential curve on Figure 3.3-27 is the Doppler contribution to the power defect and is shown in Figure 3.3-28 as a function of relative power. The Doppler coefficient becomes more negative as a function of life as the Pu-240 content increases, thus increasing the Pu-240 resonance absorption but the overall value becomes less negative since the fuel temperature changes with burnup as described in Section 3.3.3.1.

3.3.2.3.2 Moderator Coefficients

The moderator coefficient is a measure of the change in reactivity due to a change in specific coolant parameters such as density, temperature, pressure or void. The coefficients so obtained are moderator density, temperature, pressure and void coefficients.

Moderator Density and Temperature Coefficients

The moderator temperature (density) coefficient is defined as the change in reactivity per degree change in the moderator temperature. Generally, the effect of the changes in moderator density as well as the temperature are considered together. A decrease in moderator density means less moderation which results in a negative moderator coefficient. An increase in coolant temperature, keeping the density constant, leads to a hardened neutron spectrum and results in an increase in resonance absorption in U-238, Pu-240 and other isotopes. The hardened spectrum

also causes a decrease in the fission to capture ratio in U-235 and Pu-239. Both of these effects make the moderator coefficient more negative. Since water density changes more rapidly with temperature as temperature increases, the moderator temperature (density) coefficient becomes more negative with increasing temperature.

The soluble boron used in the reactor as a means of reactivity control also has an effect on moderator density coefficient since the soluble boron absorber density as well as the water density is decreased when the coolant temperature rises. A decrease in the soluble absorber concentration introduces a positive component in the moderator coefficient. Thus, if the concentration of soluble absorber is large enough, the net value of the coefficient may be positive. With the presence of sufficient numbers of IFBA fuel rods, or discrete burnable absorber rods, the initial hot boron concentration is sufficiently low that the moderator temperature coefficient is negative at full power operating temperatures. The effect of control rods on the moderator coefficient is dependent on factors such as the core loading pattern and cycle burnup, although the reduction in required soluble boron concentration to offset control rod insertion in order to maintain criticality will tend to make the moderator coefficient more negative. With burnup, the moderator coefficient becomes more negative primarily as a result of boric acid dilution but also to a significant extent from the effects of the buildup of plutonium and fission products.

The moderator coefficient is calculated for the various plant conditions discussed above by performing two group X-Y and X-Y-Z calculations, varying the moderator temperature (and density) by about ± 5°F about each of the mean temperatures. An example moderator coefficient is shown as a function of core temperature and boron concentration for the unrodded and rodded core in Figures 3.3-29 through 3.3-31. The temperature range covered is from cold (68°F) to about 600°F. The contribution due to Doppler coefficient (because of change in moderator temperature) has been subtracted from these results. Figure 3.3-32 shows the typical hot, full power moderator temperature coefficient plotted as a function of cycle exposure for the ARO critical boron concentration condition based on the design boron letdown condition.

The moderator coefficients presented here are calculated on a corewide basis, since they are used to describe the core behavior in normal and accident situations when the moderator temperature changes can be considered to affect the whole core.

Moderator Pressure Coefficient

The moderator pressure coefficient relates the change in moderator density, resulting from a reactor coolant pressure change, to the corresponding effect on neutron production. This coefficient is of much less significance in comparison with the moderator temperature

coefficient. A change of 50 psi in pressure has approximately the same effect on reactivity as a half-degree change in moderator temperature. This coefficient can be determined from the moderator temperature coefficient by relating change in pressure to the corresponding change in density. The moderator pressure coefficient may be negative over a portion of the moderator temperature range at beginning-of-life (-0.004 pcm/psi, BOL) but is always positive at operating conditions and becomes more positive during life (+0.3 pcm/psi, EOL).

Moderator Void Coefficient

The moderator void coefficient relates the change in neutron multiplication to the presence of voids in the moderator. In a PWR this coefficient is not very significant because of the low void content in the coolant. The core void content is less than 1/2 of 1 percent and is due to local or statistical boiling. The void coefficient varies from 50 pcm/percent void at BOL and at low temperatures to -250 pcm/percent void at EOL and at operating temperatures. The negative void coefficient at operating temperature becomes more negative with fuel burnup.

3.3.2.3.3 Power Coefficient

The combined effect of moderator temperature and fuel temperature change as the core power level changes is called the total power coefficient and is expressed in terms of reactivity change per percent power change. An example of total power coefficient at BOL and EOL conditions based on two group X-Y calculations is given in Figure 3.3-33. It becomes more negative with burnup reflecting the combined effect of moderator and fuel temperature coefficients with burnup. An example power defect (integral reactivity effect) at BOL and EOL is given in Figure 3.3-34.

3.3.2.3.4 Comparison of Calculated and Experimental Reactivity Coefficients

Section 3.3.3 references the comparison of calculated and experimental reactivity coefficients in detail. Based on the data presented there, the accuracy of the current analytical model is:

±0.2 percent for $\Delta\rho$ Doppler and power defect

±2 pcm/°F for the moderator coefficient

Experimental evaluation of the calculated coefficients is performed during the physics startup tests described in Chapter 13.

3.3.2.3.5 Reactivity Coefficients Used in Transient Analysis

Table 3.3-2 gives the limiting values as well as typical best estimate values for the reactivity coefficients. The limiting values are used as design limits in the transient analysis. The exact values of the coefficient used in the analysis depend on whether the transient of interest is

examined at the beginning or end-of-life, whether the most negative or the most positive (least negative) coefficients are appropriate, and whether spatial non-uniformity must be considered in the analysis. Conservative values of coefficients, considering various aspects of analysis are used in the transient analysis. This is described in Chapter 14.

The reactivity coefficients shown in Figures 3.3-26 through 3.3-34 are typical best-estimate values. The limiting values shown in Table 3.3-2 are chosen to encompass the best estimate reactivity coefficients, including the appropriate uncertainties, over appropriate operating conditions calculated for this cycle and the expected values for the subsequent cycles. The most positive as well as the most negative values are selected to form the design basis range used in the transient analysis. A direct comparison of the best estimate and design limit values shown in Table 3.3-2 can be misleading since in many instances, the most conservative combination of reactivity coefficients is used in the transient analysis even though the extreme coefficients assumed may not simultaneously occur at the conditions of lifetime, power level, temperature and boron concentration assumed in the analysis.

The need for a re-evaluation of any accident in a subsequent cycle is contingent upon whether or not the coefficients for that cycle fall within the identified range used in the analysis presented in Chapter 14 with due allowance for the appropriate calculational uncertainties. Control rod requirements are given in Table 3.3-3 for a typical core. These numbers are provided for information only and their validity in a particular cycle would be an unexpected coincidence.

3.3.2.4 Control Requirements

To ensure the shutdown margin stated in the Technical Specifications under conditions where a cooldown to ambient temperature is required, concentrated soluble boron is added to the coolant. Boron concentrations for several core conditions are listed in Table 3.3-2. For all core conditions including refueling, the boron concentration is well below the solubility limit. The rod cluster control assemblies are employed to bring the reactor to the hot shutdown condition. The minimum required shutdown margin is given in the Technical Specifications.

The ability to accomplish the shutdown for hot conditions is demonstrated in Table 3.3-3 by comparing the difference between the rod cluster control assembly reactivity available with an allowance for the worst stuck rod with that required for control and protection purposes. The shutdown margin includes an allowance of 10 percent for analytic uncertainties. The largest reactivity control requirement appears at the end-of-life when the moderator temperature coefficient reaches its peak negative value as reflected in the larger power defect.

The control rods are required to provide sufficient reactivity to account for the power defect from full power to zero power and to provide the required shutdown margin. The reactivity addition resulting from power reduction consists of contributions from Doppler, variable average moderator temperature, flux redistribution, and reduction in void content as discussed below. It should be noted that, in the current methodology for calculating shutdown margin, these components are not all calculated separately – each component is implicitly accounted for directly in the shutdown margin calculation (with the exception of the void component which is added separately).

3.3.2.4.1 Doppler

The Doppler effect arises from the broadening of U-238 and Pu-240 resonance peaks with an increase in effective pellet temperature. This effect is most noticeable over the range of zero power to full power due to the large pellet temperature increase with power generation.

3.3.2.4.2 Variable Average Moderator Temperature

When the core is shutdown to the hot, zero power condition, the average moderator temperature changes from the equilibrium full load value determined by the steam generator and turbine characteristics (steam pressure, heat transfer, tube fouling, etc.) to the equilibrium no-load value, which is based on the steam generator shell side design pressure. The shutdown margin calculation effectively allows for a conservatively large change in temperature to account for the control dead band and measurement errors.

The moderator coefficient becomes more negative as the fuel depletes because the boron concentration is reduced. This effect is the major contributor to the increased requirement at end-of-life.

3.3.2.4.3 Redistribution

During full power operation the coolant density decreases with core height, and this, together with partial insertion of control rods, results in less fuel depletion near the top of the core. Under steady-state conditions, the relative power distribution will be slightly asymmetric towards the bottom of the core. On the other hand, at hot zero power conditions, the coolant density is uniform up the core, and there is no flattening due to Doppler. The result will be a flux distribution which at zero power can be skewed toward the top of the core. The reactivity insertion due to the skewed distribution and effects of xenon distribution are implicit in the shutdown margin calculation.

3.3.2.4.4 Void Content

A small void content in the core is due to nucleate boiling at full power. The void collapse coincident with power reduction makes a small reactivity contribution.

3.3.2.4.5 Rod Insertion Allowance

The control banks are operated within a prescribed band of travel to compensate for small periodic changes in boron concentration, changes in temperature and very small changes in the xenon concentration not compensated for by a change in boron concentration. When the control bank reaches either limit of this band, a change in boron concentration is required to compensate for additional reactivity changes. The withdrawal limit is an all rods out condition. From a shutdown margin viewpoint, the allowed depth of insertion of the control banks is a function of core power level and is dictated by the inserted worth not available for shutdown and the power defect to be overcome during shutdown from at-power operating conditions. The allowance for the net reactivity difference between the inserted rod worth not available for shutdown and the reduction in power defect to be overcome during shutdown is known as the Rod Insertion Allowance (RIA). The RIA is conservatively accounted for in the shutdown margin calculation by assuming the control banks are at their insertion limit prior to the shutdown.

3.3.2.4.6 Burnup

Excess reactivity of approximately 10 percent delta-rho (hot) is installed at the beginning of each cycle to provide sufficient reactivity to compensate for fuel depletion and fission products throughout the cycle. This reactivity is controlled by the addition of soluble boron to the coolant and by burnable poison. The soluble boron concentration for several core configurations and the unit boron worth are given in Table3.3-2. Since the excess reactivity for burnup is controlled by soluble boron and/or burnable absorbers, it is not included in control rod requirements.

3.3.2.4.7 Xenon and Samarium Poisoning

Changes in xenon and samarium concentrations in the core occur at a sufficiently slow rate, even following rapid power level changes, that the resulting reactivity change is controlled by changing the soluble boron concentration.

3.3.2.4.8 pH Effects

Changes in reactivity due to a change in coolant pH, if any, are sufficiently small in magnitude and occur slowly enough to be controlled by the boron system. Further details are available in Reference (11).

3.3.2.5 Control

Core reactivity is controlled by means of a chemical poison dissolved in the coolant, rod cluster control assemblies, and IFBAs as described below.

3.3.2.5.1 Chemical Poison

Boron in solution as boric acid is used to control relatively slow reactivity changes associated with:

1. The moderator temperature defect in going from cold shutdown at ambient temperature to the hot operating temperature at zero power.
2. The transient xenon and samarium poisoning, such as that following power changes or changes in rod cluster control position.
3. The excess reactivity required to compensate for the effects of fissile inventory depletion and buildup of long-life fission products.
4. The burnable absorber depletion.

The boron concentrations for various core conditions are presented in Table 3.3-2.

3.3.2.5.2 Rod Cluster Control Assemblies

One type of rod cluster control assemblies is employed: full length assemblies as shown in Table 3.3-1. The full-length rod cluster control assemblies are used for shutdown and control purposes to offset fast reactivity changes associated with:

1. The required shutdown margin in the hot zero power, stuck rods condition.
2. The reactivity compensation as a result of an increase in power above hot zero power (power defect including Doppler, and moderator reactivity changes).
3. Unprogrammed fluctuations in boron concentration, coolant temperature, or xenon concentration (with rods not exceeding the allowable rod insertion limits).
4. Reactivity ramp rates resulting from load changes.

The allowed full-length control bank reactivity insertion is limited at full power to maintain shutdown capability. As the power level is reduced, control rod reactivity requirements are also reduced and more rod insertion is allowed. The control bank position is monitored and the operator is notified by an alarm if the limit is approached. The determination of the insertion limit uses conservative xenon distributions and axial power shapes. In addition, the rod cluster control assembly withdrawal pattern determined from these analyses is used in determining power distribution factors and in determining the maximum worth of an inserted rod cluster control assembly ejection accident.

Power distribution, rod ejection and rod misalignment analyses are based on the arrangement of the shutdown and control groups of the rod cluster control assemblies shown in Figure 3.3-35. All shutdown bank rod cluster control assemblies are withdrawn before withdrawal of the control banks is initiated. In going from zero to 100 percent power, control banks A, B, C and D are withdrawn sequentially. The limits of rod positions and further discussion on the basis for rod insertion limits are provided in the Technical Specifications and associated bases.

3.3.2.5.3 Integral Fuel Burnable Absorber (IFBA)

The IFBA coating on the fuel pellets provides partial control of the excess reactivity available during the beginning of the fuel cycle. In doing so, the burnable absorber prevents the moderator temperature coefficient from violating safety limits at normal operating conditions. The burnable absorber performs this function by reducing the requirement for soluble poison in the moderator at the beginning of the fuel cycle as described previously. For purposes of illustration, a typical IFBA pattern in the core together with the number of IFBA pins per assembly are shown in Figure 3.3-5, while example arrangements within an assembly are displayed in Figure 3.3-4. As can be seen in Figure 3.3-1, the IFBA coating on the fresh fuel is usually part-length (and possibly offset relative to the fuel centerline). The burnable absorber is usually part-length to allow a better (flatter) axial power distribution in the core. The ZrB_2 coating on the fuel pellets is depleted with burnup, but at a sufficiently slow rate so that the resulting critical concentration of soluble boron is such that the moderator temperature coefficient remains within safety limits at all times for power operating conditions.

3.3.2.5.4 Peak Xenon Startup

Compensation for the peak xenon buildup is accomplished using the boron control system. Startup from the peak xenon condition is accomplished with a combination of rod motion and boron dilution. The boron dilution may be made at any time, including during the shutdown period, provided the shutdown margin is maintained.

3.3.2.5.5 Load Follow Control and Xenon Control

During load follow maneuvers, power changes are accomplished using control rod motion and dilution or boration by the boron system as required. Control rod motion is limited by the control rod insertion limits on full-length rods as provided in the Technical Specifications and discussed in Section 3.3.2.5.2.

3.3.2.5.6 Burnup

Control of the excess reactivity for burnup is accomplished using soluble boron and/or burnable absorber. The boron concentration must be limited during operating conditions to ensure the

moderator temperature coefficient is within safety limits. Sufficient burnable absorber is installed at the beginning of a cycle to give the desired cycle lifetime without exceeding the boron concentration limit. The practical minimum boron concentration is approximately 10 ppm.

3.3.2.6 Control Rod Patterns and Reactivity Worth

The full-length rod cluster control assemblies are designated by function as the control groups and the shutdown groups. The terms "group" and "bank" are used synonymously throughout this report to describe a particular grouping of control assemblies. The rod cluster assembly pattern is displayed in Figure 3.3-35. In Nuclear Design terminology, the control banks are labeled A, B, C and D and the shutdown banks are labeled SA, SB, SC, and SD. Each bank, although operated and controlled as a unit, is comprised of two subgroups except banks SC and SD which are each a single group. The axial position of the full-length rod cluster control assemblies may be controlled manually or automatically. The rod cluster control assemblies are all dropped into the core following actuation of reactor trip signals.

Two criteria have been employed for selection of the control groups. First, the total reactivity worth of all (control and shutdown) banks must be adequate to meet the requirements specified in Table 3.3-3. Second, in view of the fact that certain control banks may be partially inserted at power operation, the total power peaking factor should be low enough to ensure that peaking factor limits and power capability requirements are met. Analyses indicate that the first requirement can be met either by a single control group or by two or more control banks with sufficiently high total worth (in addition to the worth of the shutdown banks). The axial power shape would be more peaked following movement of a single group of rods worth three to four percent $\Delta\rho$; therefore, four control banks (described as A, B, C and D in Figure 3.3-35) each worth approximately one percent $\Delta\rho$ have been selected. The worth of each bank is dependent to some extent on the fuel placement in the core typical control bank worths are shown in Table 3.3-2.

The position of control banks for criticality under any reactor condition is determined by the concentration of boron in the coolant. On an approach to criticality boron is adjusted to ensure that criticality will be achieved with control rods above the insertion limit set by shutdown and other considerations (see the Technical Specifications).

Early in the cycle there may also be a withdrawal limit at low power to maintain the moderator temperature coefficient within safety limits.

Ejected rod worths are given in Section 14.2.6 for several different conditions. Experimental confirmation of these worths can be found by reference to startup test reports such as Reference (12).

The allowable misalignment of control rods is stated in the Technical Specifications.

Calculation of control rod reactivity worth versus time following reactor trip involves both control rod velocity and differential reactivity worth. For nuclear design purposes, the reactivity worth versus rod position is calculated by a series of steady-state calculations at various control rod positions assuming all rods out of the core as the initial position in order to minimize the initial reactivity insertion rate. Also to be conservative, the rod of highest worth is assumed stuck out of the core and the flux distribution (and thus reactivity importance) is assumed to be skewed to the bottom of the core. Further discussion is provided in Section 14.

The shutdown groups provide additional negative reactivity to assure an adequate shutdown margin. Shutdown margin is defined as the amount by which the core would be subcritical at hot standby if all rod cluster control assemblies are tripped, but assuming that the highest worth assembly remains fully withdrawn and no changes in xenon or boron takes place. The loss of control rod worth due to the material irradiation is negligible since only bank D is in the core under normal full power operating conditions.

The values given in Table 3.3-3 show that the available reactivity in withdrawn rod cluster control assemblies provides the design basis minimum shutdown margin allowing for the highest worth cluster to be at its fully withdrawn position. All allowance for uncertainty in the calculated worth of N-1 rods is made before determination of the shutdown margin.

3.3.2.7 Stability

3.3.2.7.1 Introduction

The stability of the PWR cores against xenon-induced spatial oscillations and the control of such transients are discussed extensively in References (6), (13), (14) and (15). A summary of these reports is given in the following discussion and the design bases are given in Section 3.3.1.6.

In a large reactor core, xenon-induced oscillations can take place with no corresponding change in the total power of the core. The oscillation may be caused by a power shift in the core, which occurs rapidly by comparison with the xenon-iodine time constants. Such a power shift occurs in the axial direction when a plant load change is made by control rod motion and results in a change in the moderator density and fuel temperature distributions. Such a power shift could occur in the diametral plane of the core as a result of abnormal control action.

Due to the negative power coefficient of reactivity, PWR cores are inherently stable to oscillations in total power. Protection against total power instabilities is provided by the control and protection system as described in Chapter 7. Hence, the discussion on the core stability will be limited here to xenon-induced spatial oscillations.

3.3.2.7.2 Stability Index

Power distributions, either in the axial direction or in the X-Y plane, can undergo oscillations due to perturbations introduced in the equilibrium distributions without changing the total core power. The xenon-induced oscillations are essentially limited to the first flux overtones in the current PWRs, and the stability of the core against xenon-induced oscillations can be determined in terms of the eigenvalues of the first flux overtones. Writing, either in the axial direction or in the X-Y plane, the eigenvalue Σ of the first flux harmonic as:

$$\Sigma = b + ic, \tag{3.3-1}$$

then b is defined as the stability index and $T = 2\pi/c$ as the oscillation period of the first harmonic. The time-dependence of the first harmonic in the power distribution can now be represented as:

$$AO(t) = Ae^{\Sigma t} = ae^{bt}\cos(ct), \tag{3.3-2}$$

where A and a are constants. The stability index can also be obtained approximately by:

$$b = \frac{1}{T}\ln\frac{A_{n+1}}{A_n} \tag{3.3-3}$$

where A_n, A_{n+1} are the successive peak amplitudes of the oscillation and T is the time period between the successive peaks.

3.3.2.7.3 Prediction of the Core Stability

The stability of the core described herein (i.e., with 17 x 17 fuel assemblies) against xenon-induced spatial oscillations is expected to be equal to or better than that of earlier designs. The prediction is based on a comparison of the parameters which are significant in determining the stability of the core against the xenon-induced oscillations, namely 1) the overall core size is unchanged and spatial power distributions will be similar, 2) the moderator temperature coefficient is expected to be similar, and 3) the Doppler coefficient of reactivity is expected to be equal to or slightly more negative at full power.

The addition of axial blankets to VANTAGE 5 fuel, without reduced-length burnable absorber, improves stability to axial xenon oscillations by effectively shortening the core and increasing the axial peaking. Both conditions increase axial stability. The use of reduced-length burnable

absorbers with the VANTAGE 5 fuel design, without axial blankets, decreases axial xenon stability early in core life relative to an axially homogeneous design. This reduction in stability occurs because reduced-length burnable absorbers flatten the core axial power shape. Calculations indicate that as core burnup increases and reduced-length absorbers deplete, such a core becomes more stable than an axially homogeneous core due to a more center-peaked axial power distribution. Finally, the core containing both axial blankets and reduced-length burnable absorbers, while naturally unstable throughout core life, is more stable than the core with only axial blankets for the last half of the reload cycle. For more detail on this subject, see Reference (16).

Analysis of both the axial and X-Y xenon transient tests, discussed in Section 3.3.2.7.5, shows that the calculational model is adequate for the prediction of core stability.

3.3.2.7.4 Stability Measurements

1. Axial Measurements

   Two axial xenon transient tests conducted in a PWR with a core height of 12 feet and 121 fuel assemblies are reported in Reference (16) and will be briefly discussed here. The tests were performed at approximately 10 percent and 50 percent of cycle life.

   Both a free-running oscillation test and a controlled test were performed during the first test. The second test at mid-cycle consisted of a free-running oscillation test only. In each of the free-running oscillation tests, a perturbation was introduced to the equilibrium power distribution through an impulse motion of the control bank D and the subsequent oscillation period. In the controlled test conducted early in the cycle, the part length rods were used to follow the oscillations to maintain an axial offset within the prescribed limits. The axial offset of power was obtained from the excore ion chamber readings (which had been calibrated against the incore flux maps) as a function of time for both free-running tests as shown in Figure 3.3-36.

   The total core power was maintained constant during these spatial xenon tests, and the stability index and the oscillation period were obtained from a least-square fit of the axial offset data in the form of Equation (3.3-2). The axial offset of power is the quantity that properly represents the axial stability in the sense that it essentially eliminates any contribution from even order harmonics including the fundamental mode. The conclusions of the tests are:

a. The core was stable against induced axial xenon transients both at the core average burnups of 1550 MWD/MTU and 7700 MWD/MTU. The measured stability indices are -0.041 hr-1 for the first test (Curve 1 of Figure 3.3-40) and -0.014 hr-1 for the second test (Curve 2 of Figure 3.3-40). The corresponding oscillation periods are 32.4 hours and 27.2 hours, respectively.

b. The reactor core becomes less stable as fuel burnup progresses and the axial stability index was essentially zero at 12,000 MWD/MTU.

2. Measurements in the X-Y Plane

Two X-Y xenon oscillation tests were performed at a PWR plant with a core height of 12 feet and 157 fuel assemblies. The first test was conducted at a core average burnup of 1540 MWD/MTU and the second at a core average burnup of 12,900 MWD/MTU. Both of the X-Y xenon tests show that the core was stable in the X-Y plane at both burnups. The second test shows that the core became more stable as the fuel burnup increased and all Westinghouse PWR's with 121 and 157 assemblies are expected to be stable throughout their burnup cycles.

In each of the two X-Y tests, a perturbation was introduced to the equilibrium power distribution through an impulse motion of one rod cluster control unit located along the diagonal axis. Following the perturbation, the uncontrolled oscillation was monitored using the movable detector and thermocouple system and the excore power range detectors. The quadrant tilt difference (QTD) is the quantity that properly represents the diametral oscillation in the X-Y plane of the reactor core in that the differences of the quadrant average powers over two symmetrically opposite quadrants essentially eliminates the contribution to the oscillation from the azimuthal mode. The QTD data were fitted in the form of Equation (3.3-2) through a least-square method. A stability index of -0.076 hr^{-1} with a period of 29.6 hours was obtained from the thermocouple data shown in Figure 3.3-37.

It was observed in the second X-Y xenon test that the PWR core with 157 fuel assemblies had become more stable due to an increased fuel depletion and the stability index was not determined.

3.3.2.7.5 Comparison of Calculations with Measurements

The analysis of the axial xenon transient tests was performed in an axial slab geometry using a flux synthesis technique. The direct simulation of the axial offset was carried out using the PANDA Code (Reference 17). The analysis of the X-Y xenon transient tests was performed in an X-Y geometry using a modified TURTLE (Reference 10) Code. Both the PANDA and TURTLE codes solve the two-group time-dependent neutron diffusion equation with time-dependent xenon and iodine concentrations. The fuel temperature and moderator density feed back is limited to a steady-state model. All the X-Y calculations were performed in an average enthalpy plane.

The basic nuclear cross sections used in this study were generated from a unit cell depletion program, which was evolved from the codes LEOPARD (Reference 18) and CINDER (Reference 19). The detailed experimental data during the tests including the reactor power level, enthalpy rise and the impulse motion of the control rod assembly, as well as the plant follow burnup data were closely simulated in the study.

The results of the stability calculation for the axial tests are compared with the experimental data in Table 3.3-4. The calculations show conservative results for both of the axial tests with a margin of approximately -0.01 hr^{-1} in the stability index.

An analytical simulation of the first X-Y xenon oscillation test shows a calculated stability index of -0.081 hr^{-1}, in good agreement with the measured value of -0.076 hr^{-1}. As indicated earlier, the second X-Y xenon test showed that the core had become more stable compared to the first test and no evaluation of the stability index was attempted. This increase in the core stability in the X-Y plane due to increased fuel burnup is due mainly to the increased magnitude of the negative moderator temperature coefficient.

Previous studies of the physics of xenon oscillations, including three-dimensional analysis, are reported in the series of topical reports, References (13), (14) and (15). A more detailed description of the experimental results and analysis of the axial and X-Y xenon transient tests is presented in Reference (16) and Section 1 of Reference (20).

3.3.2.7.6 Stability Control and Protection

The excore detector system is utilized to provide indications of xenon-induced spatial oscillations. The readings from the excore detectors are available to the operator and also form part of the protection system.

1. Axial Power Distribution

   For maintenance of proper axial power distributions, the operator is instructed to maintain an axial offset within a prescribed operating band, based on the excore detector readings. Should the axial offset be permitted to move far enough outside this band, the protection limit will be reached and the power will be automatically reduced.

   Twelve foot PWR cores become less stable to axial xenon oscillations as fuel burnup progresses. However, free xenon oscillations are not allowed to occur except for special test. The full length control rod banks present in all modern Westinghouse PWR's are sufficient to dampen and control any axial xenon oscillations present. Should the axial offset be inadvertently permitted to move far enough outside the control band due to an axial xenon oscillation, or any other reason, the protection limit on axial offset will be reached and the power will be automatically reduced.

2. Radial Power Distribution

   The core described herein is calculated to be stable against X-Y xenon-induced oscillations at all times in life.

   The X-Y stability of large PWRs has been further verified as part of the startup physics test program for PWR cores with 193 fuel assemblies. The measured X-Y stability of the PWR cores with 157 and 193 assemblies was in good agreement with the calculated stability as discussed in Sections 3.3.2.7.4 and 3.3.2.7.5. In the unlikely event that X-Y oscillations occur, backup actions are possible and would be implemented, if necessary, to increase the natural stability of the core. This is based on the fact that several actions could be taken to make the moderator temperature coefficient more negative, which will increase the stability of the core in the X-Y plane.

   Provisions for protection against non-symmetric perturbations in the X-Y power distribution that could result from equipment malfunctions are made in the

protection system design. This includes control rod drop, rod misalignment and asymmetric loss of coolant flow.

A more detailed discussion of the power distribution control in PWR cores is presented in Reference (6) and (7).

3.3.2.8 Vessel Irradiation

A brief review of the methods and analyses used in the determination of neutron and gamma ray flux attenuation between the core and the pressure vessel is given below. A more complete discussion relative to the pressure vessel irradiation and the reactor vessel materials surveillance program is given in Chapter 4.

The materials that serve to attenuate neutrons originating in the core and gamma rays from both the core and from structural components located between the core and the pressure vessel consist of the fuel itself as well as the core baffle, core barrel, thermal shield and associated water annuli. The presence of these material zones serves to reduce the magnitude of the neutron and gamma ray flux at the pressure vessel as well as to significantly alter the energy spectra relative to those determined for the core region.

In general, few-group neutron diffusion theory codes are used to determine fission power density distributions within the active core, and the accuracy of these analyses is verified by incore measurements on operating reactors. Region and rodwise power-sharing information from the core calculations is then input as source information in two-dimensional discrete ordinates S_n transport calculations which are used to compute the neutron and gamma ray flux distributions throughout the core and vessel components.

In practice, 10 CFR 50, Appendix G and 10 CFR 50.61, which define the basis for the development of pressure temperature limit curves and the evaluation of pressure thermal shock (PTS) screening limits, require the use of best estimate neutron exposure calculations using actual fuel loading patterns. These best estimate evaluations are normally completed in conjunction with the evaluation of neutron dosimetry which is included as an integral part of the reactor vessel radiation surveillance program using the methods described in Chapter 4.

3.3.3 Analytical Methods

Calculations required in nuclear design consist of three distinct types, which are performed in sequence:

1. Determination of effective fuel temperatures.
2. Generation of macroscopic few-group parameters.
3. Space-dependent, few-group diffusion calculations.

These calculations are carried out by computer codes which can be executed individually, however, at Westinghouse most of the codes required have been linked to form an automated design sequence which minimizes design time, avoids errors in transcription of data, and standardizes the design methods.

3.3.3.1 Fuel Temperature (Doppler) Calculations

Temperatures vary radially within the fuel rod, depending on the heat generation rate in the pellet, the conductivity of the materials in the pellet, gap, and clad, and the temperature of the coolant.

The fuel temperatures for use in most nuclear design Doppler calculations are obtained from a simplified version of the Westinghouse fuel rod design model described in Section 3.2.1.3.1 which considers the effect of radial variation of pellet conductivity, expansion-coefficient and heat generation rate, elastic deflection of the clad, and a gap conductance which depends on the initial fill gap, the hot open gap dimension, and the fraction of the pellet over which the gap is closed. The fraction of the gap assumed closed represents an empirical adjustment used to produce good agreement with observed reactivity data at beginning-of-life. Further gap closure occurs with burnup and accounts for the decrease in Doppler defect with burnup which has been observed in operating plants.

Radial power distributions in the pellet as a function of burnup are obtained from LASER (Reference 21) calculations.

The effective U-238 temperature for resonance absorption is obtained from the radial temperature distribution by applying a radially dependent weighting function. The weighting function was determined from REPAD (Reference 22) Monte Carlo calculations of resonance escape probabilities in several steady-state and transient temperature distributions. In each case a flat pellet temperature was determined which produced the same resonance escape probability as the actual distribution. The weighting function was empirically determined from these results.

The effective Pu-240 temperature for resonance absorption is determined by a convolution of the radial distribution of Pu-240 densities from LASER burnup calculations and the radial weighting function. The resulting temperature is burnup dependent, but the difference between U-238 and Pu-240 temperatures, in terms of reactivity effects, is small.

The effective pellet temperature for pellet dimensional change is that value which produces the same outer pellet radius in a virgin pellet as that obtained from the temperature model. The effective clad temperature for dimensional change is its average value.

The temperature calculational model has been validated, by plant Doppler defect data as shown in Table 3.3-6, and Doppler coefficient data as shown in Figure 3.3-38. Stability index measurements also provide a sensitive measure of the Doppler coefficient near full power (see Section 3.3.2.8). It can be seen that Doppler defect data is typically within ±0.2 percent $\Delta\rho$ of prediction.

3.3.3.2 Macroscopic Group Constants

Macroscopic few-group constants and analogous microscopic cross sections (needed for feedback and microscopic depletion analysis) are generated by PHOENIX-P (Reference 3). PHOENIX-P is a two-dimensional, multi-group transport theory code, which has been approved by the USNRC. The nuclear cross-section library used by PHOENIX-P contains cross-section data based on a 70 energy-group structure derived from ENDF/B-VI files (Reference 30). The solution of the flux distribution is divided into two major steps in PHOENIX-P:

1. Solve for two-dimensional, 70 energy-group nodal fluxes which couples individual subcell regions (pellet, clad, moderator) as well as surrounding pins using a method based on collision probabilities and heterogeneous response flux which has been described in detail in Reference (27).
2. Solve for a coarse energy-group flux distribution using a standard S-4 discrete ordinates calculation and use these fluxes to normalize the detailed 70 group nodal fluxes from Step 1.

PHOENIX-P is capable of modeling all cell types necessary for PWR design applications. Nodal group constants (two group) are obtained by flux-volume homogenization of the fuel cells (including IFBA pins), guide thimbles, instrumentation thimbles, and interassembly gaps using the PHOENIX-P coarse energy-group flux distribution. Group constants for control rods are calculated in a similar manner. Validation of the cross section method is based on analysis of critical experiments, isotopic data, plant critical boron values at HZP, and at HFP conditions as a

function of burnup as discussed in detail in Reference (27). Control rod worth measurements are also discussed in the reference.

3.3.3.3 Spatial Few-Group Diffusion Calculations

Spatial few-group calculations consist primarily of two-group X-Y-Z and X-Y calculations using the Advanced Nodal Code (ANC) (Reference 27). ANC utilizes a nodal expansion method to solve the two-group diffusion equations. With this method, the partial currents and average neutron fluxes for a node are determined from continuous homogeneous neutron flux profiles described by fourth order polynomial expansions for each of the X, Y, and Z directions across the node. Discontinuity factors are used to modify the homogeneous cross-sections to preserve the node surface fluxes and currents that would be obtained from an equivalent heterogeneous model. ANC also employs a pin-power recovery process, which utilizes an analytical solution to the two-group diffusion equations coupled with pin power information from the discrete model (PHOENIX-P) applied to the calculated node average power.

The usage of ANC is in safety analysis calculations in X-Y-Z and X-Y geometry, X-Y-Z power and burnup distributions, critical boron concentrations, control bank worths, and reactivity coefficients and defects.

Axial calculations are performed using the APOLLO code (Reference 29). APOLLO is used to determine differential control rod worth curves (reactivity versus rod insertion) and to demonstrate load follow capability. Group constants for APOLLO are obtained from the three-dimensional nodal model by flux-volume weighting on an axial slicewise basis. Radial bucklings are determined by varying parameters in the buckling model while forcing the one-dimensional model to produce the axial characteristics (axial offset, midplane power) of the three-dimensional model.

Validation of the spatial codes for calculating power distributions involves the use of incore and excore detectors and is discussed in Section 3.3.2.2.9.

3.3.4 References For Section 3.3

1. Adler, M. R., "AMSAC Generic Design Package," WCAP-10858 P-A Rev.1, July 1987 (Proprietary) and WCAP-11293-A Rev.1 July 1987 (Non-Proprietary).
2. Spier, E. M. and Nguyen, T. Q., "Evaluation of Nuclear Hot Channel Factor Uncertainties," WCAP-7308-L-P-A, (Proprietary) and WCAP-7308-L-A, (Non-Proprietary), June 1988.
3. Nguyen, T. Q., et. al., "Qualification of the PHOENIX-P/ANC Nuclear Design System for Pressurized Water Reactor Cores," WCAP-11597-A, June 1988.
4. Deleted
5. Hellman, J. M. and Yang, J. W., "Effects of Fuel Densification Power Spikes on Clad Thermal Transients," WCAP-8359, July, 1974.
6. Moore, J. S., "Power Distribution Control of Westinghouse Pressurized Water Reactors," WCAP-7208, September, 1968 (Proprietary) and WCAP-7811, December, 1971 (Non-Proprietary).
7. Morita, T., et al., "Power Distribution Control and Load Follow Procedures," WCAP-8385, September, 1974 (Proprietary) and WCAP-8403, September, 1974 (Non-Proprietary).
8. Morita, T. and Lucoff, D. M., "Calculational Methods for Prediction of Elevation - Dependent Radial Power Peaking Factor," WCAP-8718 (Proprietary) and WCAP-8719, (Non-Proprietary).
9. McFarlane, A. F., "Power Peaking Factors," WCAP-7912-P-A, January, 1975 (Proprietary) and WCAP-7912-A, January, 1975 (Non-Proprietary).
10. Altomare, S. and Barry, R. F., "The TURTLE 24.0 Diffusion Depletion Code," WCAP-7213-P-A, January, 1975 (Proprietary) and WCAP-7758-A, January, 1975 (Non-Proprietary).
11. Cermak, J. O., et al., "Pressurized Water Reactor Ph - Reactivity Effect Final Report," WCAP-3696-8, (EURAEC-2074), October, 1968.
12. Outzs, J. E., "Plant Startup Test Report, H. B. Robinson Unit No. 2," WCAP-7844, January, 1972.
13. Poncelet, C. G., and Christie, A. M., "Xenon-Induced Spatial Instabilities In Large PWRs," WCAP-3680-20, (EURAEC-1974), March, 1968.

14. Skogen, F. B. and McFarlane, A. F., "Control Procedures for Xenon-Induced X-Y Instabilities in Large PWRs," WCAP-3680-21, (EURAEC-2111), February, 1969.

15. Skogen, F. B. and McFarlane, A. F., "Xenon-Induced Spatial Instabilities in Three-Dimensions," WCAP-3680-22, (EURAEC-2116), September, 1969.

16. Lee, J. C., et al., "Axial Xenon Transient Tests at the Rochester Gas and Electric Reactor," WCAP-7964, June, 1971.

17. Barry, R. F., et al., "The PANDA Code," WCAP-7048-P-A, January, 1975 (Proprietary) and WCAP-7757-A, January, 1975 (Non-Proprietary).

18. Barry, R. F., "LEOPARD, A Spectrum Dependent Non-Spatial Depletion Code for the IBM-7094," WCAP-3269-26, September, 1963.

19. England, T. R., "CINDER, A One-Point Depletion and Fission Product Program," WAPD-TM-334, August, 1962.

20. Eggleston, F. T., "Safety-Related Research and Development for Westinghouse Pressurized Water Reactors, Program Summaries," Latest revision.

21. Poncelet, C. G., "LASER, A Depletion Program for Lattice Calculations Based on MUFT and THERMOS," WCAP-6073, April, 1966.

22. Olhoeft, J. E., "The Doppler Effect for a Non-Uniform Temperature Distribution in Reactor Fuel Elements," WCAP-2048, July, 1962.

23. Deleted.

24. Kersting, P.J. et al., “Assessment of Clad Flattening and Densification Power Spike Factor Elimination in Westinghouse Nuclear Fuel”, WCAP-13589-A, March 1995 (Proprietary) and WCAP-14297-A, March 1995 (Non-Proprietary).

25. Meyer, C. E. and Stover, R. L., "Incore Power Distribution Determination in Westinghouse Pressurized Water Reactors," WCAP-8498, July 1975.

26. Deleted.

27. Liu, Y.S. et. al. “ANC: A Westinghouse Advanced Nodal Computer Code”, WCAP-10965-P-A, September 1986 (Proprietary) and WCAP-10966-A, September 1986 (Non-Proprietary).

28. Miller, R.W., “Relaxation of Constant Axial Offset Control / F_Q Surveillance Technical Specification”, WCAP-10216-P-A Revision 1-A, February 1994 (Proprietary) and WCAP-10217-A Revision 1-A, February 1994 (Non-Proprietary).

29. Yarbrough, M., et al, "APOLLO – A One Dimensional Neutron Diffusion Theory Program", WCAP-14952-NP-A Revision 1-A, September 1997.

30. McLane, V., et al, "ENDF/B-VI Summary Documentation.", BNL-NCS-17541, December 1996.

3.4 THERMAL AND HYDRAULIC DESIGN

3.4.1 Design Bases

The overall objective of the thermal and hydraulic design of the reactor core is to provide adequate heat transfer compatible with the heat generation distribution in the core and with the heat removal capability of the reactor coolant system (or the emergency core cooling system when applicable). The thermal and hydraulic design assures that the following performance and safety criteria requirements are met:

1. Fuel damage (defined as penetration of the fission product barrier, i.e., the fuel rod clad) is not expected during normal operation and operational transients (Condition I) or any transient conditions arising from faults of moderate frequency (Condition II). It is not possible, however, to preclude a very small number of rods damaged. These will be within the capability of the plant cleanup system and are consistent with the plant design bases.
2. The reactor can be brought to a safe state following a Condition III event with only a small fraction of fuel rods damaged (see above definition) although sufficient fuel damage might occur to preclude resumption of operation without considerable outage time.
3. The reactor can be brought to a safe state and the core can be kept subcritical with acceptable heat transfer geometry following transients arising from Condition IV events.

In order to satisfy the above requirements the following design bases have been established for the thermal and hydraulic design of the reactor core.

3.4.1.1 Departure from Nucleate Boiling Design Basis

Basis

There will be at least a 95 percent probability that DNB will not occur on the limiting fuel rods during normal operation and operational transients and any transient conditions arising from faults of moderate frequency (Condition I and II events) at a 95 percent confidence level.

The design method employed to meet the DNB design basis is the Revised Thermal Design Procedure (RTDP) (Reference 1). With the RTDP methodology, uncertainties in plant operating parameters, nuclear and thermal parameters, fuel fabrication parameters, and computer codes are statistically combined with the DNBR correlation uncertainties such that the probability that

DNB will not occur on the most limiting fuel rod is at least 95% (at a 95% confidence level) during normal operation and operational transients and during transient conditions arising from faults of moderate frequency (Condition I and II events as defined in ANSI N18.2). This gives the design limit DNBRs.

Using RTDP methodology and the WRB-2 DNB correlation for VANTAGE 5 fuel the design limit DNBRs are 1.23 and 1.22 for the typical and thimble cells respectively for VANTAGE 5 fuel. In order to produce margin to offset such penalties as those due to rod bow and transition core, and for design flexibility, the design limit DNBR values were increased to values designated as the safety analysis limit DNBRs. The safety analysis limit DNBRs used for this analysis are 1.69 and 1.61 in the typical and thimble cells, respectively, for VANTAGE 5 fuel.

Standard Thermal Design Procedure (STDP) is used for those analyses where RTDP is not applicable. In the STDP method the parameters used in analysis are treated in a conservative way from a DNBR standpoint, that is, plant parameter uncertainties are considered so as to give the lowest minimum DNBR. The DNBR limit for STDP is the DNB correlation limit increased to preserve the same DNBR margin that is used in RTDP. The DNB correlation limit is set so that there is at least a 95% probability at a 95% confidence level that DNB will not occur for a statepoint with DNBR ≥ correlation limit.

The WRB-2 DNB correlation with a correlation limit of 1.17 (Reference 2) is employed in the thermal hydraulic design of the VANTAGE 5 fuel. In addition the W-3 DNB correlation (References 3 and 4) is used for the analysis of the VANTAGE 5 fuel where the WRB-2 DNB correlation is not applicable.

By preventing departure from nucleate boiling, adequate heat transfer is assured between the fuel clad and the reactor coolant, thereby preventing clad damage as a result of inadequate cooling. Maximum fuel rod surface temperature is not a design basis as it will be within a few degrees of coolant temperature during operation in the nucleate boiling region. Limits provided by the nuclear control and protection systems are such that this design basis will be met for transients associated with Condition II events including overpower transients. There is an additional large DNBR margin at rated power operation and during normal operating transients.

3.4.1.2 Fuel Temperature Design Basis

Basis

During modes of operation associated with Condition I and Condition II events, the maximum fuel temperature for at least 95 percent of the peak Kw/ft fuel rods will not exceed the UO_2 melting temperature with 95 percent confidence. Melting temperature of UO_2 is taken as 5080°F

(Reference 5) unirradiated and decreasing by 58°F per 10,000 MWD/MTU. By precluding UO_2 melting the fuel geometry is preserved and possible adverse effects of molten UO_2 on the cladding are eliminated. To preclude center melting and as a basis for overpower protection system setpoints, a calculated centerline fuel temperature of 4700°F has been selected as the overpower limit. This provides sufficient margin for uncertainties in the thermal evaluation as discussed in Section 3.4.2.10.1.

Discussion

Fuel rod thermal evaluations are performed at rated power, maximum overpower and during transients at various burnups. These analyses assure that this design basis as well as the fuel integrity design bases given in Section 3.2 are met. They also provide input for the evaluation of Condition III and IV faults given in Chapter 14.

3.4.1.3 Core Flow Design Basis

Basis

A minimum of 91.4 percent of the thermal flow rate will pass through the fuel rod region of the core and be effective for fuel rod cooling. Coolant flow through the thimble tubes as well as that leakage from the core barrel-baffle region into the core are not considered effective for heat removal.

Discussion

Core cooling evaluations are based on the thermal flow rate (minimum flow) entering the reactor vessel. A maximum of 8.6 percent of this value is allotted as bypass flow (Reference 87). This includes RCC guide thimble cooling flow, head-cooling flow, baffle leakage, and leakage to the vessel outlet nozzle.

3.4.1.4 Hydrodynamic Stability Design Bases

Basis

Modes of operation associated with Condition I and II events shall not lead to hydrodynamic instability.

3.4.1.5 Other Considerations

The above design bases together with the fuel clad and fuel assembly design bases given in Section 3.2.1.1 are sufficiently comprehensive so additional limits are not required.

Fuel rod diametral gap characteristics, moderator flow velocity and distribution, and moderator void are not inherently limiting. Each of these parameters is incorporated into the thermal and

hydraulic models used to ensure that the above mentioned design criteria are met. For instance, the fuel rod diametral gap characteristics change with time (see Section 3.2.1.3.1) and the fuel rod integrity is evaluated on that basis. The effects of the moderator flow velocity and distribution (see Section 3.4.2.3) and moderator void distribution (see Section 3.4.2.5) are included in the core thermal (THINC) evaluation and thus affect the design bases.

Meeting the fuel clad integrity criteria covers possible effects of clad temperature limitations. As noted in Section 3.2.1.3.1, the fuel rod conditions change with time. A single clad temperature limit for Condition I or Condition II events is not appropriate since of necessity it would be overly conservative. An appropriate clad temperature limit is applied in each case to the following Condition IV events: loss of coolant accident (Section 14.3.1, 14.3.2, and 14.3.9), control rod ejection accident (14.2.6) (Reference 6) and locked rotor accident (14.1.6.2).

3.4.2 Description

3.4.2.1 Summary Comparison

Table 3.4-1 provides a comparison of the current design parameters for the Cook Nuclear Plant Unit 2 core described herein with those for the initial cycle.

The Cook Nuclear Plant Unit 2 core described herein is demonstrated to meet all design bases by considering the values of plant parameters and the uncertainties in these parameters through the use of the Revised Thermal Design Procedure (Reference 1). The justification for the analytical techniques used in determining the values presented for the Cook Nuclear Plant Unit 2 core are presented in the relevant chapters in this document.

3.4.2.2 Fuel and Cladding Temperatures

Consistent with the thermal-hydraulic design bases described in Section 3.4.1, the following discussion pertains mainly to fuel pellet temperature evaluation. A discussion of fuel clad integrity is presented in Section 3.2.1.3.1.

The thermal-hydraulic design assures that the maximum fuel temperature is below the melting point of UO_2 (melting point of 5080°F (Reference 5) unirradiated and decreasing by 58°F per 10,000 MWD/MTU). To preclude center melting and as a basis for overpower protection system setpoints, a calculated centerline fuel temperature of 4700°F has been selected as the overpower limit. This provides sufficient margin for uncertainties in the thermal evaluation as described in Section 3.4.2.10.1. The temperature distribution within the fuel pellet is predominantly a function of the local power density and the UO_2 thermal conductivity. However, the computation of radial fuel temperature distributions combines crud, oxide, clad, gap and pellet

conductances. The factors which influence these conductances, such as gap size (or contact pressure), internal gas pressure, gas composition, pellet density, and radial power distribution within the pellet, etc., have been combined into a semiempirical thermal model (see Section 3.2.1.3.1) which includes a model for time dependent fuel densification, as given in Reference (7). This thermal model enables the determination of these factors and their net effects on temperature profiles. The temperature predictions have been compared to inpile fuel temperature measurements (References 7, 8, and 85) and melt radius data (References 9 and 10) with good results.

Fuel rod thermal evaluations (fuel centerline, average and surface temperatures) are performed for several times in the fuel rod lifetime, with consideration of time dependent densification, to determine the maximum fuel temperatures.

The principal factors, which are employed in the determination of the fuel temperature, are discussed below.

3.4.2.2.1 UO2 Thermal Conductivity

The thermal conductivity of uranium dioxide was evaluated from data reported by Howard, et al. (Reference 11); Lucks, et al. (Reference 12); Daniel, et al. (Reference 13); Feith (Reference 14); Vogt, et al. (Reference 15); Nishijima, et al. (Reference 16); Ainscough, et al. (Reference 17); Godfrey, et al. (Reference 18); Stora, et al. (Reference 19); Bush (Reference 20); Asamato, et al. (Reference 21); Kruger (Reference 22); and Gyllander (Reference 23).

At the higher temperatures, thermal conductivity is best obtained utilizing the integral conductivity to melt which can be determined with more certainty. From an examination of the data, it has been concluded that the best estimate for the value of $\int_{0^\circ C}^{2800^\circ C} k\,dt$ is 93 watts/cm. This conclusion is based on the integral values reported by Duncan (Reference 9), Gyllander (Reference 23), Lyons, et al. (Reference 24), Coplin, et al. (Reference 25), Bain (Reference 26), and Stora (Reference 27).

The design curve for the thermal conductivity is shown in Figure 3.4-1. The section of the curve at temperatures between 0°C and 1300°C is in excellent agreement with the recommendation of the IAEA panel (Reference 28). The section of the curve above 1300°C is derived for an integral value of 93 watts/cm (References 9, 23, and 27).

Thermal conductivity for UO_2 at 95 percent theoretical density can be presented best by the following equation:

$$K = \frac{1}{11.8 + .0238T} + 8.775 \times 10^{-13} T^3 \qquad (3.4\text{-}1)$$

Where:

K = watts/cm-°C.

T = °C.

3.4.2.2.2 Radial Power Distribution in UO2 Fuel Rods

An accurate description of the radial power distribution as a function of burnup is needed in determining the power level for incipient fuel melting and other important performance parameters such as pellet thermal expansion, fuel swelling and fission gas release rates.

This information on radial power distributions in UO_2 fuel rods is determined with the neutron transport theory code, LASER. The LASER Code has been validated by comparing the code predictions on radial burnup and isotopic distributions with measured radial microdrill data (References 29, and 30). A "radial power depression factor," f, is determined using radial power distributions predicted by LASER. The factor f enters into the determination of the pellet centerline temperature, T_c, relative to the pellet surface temperature, T_s, through the expression:

$$\int_{T_s}^{T_c} k(T)dT = \frac{q'f}{4\pi} \qquad (3.4\text{-}2)$$

Where:

k(T) = the thermal conductivity for UO_2 with a uniform density distribution.

q' = the linear power generation rate.

3.4.2.2.3 Gap Conductance

The temperature drop across the pellet-clad gap is a function of the gap size and the thermal conductivity of the gas in the gap. The gap conductance model is selected such that when combined with the UO_2 thermal conductivity model, the calculated fuel centerline temperatures reflect the inpile temperature measurements. A detailed discussion of the gap conductance model is given in References 7 and 8.

3.4.2.2.4 Surface Heat Transfer Coefficients

The fuel rod surface heat transfer coefficients during subcooled forced convection and nucleate boiling are presented in Section 3.4.2.8.1.

3.4.2.2.5 Fuel Clad Temperatures

The outer surface of the fuel rod at the hot spot operates at a temperature of approximately 660°F for steady-state operation at rated power throughout core life due to the onset of nucleate boiling. Initially (beginning-of-life), this temperature is that of the clad metal outer surface.

During operation over the life of the core, the buildup of oxides and crud on the fuel rod surface causes the clad surface temperature to increase. Allowance is made in the fuel center melt evaluation for this temperature rise. Since the thermal-hydraulic design basis limits DNB, adequate heat transfer is provided between the fuel clad and the reactor coolant so that the core thermal output is not limited by considerations of the clad temperature.

3.4.2.2.6 Treatment of Peaking Factors

The total heat flux hot channel factor, F_Q, is defined by the ratio of the maximum to core average heat flux. As presented in Table 3.3-2 and discussed in Section 3.3.2.2.6, the design value of F_Q for normal operation in a typical cycle with the Westinghouse VANTAGE 5 design was 2.335. This resulted in a peak local power of 12.9 Kw/ft at full power conditions.

As described in Section 3.3.2.2.8 the peak linear power resulting from overpower transients/operator errors (assuming a maximum overpower of 118 percent) is considerably less than 22.0 Kw/ft. The centerline temperature Kw/ft must be below the UO_2 melt temperature over the lifetime of the rod, including allowances for uncertainties. The fuel temperature design basis is discussed in 3.4.1.2 and results in a maximum allowable calculated centerline temperature of 4700°F. The peak linear power for prevention of centerline melt is < 22.0 kW/ft. The centerline temperature at the peak linear power resulting from overpower transients/overpower errors (assuming a maximum overpower of 118 percent) is below that required to produce melting.

3.4.2.3 Critical Heat Flux Ratio or Departure from Nucleate Boiling Ratio and Mixing Technology

The minimum DNBRs for the rated power and anticipated transient conditions are given in Table 3.4-1. The core average DNBR is not a safety-related item as it is not directly related to the minimum DNBR in the core, which occurs at some elevation in the limiting flow channel which is typically downstream of the peak heat flux location (hot spot) due to the increased downstream enthalpy rise.

DNBRs are calculated by using the correlation and definitions described in the following Sections 3.4.2.3.1 and 3.4.2.3.2. The THINC-IV computer code (discussed in Section 3.4.3.4.1)

is used to determine the flow distribution in the core and the local conditions in the hot channel for use in the DNB correlation. The use of hot channel factors is discussed in Section 3.4.3.2.1 (nuclear hot channel factors) and in Section 3.4.2.3.4 (engineering hot channel factors).

3.4.2.3.1 Departure from Nucleate Boiling Technology

Early experimental studies of DNB were conducted with fluid flowing inside single heated tubes or channels and with single annulus configurations with one or both walls heated. The results of the experiments were analyzed using many different physical models for describing the DNB phenomenon but all resultant correlations are highly empirical in nature. The evolution of these correlations is given by Tong (References 3, and 31) including the W-3 Correlation which is in wide use in the pressurized water reactor industry.

As testing methods progressed to the use of rod bundles, instead of single channels, it became apparent that the bundle average flow conditions cannot be used in DNB correlations. As outlined by Tong (Reference 4) test results showed that correlations based on average conditions were not accurate predictors of DNB heat flux. This indicates that a knowledge of the local subchannel conditions within the bundle is necessary.

In order to determine the local subchannel conditions, the THINC (Reference 32,33,34) computer codes were developed. In the THINC Codes, a rod bundle is considered to be an array of subchannels each of which includes the flow area formed by four adjacent rods. The subchannels are also divided into axial steps such that each may be treated as a control volume. By solving simultaneously the mass, energy, and momentum equations, the local fluid conditions in each control volume are calculated. The W-3 Correlation, developed from single channel data, can be applied to rod bundles by using the subchannel local fluid conditions calculated by the THINC Code.

It was shown by Tong (Reference 4) that the above approach yielded conservative predictions particularly in rod bundles with mixing vane grid spacers. Hence a correction factor was developed to adapt the W-3 Correlation (which was developed based on single channel data), to rod bundles with spacer grids. This correlation factor, termed the "Modified Spacer Factor," (Reference 35, and 36) was developed as a multiplier on the W-3 Correlation and was applied to previous designs.

The WRB-2 Correlation, (Reference 2) was developed to take credit for the VANTAGE 5 fuel assemblies mixing vane grid design. A DNBR limit of 1.17 is applicable for the WRB-2 correlation. This correlation accounts directly for both typical and thimble cold wall cell effects, uniform and non-uniform heat flux profiles, and variations in rod heated length and in grid spacing.

The applicable range of variables is:

Pressure	:	$1440 \leq P \leq 2490$ psia
Local Mass Velocity	:	$0.9 \leq G_{loc}/10^6 \leq 3.7$ lb/ft^2-hr
Local Quality	:	$-0.1 \leq X_{loc} \leq 0.3$[1]
Heated Length[2]	:	$L_h \leq 14$ feet
Grid Spacing	:	$10 \leq g_{sp} \leq 26$ inches
Equivalent Hydraulic Diameter	:	$0.37 \leq d_e \leq 0.51$ inches
Equivalent Heated Hydraulic Diameter	:	$0.46 \leq d_h \leq 0.59$ inches

Figure 3.4-2 shows measured critical heat flux plotted against predicted critical heat flux using the WRB-2 Correlation.

3.4.2.3.2 Definition of Departure from Nucleate Boiling Ratio

The DNBR as applied to this design for both typical and thimble cold wall cells is:

$$DNBR = \frac{q''_{DNB,N}}{q''_{loc}} \quad (3.4\text{-}3)$$

Where:

$$q''_{DNB,N} = \frac{q''_{DNB,EU}}{F} \quad (3.4\text{-}4)$$

and $q''_{DNB,\,EU}$ is the equivalent uniform critical heat flux as predicted by the WRB-2 Correlation (Reference 2); q''_{loc} is the actual local heat flux.

F is the flux shape factor to account for non-uniform axial heat flux distributions (Reference 37).

3.4.2.3.3 Mixing Technology

The rate of heat exchange by mixing between flow channels is proportional to the difference in the local mean fluid enthalpy of the respective channels, the local fluid density and flow velocity. The proportionality is expressed by the dimensionless thermal diffusion coefficient, TDC, which is defined as:

[1] A penalty is applied when local quality is ≥0.26 per Westinghouse Letter AEP-15-59 (Reference 86).

[2] Inlet to CHF location.

$$TDC = \frac{w'}{qVa} \qquad (3.4\text{-}5)$$

Where:

w' = flow exchange rate per unit length, lb/ft-sec.

q = fluid density, lb/ft^3.

V = fluid velocity, ft/sec.

a = lateral flow area between channels per unit length, ft^2/ft.

The application of the TDC in the THINC analysis for determining the overall mixing effect or heat exchange rate is presented in Reference (32).

As part of an ongoing research and development program, Westinghouse has sponsored and directed mixing tests at Columbia University (Reference 38). These series of tests, using the "R" mixing vane grid design on 13, 26 and 32 inch grid spacing, were conducted in pressurized water loops at Reynolds numbers similar to that of a PWR core under the following single and two phase (subcooled boiling) flow conditions:

Pressure	1500 to 2400 psia
Inlet temperature	332 to 642°F
Mass velocity	1.0 to 3.5 x 10^6 lbm/hr ft^2
Reynolds number	1.34 to 7.45 x 10^5
Bulk outlet quality	-52.1 to -13.5%

TDC is determined by comparing the THINC Code predictions with the measured subchannel exit temperatures. Data for 26-inch axial grid spacing are presented in Figure 3.4-3 where the thermal diffusion coefficient is plotted versus the Reynolds number. TDC is found to be independent of Reynolds number, mass velocity, pressure and quality over the ranges tested. The two-phase data (local, subcooled boiling) fell within the scatter of the single phase data. The effect of two-phase flow on the value of TDC has been demonstrated by Cadek (Reference 38), Rowe and Angle (References 39, and 40) and Gonzalez-Santalo and Griffith (Reference 41). In the subcooled boiling region the values of TDC were indistinguishable from the single-phase

values. In the quality region, Rowe and Angle show that in the case with rod spacing similar to that in PWR reactor core geometry, the value of TDC increased with quality to a point and then decreases, but never below the single phase value. Gonzalez-Santalo and Griffith showed that the mixing coefficient increased as the void fraction increased.

The data from these tests on the "R" grid showed that a design TDC value of 0.038 (for 26-inch grid spacing) can be used in determining the effect of coolant mixing in the THINC analysis.

A mixing test program similar to the one described above was conducted at Columbia University for the 17 x 17 geometry and mixing vane grids on 26 inch spacing (Reference 42). The mean value of TDC obtained from these tests was 0.059, and all data was well above the current design value of 0.038.

The inclusion of three intermediate flow mixer (IFM) grids in the upper span of the VANTAGE 5 fuel assembly results in a grid spacing of approximately 10 inches. Therefore, the design value of 0.038 for TDC is a conservatively low value for use in VANTAGE 5 to determine the effect of coolant mixing in the core thermal performance analysis.

Since the actual reactor grid spacing is approximately 21 inches, additional margin is available for this design, as the value of TDC increases as grid spacing decreases (Reference 38).

3.4.2.3.4 Hot Channel Factors

The total hot channel factors for heat flux and enthalpy rise are defined as the maximum to core-average ratios of these quantities. The heat flux hot channel factor considers the local maximum linear heat generation rate at a point (the "hot spot"), and the enthalpy rise hot channel factor involves the maximum integrated value along a channel (the "hot channel").

Each of the total hot channel factors considers a nuclear hot channel factor (see Table 3.3-2 and Section 3.4.3.2) describing the neutron power distribution and an engineering hot channel factor, which allows for variations in flow conditions and fabrication tolerances. The engineering hot channel factors are made up of subfactors which account for the influence of the variations of fuel pellet diameter, density, enrichment and eccentricity; fuel rod diameter pitch and bowing; inlet flow distribution; flow redistribution; and flow mixing.

kW/ft Engineering Heat Flux Hot Channel Factor, F_Q^E

The kW/ft engineering hot channel factor is used to evaluate the maximum linear heat generation rate in the core. This subfactor is determined by statistically combining the fabrication variations for fuel pellet diameter, density, and enrichment, and has a value of 1.03 at the 95 percent probability level with 95 percent confidence. As shown in Reference (43), no DNB penalty need

be taken for the short relatively low intensity heat flux spikes caused by variations in the above parameters, as well as fuel pellet eccentricity and fuel rod diameter variation.

Engineering Enthalpy Rise Hot Channel Factor, $F_{\Delta H}^{E}$

The effect of variations in flow conditions and fabrication tolerances on the hot channel enthalpy rise is directly considered in the THINC code thermal subchannel analysis (see Section 3.4.3.4.1) under any reactor operating condition. The items considered contributing to the enthalpy rise engineering hot channel factor are discussed below:

1. Pellet diameter, density and enrichment:

   Variations in pellet diameter, density and enrichment are considered statistically in establishing the limit DNBRs (see Section 3.4.1.1) for the Revised Thermal Design Procedure (Reference 1) employed in this application. Uncertainties in these variables are determined from sampling of manufacturing data.

2. Inlet Flow Maldistribution:

   The consideration of inlet flow maldistribution in core thermal performances is discussed in Section 3.4.3.1.2. A design basis of 5 percent reduction in coolant flow to the hot assembly is used in the THINC-IV analysis.

3. Flow Redistribution:

   The flow redistribution accounts for the reduction in flow in the hot channel resulting from the high flow resistance in the channel due to the local or bulk boiling. The effect of the non-uniform power distribution is inherently considered in the THINC analysis for every operating condition which is evaluated.

4. Flow Mixing:

   The subchannel mixing model incorporated in the THINC Code and used in reactor design is based on experimental data (Reference 44) discussed in Section 3.4.3.4.1. The mixing vanes incorporated in the spacer grid design induce additional flow mixing between the various flow channels in a fuel assembly as well as between adjacent assemblies. This mixing reduces the enthalpy rise in the hot channel resulting from local power peaking or unfavorable mechanical tolerances.

5. Effects of Rod Bow on DNBR

   The phenomenon of fuel rod bowing must be accounted for in the DNBR safety analysis of Condition I and Condition II events (Reference 45). A portion of the

margin resulting from the difference between the design and safety analysis limit DNBRs is used to counteract the rod bow penalties.

The maximum rod bow penalties accounted for in the design safety analysis are based on an assembly average burnup of 24,000 MWD/MTU. At burnups greater than 24,000 MWD/MTU, credit is taken for the effect of $F^N_{\Delta H}$ burndown, due to the decrease in fissionable isotopes and the buildup of fission product inventory, and no additional rod bow penalty is required (Reference 46).

In the upper spans of the VANTAGE 5 fuel assembly, additional restraint is provided with the intermediate flow mixer (IFM) grids such that the grid-to-grid spacing in those spans with IFM grids is approximately 10 inches compared to approximately 20 inches in the other spans. Using the NRC approved scaling factor results in predicted channel closure in the limiting 10 inch spans of less than 50% closure. Therefore, no rod bow DNBR penalty is required in the 10 inch spans in the VANTAGE 5 safety analyses.

3.4.2.4 Flux Tilt Considerations

Significant quadrant power tilts are not anticipated during normal operation since this phenomenon is caused by some asymmetric perturbation. A dropped or misaligned RCCA could cause changes in hot channel factors; however, these events are analyzed separately in Chapter 14. This discussion will be confined to flux tilts caused by x-y xenon transients, inlet temperature mismatches, enrichment variations within tolerances and so forth.

The design value of the enthalpy rise hot channel factor $F_{\Delta H}$ as discussed in Section 3.3.2.2.7 together with the uncertainty accounted for in the Revised Thermal Design Procedure (Reference 1) is assumed to be sufficiently conservative that flux tilts up to and including the alarm point (see the Technical Specifications) will not result in values of $F^N_{\Delta H}$ greater than that assumed in the analysis. The design value of F_Q does not include a specific allowance for quadrant flux tilts.

3.4.2.5 Void Fraction Distribution

The calculated core average and the hot subchannel maximum and average void fractions are presented in Table 3.4-2 for operation at full power with design hot channel factors. The void fraction distribution in the core at various radial and axial locations for a representative Westinghouse four-loop plant is presented in Reference (33). The void models used in the THINC-IV computer code are described in Section 3.4.2.8.3.

Since void formation due to subcooled boiling is an important promoter of interassembly flow redistribution, a sensitivity study was performed with THINC-IV using the void model referenced above (Reference 33).

The results of this study showed that because of the realistic crossflow model used in THINC-IV, the minimum DNBR in the hot channel is relatively insensitive to variations in this model. The range of variations considered in this sensitivity study covered the maximum uncertainty range of the data used to develop each part of the void fraction correlation.

3.4.2.6 Core Coolant Flow Distribution

Assembly average coolant mass velocity and enthalpy at various radial and axial core locations are given in Figures 3.4-4 to 3.4-6 for a representative Westinghouse plant. Coolant enthalpy rise and flow distributions are shown for the elevations of 1/3 of core height in Figure 3.4-4, 2/3 of the core height in Figure 3.4-5 and at the core exit in Figure 3.4-6. The THINC Code analysis for this case utilized a uniform core inlet enthalpy and inlet flow distribution.

Reactor Coolant Flow

The reactor coolant flow, a major parameter in the design of the system and its components, is established by a detailed design procedure supported by operating plant performance data and component hydraulics experimental data. The procedure establishes a best estimate flow as well as conservatively high and low flows for the applicable mechanical and thermal design considerations. In establishing the range of design flows, the procedure accounts for the uncertainties in the component flow resistances and the pump head-flow capability, established by analysis of the available experimental data. The procedure also accounts for the uncertainties in the technique used to measure flow in the operating plant.

Best Estimate Flow

The best estimate flow is considered to be the most likely value for the plant operating condition. This flow is based on the best estimate of the reactor vessel, steam generator and piping flow resistances, and on the best estimate of the reactor coolant pump head-flow capability, with no known uncertainties assigned to either the system flow resistance or the pump head. The best estimate flow provides the basis for the establishment of the other design flows required for the system and component design.

The best estimate flow analysis has been based on extensive experimental data, including very accurate flow and pressure drop data from one operating plant, flow resistance measurements from several fuel assembly hydraulics tests, and hydraulic performance measurements from several pump impeller model tests. Since operating plant flow measurements have been shown

to be in good agreement with the calculated best estimate flows, the flows established with this design procedure can be applied to the plant design with a high level of confidence.

Thermal Design Flow

Thermal design flow is the basis for the reactor core thermal performance, with steam generator thermal performance, and the nominal plant parameters used throughout the design. To provide the required margin, the thermal design flow accounts for the uncertainties in reactor vessel, steam generator and piping flow resistances, reactor coolant pump head, and the technique used to measure flow rate. The combination of these uncertainties provides an overall thermal design flow margin of 7 percent. The thermal design flow is confirmed when the plant is placed in operation. The thermal design flow is provided in Table 3.4-3.

Minimum Measured Flow

The minimum measured flow is the flow defined by adding the applicable plant flow measurement uncertainty to the Thermal Design Flow. The minimum measured flow is specified in the Technical Specifications as the flow that must be confirmed or exceeded by a flow measurement at the plant, and where applicable, is the flow used in the ITDP or RTDP DNB analyses.

Mechanical Design Flow

Mechanical design flow is the conservatively high flow used in the mechanical design of the reactor vessel internals and fuel assemblies. To assure that a conservatively high flow is specified, the mechanical design flow accounts for the same uncertainties applied to the thermal design flow margin, thereby providing an overall mechanical design flow margin of 6 percent. The mechanical design flow is listed in Table 3.4-3.

3.4.2.7 Core Pressure Drops and Hydraulic Load

3.4.2.7.1 Core Pressure Drops

The analytical model and experimental data used to calculate the pressure drops shown in Table 3.4-1 are described in Section 3.4.2.8. The full power operation pressure drop values shown in the Table are the unrecoverable pressure drops across the vessel, including the inlet and outlet nozzles, and across the core. These pressure drops are based on the Best Estimate Flow (most likely value for actual plant operating conditions) described in Section 3.4.2.6. Section 3.4.2.6 also defines and describes the thermal design flow (minimum flow) and minimum measured flows which are the basis for reactor core thermal performance and the mechanical design flow

(maximum flow) which is used in the mechanical design of the reactor vessel internals and fuel assemblies.

Uncertainties associated with the core pressure drop values are discussed in Section 3.4.2.10.2.

The pressure drops quoted in Table 3.4-1 are based on the VANTAGE 5 fuel assembly pressure loss coefficients.

3.4.2.7.2 Hydraulic Loads

Hydraulic loads at normal operating conditions are calculated considering the mechanical design flow described above and accounting for the minimum core bypass flow based on manufacturing tolerances. Core hydraulic loads at cold plant startup conditions also consider this flow but are adjusted to account for the coolant density difference. Conservative core hydraulic loads for a pump overspeed transient, which could possibly create flow rates 18 percent greater than the mechanical design flow, are evaluated to be greater than twice the fuel assembly weight.

The fuel assembly hold down springs are designed to keep the fuel assemblies resting on the lower core plate under all Condition I and II events with the exception of the turbine overspend transient associated with a loss of external load. Under the transient flow rate and core pressure drop resulting from increased pump outputs with turbine overspeed, fuel assembly lift may occur. However, the hold down springs are designed to tolerate the over-deflection for this case and to provide the required hold down force following the transient. Maximum flow conditions are usually limiting because hydraulic loads are a maximum. The most adverse hydraulic loads occur during a LOCA. This accident is discussed in Section 14.3.

Core hydraulic loads were measured during the prototype assembly tests. Reference (2) contains a detailed discussion of the results.

3.4.2.8 Correlation and Physical Data

3.4.2.8.1 Surface Heat Transfer Coefficients

Forced convection heat transfer coefficients are obtained from the familiar Dittus-Boelter correlation, (Reference 51) with the properties evaluated at bulk fluid conditions:

$$\frac{hD_e}{k} = 0.023\left[\frac{D_eG}{\mu}\right]^{0.8}\left[\frac{C_p\mu}{k}\right]^{0.4} \qquad (3.4\text{-}6)$$

Where:

h = heat transfer coefficient, BTU/hr-ft^2-°F.

D_e = equivalent diameter, ft.

k = thermal conductivity, BTU/hr-ft-°F.

G = mass velocity, lb/hr-ft^2.

μ = dynamic viscosity, lb/ft-hr.

C_p = heat capacity, BTU/lb-°F.

This correlation has been shown to be conservative (Reference 55) for rod bundle geometries with pitch to diameter ratios in the range used by PWRs.

The onset of nucleate boiling occurs when the clad wall temperature reaches the amount of superheat predicted by Thom's (Reference 56) correlation. After this occurrence the outer clad wall temperature is determined by:

$$\Delta T_{sat} = \left[0.072\exp\left(-P/1260\right)\right](q'')^{0.5} \qquad (3.4\text{-}7)$$

Where:

ΔT_{sat} = wall superheat, $T_w - T_{sat}$, °F.

q" = wall heat flux, BTU/hr-ft^2.

P = pressure, psia.

T_w = outer clad wall temperature, °F.

T_{sat} = saturation temperature of coolant at P, °F.

3.4.2.8.2 Total Core and Vessel Pressure Drop

Unrecoverable pressure losses occur as a result of viscous drag (friction) and/or geometry changes (form) in the fluid flow path. The flow field is assumed to be incompressible, turbulent,

single-phase water. These assumptions apply to the core and vessel pressure drop calculations for the purpose of establishing the primary loop flow rate. Two-phase considerations are neglected in the vessel pressure drop evaluation because the core average void is negligible (see Section 3.4.2.5 and Table 3.4-2). Two phase flow considerations in the core thermal subchannel analyses are considered and the models are discussed in Section 3.4.3.1.3. Core and vessel pressure losses are calculated by equations in the form:

$$P_L = \left(K + F\frac{L}{D_e}\right)\frac{\rho V^2}{2g_c(144)} \qquad (3.4\text{-}8)$$

Where:

P_L = unrecoverable pressure drop, lb_f/in^2

ρ = fluid density, lb_m/ft^3

L = length, ft

D_e = equivalent diameter, ft

V = fluid velocity, ft/sec

$$g_c = 32.174\frac{lb_m - ft}{lb_f - sec^2}$$

K = form loss coefficient, dimensionless

F = friction loss coefficient, dimensionless

Fluid density is assumed to be constant at the appropriate value for each component in the core and vessel. Because of the complex core and vessel flow geometry, precise analytical values for the form and friction loss coefficients are not available. Therefore, experimental values for these coefficients are obtained from geometrically similar models.

Values are quoted in Table 3.4-1 for unrecoverable pressure loss across the reactor vessel, including the inlet and outlet nozzles, and across the core. The results of full-scale tests of core components and fuel assemblies were utilized in developing the core pressure loss characteristic. The pressure drop for the vessel was obtained by combining the core loss with correlation of 1/7th scale model hydraulic test data on a number of vessels (References 57, and 58) and form loss relationships (Reference 59). Moody (Reference 60) curves were used to obtain the single-phase friction factors.

Core pressure drops were confirmed by full-scale hydraulic flow tests performed in the fuel assembly test system (FATS) facility (Reference 2). These hydraulic verification tests include

hydraulic head losses and effects of velocity changes as well as unrecoverable pressure losses. The effects of velocity changes are small since the static pressure taps are located at elevations of approximately equal flow areas (and therefore approximately equal velocities). When wall static pressure taps are used near ambient fluid conditions, it can be shown analytically that the elevation head losses do not contribute to the measured core pressure drops. Therefore, data from the hydraulic verification tests can be directly applied to confirm the pressure drop values quoted in Table 3.4-1 which are based on unrecoverable pressure losses only.

Tests of the primary coolant loop flow rates were performed (see Section 3.4.4.1) prior to initial criticality to verify that the flow rates used in the design, which were determined in part from the pressure losses calculated by the method described here, are conservative.

3.4.2.8.3 Void Fraction Correlation

There are three separate void regions considered in flow boiling in a PWR as illustrated in Figure 3.4-7. They are the wall void region (no bubble detachment), the subcooled boiling region (bubble detachment) and the bulk boiling region.

In the wall void region, the point where local boiling begins is determined when the clad temperature reaches the amount of superheat predicted by Thom's (Reference 56) correlation (discussed in Section 3.4.2.8.1). The void fraction in this region is calculated using Maurer's (Reference 61) relationship. The bubble detachment point, where the superheated bubbles break away from the wall, is determined by using Griffith's (Reference 62) relationship.

The void fraction in the subcooled boiling region (that is, after the detachment point) is calculated from the Bowring (Reference 63) correlation. This correlation predicts the void fraction from the detachment point to the bulk-boiling region.

The void fraction in the bulk boiling region is predicted by using homogeneous flow theory and assuming no slip. The void fraction in this region is therefore a function only of the thermodynamic quality.

3.4.2.9 Thermal Effects of Operational Transients

DNB core safety limits are generated as a function of coolant temperature, pressure, core power, and the axial and radial power distributions. Operation within these DNB safety limits insures that the DNB design basis is met for both steady-state operation and for anticipated operational transients that are slow with respect to fluid transport delays in the primary system. In addition, for fast transients, e.g., uncontrolled rod bank withdrawal at power incident, specific protection functions are provided as described in Chapter 7 and the use of these protection functions are described in Chapter 14. The thermal response of the fuel is discussed in Section 3.4.3.7.

3.4.2.10 Uncertainties in Estimates

3.4.2.10.1 Uncertainties in Fuel and Clad Temperatures

As discussed in Section 3.4.2.2, the fuel temperature is a function of crud, oxide, clad, gap, and pellet conductances. Uncertainties in the fuel temperature calculation are essentially of two types: fabrication uncertainties such as variations in the pellet and clad dimensions and the pellet density; and model uncertainties such as variations in the pellet conductivity and the gap conductance. These uncertainties have been quantified by comparison of the thermal model to the inpile thermocouple measurements, (References 7, and 8) by out-of-pile measurements of the fuel and clad properties, (11-22) and by measurements of the fuel and clad dimensions during fabrication. The resulting uncertainties are then used in all evaluations involving the fuel temperature. The effect of densification on fuel temperature uncertainties is also included in the calculation of the total uncertainty.

In addition to the temperature uncertainty described above, the measurement uncertainty in determining the local power, and the effect of density and enrichment variations on the local power are considered in establishing the heat flux hot channel factor. These uncertainties are described in Section 3.3.2.2.1.

Reactor trip setpoints are as specified in the Technical Specifications and include allowance for instrument and measurement uncertainties such as calorimetric error, instrument drift and channel reproducibility, temperature measurement uncertainties, and noise.

Uncertainty in determining the cladding temperature results from uncertainties in the crud and oxide thicknesses. Because of the excellent heat transfer between the surface of the rod and the coolant, the film temperature drop does not appreciably contribute to the uncertainty.

3.4.2.10.2 Uncertainties in Pressure Drops

Core and vessel pressure drops based on the best estimate flow, described in 3.4.2.6, are quoted in Table 3.4-1. The uncertainties quoted are based on the uncertainties in both the test results and the analytical extension of these values to the reactor application.

A major use of the core and vessel pressure drops is to determine the primary system coolant flow rates as discussed in 3.4.2.6. In addition, as discussed in Section 3.4.4.1, tests on the primary system prior to initial criticality were made to verify that a conservative primary system coolant flow rate has been used in the design and analyses of the plant.

3.4.2.10.3 Uncertainties Due to Inlet Flow Maldistribution

The effects of uncertainties in the inlet flow maldistribution criteria used in the core thermal analyses is discussed in Section 3.4.3.1.2.

3.4.2.10.4 Uncertainty in DNB Correlation

The uncertainty in the DNB correlation (Section 3.4.2.3) can be written as a statement on the probability of not being in DNB based on the statistics of the DNB data. This is discussed in Section 3.4.1.1.

3.4.2.10.5 Uncertainties in DNBR Calculations

The uncertainties in the DNBRs calculated by THINC analysis (see Section 3.4.3.4.1) due to nuclear peaking factors are accounted for by applying conservatively high values of the nuclear peaking factors and including measurement error allowances in the statistical evaluation of the limit DNBR (see Section 3.4.1.1) using the Revised Thermal Design Procedure (Reference 1). In addition, engineering hot channel factors are employed as discussed in Section 3.4.2.3.4.

The results of the sensitivity study (Reference 33) with THINC-IV show that the minimum DNBR in the hot channel is relatively insensitive to variations in the corewide radial power distribution (for the same value of $F^N_{\Delta H}$).

The ability of the THINC-IV computer code to accurately predict flow and enthalpy distributions in rod bundles is discussed in Section 3.4.3.4.1 and in Reference (34). Studies have been performed (Reference 33) to determine the sensitivity of the minimum DNBR in the hot channel to the void fraction correlation (see also Section 3.4.2.8.3); the inlet velocity and exit pressure distributions assumed as boundary conditions for the analysis; and the grid pressure loss coefficients. The results of these studies show that the minimum DNBR in the hot channel is relatively insensitive to variations in these parameters. The range of variations considered in these studies covered the range of possible variations in these parameters.

3.4.2.10.6 Uncertainties in Flow Rates

The uncertainties associated with loop flow rates are discussed in Section 3.4.2.6. For core thermal performance evaluations, a thermal design flow is used which is approximately 7 percent less than the best estimate flow.

In addition, a maximum of 8.6 percent of the thermal design flow is assumed to be ineffective for core heat removal capability because it bypasses the core through the various available vessel flow paths described in Section 3.4.3.1.1.

3.4.2.10.7 Uncertainties in Hydraulic Loads

As discussed in Section 3.4.2.7.2, hydraulic loads on the fuel assembly are evaluated for a pump overspeed transient which create flow rates 18 percent greater than the mechanical design flow. The mechanical design flow as stated in 3.4.2.6 is approximately 6 percent greater than the best estimate flow or most likely flow rate value for the actual plant operating condition.

3.4.2.10.8 Uncertainty in Mixing Coefficient

The value of the mixing coefficient, TDC, used in THINC analyses for this application is 0.038. The mean value of TDC obtained in the "R" grid mixing tests described in Section 3.4.2.3.3 was 0.042 (for 26-inch grid spacing). The value of 0.038 is one standard deviation below the mean value; and 90 percent of the data gives values of TDC greater than 0.038 (Reference 38).

The results of the mixing tests done on 17 x 17 geometry, as discussed in Section 3.4.2.3.3, had a mean value of TDC of 0.059 and standard deviation of 0.007. Hence the current design value of TDC is almost 3 standard deviations below the mean for 26-inch grid spacing.

3.4.2.11 Plant Configuration Data

Plant configuration data for the thermal-hydraulic and fluid systems external to the core are provided in the appropriate Chapters 4, 6 and 9. Implementation of the emergency core cooling systems (ECCS) is discussed in Chapter 6 and evaluation of ECCS performance appears in Chapter 14. Some specific areas of interest are the following:

1. Total coolant flow rates for the reactor coolant system (RCS) and each loop are provided in 3.4.2.6. Flow rates employed in the evaluation of the core are presented in Section 3.4.3.
2. Total RCS volume including pressurizer and surge line, RCS liquid volume including pressurizer water at steady-state power conditions are given in Table 3.4-3. The components of the RCS are water filled during power operation with the pressurizer being approximately 50 percent water filled.

3.4.3 Evaluation

3.4.3.1 Core Hydraulics

3.4.3.1.1 Flow Paths Considered in Core Pressure Drop and Thermal Design

The following flow paths or core bypass flow are considered:

1. Flow through the spray nozzles into the upper head for head cooling purposes.
2. Flow entering into the RCCA guide thimbles to cool the core components.
3. Leakage flow from the vessel inlet nozzle directly to the vessel outlet nozzle through the gap between the vessel and the barrel.
4. Flow introduced between the baffle and the barrel for the purpose of cooling these components, and which is not considered available for core cooling.
5. Flow in the gaps between the fuel assemblies on the core periphery and the adjacent baffle.

The above contributions are evaluated to confirm that the design basis value of not more than 8.6 percent core bypass flow is met. Of the total allowance, 4.6 percent is associated with the internals (items 1, 3, 4, and 5 above) and 4.0 percent for the core. Calculations have been performed using drawing tolerances on a worst case basis and accounting for uncertainties in pressure losses. Based on these calculations, the core bypass flow for this plant is not more than 8.6 percent. This design bypass value is also used in the evaluation of the core pressure drops quoted in Table 3.4-1, and the determination of reactor flow rates in Section 3.4.2.6.

Flow model test results for the flow path through the reactor are discussed in Section 3.4.2.8.2.

3.4.3.1.2 Inlet Flow Distributions

Data has been considered from several 1/7 scale hydraulic reactor model tests (References 57, 58, and 64) in arriving at the core inlet flow maldistribution criteria to be used in the THINC analyses (see Section 3.4.3.4.1). THINC I analyses made using this data have indicated that a conservative design basis is to consider a 5 percent reduction in the flow to the hot assembly (Reference 65). The same design basis of 5 percent reduction to the hot assembly inlet is used in THINC-IV analyses.

The experimental error estimated in the inlet velocity distribution has been considered as outlined in Reference (33) where the sensitivity of changes in inlet velocity distributions to hot channel thermal performance is shown to be small. Studies (Reference 33) made with the THINC model (THINC-IV) show that it is adequate to use the 5 percent reduction in inlet flow

to the hot assembly for a loop out of service based on the experimental data in References (57) and (58).

The effect of the total flow rate on the inlet velocity distribution was studied in the experiments of Reference (57). As was expected, on the basis of the theoretical analysis, no significant variation could be found in inlet velocity distribution with reduced flow rate.

3.4.3.1.3 Empirical Friction Factor Correlations

The empirical friction factor correlations are used in the THINC-IV computer code (described in Section 3.4.3.4.1).

The friction factor in the axial direction, parallel to the fuel rod axis, is evaluated using the Novendstern-Sandberg correlation (Reference 66). This correlation consists of the following:

1. For isothermal conditions, this correlation uses the Moody (Reference 60) friction factor including surface roughness effects,
2. Under single-phase heating conditions a factor is applied based on the values of the coolant density and viscosity at the temperature of the heated surface and at the bulk coolant temperature, and
3. Under two-phase flow conditions the homogeneous flow model proposed by Owens (Reference 67) is used with a modification to account for a mass velocity and heat flux effect.

The flow in the lateral directions, normal to the fuel rod axis, views the reactor core as a large tube bank. Thus, the lateral friction factor proposed by Idel'chick (Reference 59) is applicable. This correlation is of the form:

$$F_L = A \ Re_L^{-0.2} \qquad (3.4\text{-}9)$$

Where:

A is a function of the rod pitch and diameter as given in Reference (59).

Re_L is the lateral Reynolds number based on the rod diameter.

Extensive comparisons of THINC-IV predictions using these correlations to experimental data are given in Reference (34), and verify the applicability of these correlations in PWR design.

3.4.3.2 Influence of Power Distribution

The core power distribution which is largely established at beginning-of-life by fuel enrichment, loading pattern, and core power level is also a function of variables such as control rod worth and position, and fuel depletion throughout lifetime. Radial power distributions in various planes of

the core are often illustrated for general interest, however, the core enthalpy rise distribution as determined by the integral of power up each channel is of greater importance for DNB analyses. These radial power distributions, characterized by $F^N_{\Delta H}$ (defined in Section 3.3.2.2.2) as well as axial heat flux profiles are discussed in the following two sections.

3.4.3.2.1 Nuclear Enthalpy Rise Hot Channel Factor, $F^N_{\Delta H}$

Given the local power density q'(kW/ft) at a point x, y, z in a core with N fuel rods and height H,

$$F^N_{\Delta H} = \frac{\text{hot rod power}}{\text{average rod power}} = \frac{MAX\int_0^H q'(x_o, y_o, z)dz}{\frac{1}{N}\sum_{\text{all rods}}\int_0^H q'(x, y, z)dz} \qquad (3.4\text{-}10)$$

The way in which $F^N_{\Delta H}$ is used in the DNB calculation is important. The location of minimum DNBR depends on the axial profile and the value of DNBR depends on the enthalpy rise to that point. Basically, the maximum value of the rod integral is used to identify the most likely rod for minimum DNBR. An axial power profile is obtained which when normalized to the design value of $F^N_{\Delta H}$, recreates the axial heat flux along the limiting rod. The surrounding rods are assumed to have the same axial profile with rod average powers which are typical distributions found in hot assemblies. In this manner worst case axial profiles can be combined with worst case radial distributions for reference DNB calculations.

It should be noted again that $F^N_{\Delta H}$ is an integral and is used as such in DNB calculations. Local heat fluxes are obtained by using hot channel and adjacent channel explicit power shapes which take into account variations in horizontal power shapes throughout the core. The sensitivity of the THINC-IV analysis to radial power shapes is discussed in Reference (33).

For operation at a fraction P of full power, the $F^N_{\Delta H}$ used is given by:

$$F^N_{\Delta H} = 1.61\ [1 + 0.3\ (1\text{-}P)] \qquad (3.4\text{-}11)$$

The permitted relaxation of $F^N_{\Delta H}$ for lower powers is included in the DNB protection setpoints and allows radial power shape changes with rod insertion to the insertion limits (Reference 68), thus allowing greater flexibility in the nuclear design.

3.4.3.2.2 Axial Heat Flux Distributions

As discussed in Section 3.3.2.2, the axial heat flux distribution can vary as a result of rod motion, power change, or due to a spatial xenon transients which may occur in the axial direction. Consequently, it is necessary to measure the axial power imbalance by means of the excore nuclear detectors (as discussed in Section 3.3.2.2.7) and protect the core from excessive axial power imbalance.

The reference axial shape used in establishing core DNB limits (that is Overtemperature ΔT protection system setpoints) is a chopped cosine with a peak to average value of 1.55. The reactor trip system provides automatic reduction of the trip setpoints on excessive axial power imbalance. To determine the magnitude of the setpoint reduction, the reference shape is supplemented by other axial shapes skewed to the bottom and top of the core.

The course of those accidents in which DNB is a concern is analyzed in Chapter 14 assuming that the protection setpoints have been set on the basis of these shapes. In many cases the axial power distribution in the hot channel changes throughout the course of the accident due to rod motion, coolant temperature and power level changes.

The initial conditions for accidents for which DNB protection is required are assumed to be those permissible within the constant axial offset control strategy for the load maneuvers described in Reference (69). In the case of the loss of flow accident the hot channel heat flux profile is very similar to the power density profile in normal operation preceding the accident. It is therefore possible to illustrate the calculated minimum DNBR for conditions representative of the loss of flow accident as a function of the flux difference initially in the core. A plot of this type is provided in Figure 3.4-8. As noted on this figure all power shapes were evaluated with a full power radial peaking factor ($F^N_{\Delta H}$) of 1.59. The radial contribution to the hot rod power shape is conservative both for the initial condition and for the condition at the time of minimum DNBR during the loss of flow transient. Also shown is the minimum DNBR calculated at the same conditions for the design power shape for non-overpower/overtemperature DNB events. It can be seen that this arbitrary design shape results in a lower calculated DNBR than any of the actual normal operation power shapes.

3.4.3.3 Core Thermal Response

A general summary of the steady-state thermal-hydraulic design parameters including thermal output, flow rates, etc., is provided in Table 3.4-1 for all loops in operation.

As stated in Section 3.4.1, the design bases of the application are to prevent departure from nucleate boiling and to prevent fuel melting for Condition I and II events. The protective systems described in Chapter 7 are designed to meet these bases. The response of the core to Condition II transients is given in Chapter 14.

3.4.3.4 Analytical Techniques

3.4.3.4.1 Core Analysis

The objective of reactor core thermal design is to determine the maximum heat removal capability in all flow subchannels and show that the core safety limits, as presented in the Technical Specifications are not exceeded while compounding engineering and nuclear effects. The thermal design takes into account local variations in dimensions, power generation, flow redistribution, and mixing. THINC-IV is a realistic three-dimensional matrix model which has been developed to account for hydraulic and nuclear effects on the enthalpy rise in the core (References 33, and 34). The behavior of the hot assembly is determined by superimposing the power distribution among the assemblies upon the inlet flow distribution while allowing for flow mixing and flow distribution between assemblies. The average flow and enthalpy in the hottest assembly is obtained from the corewide, assembly by assembly analysis. The local variations in power, fuel rod and pellet fabrication, and mixing within the hottest assembly are then superimposed on the average conditions of the hottest assembly in order to determine the conditions in the hot channel.

The following sections describe the use of the THINC Code in the thermal-hydraulic design evaluation to determine the conditions in the hot channel and to assure that the safety-related design bases are not violated.

Steady-State Analysis

The THINC-IV computer program determines coolant density, mass velocity, enthalpy, vapor void, static pressure, and DNBR distributions along parallel flow channels within a reactor core under all expected operating conditions. The core region being studied is considered to be made up of a number of contiguous elements in a rectangular array extending the full length of the core. An element may represent any region of the core from a single assembly to a subchannel.

The momentum and energy exchange between elements in the array are described by the equations for the conservation of energy and mass, the axial momentum equation and two lateral momentum equations which couple each element with its neighbors. The momentum equations used in THINC-IV are similar to the Euler equations (Reference 70) excepting that frictional loss terms have been incorporated which represent the combined effects of frictional and form drag

due to the presence of grids and fuel assembly nozzles in the core. The crossflow resistance model used in the lateral momentum equations was developed from experimental data for flow normal to tube banks (References 59, and 71). The energy equation for each element also contains additional terms which represent the energy gain or loss due to the crossflow between elements.

The unique feature of THINC-IV is that lateral momentum equations, which include both inertial and crossflow resistance terms, have been incorporated into the calculational scheme. This differentiates THINC-IV from other thermal-hydraulic programs in which only the lateral resistance term is modeled. Another important consideration in THINC-IV is that the entire velocity field is solved, en masse, by a field equation while in other codes such as THINC-I (Reference 32) and COBRA (Reference 72) the solutions are obtained by stepwise integration throughout the array.

The resulting formulation of the conservation equations are more rigorous for THINC-IV; therefore, the solution is more accurate. In addition, the solution method is complex and some simplifying techniques must be employed. Since the reactor flow is chiefly in the axial direction, the core flow field is primarily one-dimensional and it is reasonable to assume that the lateral velocities and the parameter gradients are larger in the axial direction than the lateral direction. Therefore, a perturbation technique can be used to represent the axial and lateral parameters in the conservation equations. The lateral velocity components are regarded as perturbed quantities, which are smaller than the unperturbed axial velocity. The core parameters are split into an unperturbed and perturbed component with the unperturbed component equaling the core average value at a given elevation and the perturbed value is the difference between the local value and the unperturbed component. Since the magnitudes of the unperturbed and perturbed parameters are significantly different, they can be solved separately. The unperturbed equations are one-dimensional and can be solved with the resulting solutions becoming the coefficients of the perturbed equations. An interactive method is then used to solve the system of perturbed equations which couples all the elements in the array.

Three THINC-IV computer runs constitute one design run; a corewide analysis, a hot assembly analysis, and a hot subchannel analysis. While the calculational method is identical for each run, the elements, which are modeled by THINC-IV, change from run-to-run. In the corewide analysis, the computational elements represent full fuel assemblies, in the second computation the elements represent a quarter of the hot assembly. For the last computation, a quarter of the hot assembly is analyzed and each individual subchannel is represented as a computational element. The channel layout and inlet flow distribution used in the THINC analysis are

consistent with those used in Reference (33). Appropriate pressure loss coefficients are used in modeling the various channels, and the output parameters specified below are then calculated as a function of distance along the channels.

The first computation is a corewide, assembly-by-assembly analysis which uses an inlet velocity distribution modeled from experimental reactor models (References 57, 58, and 64) (see Section 3.4.3.1.2). In the corewide analysis the core is considered to be made up of a number of contiguous fuel assemblies divided axially into increments of equal length. The system of perturbed and unperturbed equations are solved for this array giving the flow, enthalpy, pressure drop, temperature and void fraction in each assembly. The system of equations is solved using the specified inlet velocity distribution and a known exit pressure condition at the top of the core. This computation determines the interassembly energy and flow exchange at each elevation for the hot assembly. THINC-IV stores this information and then uses it for the subsequent hot assembly analysis.

In the second computation, each computational element represents one-fourth of the hot assembly. The inlet flow and the amount of momentum and energy interchange at each elevation is known from the previous corewide calculation. The same solution technique is used to solve for the local parameters in the hot quarter assembly.

While the second computation provides an overall analysis of the thermal and hydraulic behavior of the hot quarter assembly, it does not consider the individual channels in the hot assembly. The third computation further divides the hot assembly into channels consisting of individual fuel rods to form flow channels. The local variations in power, fuel rod and pellet fabrication, fuel rod spacing and mixing (engineering hot channel factors) within the hottest assembly are imposed on the average conditions of the hottest fuel assembly in order to determine the conditions in the hot channel. The engineering hot channel factors are described in Section 3.4.2.3.4.

Experimental Verification

An experimental verification (Reference 34) of the THINC-IV analysis for corewide, assembly-to-assembly enthalpy rises as well as enthalpy rise in a non-uniformly heated rod bundle have been obtained. In these experimental tests, the system pressure, inlet temperature, mass flow rate and heat fluxes were typical of present PWR core designs.

During the operation of a reactor, various incore monitoring systems obtain measured data indicating the core performance. Assembly power distributions and assembly mixed mean temperature are measured and can be converted into the proper three-dimensional power input

needed for the THINC program. This data can then be used to verify the Westinghouse thermal-hydraulic design codes.

One standard startup test is the natural circulation test in which the core is held at a very low power (2 percent) and the pumps are turned off. The core is cooled by the natural circulation currents created by the power differences in the core. During natural circulation, a thermal siphoning effect occurs resulting in the hotter assemblies gaining flow, thereby creating significant interassembly crossflow. As described in the preceding section the most important feature of THINC-IV is the method by which crossflow is evaluated. Thus, tests with significant crossflow are of more value in the code verification. Interassembly crossflow is caused by radial variation in pressure. Radial pressure gradients are in turn caused by variations in the axial pressure drop, which is due mainly to friction losses. Since all assemblies have the same geometry, all assemblies have nearly the same axial pressure drops and crossflow velocities are small. However, under natural circulation conditions (low flow) the axial pressure drop is due primarily to the difference in elevation head (or coolant density) between assemblies (axial velocity is low and therefore axial friction losses are small). This phenomenon can result in relatively large radial pressure gradients and therefore higher crossflow velocities than at normal reactor operation conditions.

The incore instrumentation was used to obtain the assembly-by-assembly core power distribution during a natural circulation test. Assembly exit temperatures during the natural circulation test on a 157 assembly, three-loop plant were predicted using THINC-IV. The predicted data points were plotted as assembly temperature rise versus assembly power and a least squares fitting program used to generate an equation which best fit the data. The result is the straight line presented in Figure 3.4-9. The measured assembly exit temperatures are reasonably uniform, as indicated in this figure, and are predicted closely by the THINC-IV Code. This agreement verifies the lateral momentum equations and the crossflow resistance model used in THINC-IV. The larger crossflow resistance used in THINC-I reduces flow redistribution, so that THINC-IV gives better agreement with the experimental data.

Data has also been obtained for Westinghouse plants operating from 67 percent to 101 percent of full power. A representative cross section of the data obtained from a two-loop and three-loop reactor were analyzed to verify the THINC-IV calculational method. The THINC-IV predictions were compared with the experimental data as shown in Figures 3.4-10 and 3.4-11. The predicted assembly exit temperatures were compared with the measured exit temperature for each data run. The standard deviation of the measured and predicted assembly exit temperatures were calculated and compared for both THINC-IV and THINC-I and are given in Table 3.4-4. As the

standard deviations indicate, THINC-IV generally fits the data somewhat more accurately than THINC-I. For the core inlet temperatures and power of the data examined, the coolant flow is essentially single phase. Thus, one would expect little interassembly crossflow and small differences between THINC-IV and THINC-I predictions as seen in the tables. Both codes are conservative and predict exit temperatures higher than measured values for the high powered assemblies.

An experimental verification of the THINC-IV subchannel calculation method has been obtained from exit temperature measurements in a non-uniformly heated rod bundle (Reference 73). The inner nine heater rods were operated at approximately 20 percent more power than the outer rods to create a typical PWR intra-assembly power distribution. The rod bundle was divided into 36 subchannels and the temperature rise was calculated by THINC-IV using the measured flow and power for each experimental test.

Figure 3.4-12 shows, for a typical run, a comparison of the measured and predicted temperature rises as a function of the power density in the channel. The measurements represent an average of two to four measurements taken in various quadrants of the bundle. It is seen that the THINC-IV results predict the temperature gradient across the bundle very well. In Figure 3.4-13, the measured and predicted temperature rises are compared for a series of runs at different pressures, flows, and power levels.

Again, the measured points represent the average of the measurements taken in the various quadrants. It is seen that the THINC-IV predictions provide a good representation of the data.

Extensive additional experimental verification is presented in Reference (34).

The THINC-IV analysis is based on a knowledge and understanding of the heat transfer and hydrodynamic behavior of the coolant flow and the mechanical characteristics of the fuel elements. The use of the THINC-IV analysis provides a realistic evaluation of the core performance and is used in the thermal analyses as described above.

Transient Analysis

The THINC-IV thermal-hydraulic computer code does not have a transient capability since the third section of the THINC-I program (Reference 32) does have this capability, this code (THINC-III) continues to be used for transient DNB analysis.

The conservation equations needed for the transient analysis are included in THINC-III by adding the necessary accumulation terms to the conservation equations used in the steady-state (THINC-I) analysis. The input description must now include one or more of the following dependent arrays:

1. Inlet flow variation.
2. Heat flux distribution.
3. Inlet pressure history.

At the beginning of the transient, the calculation procedure is carried out as in the steady-state analysis. The THINC-III Code is first run in the steady-state mode to ensure conservatism with respect to THINC-IV and in order to provide the steady initial conditions at the start of the transient. The time is incremented by an amount determined either by the user or by the program itself. At each new time step the calculations are carried out with the addition of the accumulation terms which are evaluated using the information from the previous time step. This procedure is continued until a present maximum time is reached.

At preselected intervals, a complete description of the coolant parameter distributions within the array as well as DNBR are printed out. In this manner the variation of any parameter with time can be readily determined. At various times during the transient, steady-state THINC-IV is applied to show that the application of the transient version of THINC-I is conservative.

The THINC-III Code does not have the capability for evaluating fuel rod thermal response. This is treated by the methods described in Chapter 14.

3.4.3.4.2 Fuel Temperatures

As discussed in 3.4.2.2, the fuel rod behavior is evaluated utilizing a semi-empirical thermal model which considers in addition to the thermal aspects such items as clad creep, fuel swelling, fission gas release, release of absorbed gases, cladding corrosion and elastic deflection, and helium solubility.

A detailed description of the thermal model can be found in Reference (8) with the modification for time dependent densification given in Reference (7).

3.4.3.4.3 Hydrodynamic Instability

The analytical methods used to assess hydrodynamic instability are discussed in Section 3.4.3.5.

3.4.3.5 Hydrodynamic and Flow, Power Coupled, Instability

Boiling flows may be susceptible to thermohydraulic instabilities (Reference 74). These instabilities are undesirable in reactors because they may cause a change in thermohydraulic

conditions that may lead to a reduction in the DNB heat flux relative to that observed during a steady flow condition or to undesired forced vibrations of core components. Therefore, a thermohydraulic design criterion was developed which states that modes of operation under Condition I and II events will not lead to thermohydrodynamic instabilities.

Two specific types of flow instabilities are considered for Westinghouse PWR operation. These are the Ledinegg or flow excursion types of static instability and the density wave type of dynamic instability.

A Ledinegg instability involves a sudden change in flow rate from one steady state to another. This instability occurs (Reference 74) when the slope of the reactor coolant system pressure drop-flow rate curve ($\partial\Delta P/\partial Gl$ internal) becomes algebraically smaller than the loop supply (pump head) pressure drop-flow rate curve ($\partial\Delta P/\partial Gl$ external). The criterion for stability is $\partial\Delta P/\partial Gl$ internal > $\partial\Delta P/\partial Gl$ external. The Westinghouse pump head curve has a negative slope ($\partial\Delta P/\partial Gl$ external < 0) whereas the reactor coolant system pressure drop-flow curve has a positive slope ($\partial\Delta P/\partial Gl$ internal > 0) over the Condition I and Condition II operational ranges. Thus, the Ledinegg instability will not occur.

The mechanism of density wave oscillations in a heated channel has been described by Lahey and Moody (Reference 75). Briefly, an inlet flow fluctuation produces an enthalpy perturbation. This perturbs the length and the pressure drop of the single-phase region and causes quality or void perturbations in the two-phase regions, which travel up the channel with the flow. The quality and length perturbations in the two-phase region create two-phase pressure drop perturbations. However, because the total pressure drop across the core is maintained by the characteristics of the fluid system external to the core, the two-phase pressure drop perturbation feeds back to the single-phase region. These resulting perturbations can be either attenuated or self-sustained.

A simple method has been developed by Ishii (Reference 76) for parallel closed channel systems to evaluate whether a given condition is stable with respect to the density wave type of dynamic instability. This method has been used to assess the stability of typical Westinghouse reactor designs under Condition I and II operation. The results indicate that a large margin to density wave instability exists; for example, increases on the order of 150-200 percent of rated reactor power would be required for the predicted inception of this type of instability.

The application of Ishii's method (Reference 76) to Westinghouse reactor designs is conservative because of the parallel open channel feature of Westinghouse PWR cores. For such cores, there is little resistance to lateral flow leaving the flow channels of high power density. There is also

energy transfer from high power density channels to lower power density channels. This coupling with cooler channels causes an open channel configuration to be more stable than the above closed channel configuration under the same boundary conditions. Flow stability tests (References 77, and 78) have been conducted in which the closed channel systems were shown to be less stable than when the same channels were cross-connected at several locations. The cross-connections were such that the resistance to channel-to-channel crossflow and enthalpy perturbations would exist in a PWR core, which has a relatively low resistance to cross flow.

Flow instabilities, which have been observed, have occurred almost exclusively in closed channel systems operating at low pressures relative to the Westinghouse PWR operation pressures. Kao, Morgan and Parker (Reference 79) analyzed parallel closed channel stability experiments simulating a reactor core flow. These experiments were conducted at pressures up to 2200 psia. The results showed that for flow and power levels typical of power reactor conditions, no flow oscillations could be induced above 1200 psia.

Additional evidence that flow instabilities do not adversely affect thermal margin is provided by the data from the rod bundle DNB tests. Many Westinghouse rod bundles have been tested over wide ranges of operating conditions with no evidence of premature DNB or of inconsistent data which might indicate flow instabilities in the rod bundle.

In summary, it is concluded that thermohydrodynamic instabilities will not occur under Condition I and II modes of operation for Westinghouse PWR reactor designs. A large power margin, exists to predicted inception of such instabilities. Analysis has been performed which shows that minor plant-to-plant differences in Westinghouse reactor designs - such as fuel assembly arrays, core power to flow ratios, and fuel assembly length - will not result in gross deterioration of the above power margins.

3.4.3.6 Waterlogging

Local cladding deformations of waterlogging* bursts have never been observed in commercial Westinghouse fuel.

Experience has shown that the small number of rods, which have acquired clad defects, regardless of primary mechanism, remain intact and do not progressively distort or restrict

* Waterlogging damage of a previously defected fuel rod has occasionally been postulated as a mechanism for subsequent rupture of the cladding. Such damage has been postulated as a consequence of a power increase on a rod after water has entered such a rod through a clad defect of appropriate size. Rupture is postulated upon power increase if the rod internal pressure increase is excessive due to insufficient venting of water to the reactor coolant.

coolant flow. In fact such small defects are normally observed through reductions in coolant activity to be progressively closed upon further operation due to the buildup of zirconium oxide and other substances. Secondary failures, which have been observed in defected rods, are attributed to hydrogen embrittlement of the cladding. Post-irradiation examinations point to the hydriding failure mechanism rather than a waterlogging mechanism; the secondary failures occur as axial cracks in the cladding and are similar regardless of the primary failure mechanism. Such cracks do not result in flow blockage. Hence the presence of such fuel, the quantity of which must be maintained below Technical Specification limits, does not in any way exacerbate the effects of any postulated transients.

3.4.3.7 Potentially Damaging Temperature Effects During Transients

The fuel rod experiences many operational transients (intentional maneuvers) during its residency in the core. A number of thermal effects must be considered when analyzing the fuel rod performance.

The clad can be in contact with the fuel pellet at some time in the fuel lifetime. Clad-pellet interaction occurs if the fuel pellet temperature is increased after the clad is in contact with the pellet. Clad-pellet interaction is discussed in Section 3.2.1.3.1.

The potential effects of operation with waterlogged fuel are discussed in Section 3.4.3.6, which concluded that waterlogging is not a concern during operational transients.

Clad flattening, as noted in Section 3.2.1.3.1, has been observed in some operating power reactors. Thermal expansion (axial) of the fuel rod stack against a flattened section of clad could cause failure of the clad. This is no longer a concern because clad flattening is precluded during the fuel residence in the core (see Section 3.2.1.3.1).

There can be a differential thermal expansion between the fuel rods and the guide thimbles during a transient. Bowing of the fuel rods could occur if the grid assemblies did not allow axial movement of the fuel rods relative to the grid. Thermal expansion of the fuel rods is considered in the grid design so that axial loads imposed on the fuel rods during a thermal transient will not result in bowed fuel rods (see Section 3.2.1.2.2).

3.4.3.8 Energy Release During Fuel Element Burnout

As discussed in Section 3.4.3.3 the core is protected from going through DNB over the full range of possible operating conditions. At full power nominal operation, the minimum DNBR was found to be 2.28. This means that for these conditions, the probability of the peak power rod going through DNB is much less than 0.1 percent with 95 percent confidence. In the extremely

unlikely event that DNB should occur, the clad temperature will rise due to the steam blanketing at the rod surface and the consequent degradation in heat transfer. During this time there is potential for a chemical reaction between the cladding and the coolant. However, because of the relatively good film boiling heat transfer following DNB, the energy release resulting from this reaction is insignificant compared to the power produced by the fuel.

DNB With Physical Burnout

Westinghouse (Reference 73) has conducted DNB tests in a 25-rod bundle where physical burnout occurred with one rod. After this occurrence, the 25-rod test section was used for several days to obtain more DNB data from the other rods in the bundle. The burnout and deformation of the rod did not affect the performance of neighboring rods in the test section during the burnout or the validity of the subsequent DNB data points as predicted by the W-3 correlation. No occurrences of flow instability or other abnormal operation were observed.

DNB With Return to Nucleate Boiling

Additional DNB tests have been conducted by Westinghouse (Reference 80) in 19 and 21 rod bundles. In these tests, DNB without physical burnout was experienced more than once on single rods in the bundles for short periods of time. Each time, a reduction in power of approximately 10 percent was sufficient to reestablish nucleate boiling on the surface of the rod. During these and subsequent tests, no adverse effects were observed on this rod or any other rod in the bundle as a consequence of operating in DNB.

3.4.3.9 Fuel Rod Behavior Effects from Coolant Flow Blockage

Coolant flow blockages can occur within the coolant channels of a fuel assembly or external to the reactor core. The effects of fuel assembly blockage within the assembly on fuel rod behavior is more pronounced than external blockages of the same magnitude. In both cases the flow blockages cause local reductions in coolant flow. The amount of local flow reduction, where it occurs in the reactor, and how far along the flow stream the reduction persists are considerations which will influence the fuel rod behavior. The effects of coolant flow blockages in terms of maintaining rated core performance are determined both by analytical and experimental methods. The experimental data are usually used to augment analytical tools such as computer programs similar to the THINC-IV program. Inspection of the DNB correlation (Section 3.4.2.3 and Reference (2)) shows that the predicted DNBR is dependent upon the local values of quality and mass velocity.

The THINC-IV Code is capable of predicting the effects of local flow blockages on DNBR within the fuel assembly on a subchannel basis, regardless of where the flow blockage occurs. In

Reference (34), it is shown that for a fuel assembly similar to the Westinghouse design, THINC-IV accurately predicts the flow distribution within the fuel assembly when the inlet nozzle is completely blocked. Full recovery of the flow was found to occur about 30 inches downstream of the blockage. With the reference reactor operating at the nominal full power conditions specified in Table 3.4-1, the effects of an increase in enthalpy and decrease in mass velocity in the lower portion of the fuel assembly would not result in the reactor reaching the limiting DNBR specified in Section 3.4.1.1.

From a review of the open literature it is concluded that flow blockage in "open lattice cores" similar to the Westinghouse cores cause flow perturbations which are local to the blockage. For instance, A. Ohtsubo, et. al., (Reference 81) shows that the mean bundle velocity is approached asymptotically about 4 inches downstream from a flow blockage in a single flow cell. Similar results were also found for 2 and 3 cells completely blocked. Basmer (Reference 82), et. al., tested an open lattice fuel assembly in which 41 percent of the subchannels were completely blocked in the center of the test bundle between spacer grids. Their results show the stagnant zone behind the flow blockage essentially disappears after 1.65 L/De or about 5 inches for their test bundle. They also found that leakage flow through the blockage tended to shorten the stagnant zone or in essence the complete recovery length. Thus, local flow blockages within a fuel assembly have little effect on subchannel enthalpy rise. The reduction in local mass velocity is then the main parameter, which affects the DNBR. If this plant were operating at full power and nominal steady-state conditions as specified in Table 3.4-1, a reduction in local mass velocity greater than 50 percent would be required to reduce the DNBR from 2.28 to the safety analysis limit DNBR. The above mass velocity effect on the DNB correlation was based on the assumption of fully developed flow along the full channel length. In reality a local flow blockage is expected to promote turbulence and thus would likely not affect DNBR at all.

Coolant flow blockages induce local crossflows as well as promote turbulence. Fuel rod behavior is changed under the influence of a sufficiently high crossflow component. Fuel rod vibration could occur, caused by this crossflow component, through vortex shedding or turbulent mechanisms. If the crossflow velocity exceeds the limit established for fluidelastic stability, large amplitude whirling results. The limits for a controlled vibration mechanism are established from studies of vortex shedding and turbulent pressure fluctuations. Crossflow velocity above the established limits can lead to mechanical wear of the fuel rods at the grid support locations. Fuel rod wear due to flow induced vibration is considered in the fuel rod fretting evaluation (see Section 3.2.1.3.2).

3.4.4 Testing And Verification

3.4.4.1 Tests Prior to Initial Criticality

A reactor coolant flow test was performed following fuel loading but prior to initial criticality. Coolant loop pressure drop data is obtained in this test. This data in conjunction with coolant pump performance information allows determination of the coolant flow rates at reactor operating conditions. This test verifies that proper coolant flow rates have been used in the core thermal and hydraulic analysis.

3.4.4.2 Initial Power and Plant Operation

Core power distribution measurements are made at several core power levels (see Section 3.3.2.2.7). These tests are used to insure that conservative peaking factors are used in the core thermal and hydraulic analysis.

Additional demonstration of the overall conservatism of the THINC analysis was obtained by comparing THINC predictions to incore thermocouple measurements. These measurements were performed on the Zion reactor (Reference 83). No further in-reactor testing is planned.

3.4.4.3 Component and Fuel Inspections

Inspections performed on the manufactured fuel are delineated in Section 3.2.1.4. Fabrication measurements critical to thermal and hydraulic analysis are obtained to verify that the engineering hot channel factors employed in the design analyses (Section 3.4.2.3.4) are met.

3.4.5 Instrumentation Application

3.4.5.1 Incore Instrumentation

Instrumentation is located in the core so that by correlating movable neutron detector information with fixed thermocouple information radial, axial, and azimuthal core characteristics may be obtained for all core quadrants.

The incore instrumentation system is comprised of thermocouples positioned to measure fuel assembly coolant outlet temperatures at preselected positions, and fission chamber detectors positioned in guide thimbles, which run the length of, selected fuel assemblies to measure the neutron flux distribution. Figure 3.4-14 shows the typical number and location of instrumented assemblies in the core.

The core-exit thermocouples provide a backup to the flux monitoring instrumentation for monitoring power distribution. Normally, a thermocouple map using the core exit

thermocouples, is taken monthly when incore flux mapping is performed. Abnormal power distributions may be deduced by comparing the recent thermocouple map(s) with a reference thermocouple map.

The movable incore neutron detector system could be used for more detailed mapping if the thermocouple system were to indicate an abnormality. These two complementary systems are more useful when taken together than either system alone would be. The incore instrumentation system is described in more detail in Chapter 7.

The incore instrumentation is provided to obtain data from which fission power density distribution in the core, coolant enthalpy distribution in the core, and fuel burnup distribution may be determined.

3.4.5.2 Overtemperature and Overpower ΔT Instrumentation

The Overtemperature ΔT trip protects the core against low DNBR. The Overpower ΔT trip protects against excessive power (fuel rod rating protection).

As discussed in Chapter 7, factors included in establishing the Overtemperature ΔT and Overpower ΔT trip setpoints includes the reactor coolant temperature in each loop and the axial distribution of core power through the use of the two section excore neutron detectors.

3.4.5.3 Instrumentation to Limit Maximum Power Output

The output of the three ranges (source, intermediate, and power) of detectors, with the electronics of the nuclear instruments, are used to limit the maximum power output of the reactor within their respective ranges.

There are six radial locations containing a total of eight neutron flux detectors installed around the reactor in the primary shield, two proportional counters for the source range installed on opposite "flat" portions of the core containing the primary startup sources at an elevation approximately 1/4 of the core height. Two compensated ionization chambers for the intermediate range, located in the same instrument walls and detector assemblies as the source range detectors, are positioned at an elevation corresponding to one half of the core height; four dual section uncompensated ionization chamber assemblies for the power range installed vertically at the four corners of the core and located equidistant from the reactor vessel at all points, and, to minimize neutron flux pattern distortions, within one foot of the reactor vessel. Each power range detector provides two signals corresponding to the neutron flux in the upper and in the lower sections of the core quadrant. The three ranges of detectors are used as inputs to

monitor neutron flux from a completely shutdown condition to 120 percent of full power with the capability of recording overpower excursions up to 200 percent of full power.

The difference in neutron flux between the upper and lower sections of the power range detectors are used to limit the Overtemperature ΔT and Overpower ΔT trip setpoints and to provide the operator with an indication of the core axial flux difference. Power range channels are also used for:

1. The rod speed control function.
2. To alert the operator to an excessive power unbalance between the quadrants.
3. Protect the core against RCCA ejection accidents.
4. Protect the core against adverse power distributions resulting from dropped rods.

Details of the neutron detectors and nuclear instrumentation design and the control and trip logic are given in Chapter 7. The limits on neutron flux operation and trip setpoints are given in the Technical Specifications.

3.4.6 References for Section 3.4

1. Friedland, A. J., and Ray, S., "Revised Thermal Design Procedure," WCAP-11397-P-A, April 1989.
2. Davidson, S. L. and Kramer, W. R.; (Ed.) "Reference Core Report VANTAGE 5 Fuel Assembly," WCAP-10444-P-A, September 1985.
3. Tong, L. S., "Boiling Crisis and Critical Heat Flux," AEC Critical Review Series, TID-25887, 1972.
4. Tong, L. S., "Critical Heat Fluxes on Rod Bundles," in "Two-Phase Flow and Heat Transfer in Rod Bundles," pp. 31-41, American Society of Mechanical Engineers, New York, 1969.
5. Christensen, J. A., Allio, R. J. and Biancheria, A., "Melting Point of Irradiated UO_2," WCAP-6065, February 1965.
6. Risher, D. H., "An Evaluation of the Rod Ejection Accident in Westinghouse Pressurized Water Reactors Using Spatial Kinetics Methods," WCAP-7588, Revision 1-A, January, 1975.
7. Weiner, R. A., et. al., "Improved Fuel Performance Models for Westinghouse Fuel Rod Design and Safety Evaluations," WCAP-11873-A, August 1988.

8. Leech, W. J., et. al., "Revised PAD Code Thermal Safety Model," WCAP-8720 Addendum 2 (Proprietary), October 1982.

9. Duncan, R. N., "Rabbit Capsule Irradiation of UO_2," CVTR Project, CVNA-142, June, 1962.

10. Nelson, R. C., Coplin, D. H., Lyons, M. F. and Weidenbaum, B., "Fission Gas Release from UO_2 Fuel Rods with Gross Central Melting," GEAP-4572, July, 1964.

11. Howard, V. C. and Gulvin, T. G., "Thermal Conductivity Determinations on Uranium Dioxide by a Radial Flow Method," UKAEA IG-Report 51, November, 1960.

12. Lucks, C. F. and Deem, H. W., "Thermal Conductivity and Electrical Conductivity of UO_2," in Progress Reports Relating to Civilian Applications, BMI-1448 (Rev.) for June, 1960; BMI-1489 (Rev.) for December, 1960 and BMI-1518 (Rev.) for May, 1961.

13. Daniel, J. L. , Matolich, Jr., J. and Deem, H. W., "Thermal Conductivity of UO_2," HW-69945, September, 1962.

14. Feith, A. D., "Thermal Conductivity of UO_2 by a Radial Heat Flow Method," TID-21668, 1962.

15. Vogt, J., Grandell, L. and Runfors, U., "Determination of the Thermal Conductivity of Unirradiated Uranium Dioxide," AB Atomenergi Report RMB-527, 1964, Quoted by IAEA Technical Report Series No. 59, "Thermal Conductivity of Uranium Dioxide."

16. Nishijima, T., Kawada, T. and Ishihata, A., "Thermal Conductivity of Sintered UO_2 and $A1_2O_3$ at High Temperatures," J. American Ceramic Society, 48, 31 34 (1965).

17. Ainscough, J. B. and Wheeler, M. J., "The Thermal Diffusivity and Thermal Conductivity of Sintered Uranium Dioxide," in Proceedings of the Seventh Conference of Thermal Conductivity, p. 467, National Bureau of Standards, Washington, 1968.

18. Godfrey, T. G., Fulkerson, W., Killie, T. G., Moore, J. P. and McElroy, D. L., "Thermal Conductivity of Uranium Dioxide and Armco Iron by an Improved Radial Heat Flow Technique," ORNL-3556, June, 1964.

19. Stora, J. P., et. al., "Thermal Conductivity of Sintered Uranium Oxide Under In-Pile Conditions," EURAEC-1095, August, 1964.

20. Bush, A., J., "Apparatus for Measuring Thermal Conductivity to 2500°C," Westinghouse Research Laboratories Report 64-1P6-401-R3, February, 1965 (Proprietary).

21. Asamoto, R. R., Anselin, F. L. and Conti, A. E., "The Effect of Density on the Thermal Conductivity of Uranium Dioxide," GEAP-5493, April, 1968.

22. Kruger, O. L., "Heat Transfer Properties of Uranium and Plutonium Dioxide," Paper 11-N-68F presented at the Fall meeting of Nuclear Division of the American Ceramic Society, September, 1968, Pittsburgh.

23. Gyllander, J. A., "In-Pile Determination of the Thermal Conductivity of UO_2 in the Range 500-2500°C," AE-411, January, 1971.

24. Lyons, M. F., et. al., "UO_2 Powder and Pellet Thermal Conductivity During Irradiation," GEAP-5100-1, March, 1966.

25. Coplin, C. H., et al., "The Thermal Conductivity of UO_2 by Direct In-Reactor Measurements," GEAP-5100-6, March, 1968.

26. Bain, A. S., "The Heat Rating Required to Produce Center Melting in Various UO_2 Fuels," ASTM Special Technical Publication, NO. 306, pp. 30-46, Philadelphia, 1962.

27. Stora, J. P., "In-Reactor Measurements of the Integrated Thermal Conductivity of UO_2 - Effect of Porosity," Trans. ANS, 13, 137-138 (1970).

28. International Atomic Energy Agency, "Thermal Conductivity of Uranium Dioxide," Report of the Panel held in Vienna, April, 1965, IAEA Technical Reports Series, No. 59, Vienna, The Agency, 1966.

29. Poncelot, C. G., "Burnup Physics of Heterogeneous Reactor Lattices, WCAP-6069, June, 1965.

30. Nodvick, R. J., "Saxton Core II Fuel Performance Evaluation," WCAP-3385-56, Part II, "Evaluation of Mass Spectrometric and Radiochemical Analyses of Irradiated Saxton Plutonium Fuel," July, 1970.

31. Tong, L. S., "Boiling Heat Transfer and Two-Phase Flow," John Wiley & Sons, New York, 1965.

32. Chelemer, H., Weisman, J. and Tong, L. S., "Subchannel Thermal Analysis of Rod Bundle Cores," WCAP-7015, Revision 1, January,1969.

33. Hochreiter, L. E., and Chelemer, H., "Application of the THINC-IV Program to PWR Design," WCAP-8054-P-A, February 1989.

34. Hochreiter, L. E., Chelemer, H. and Chu, P. T., "THINC-IV An Improved Program for Thermal-Hydraulic Analysis of Rod Bundle Cores," WCAP-7956-P-A, February 1989 (Proprietary).

35. Motley, F. E. and Cadek, F. F., "DNB Tests Results for New Mixing Vane Grids (R)," WCAP-7695-P-A, January 1975 (Proprietary) and WCAP-7958-A, January 1975 (Proprietary).

36. Motley, F. E. and Cadek, F. F., "DNB Tests Results for R Grid Thimble Cold Wall Cells," WCAP-7695-Addendum 1-P-A, January, 1975 (Proprietary) and WCAP-7958-Addendum 1-A, January, 1975 (Non-Proprietary).

37. Tong, L. S., "Prediction of Departure from Nucleate Boiling for an Axially Non-Uniform Heat Flux Distribution," J. Nucl. Energy, 21, 241-248 (1967).

38. Cadek, F. F., Motley, F. E. and Dominicis, D. P., "Effect of Axial Spacing on Interchannel Thermal Mixing with R Mixing Vane Grid, WCAP-7941-P-A, January, 1975 (Proprietary) and WCAP-7959-A, January, 1975 (Non-Proprietary).

39. Rowe, D. S. and Angle, C. W., "Crossflow Mixing Between Parallel Flow Channels During Boiling, Part II Measurement of Flow and Enthalpy in Two Parallel Channels," BNWL-371, Part 2, December, 1967.

40. Rowe, D. S. and Angle, C. W., "Crossflow Mixing Between Parallel Flow Channels During Boiling, Part III Effect of Spacers on Mixing Between Two Channels," BNWL-371, part 3, January, 1969.

41. Gonzalez-Santalo, J. M. and Griffith, P., "Two-Phase Flow Mixing in Rod Bundle Subchannels," ASME Paper 72-WA/NE-19.

42. Motley, F. E., Wenzel, A. H. and Cadek, F. F., "The Effect of 17 x 17 Fuel Geometry on Interchannel Thermal Mixing," WCAP-8298 P-A, January, 1975 (Proprietary) and WCAP-8299-A, January, 1975 (Non-Proprietary).

43. Hill, K. W., Motley, F. E. and Cadek, F. F., "Effect of Local Heat Flux Spikes on DNB in Non-Uniform Heated Rod Bundles," WCAP-8174, August 1973 (Proprietary) and WCAP-8202, August 1973 (Non-Proprietary).

44. Cadek, F. F., "Interchannel Thermal Mixing with Mixing Vane Grids," WCAP-7667-P-A, January, 1975 (Proprietary) and WCAP-7755-A, January, 1975 (Non-Proprietary).

45. Skaritka, J., (Ed.), "Fuel Rod Bow Evaluation," WCAP-8691, Revision 1 (Proprietary), July 1979.

46. Letter from C. Berlinger (NRC) to E. P. Rahe Jr. (W), Subject: Request for Reduction in Fuel Assembly Burnup Limit for Calculation of Maximum Rod Bow Penalty, June 18, 1986.

47. Corsetti, L. V. and Joffre, P. F., "Mechanical and Hydraulic Compatibility Characterization of D. C. Cook 2 Fuel Assemblies," Combustion Engineering report, December 1986.

48. Davidson, S. L., Iorii, J. A., "Reference Core Report - 17 x 17 Optimized Fuel Assembly," WCAP-9500-A, May 1982.

49. Letter from E. P. Rahe (W) to Miller (NRC) dated March 19, 1982, NS-EPR-2573, WCAP-9500 and WCAPS 9401/9402 NRC SER Mixed Core Compatibility Items.

50. Letter from C. O. Thomas (NRC) to Rahe (W) - Supplemental Acceptance No. 2 for Referencing Topical Report WCAP-9500, January 1983.

51. Dittus, F. W., and Boelter, L. M. K., "Heat Transfer in Automobile Radiators of the Tubular Type," University of California, Berkeley, Publication in Eng. 2, No. 13, 443-461 (1930).

52. Letter from W. J. Johnson (Westinghouse) to M. W. Hodges (NRC), NS-NRC-87-3208, dated October 2, 1987, Subject: "VANTAGE 5 DNB Transition Core Effects."

53. Letter from M. W. Hodges (NRC), to W. J. Johnson (W), NRC SER on VANTAGE 5 Transition Core Effects, dated February 24, 1988.

54. Schueren, P., McAtee, K. R., "Extension of Methodology for Calculating Transition Core DNBR Penalties," WCAP-11837, May 1988.

55. Weisman, J., "Heat Transfer to Water Flowing Parallel to Tube Bundles," Nucl. Sci. Eng., 6, 78-79 (1959).

56. Thom, J. R. S., Walker, W. M., Fallon, T. A. and Reising, G. F. S.,"Boiling in Sub-cooled Water During Flowup Heated Tubes or Annuli," Prc. Instn. Mech. Engrs., 180, Pt. C, 226-46 (1955-66).

57. Hetsroni, G., "Hydraulic Tests of the San Onofre Reactor Model, "WCAP-3269-8, June, 1964.

58. Hetsroni, G., "Studies of the Connecticut-Yankee Hydraulic Model," NYO-3250-2, June, 1965.

59. Idel'chik, I. E., "Handbook of Hydraulic Resistance," AEC-TR-6630, 1960.

60. Moody, L. F., "Friction Factors for Pipe Flow," Transaction of the American Society of Mechanical Engineers, 66, 671-684 (1944).

61. Maurer, G. W., "A Method of Predicting Steady State Boiling Vapor Fractions in Reactor Coolant Channels," WAPD-BT-19, pp. 59-70. June, 1960.

62. Griffith, P., Clark, J. A. and Rohsenow, W. M., "Void Volumes in Subcooled Boiling Systems," ASME Paper No. 58-HT-19.

63. Bowring, R. W., "Physical Model, Based on Bubble Detachment, and Calculation of Steam Voidage in the Subcooled Region of a Heated Channel," HPR-10, December, 1962.

64. Carter, F. D., "Inlet Orificing of Open PWR Cores," WCAP-7836, January, 1972.

65. Shefcheck, J., "Application of the THINC Program to PWR Design," WCAP-7359-L, August, 1969 (Proprietary) and WCAP-7838, January, 1972 (Non-Proprietary).

66. Novendstern, E. H. and Sandberg, R. O., "Single Phase Local Boiling and Bulk Boiling Pressure Drop Correlations," WCAP-2850, April, 1966 (Proprietary) and WCAP-7916, June, 1972 (Non-Proprietary).

67. Owens, Jr., W. L., "Two-Phase Pressure Gradient," in International Developments in Heat Transfer, Part II, pp. 363-368, ASME, New York, 1961.

68. McFarlane, A. F., "Power Peaking Factors," WCAP-7912-P-A, January, 1975 (Proprietary) and WCAP-7912-A, January, 1975 (Non-Proprietary).

69. Morita, T., et al., "Power Distribution Control and Load Follow Procedures," WCAP-8385, September, 1974 (Proprietary) and WCAP-8403, September, 1974 (Non-Proprietary).

70. Vallentine, H. R., "Applied Hydrodynamics," Buttersworth Publishers, London, 1959.

71. Kays, W. M. and London, A. L., "Compact Heat Exchangers," National Press, Palo Alto, 1955.

72. Rowe, D. S., "COBRA-II, a Digital Computer Program for Steady State and Transient Thermal-Hydraulic Analysis of Rod Bundle Nuclear Fuel Elements," BNWL-B-82, 1971.

73. Weisman, J., Wenzel, A. H., Tong, L. S., Fitzsimmons, D., Thorne, W. and Batch, J., "Experimental Determination of the Departure from Nucleate Boiling in Large Rod Bundles at High Pressures," Chem. Eng. Prog. Symp. Ser. 64, No. 82, 114-125 (1968).

74. Boure, J. A., Bergles, A. E., and Tong. L. S., "Review of Two-Phase Flow Instability," Nuclear Engineering Design 25 (1973) p. 165-192.

75. Lahey, R. T. and Moody, F. J., "The Thermal Hydraulics of a Boiling Water Reactor," American Nuclear Society, 1977.

76. Saha, P., Ishii, M. and Zuber, N., "An Experimental Investigation of the Thermally Induced Flow Oscillations in Two-Phase Systems," J. of Heat Transfer, November 1976, pp. 616-622.

77. Kakac, S., Veziroglu, T. N., Akyuzlu, K., Berkol, O., "Sustained and Transient Boiling Flow Instabilities in a Cross-Connected Four-Parallel-Channel Upflow System," Proceedings of 5th International Heat Transfer Conference, Tokyo, September 3-7, 1974.

78. Taleyarkhan, R., Podowski, M., Lahey, Jr., R. T., "An Analysis of Density - Wave Oscillations in Ventilated Channels," NUREG/CR-2972, March 1983.

79. Kao, H. S., Morgan, C. D., and Parker, W. B., "Prediction of Flow Oscillation in Reactor Core Channel," Transactions of the ANS, Vol. 16, 1973, pp. 212-213.

80. Tong, L. S., et al., "Critical Heat Flux (DNB) in Square and Tri-Angular Array Rod Bundles," presented at the Japan Society of Mechanical Engineers Semi-International Symposium held at Tokyo, Japan, September 4-8, 1967, pp. 25-34.

81. Ohtsubo, A., and Uruwashi, S., "Stagnant Fluid Due to Local Flow Blockage," J. Nucl. Sci. Technol. 9 No. 7, 433-434 (1972).

82. Basmer, P., Kirsh, D. and Schultheiss, G. F., "Investigation of the Flow Pattern in the Recirculation Zone Downstream of Local Coolant Blockages in Pin Bundles," Atomwirtchaft, 17 No. 8, 416-417 (1972). (In German.)

83. Burke, T. M., Meyer, C. E. and Shefcheck, J., "Analysis of Data from the Zion (Unit 1) THINC Verification Test," WCAP-8453-A, May, 1976.

84. Chelemer, H., Boman, L. H. and Sharp, D. R., "Improved Thermal Design Procedure," WCAP-8567-P, July 1975 (Proprietary) and WCAP-8568, July 1975 (Proprietary).

85. Slagle, W. H. (Ed.) et. al., "Westinghouse Improved Performance Analysis and Design Model (PAD 4.0)," WCAP-15063-P-A, Revision 1 with Errata, July 2000.

86. AEP-15-59, "American Electric Power, Donald C. Cook Units 1 & 2, Westinghouse Resolution Plan and Technical Basis for NSAL-14-5, "Lower Than Expected Critical Heat Flux Results Obtained During DNB Testing," December 1, 2015.

87. Good, B. F., Allen, J. J., and Szweda, N. A., "Reactor Internals Upflow Conversion Program Engineering Report for Donald C. Cook Generation Station Unit 2," WCAP-18282-P, Rev 2, March 2018 (Proprietary).

REACTOR DESIGN COMPARISON TABLE [1]

Thermal and Hydraulic Design Parameters		Initial Cycle	Typical Cycle Before MUR Power Uprate	Typical Cycle After MUR Power Uprate
1.	Reactor Core Heat Output, MWt	3,391	3,411	3468
2.	Reactor Core Heat Output, 10^6 Btu/hr	11,573.5	11,639	11,833
3.	Heat Generated in Fuel, %	97.4	97.4	97.4
4.	System Pressure, Nominal, psia	2,280	2,280	2,280
5.	System Pressure, Minimum Steady-State, psia	2,250	2,250	2,250
6.	Minimum Departure from Nucleate Boiling Ratio for Design Transients			
	Typical Flow Channel	1.80 (2)	1.69 (3)	1.69 (3)
	Thimble Flow Channel	1.77 (2)	1.61 (3)	1.61 (3)

1 The fresh fuel assemblies for Cycle 21 and beyond will have **Optimized ZIRLO™** clad fuel rods and ZIRLO® guide thimbles, instrumentation tubes, mid-grids and IFM grids with balanced vanes. The option to remove thimble plugs will exist for Cycle 13 and beyond. This will increase the bypass flow and cause small changes in the core flow rates and temperatures.

2 These numbers are based on Improved Thermal design Procedure in Reference 2.

3 These numbers are based on Revised Thermal Design Procedure in Reference 3.

REACTOR DESIGN COMPARISON TABLE [1]

	Thermal and Hydraulic Design Parameters	Initial Cycle	Typical Cycle Before MUR Power Uprate	Typical Cycle After MUR Power Uprate
	COOLANT FLOW			
7.	Total Thermal Design Flow Rate, 10^6 lb_m/hr	142.7	134.4	134.7
8.	Effective Flow Rate for Heat Transfer, 10^6 lb/hr	136.3	127.5	125.15
9.	Effective Flow Area for Heat Transfer, ft^2	51.1	54.1	54.1
10.	Average Velocity Along Fuel Rods, ft/sec	16.7	14.6	13.5
11.	Average Mass Velocity, 10^6 lb_m/hr-ft^2	2.72	2.36	2.31
	COOLANT TEMPERATURE, °F			
12.	Nominal Inlet	541.3	543.4 (4)	540.8 (4)
13.	Average Rise in Vessel	61.8	65.3 (4)	66.4 (4)
14.	Average Rise in Core	63.4	68.4 (4)	71.0 (4)
15.	Average in Core	574.3	579.3 (4)	578.05 (4)

4 Based on thermal design flow

REACTOR DESIGN COMPARISON TABLE [1]

	Thermal and Hydraulic Design Parameters	Initial Cycle	Typical Cycle Before MUR Power Uprate	Typical Cycle After MUR Power Uprate
16.	Average in Vessel	572.2	576.0 (4)	574.0 (4)
	HEAT TRANSFER			
17.	Active Heat Transfer, Surface Area, ft^2	59,700	57,505	57,505
18.	Average Heat Flux, Btu/hr-ft^2	188,700	197,180	200,477
19.	Maximum Heat Flux for Normal Operation, Btu/hr-ft^2	437,800(5)	460,420	468,114
20.	Average Thermal Output, kW/ft	5.41	5.45	5.54
21.	Maximum Thermal Output for Normal Operation, kW/ft	12.6 (6)	12.7	12.9
22.	Maximum Thermal Output at Maximum Overpower Trip Point (118% power), kW/ft	18.0 (7)	22.5	22.5
23.	Heat Flux Hot Channel Factor, F_Q	2.32 (8)	2.335	2.335

5 The value of 437,800 Btu/hr-ft^2 is associated with a Cycle 1 value of F_Q of 2.32.

6 This value of 12.6 kW/ft is associated with a Cycle 1 value of F_Q of 2.32.

7 See Section 3.3.2.2.6.

8 The value of F_Q = 2.32 was the value of F_Q for normal operation reported in the original FSAR.

REACTOR DESIGN COMPARISON TABLE [1]

	Thermal and Hydraulic Design Parameters	Initial Cycle	Typical Cycle Before MUR Power Uprate	Typical Cycle After MUR Power Uprate
24.	Peak Fuel Central Temperature at 100% Power, °F	< 4700	< 4700	< 4700
25.	Peak Fuel Central Temperature at Maximum Thermal Output for Maximum Overpower Trip Point, °F	< 4700	< 4700	< 4700
	FUEL ASSEMBLIES			
26.	Design	RCC Canless	RCC Canless	RCC Canless
27.	Number of Fuel Assemblies	193	193	193
28.	UO_2 Rods per Assembly	264	264	264
29.	Rod Pitch, in	0.496	0.496	0.496
30.	Overall Dimensions, in	8.426 x 8.426	8.426 x 8.426	8.426 x 8.426
31.	Fuel Weight (as UO_2), lb	222,739	204,200	204,200
32.	Zircaloy Weight, lb	50,913	45, 914	45, 914

REACTOR DESIGN COMPARISON TABLE [1]

Thermal and Hydraulic Design Parameters		Initial Cycle	Typical Cycle Before MUR Power Uprate	Typical Cycle After MUR Power Uprate
33.	Number of Grids per Assembly	8 – Type R	6 – Flow mixer grids 2 – Non-flow mixer grids 3 – IFM grids 1 – Protective Grid	6 – Flow mixer grids 2 – Non-flow mixer grids 3 – IFM grids 1 – Protective Grid
34.	Loading Techniques	Out – In Checkerboard	3 – Region Low Leakage	3 – Region Low Leakage
FUEL RODS				
35.	Number	50,952	50,952	50,952
36.	Outside Diameter, in	0.374	0.360	0.360
37.	Diametral Gap, in	0.0065	0.0062	0.0062
38.	Clad Thickness, in	0.0225	0.0225	0.0225
39.	Clad Material	Zircaloy-4	Zircaloy-4	**Optimized ZIRLO™** starting with Cycle 21

REACTOR DESIGN COMPARISON TABLE [1]

	Thermal and Hydraulic Design Parameters	Initial Cycle	Typical Cycle Before MUR Power Uprate	Typical Cycle After MUR Power Uprate
	FUEL PELLETS			
40.	Material	UO_2 Sintered	UO_2 Sintered 0.370 Enriched	UO_2 Sintered 0.370 Enriched
41.	Density (% of Theoretical)	95	95.5	95.5
42.	Diameter, in	0.3225	0.3088	0.3088
43.	Length, in	0.530 (4)	0.462 Axial Blankets	0.462 Axial Blankets
	ROD CLUSTER CONTROL ASSEMBLIES			
44.	Neutron Absorber, Full/Part Length (9)	Ag-In-Cd	Ag-In-Cd	Ag-In-Cd
45.	Cladding Material	Type 304 SS-Cold Worked	Type 304 SS-Cold Worked	Type 304 SS-Cold Worked
46.	Clad Thickness, in	0.0185	0.0185	0.0185
47.	Number of Clusters, Full and Part Length (9)	53/0	53/0	53/0

[9] Part Length CRDMs were eliminated.

REACTOR DESIGN COMPARISON TABLE [1]

	Thermal and Hydraulic Design Parameters	Initial Cycle	Typical Cycle Before MUR Power Uprate	Typical Cycle After MUR Power Uprate
48.	Number of Absorber Rods per Cluster	24	24	24
	CORE STRUCTURE			
49.	Core Barrel, I.D./O.D., in	148.0/152.5	148.0/152.5	148.0/152.5
50.	Thermal Shield, I.D./O.D., in	158.5/164.0	158.5/164.0	158.5/164.0
	STRUCTURE CHARACTERISTICS			
51.	Core Diameter, in (Equivalent)	132.7	132.7	132.7
52.	Core Height, in (Active Fuel)	144.0	144.0	144.0
	REFLECTOR THICKNESS AND COMPOSITION			
53.	Top - Water plus Steel, in	10	10	10
54.	Bottom - Water plus Steel, in	10	10	10
55.	Side - Water plus Steel, in	15	15	15
56.	H_2O/U Molecular Ratio Core, Lattice (Cold)	2.41	2.73	2.73

REACTOR DESIGN COMPARISON TABLE [1]

	Thermal and Hydraulic Design Parameters	Initial Cycle	Typical Cycle Before MUR Power Uprate	Typical Cycle After MUR Power Uprate
	FEED ENRICHMENT, W/O			
57.	Region 1	2.10	4.0/2.6 (10)	4.0/2.6 (10)
58.	Region 2	2.60	4.0/2.6 (10)	4.0/2.6 (10)
59.	Region 3	3.10	4.0/2.6 (10)	4.0/2.6 (10)

10 Reload enrichments are cycle-specific, 2.6 w/o value corresponds to the axial blanket.

ANALYTIC TECHNIQUES IN CORE DESIGN

Analysis	Technique	Computer Code	Section Referenced
Mechanical Design of Core Internals			
Loads, Deflections, and Stress Analysis	Static and Dynamic Modeling	Blowdown code, FORCE, Finite element structural analysis code, and others	14.3.3
Fuel Rod Design			
Fuel Performance Characteristics (temperature, internal pressure, clad stress, etc.)	Semi-empirical thermal model of fuel rod with consideration of fuel density changes, heat transfer, fission gas release, etc.	Westinghouse fuel rod design model	3.2.1.3.1 3.3.3.1 3.4.2.2 3.4.3.4.2
Nuclear Design			
1. Cross Sections and Group Constants	Microscopic data Macroscopic constants for homogenized core regions	Modified ENDF/B-V or ENDF/B-VI library PHOENIX-P	3.3.3.2 3.3.3.2
	Group constants for control rods with self-shielding	PHOENIX-P	3.3.3.2
Nuclear Design (Continued)			
2. X-Y Power Distributions, Fuel Depletion, Critical Boron Concentrations, X-Y Xenon Distributions,	3D, 2-Group Nodal Expansion Method	ANC	3.3.3.3

ANALYTIC TECHNIQUES IN CORE DESIGN

Analysis	Technique	Computer Code	Section Referenced
Reactivity Coefficients			
3. Axial Power Distributions, Control Rod Worths, and Axial Xenon Distribution	1-D, 2-Group Diffusion Theory	APOLLO	3.3.3.3
4. Fuel Rod Power	Integral Transport Theory	LASER	3.3.3.1
Effective Resonance Temperature	Monte Carlo Weighting Function	REPAD	
Thermal-Hydraulic Design			
1. Steady-State	Subchannel analysis of local fluid conditions in rod bundles, including inertial and crossflow resistance terms, solution - progresses from core-wide to hot assembly to hot channel	THINC-IV	3.4.3.4.1
2. Transient Departure from Nucleate Boiling Analysis	Subchannel analysis of local fluid conditions in rod bundles during transients by including accumulation terms in conservation equations solution progresses from core-wide to hot assembly to hot channel	THINC-I (THINC-III)	3.4.3.4.1

DESIGN LOADING CONDITIONS FOR REACTOR CORE COMPONENTS

1.	Fuel Assembly Weight
2.	Fuel Assembly Spring Forces
3.	Internals Weight
4.	Control Rod Trip (equivalent static load)
5.	Differential Pressure
6.	Spring Preloads
7.	Coolant Flow Forces (static)
8.	Temperature Gradients
9.	Differences In Thermal Expansion a. Due to temperature differences b. Due to expansion of different materials
10.	Interference Between Components
11.	Vibration (mechanically or hydraulically induced)
12.	One Or More Loops Out Of Service
13.	Operational Transients
14.	Pump Overspeed
15.	Seismic Loads (operating basis earthquake and design basis earthquake)
16.	Blowdown Forces (due to cold and hot leg break)

Maximum Deflections Allowed For Reactor Internal Support Structure

Component	Allowable Deflections (in)	No Loss-of-Function Deflections (in)
Upper Barrel		
Radial inward	4.1	8.2
Radial outward	1.0	1.0
Upper Package	0.10	0.15
Rod Cluster Guide Tubes	1.00	1.75

Reactor Core Description

Active Core	
Equivalent Diameter, in	132.7
Active Fuel Height, First Core, in	144.0
Height-to-Diameter Ratio	1.09
Total Cross Section Area, ft^2	96.06
H_2O/U Molecular Ratio, lattice (Cold)	2.73
Reflector Thickness And Composition	
Top - Water plus Steel, in	10
Bottom - Water plus Steel, in	10
Side - Water plus Steel, in	15
Fuel Assemblies	
Number	193
Rod Array	17 x 17
Rods per Assembly	264
Rod Pitch, in	0.496
Overall Transverse Dimensions, in	8.426 x 8.426
Fuel Weight (as UO_2), lb - per assembly	1058
Zircaloy Weight, lb - per assembly	238
Number of Grids per Assembly	2-R
	6-Z
	3-IFM
	1-P

Reactor Core Description

Composition of Grids	R-Inconel 718
	Zircaloy 4/ZIRLO™
	IFM - Zircaloy 4/ZIRLO™
	P-Debris Resistant- Inconel 718
Weight of Grids (Effective in Core), lb - per assembly	20.10
Number of Guide Thimbles per Assembly	24
Composition of Guide Thimbles	Zircaloy 4/ZIRLO™
Diameter of Guide Thimbles (upper part), in	0.442 I.D. x 0.474 O.D.
Diameter of Guide Thimbles (lower part), in	0.397 I.D. x 0.429 O.D.
Diameter of Instrument Guide Thimbles, in	0.440 I.D. x 0.474 O.D.
Fuel Rods	
Number	50,952
Outside Diameter, in	0.360
Diameter Gap, in	0.0062
Clad Thickness, in	0.0225
Clad Material	Zircaloy-4 / ZIRLO / **Optimized ZIRLO™**
Fuel Pellets	
Material	UO_2 Sintered
Density (percent of Theoretical)	Approx. 95.5
Maximum Fuel Enrichments w/o	4.95
Diameter, in	0.3088
Length, in	0.370 Enriched

Reactor Core Description

	0.462 Axial Blanket
Mass of UO_2 per Foot of Fuel Rod, lb/ft	0.336 [1]
Rod Cluster Control Assemblies	
Neutron Absorber	Ag-In-Cd
Composition	80%, 15%, 5%
Diameter, in	0.341
Density, lb/in^3	0.367
Cladding Material	Type 304, Cold Worked Stainless Steel
Clad Thickness, in	0.0185
Number of Clusters	
Full Length	53
Number of Absorber Rods per cluster	24
Full Length Assembly Weight (dry), lb	149
Excess Reactivity	
Maximum Fuel Assembly k (Cold, Clean, Unborated Water)	1.476 [2]
Maximum Core Reactivity (Cold, Zero Power Beginning of Cycle)	1.224 [2]

[1] Based on fuel at 95.5% theoretical density

[2] Typical values

Reactor Core Description

Integral Fuel Burnable Absorber	
Number	~8640 [2]
Material	ZrB_2
Coating Thickness, mil	~0.2
Boron 10 Loading, mg/in	2.25

Nuclear Design Parameters
(Best-Estimate Values Are Representative Of A Typical Cycle)

Core Average Linear Power, kW/ft, including densification effects[1]		5.45 / 5.54
Total Heat Flux Hot Channel Factor, F_Q		2.335
Nuclear Enthalpy Rise Hot Channel Factor, $F^N_{\Delta H}$		1.61 [1+0.3(1-P)]
Reactivity Coefficients[2]	**Design Limits**	**Best Estimate**
Doppler-only Power, Coefficients, pcm/°F		
Upper Curve	-19.4 to -12.224	-12.4 to -7.9
Lower Curve	-9.55 to -5.818	-10.9 to -7.5
Doppler Temperature Coefficient, pcm/°F	-3.20 to -0.91	-1.9 to -1.3
Moderator Temperature Coefficient, pcm/°F	+5 to -38[3]	< + 5.0[4] to -29.54[3]
Boron Coefficient, pcm/ppm		-10.9 to -7.6
Rodded Moderator Density, pcm/gm/cc	0.54 x 10 E + 05	0.40 x 10 E + 05
Radial Assembly Peaking Factor	**Design Limits**	**Best Estimate**
Radial Assembly Peaking Factor[5]		
Unrodded		1.36 to 1.49
D bank		1.51 to 1.58
D + C		1.61 to 1.70
Boron Concentrations (ppm)	**Design Limits**	**Best Estimate**
Zero Power, K_{eff} = 0.99, Cold, Rod Cluster Control Assemblies Out		1804
Zero Power, K_{eff} = 0.99, Hot, Rod Cluster Control Assemblies Out		1930
Design Basis Refueling Boron Concentration	2400	1855

1 Before and After MUR power uprate values listed.
2 Uncertainties are referenced in Section 3.3.3.3.
3 Design limit dependent on vessel average moderator temperature. Value reported is for Cycle 14 temperature of 574.0 °F.
4 Administrative rod withdrawal limits are required if an MTC violation is observed during startup physics testing, as specified by an action statement in Technical Specification 3.1.3.A.1.
5 Typical values.

Nuclear Design Parameters
(Best-Estimate Values Are Representative Of A Typical Cycle)

Zero Power, K_{eff} = 0.95, Cold, Rod Cluster Control Assemblies In			1754
Zero Power, K_{eff} = 1.00, Hot, Rod Cluster Control Assemblies Out			1795
Full Power, No Xenon, K_{eff} = 1.0, Hot, Rod Cluster Control Assemblies Out			1648
Full Power, Equilibrium Xenon, K_{eff} Hot, Rod Cluster Control Assemblies Out			1316
Reduction with Fuel Burnup Reload Cycle, ppm/GWD/MTU[6]			~84
Delayed Neutron Fraction and Lifetime		**Design Limits**	**Best Estimate**
β	eff BOL, (EOL	0.0075, (0.0040)	0.0062, (0.0050)
ℓ	BOL, (EOL) μsec[5]		20.1, (22.3)
Control Rods		**Best Estimate**	**Best Estimate**
Rod Requirements			See Table 3.3-3
Maximum Bank Worth, pcm			1380
Maximum Ejected Rod Worth			See Chapter 14
Bank Worth, pcm[7]		BOL, Xe free HZP	EOL, Xe free HZP
	Bank D	1135	1380
	Bank C	966	1222
	Bank B	851	1259
	Bank A	572	617

[6] Gigawatt Day (GWD) = 1000 Megawatt Day (1000 MWD).
[7] Note: For two statepoint values of k_{eff}, k_1 and k_2, the reactivity change in pcm (percent milli) is given by In (k_2/k_1) x10^5.

SHUTDOWN REQUIREMENTS AND MARGINS

	Typical Values	
	BOC	**EOC**
Control Rod Worth (pcm)		
Available Rod Worth Less Worst Stuck Rod	4856	5879
(A) less 10%	4371	5291
Control Rod Requirements (pcm)		
Reactivity Defects (Doppler, Tavg, RIA, Redistribution)	1431	2764
Void Allowance	50	50
(B) Total Requirements	1481	2814
(C) Available Shutdown Margin [(A) – (B)] (pcm)	2890	2477
(D) Required Shutdown Margin (pcm)	1300	1300
Excess Shutdown Margin [(C) – (D)] (pcm)	1590	1177

AXIAL STABILITY INDEX PRESSURIZED WATER REACTOR CORE WITH A 12 FOOT HEIGHT

			Stability Index (hr^{-1})		
Burnup (MWD/MTU)	**F_Z**	**C_B (ppm)**	**Exp**	**Calc**	**Difference (Exp-Calc)**
1550	1.34	1065	-0.041	-0.032	-0.009
7700	1.27	700	-0.014	-0.006	-0.008
		Difference:	+0.027	+0.026	

COMPARISON OF MEASURED AND CALCULATED DOPPLER DEFECTS

Plant	Fuel Type	Core Burnup (MWD/MTU)	Measured (pcm)[1]	Calculated (pcm)
1	Air-filled	1800	1700	1710
2	Air-filled	7700	1300	1440
3	Air and helium-filled	8460	1200	1210

[1] 1 pcm = 10^{-5} $\Delta\rho$

Cook Nuclear Plant Unit 2 Reactor Design Comparison Table [1]

Thermal and Hydraulic Design Parameters	Initial Cycle	Typical Cycle Before MUR Power Uprate	Typical Cycle After MUR Power Uprate
Reactor Core Heat Output, MWt	3391	3411	3468
Reactor Core Heat Out, 10^6 BTU/hr	11,573.5	11,639	11,833
Heat Generated in Fuel, %	97.4	97.4	97.4
System Pressure, Nominal, psia [2]	2280	2280	2280
System Pressure, Minimum			
Steady-State, psia	2250	2250	2250
Minimum DNBR at Nominal Conditions			
Typical Flow Channel	3.03 [3]	2.42	2.66
Thimble (Cold Wall) Flow Channel	2.70 [3]	2.28	2.49
Design DNBR for Design Transients			
Typical Flow Channel	1.80 [4]	1.69 [5]	1.69 [5]
Thimble Flow Channel	1.77 [4]	1.61 [5]	1.61 [5]

1 The fresh fuel assemblies for Cycle 21 and beyond will have **Optimized ZIRLO™** clad fuel rods and ZIRLO® guide thimbles, instrumentation tubes, mid-grids and IFM grids with balanced vanes. The option to remove thimble plugs will exist for Cycle 13 and beyond. This will increase the bypass flow and cause small changes in the core flow rates, temperatures and pressure drops.

2 Pressure in the core. See Reference (1).

3 Based on Improved Thermal Design Procedure, Reference (84).

4 Including 31.1 percent rod bow penalty.

5 Value used in DNB analyses (RTDP Transients).

Cook Nuclear Plant Unit 2 Reactor Design Comparison Table [1]

Thermal and Hydraulic Design Parameters	Initial Cycle	Typical Cycle Before MUR Power Uprate	Typical Cycle After MUR Power Uprate
DNB Correlation	WRB-1	WRB-2	WRB-2
Coolant Flow [6]			
Total Thermal Design Flow Rate, 10^6 lb_m/hr	142.7	134.3	134.7
Best Estimate Flow, 10^6 lb_m/hr	148.4	145.2	145.2
Mechanical Design Flow, 10^6 lb_m/hr	154.3	154.5	154.5
Minimum Effective Flow Rate for Heat Transfer, 10^6 lb_m/hr	136.3	127.4	125.15
Effective Flow Area for Heat Transfer, ft^2	51.1	54.1	54.1
Average Velocity Along Fuel Rods, ft/sec	16.7	14.6	13.5
Average Mass Velocity, 10^6 lb_m/hr	2.72	2.35	2.31
Coolant Temperature [6]			
Nominal Inlet, °F	541.3	543.4	540.8
Average Rise in Vessel, °F	61.8	65.3	66.4
Average Rise in Core, °F	63.4	68.4	71.0
Average in Core, °F	574.3	579.3	578.05

6 Based on Thermal Design Flow.

Cook Nuclear Plant Unit 2 Reactor Design Comparison Table [1]

Thermal and Hydraulic Design Parameters	Initial Cycle	Typical Cycle Before MUR Power Uprate	Typical Cycle After MUR Power Uprate
Average in Vessel, °F	572.2 [7]	576.0	574.0
Heat Transfer			
Active Heat Transfer, Surface Area, ft^2	59,700	57,505	57,505
Average Heat Flux, BTU/hr-ft^2	188,700	197,180	200,477
Maximum Heat Flux for Normal Operation, BTU/hr-ft^2	437,800 [8]	460,420 [9]	468,114 [9]
Average Linear Power, kW/ft	5.41	5.45	5.54
Peak Linear Power for Normal Operation, kW/ft	12.6 [8]	12.7 [9]	12.9 [9]
Peak Linear Power Resulting from Overpower Transients/Operator Errors, (assuming a maximum overpower of 118%), kW/ft	18.0 [10]	22.5	22.0
Peak Linear Power for Prevention of Centerline Melt, kW/ft [11]	18.0	>22.5	>22.5
Fuel Central Temperature			
Peak at Peak Linear Power for Prevention of Centerline Melt, °F	4700	4700	4700

7 The vessel average temperature was increased to 573.8°F as per amendment 19 of May 13, 1980.
8 This limit is associated with the value of FQ = 2.32.
9 This limit is associated with the value of FQ = 2.335.
10 See Section 3.3.2.2.6.
11 See Section 3.4.2.2.6.

Cook Nuclear Plant Unit 2 Reactor Design Comparison Table [1]

Thermal and Hydraulic Design Parameters	Initial Cycle	Typical Cycle Before MUR Power Uprate	Typical Cycle After MUR Power Uprate
Pressure Drop [12]			
Across Core, psi	23.3 ± 2.3	27.0 ± 2.7	27.0 ± 2.7
Across Vessel, including nozzles, psi	43.2 ± 4.3	50.1 ± 5.0	50.1 ± 5.0

12 Based on Best Estimate Flow as discussed in 3.4.2.6.

VOID FRACTIONS AT NOMINAL REACTOR CONDITIONS [1] WITH DESIGN HOT CHANNEL FACTORS

	Average	Maximum
Core	0.2%	-------
Hot Subchannel	0.9%	2.1%

[1] Based upon Minimum Measured Flow.

SYSTEM DESIGN AND OPERATING PARAMETERS
(TYPICAL CYCLES BEFORE AND AFTER MUR POWER UPRATE)[1]

	At 70°	At Hot[2]
Approximate total RCS volume (including pressurizer and surge line), with 0% steam generator tube plugging. ($ft.^3$)	12,470	12,845
Approximate system liquid volume, (including pressurizer water) at maximum guaranteed power with 0% steam generator tube plugging. ($ft.^3$)		12,019 [3]

SYSTEM THERMAL AND HYDRAULIC DATA
(BASED ON THERMAL DESIGN FLOW)

	Typical Cycle Before MUR Power Uprate	Typical Cycle After MUR Power Uprate[4]
NSSS Power, MWt	3423	3480
Reactor Power, MWt	3411	3468
Thermal Design Flows, gpm		
Active Loop	88,500	88,500
Reactor	354,000	354,000
Total Reactor Flow, 10^6lb/hr	134.4	134.4
Temperatures, °F		
Reactor Vessel Outlet	606.4	611.1
Reactor Vessel Inlet	541.2	545.1
Steam Generator Outlet	541.0	544.8
Steam Generator Steam	521.1	524.0
Feedwater	431.0	444.1
Steam Pressure, psia	820.0	840.9
Total Steam Flow, 10^6 lb/hr	14.78	15.37

1 The option to remove thimble plugs will exist for Cycle 13 and beyond. This will increase bypass flow and cause small changes in the core flow rates and temperatures.

2 This includes a 3% volume increase (1.3% for thermal expansion and 1.7% for pipe connections to the reactor coolant loops, volume in the rod drive mechanisms and calculation inaccuracies). Refer to Westinghouse letters AEP-97-151, AEP-98-078, AEP-98-082, AEP-98-161, and the Westinghouse IMP database SEC-SAI-4824-CO.

3 Total RCS Volume (12,845 $ft.^3$) - Pressurizer steam volume at full power (826 $ft.^3$).

4 Based upon reactor loop average temperature of 578.1°F.

SYSTEM FLOW SUMMARY

Flows, gpm	Thermal Design [5]	Minimum Measured[6]	Best Estimate	Mechanical Design
4 Pumps Running, each loop	88,500	91,600	95,500	101,600

[5] Fixed value analyses (non-RTDP transients).
[6] DNB analyses values (RTDP transients).

COMPARISON OF THINC-IV AND THINC-I PREDICTIONS WITH DATA FROM REPRESENTATIVE WESTINGHOUSE TWO AND THREE LOOP REACTORS

Reactor	Power (MWt)	% Full Power	Measured Inlet Temp (^{o}F)	rms(^{o}F) THINC-I	(^{o}F) THINC-IV	Improvement (^{o}F) for THINC-IV over THINC-I
Ginna	847	65.1	543.7	1.97	1.83	0.14
	854	65.7	544.9	1.56	1.46	0.10
	857	65.9	543.9	1.97	1.82	0.15
	947	72.9	543.8	1.92	1.74	0.18
	961	74.0	543.7	1.97	1.79	0.18
	1091	83.9	542.5	1.73	1.54	0.19
	1268	97.5	542.0	2.35	2.11	0.24
	1284	98.8	540.2	2.69	2.47	0.22
	1284	98.9	541.0	2.42	2.17	0.25
	1287	99.0	544.4	2.26	1.97	0.29
	1294	99.5	540.8	2.20	1.91	0.29
	1295	99.6	542.0	2.10	1.83	0.27
Robinson	1427.0	65.1	548.0	1.85	1.88	0.03
	1422.6	64.9	549.4	1.39	1.39	0.00

COMPARISON OF THINC-IV AND THINC-I PREDICTIONS WITH DATA FROM REPRESENTATIVE WESTINGHOUSE TWO AND THREE LOOP REACTORS

Reactor	Power (MWt)	% Full Power	Measured Inlet Temp (^{o}F)	rms(^{o}F) THINC-I	(^{o}F) THINC-IV	Improvement (^{o}F) for THINC-IV over THINC-I
	1529.0	88.0	550.0	2.35	2.34	0.01
	2207.3	100.7	534.0	2.41	2.41	0.00
	2213.9	101.0	533.8	2.52	2.44	0.08

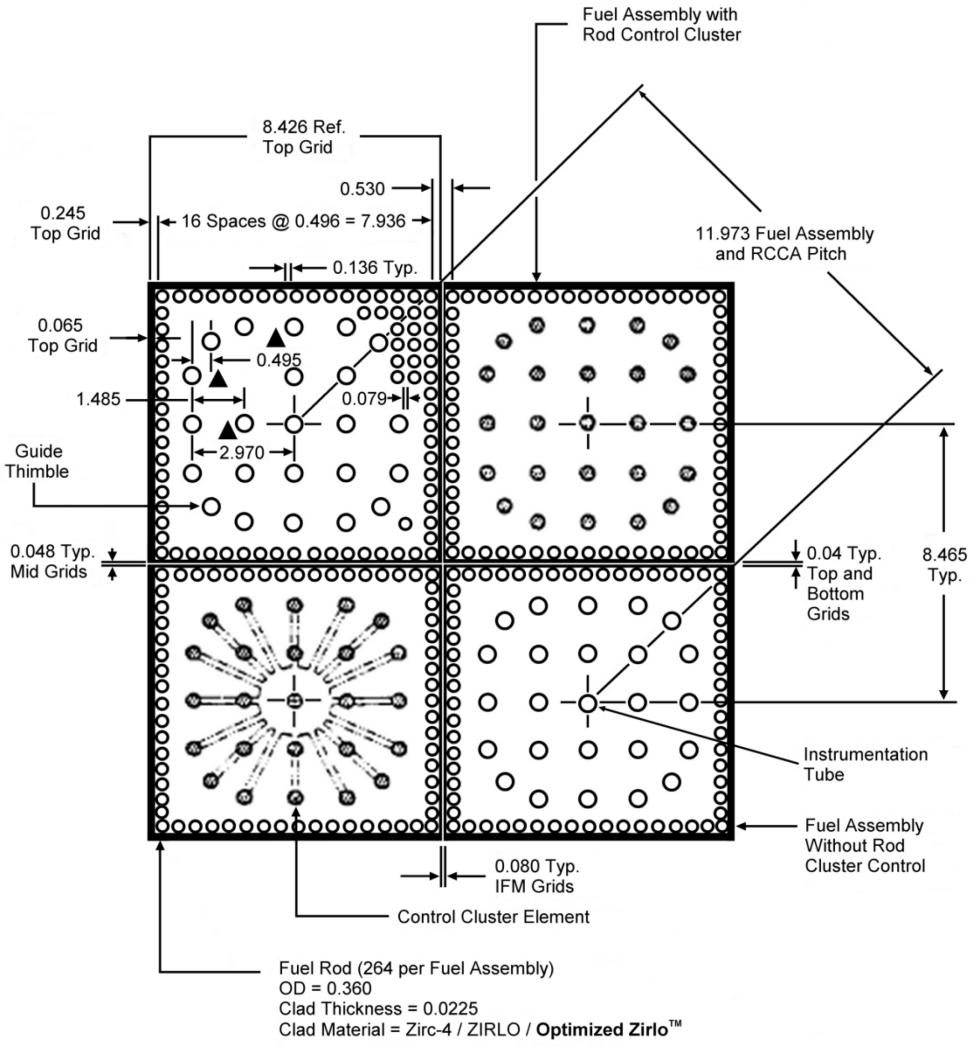

UFSAR Figure: 3.2-1	Change Description: UCR-2052, Rev. 0	Unit: 2

Title: Fuel Assembly Cross Section 17 x 17 Vantage 5 Update

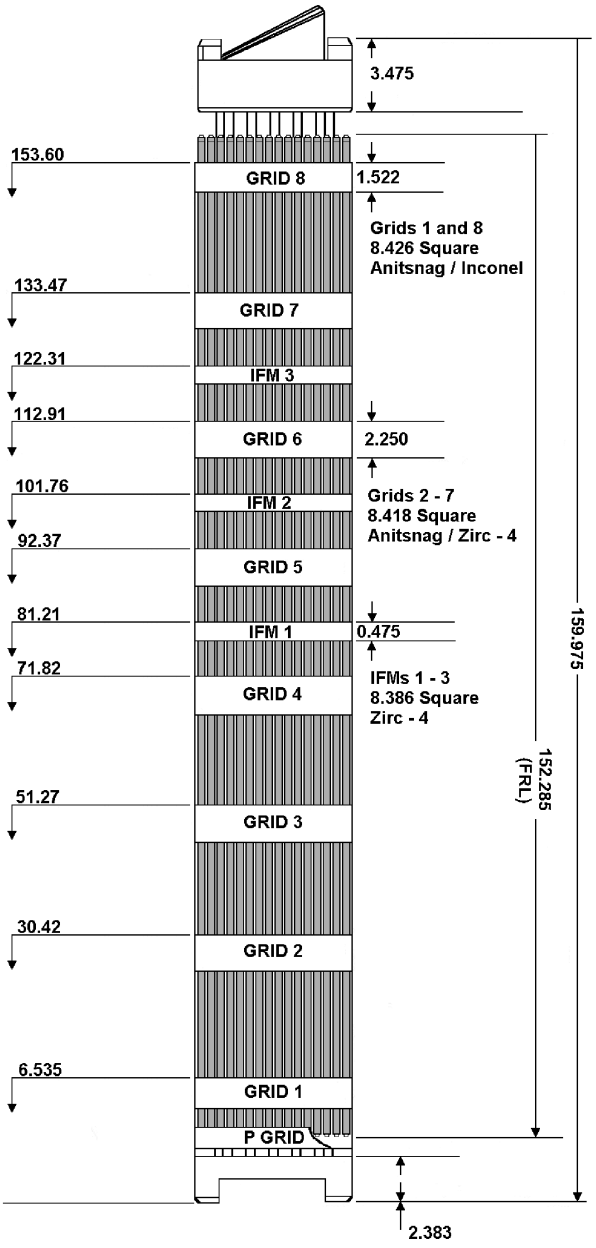

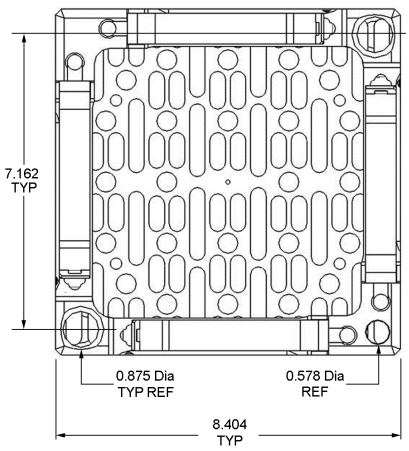

Top Nozzle

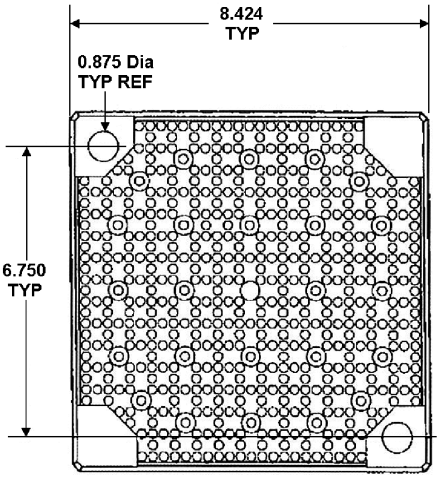

UFSAR Figure: 3.2-2	Change Description: UCR-2116, Rev. 0	Unit: 2

Title: Vantage 5 Fuel Assembly

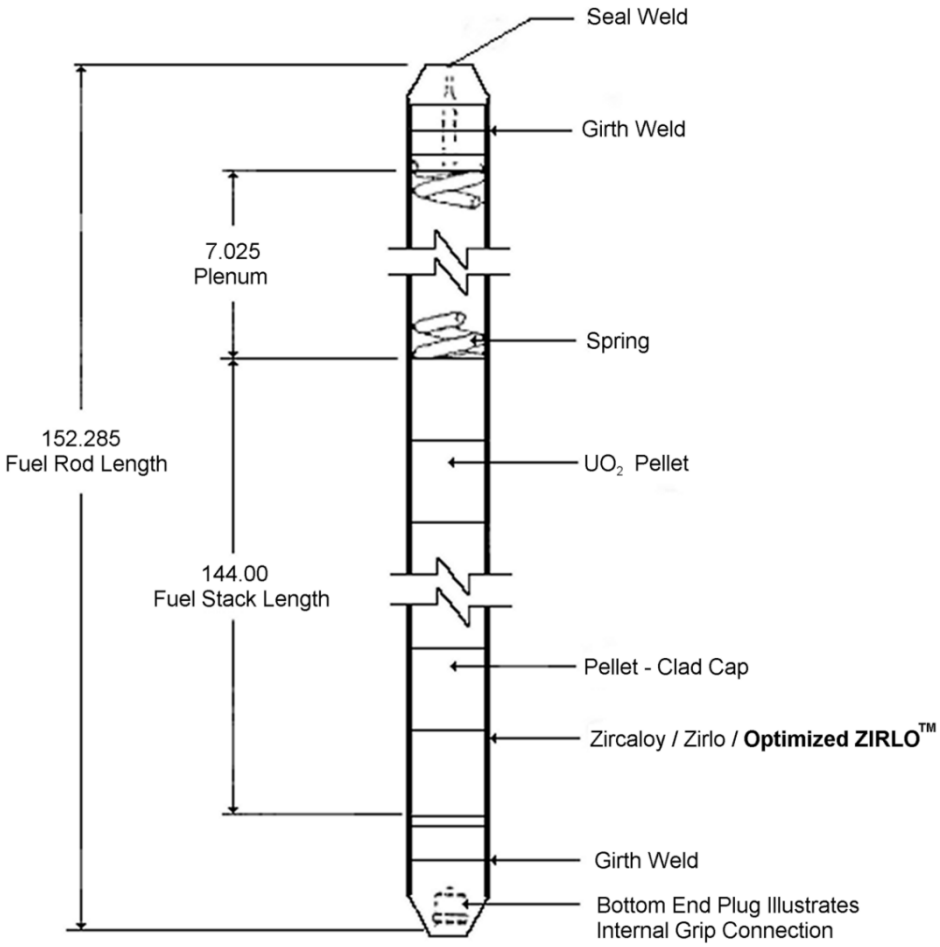

17 X 17 FUEL ROD ASSEMBLY

Specific Dimensions Depend on Design Variables Such as Prepressurization, Power History, and Discharge Burnup

Dimensions are in Inches (Nominal)

UFSAR Figure: 3.2-3	Change Description: UCR-2052, Rev. 0	Unit: 2

Title: 17 X 17 Fuel Rod Assembly

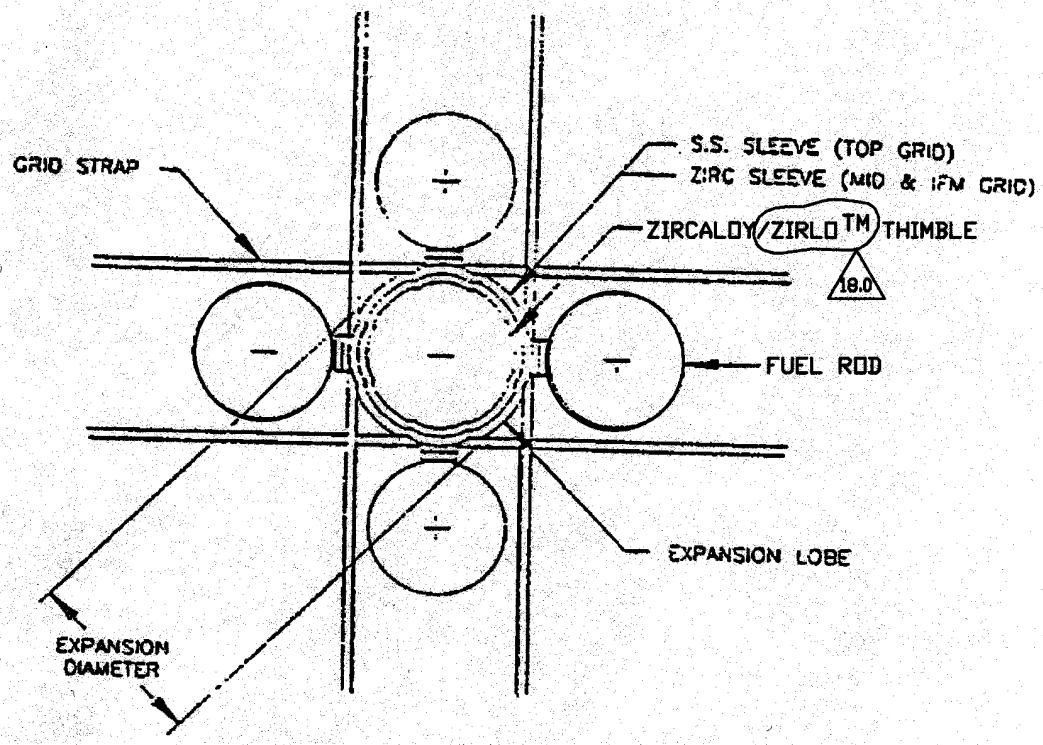

GRID EXPANSION JOINT DESIGN

Revision: **19.0**	Change Description: **UCR-1703**

AMERICAN ELECTRIC POWER COOK NUCLEAR PLANT NUCLEAR GENERATION GROUP BRIDGMAN, MICHIGAN	Title: **D.C. Cook Unit 2 Plan View**	
	UFSAR Figure: **3.2-4**	Sheet 1 of 1

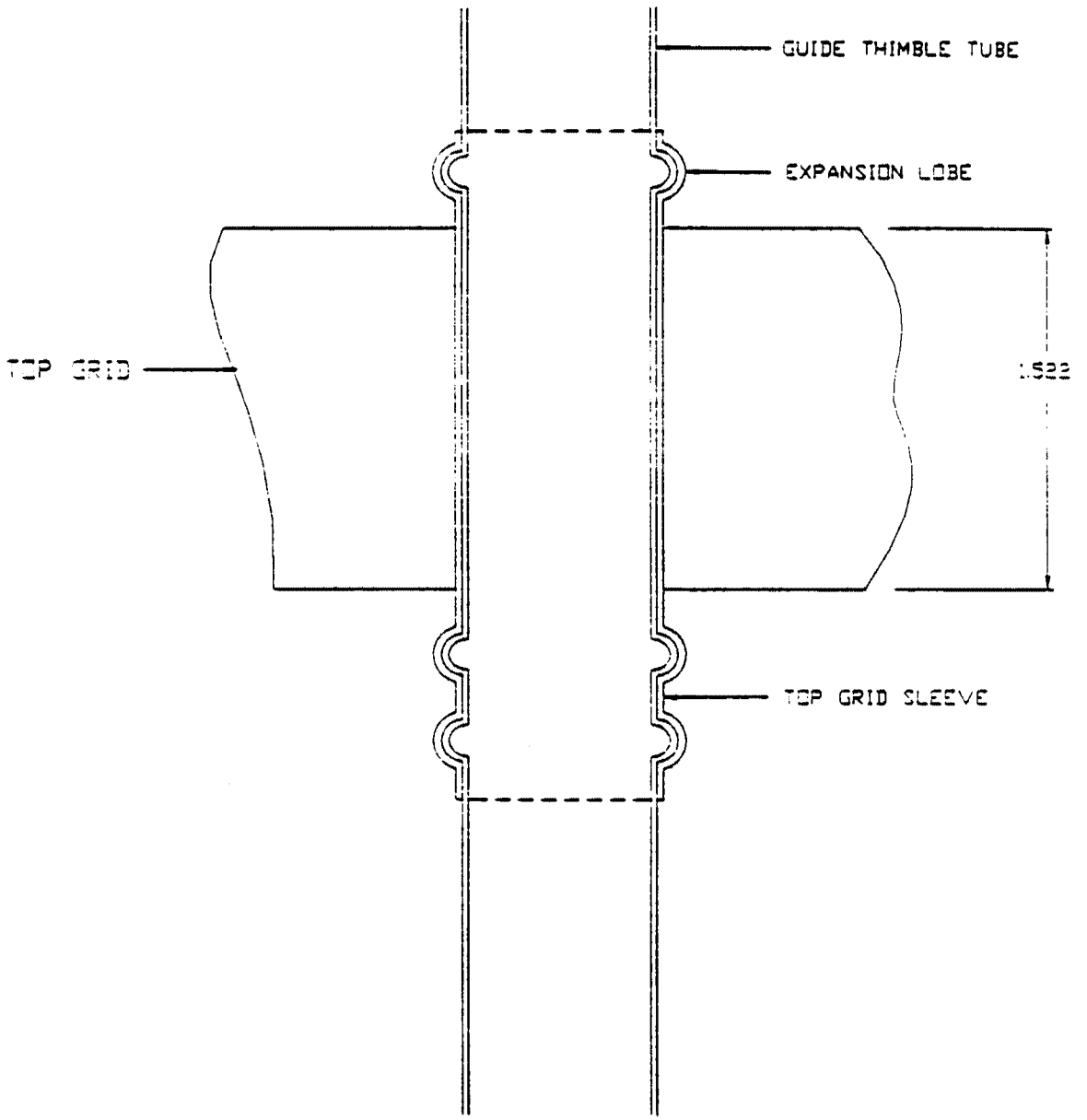

REV. 05/91

D.C. COOK UNIT 2
TOP GRID TO THIMBLE ATTACHMENT
FIGURE 3.2-5

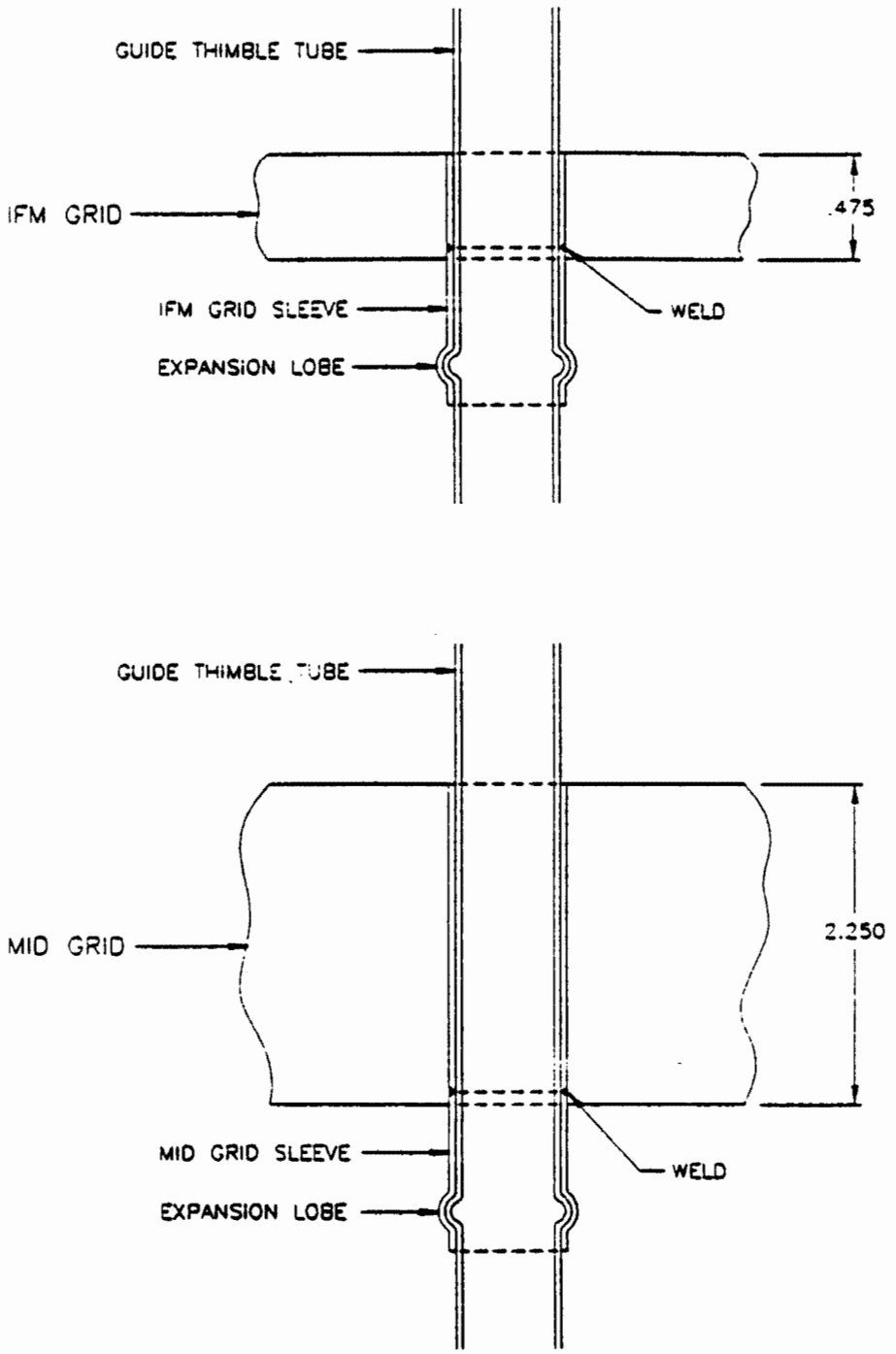

DIMENSIONS ARE IN INCHES (NOMINAL)

REV 05/91

D.C. COOK UNIT 2
GRID TO THIMBLE ATTACHMENT JOINTS
FIGURE 3.2-5A

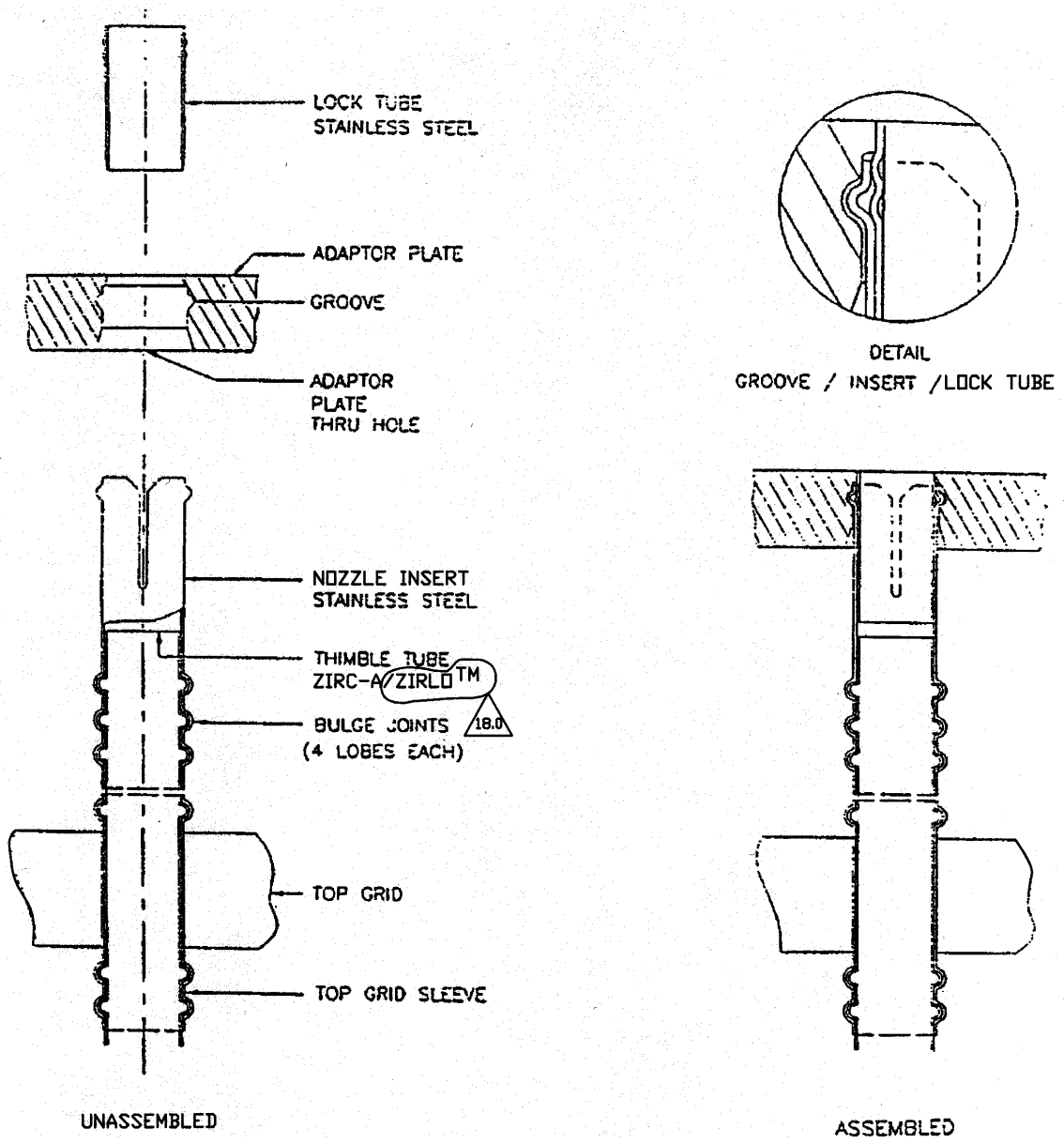

Revision: **19.0**	Change Description: **UCR-1703**

AMERICAN ELECTRIC POWER **COOK NUCLEAR PLANT** **NUCLEAR GENERATION GROUP** **BRIDGMAN, MICHIGAN**	Title: **D. C. Cook Unit 2** **Top Nozzle to Thimble Attachment**	
	UFSAR Figure: **3.2-6**	Sheet 1 of 1

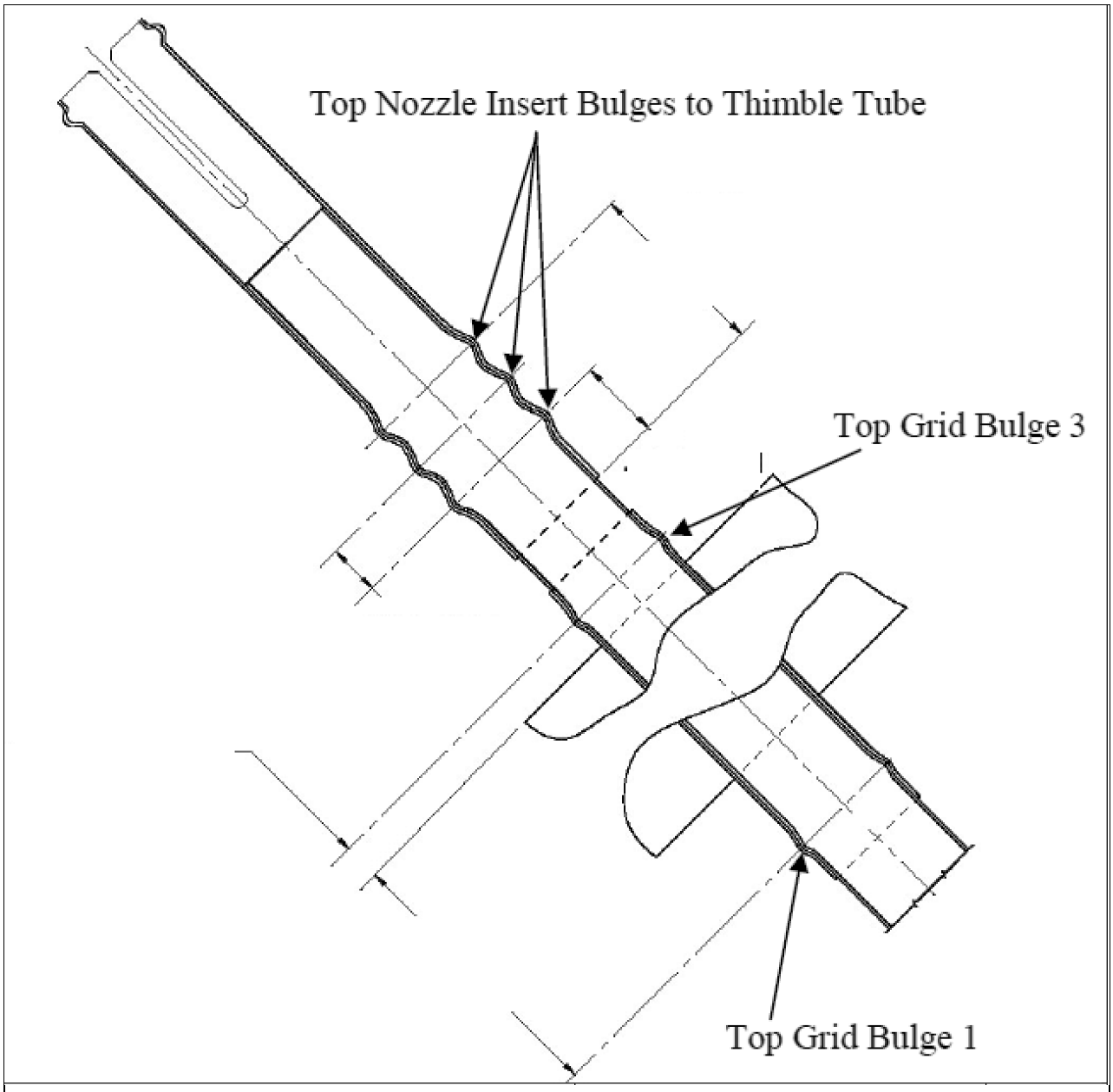

UFSAR Figure: 3.2-6A	Change Description: UCR-2330,. Rev. 0	Unit: 2
Title: Top Nozzle and Top Grid* Attachment Illustration		

* There is a double top grid bulge configuration starting with the Unit 2 fresh fuel in Cycle 24, where a triple top grid bulge configuration was the previous configuration.

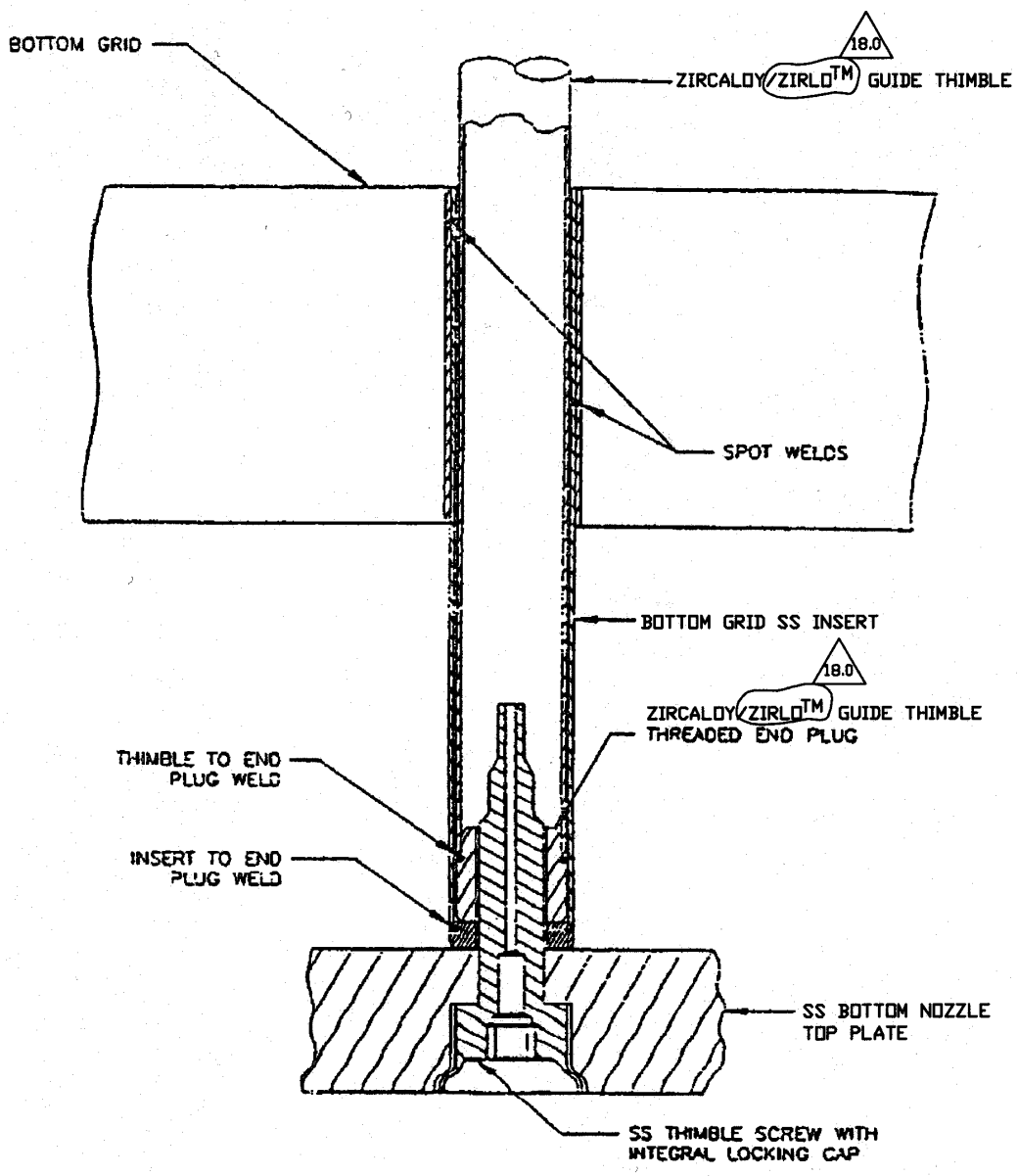

Revision: **19.0**	Change Description: **UCR-1703**

AMERICAN ELECTRIC POWER **COOK NUCLEAR PLANT** **NUCLEAR GENERATION GROUP** **BRIDGMAN, MICHIGAN**	Title: **D.C. Cook Unit 2** **Guide Thimble to Bottom Nozzle Joint**	
	UFSAR Figure: **3.2-7**	Sheet 1 of 1

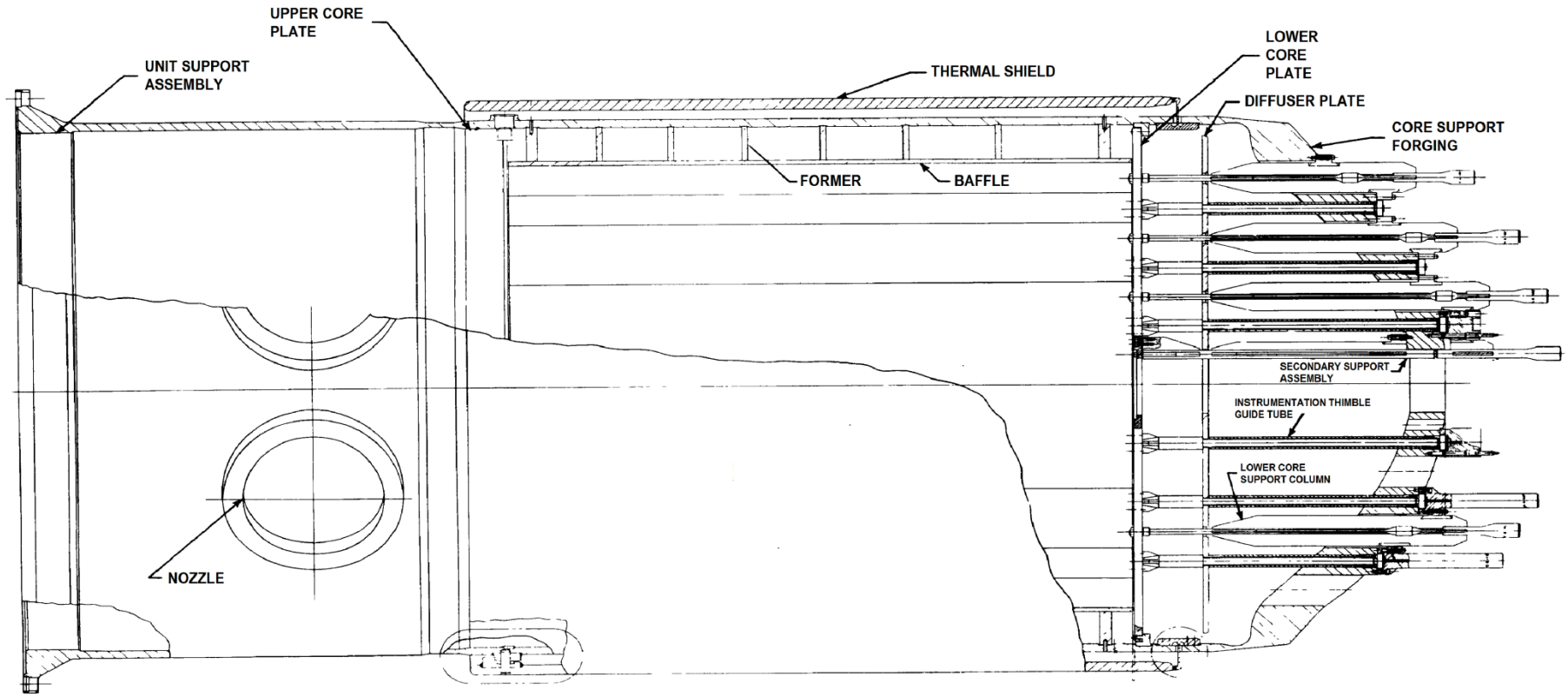

UFSAR Figure: 3.2-8	Change Description: **UCR-2221, Rev. 0**	**Unit: 2**

Title: Typical Core Barrel Assembly

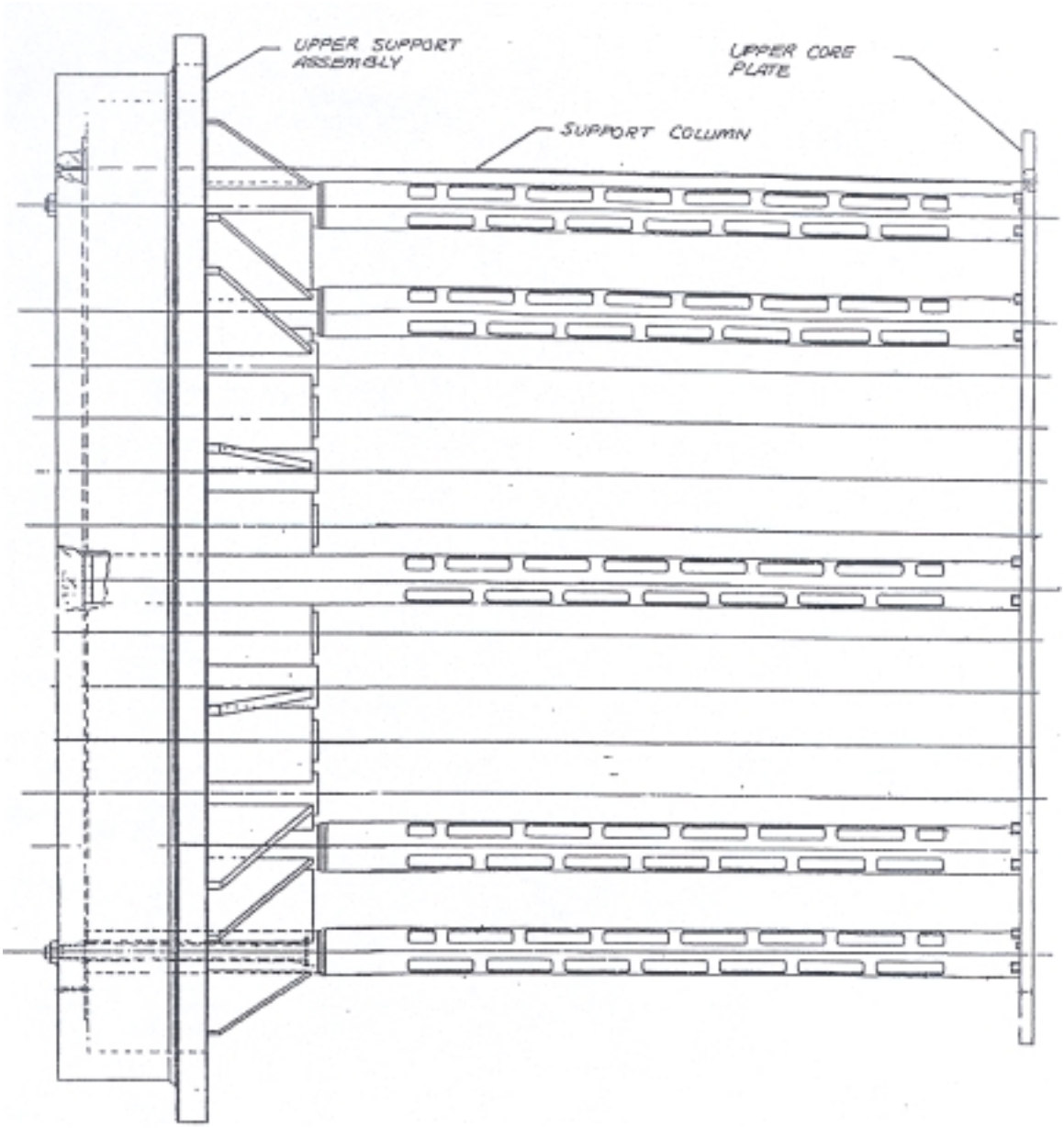

Revision: **19.1**	Change Description**: UCR-1727**

AMERICAN ELECTRIC POWER COOK NUCLEAR PLANT NUCLEAR GENERATION GROUP BRIDGMAN, MICHIGAN	Title: **Upper Core Support Structure**	
	UFSAR Figure: **3.2-9**	Sheet 1 of 1

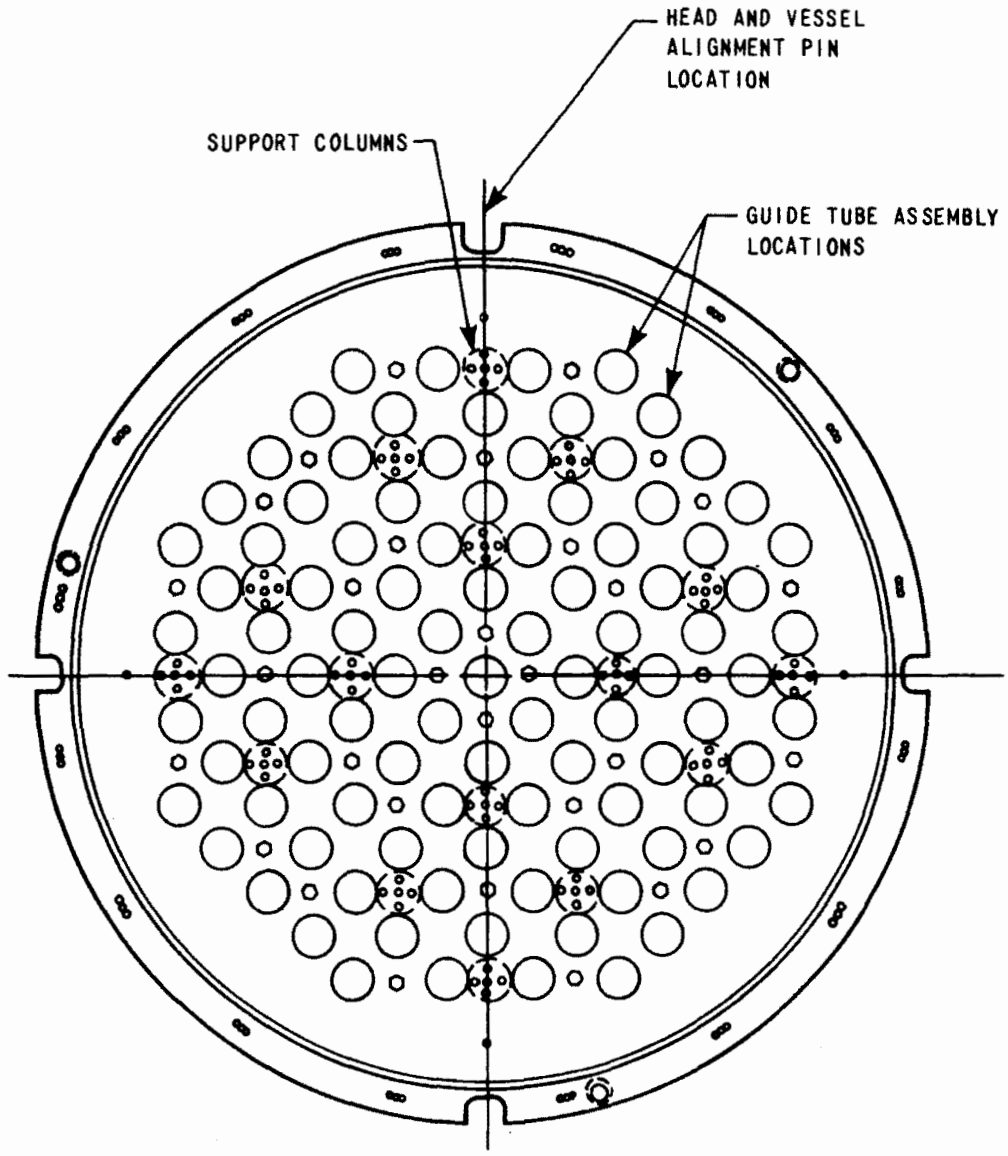

Figure 3.2-10 Plan View of Upper Core Support Structure

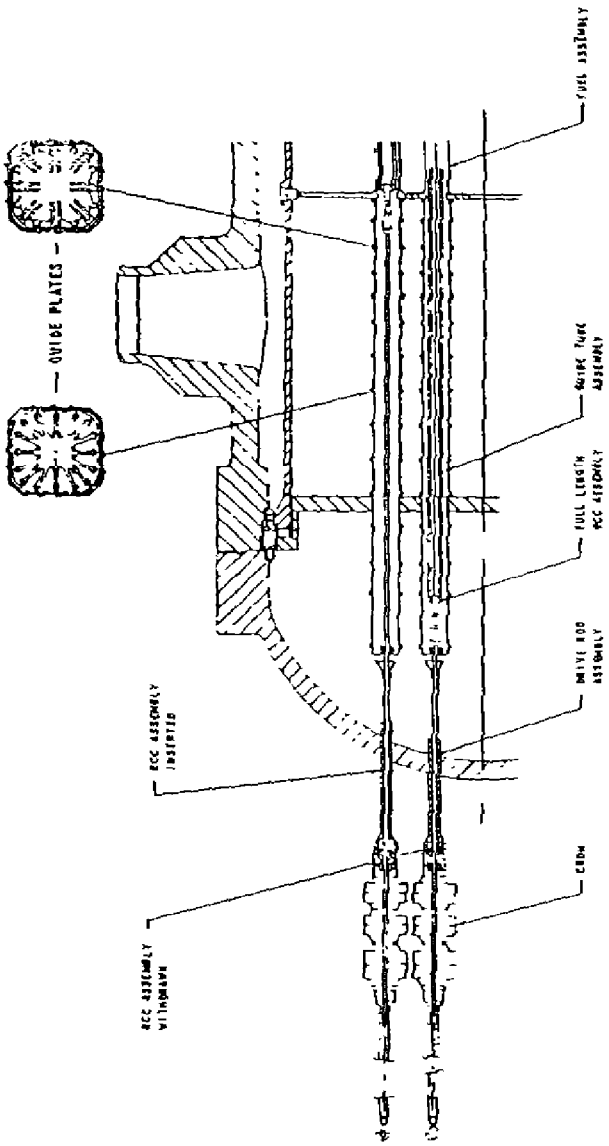

UNIT 2

16.4	REVISED PER 99-UFSAR-1243
REV. NO.	**DESCRIPTION**

REVISIONS

AMERICAN ELECTRIC POWER **COOK NUCLEAR PLANT** **NUCLEAR GENERATION GROUP** **BRIDGMAN, MICHIGAN**	**TITLE** **TYPICAL FULL LENGTH ROD CLUSTER CONTROL AND DRIVE ROD ASSEMBLY WITH INTERFACING COMPONENTS**	
	DWG. NO. **FSAR FIG. 3.2-11**	SH 1 of 1

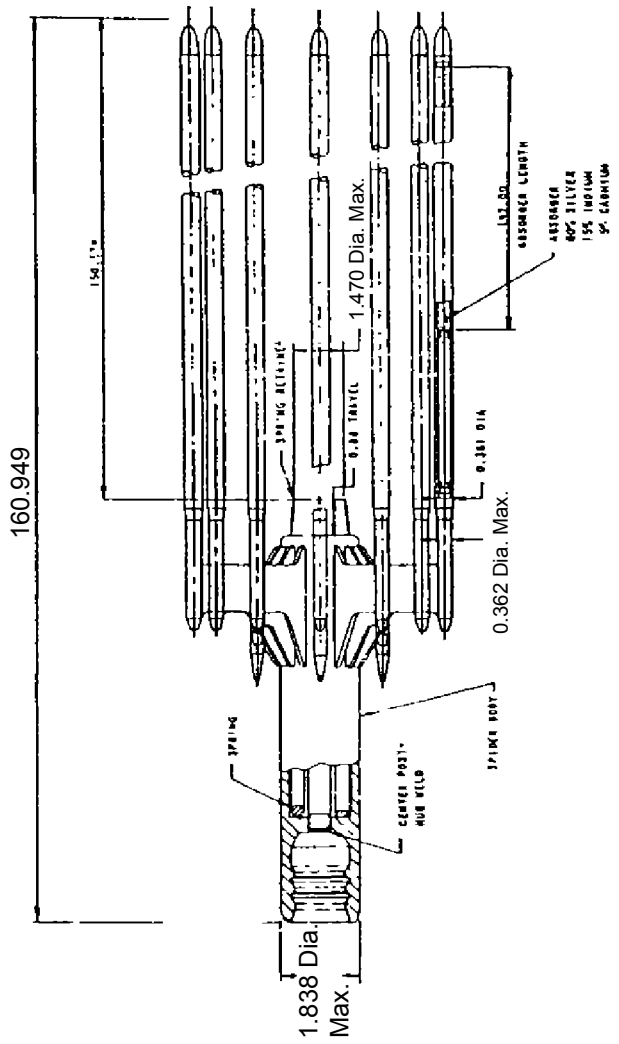

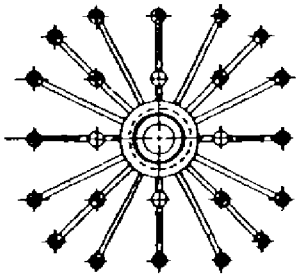

UNIT 2

16.4	REVISED PER 99-UFSAR-1243
REV. NO.	**DESCRIPTION**

REVISIONS

AMERICAN ELECTRIC POWER **COOK NUCLEAR PLANT** **NUCLEAR GENERATION GROUP** **BRIDGMAN, MICHIGAN**	**TITLE** **FULL LENGTH ROD CLUSTER CONTROL ASSEMBLY OUTLINE**
	DWG. NO. **FSAR FIG. 3.2-12** — SH 1 of 1

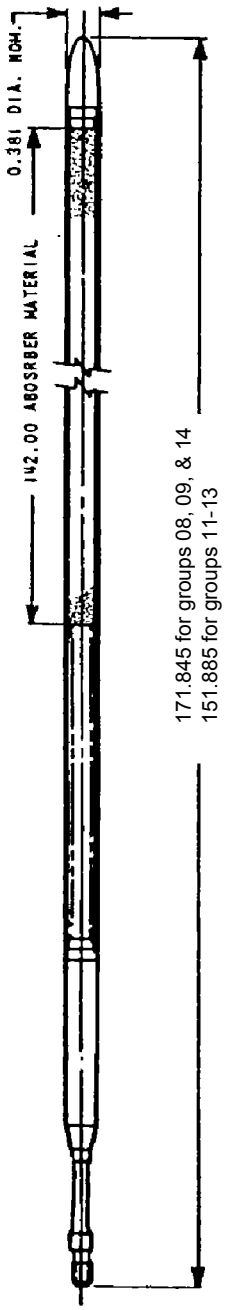

UNIT 2

16.4	REVISED PER 99-UFSAR-1243
REV. NO.	**DESCRIPTION**
REVISIONS	

AMERICAN ELECTRIC POWER **COOK NUCLEAR PLANT** **NUCLEAR GENERATION GROUP** **BRIDGMAN, MICHIGAN**	**TITLE** **FULL LENGTH ABSORBER ROD**
	DWG. NO. **FSAR FIG. 3.2-13** SH 1 of 1

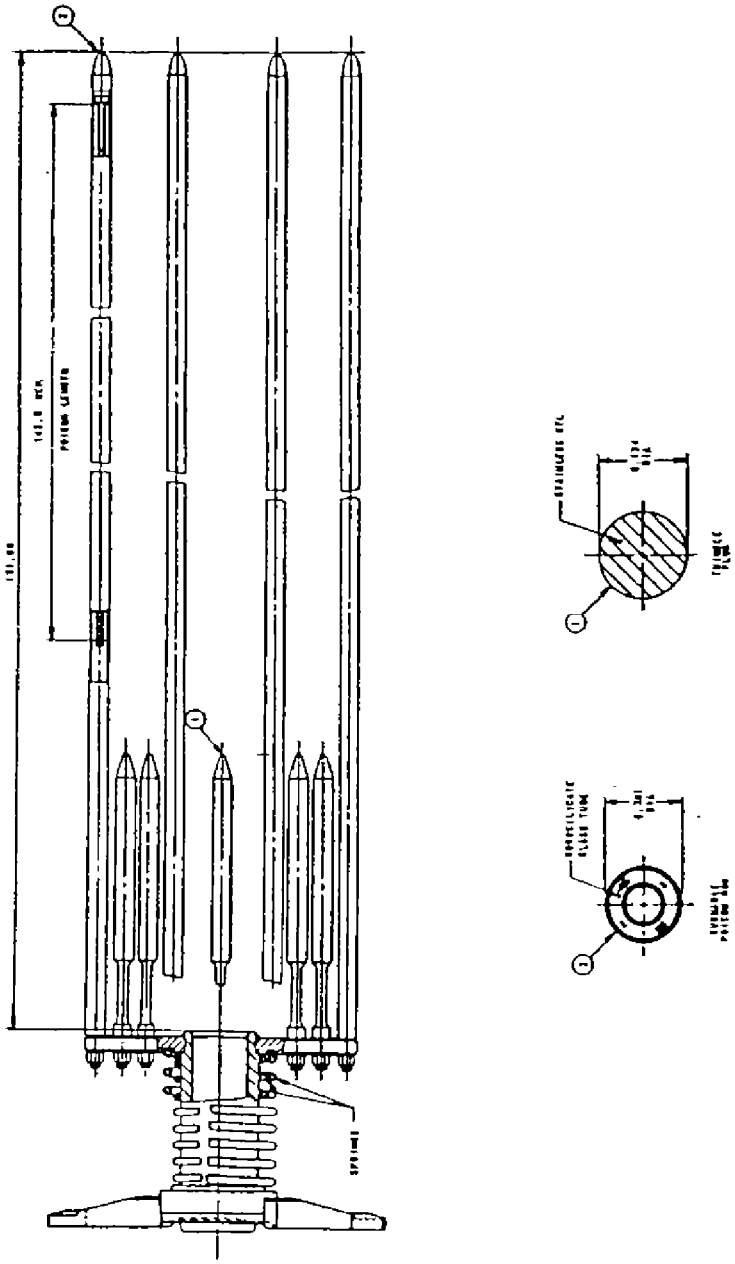

UNIT 2

16.4	REVISED PER 99-UFSAR-1243
REV. NO.	**DESCRIPTION**

REVISIONS

AMERICAN ELECTRIC POWER **COOK NUCLEAR PLANT** **NUCLEAR GENERATION GROUP** **BRIDGMAN, MICHIGAN**	**TITLE** **TYPICAL BURNABLE POISON ASSEMBLY**	
	DWG. NO. **FSAR FIG. 3.2 - 15A**	SH 1 of 1

AEP AMERICAN ELECTRIC POWER - COOK NUCLEAR PLANT

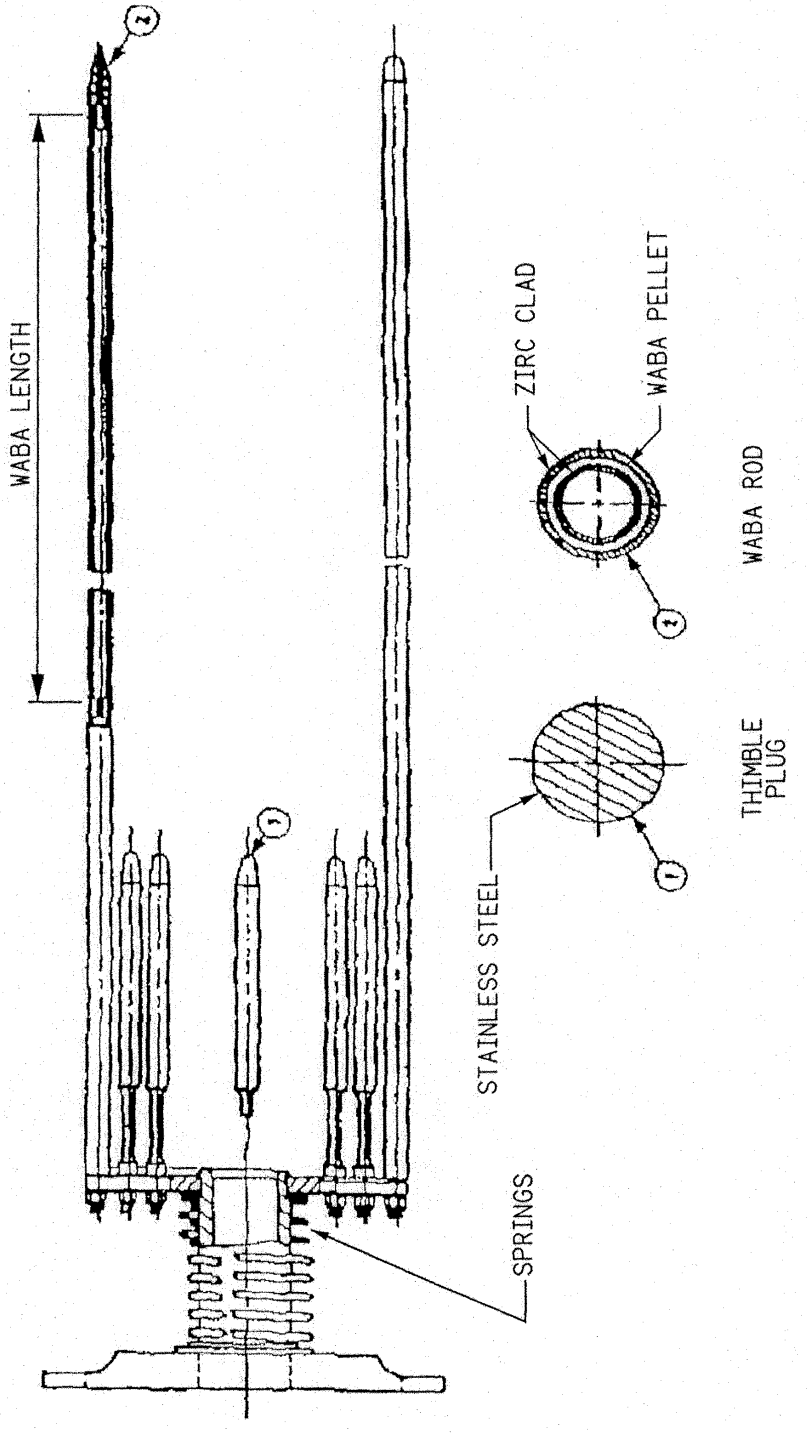

DATE	NO.	DESCRIPTION	DR.	CHK'D.	APP'D.
	19.2	REVISED PER UCR-1743			

FILENAME: fsar-fig-3-2-15b 19-2.dgn
(raster file): fsar-fig-3-2-15b 19-2.tif

REVISIONS

OTHER:

REF. DWGS:

DR.	CK'D.	APP'D.	DATE:

TITLE - WET ANNULAR BURNABLE ABSORBER (WABA) ASSEMBLY

UNIT NO. 2

SH. 1 OF 1

DRAWING NO. FSAR FIG. 3.2-15B

REV. NO. 19.2

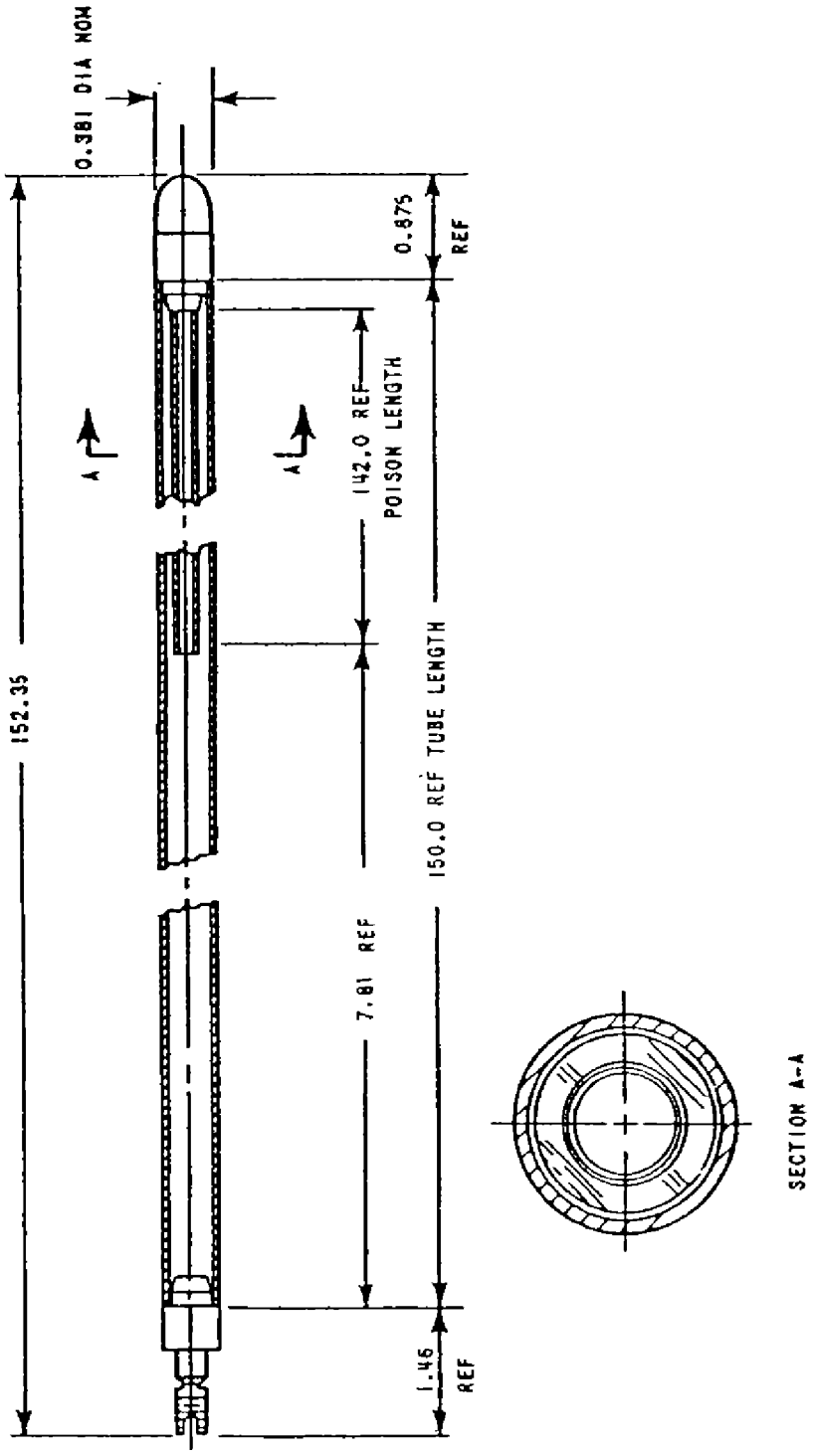

UNIT 2

16.4	REVISED PER 99-UFSAR-1243
REV. NO.	**DESCRIPTION**

REVISIONS

AMERICAN ELECTRIC POWER **COOK NUCLEAR PLANT** **NUCLEAR GENERATION GROUP** **BRIDGMAN, MICHIGAN**	**TITLE** **TYPICAL BURNABLE POISON ROD CROSS SECTION**
	DWG. NO. **FSAR FIG. 3.2-16A** — SH 1 of 1

AEP AMERICAN ELECTRIC POWER - COOK NUCLEAR PLANT

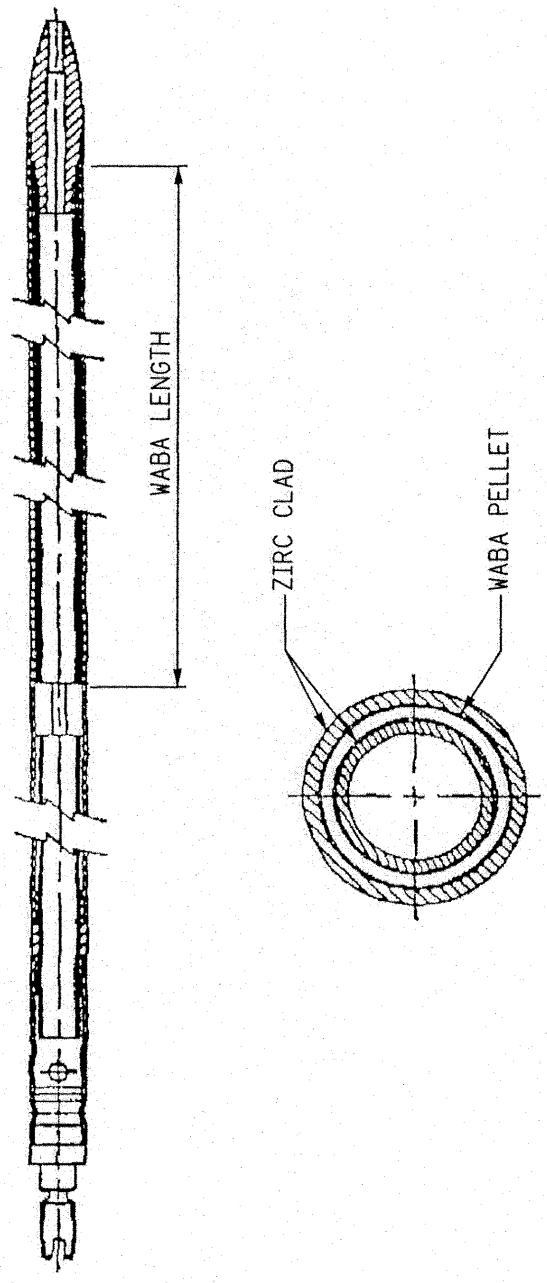

	19.2	REVISED PER UCR-1743			
DATE	NO.	DESCRIPTION	DR.	CHK'D.	APP'D.

FILENAME: fsar-fig-3-2-16b 19-2.dgn
(raster file): fsar-fig-3-2-16b 19-2.tif

REVISIONS

OTHER:

REF. DWGS:

DR.	CK'D.	APP'D.	DATE:

TITLE - BA ROD CROSS SECTION (WET ANNULAR BURNABLE ABSORBER)

UNIT NO. 2

SH. 1 OF 1

DRAWING NO. FSAR FIG. 3.2-16B **REV. NO.** 19.2

HISTORICAL

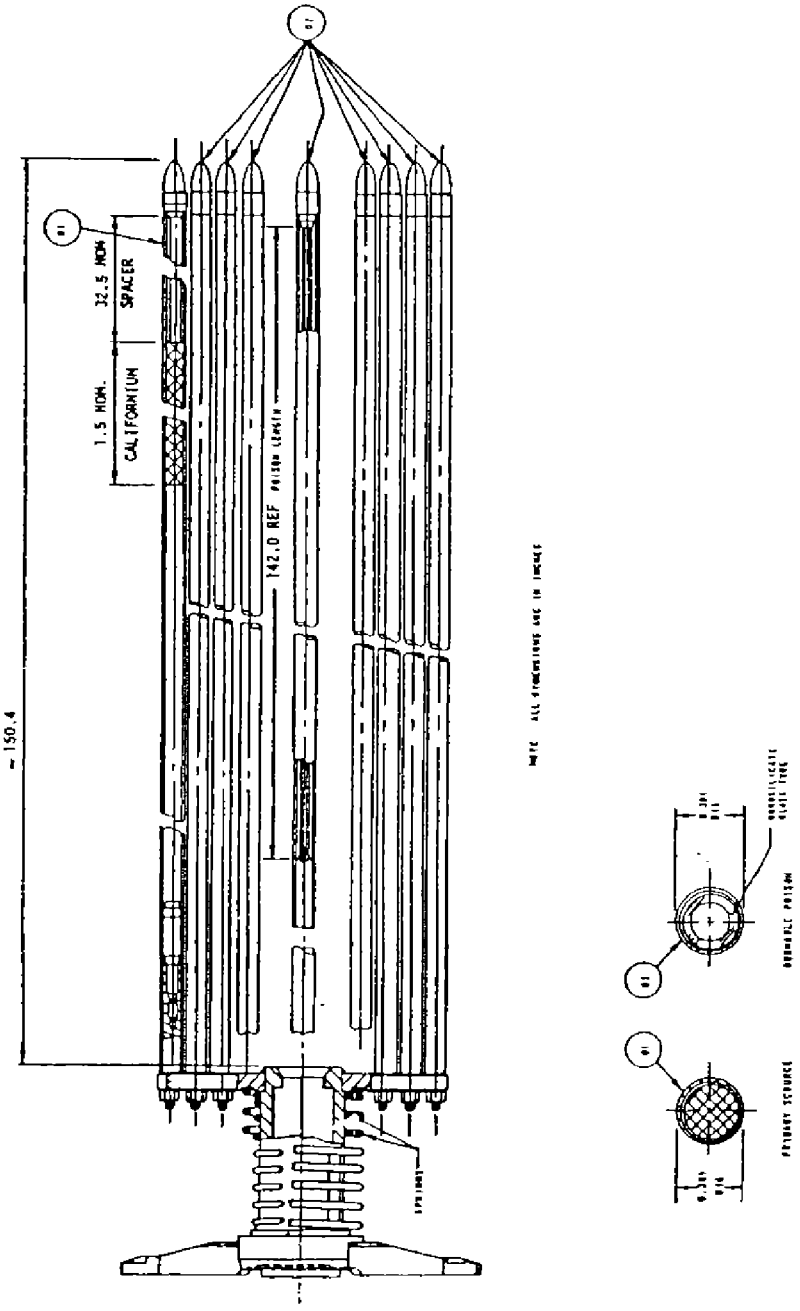

UNIT 2

16.4	REVISED PER 99-UFSAR-1243
REV. NO.	**DESCRIPTION**

REVISIONS

AMERICAN ELECTRIC POWER **COOK NUCLEAR PLANT** **NUCLEAR GENERATION GROUP** **BRIDGMAN, MICHIGAN**	**TITLE** **PRIMARY SOURCE ASSEMBLY**	
	DWG. NO. **FSAR FIG. 3.2-17**	SH 1 of 1

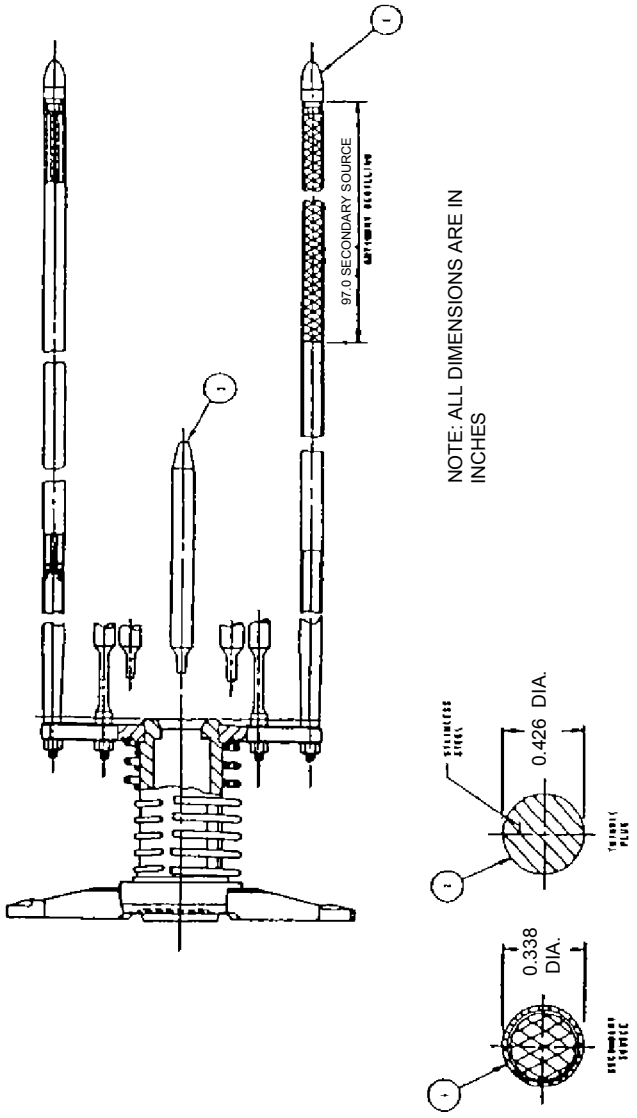

UNIT 2

16.4	REVISED PER 99-UFSAR-1243
REV. NO.	**DESCRIPTION**

REVISIONS

AMERICAN ELECTRIC POWER **COOK NUCLEAR PLANT** **NUCLEAR GENERATION GROUP** **BRIDGMAN, MICHIGAN**	**TITLE** **SECONDARY SOURCE ASSEMBLY**
	DWG. NO. **FSAR FIG. 3.2 - 18** SH 1 of 1

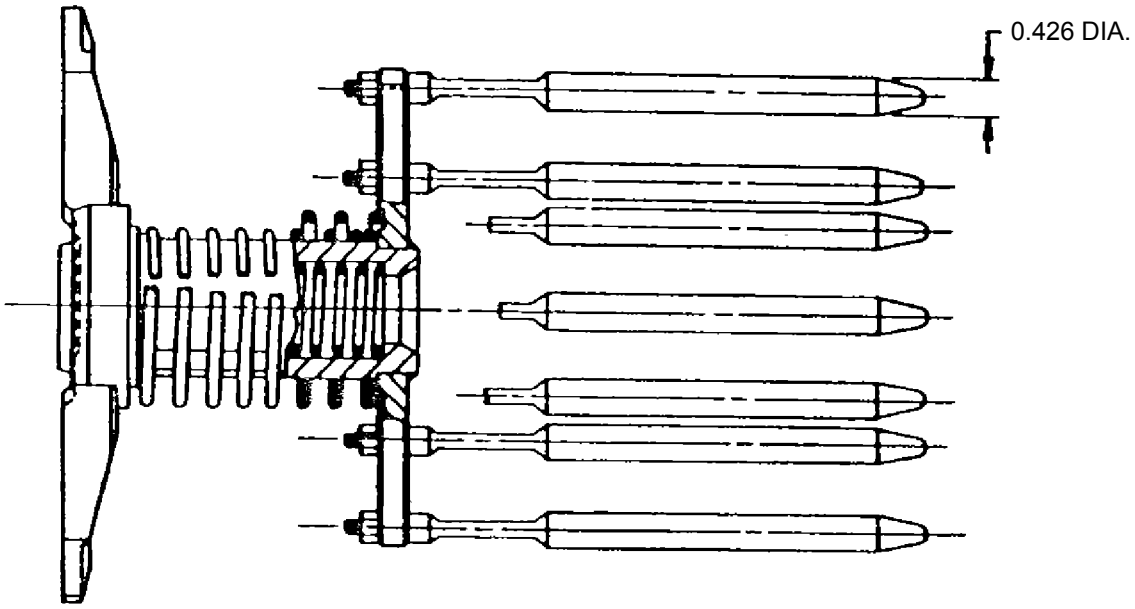

UNIT 2

16.4	REVISED PER 99-UFSAR-1243
REV. NO.	**DESCRIPTION**

REVISIONS

AMERICAN ELECTRIC POWER
COOK NUCLEAR PLANT
NUCLEAR GENERATION GROUP
BRIDGMAN, MICHIGAN

TITLE **THIMBLE PLUG ASSEMBLY**

DWG. NO. **FSAR FIG. 3.2-19**

SH 1 of 1

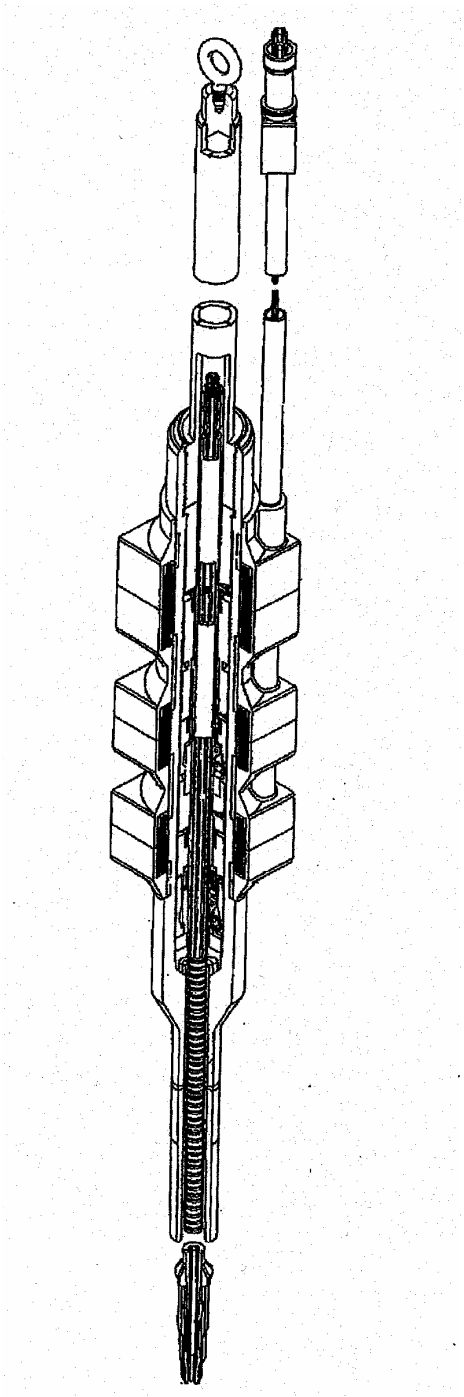

Revision: **21.2**	Change Description**: UCR-1836**

AMERICAN ELECTRIC POWER COOK NUCLEAR PLANT NUCLEAR GENERATION GROUP BRIDGMAN, MICHIGAN	Title: **Full Length Control Rod Drive Mechanism**	
	UFSAR Figure: **3.2-20**	Sheet 1 of 1

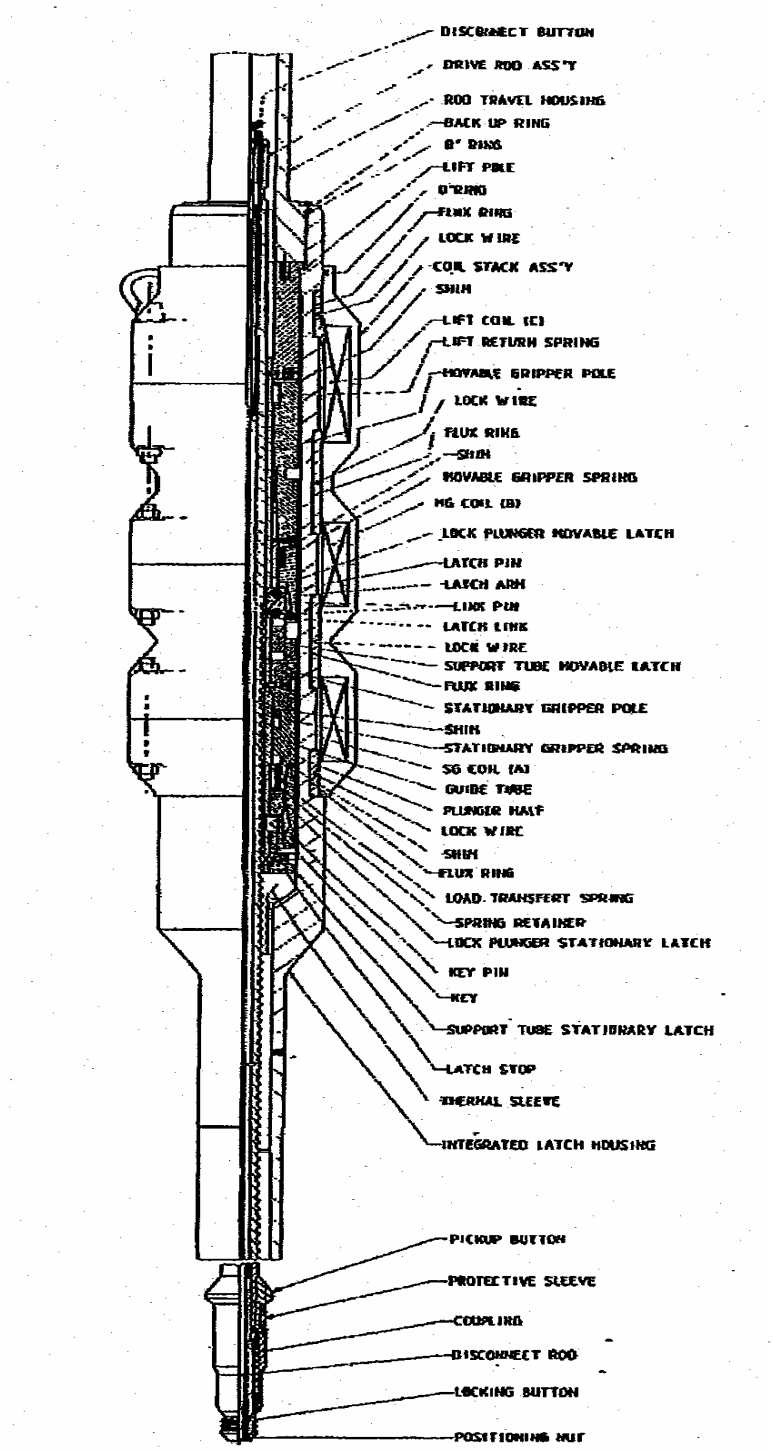

Revision: **21.2**	Change Description**: UCR-1836**

AMERICAN ELECTRIC POWER COOK NUCLEAR PLANT NUCLEAR GENERATION GROUP BRIDGMAN, MICHIGAN	Title: **Full Length Control Rod Drive Mechanism Schematic**	
	UFSAR Figure: **3.2-21**	Sheet 1 of 1

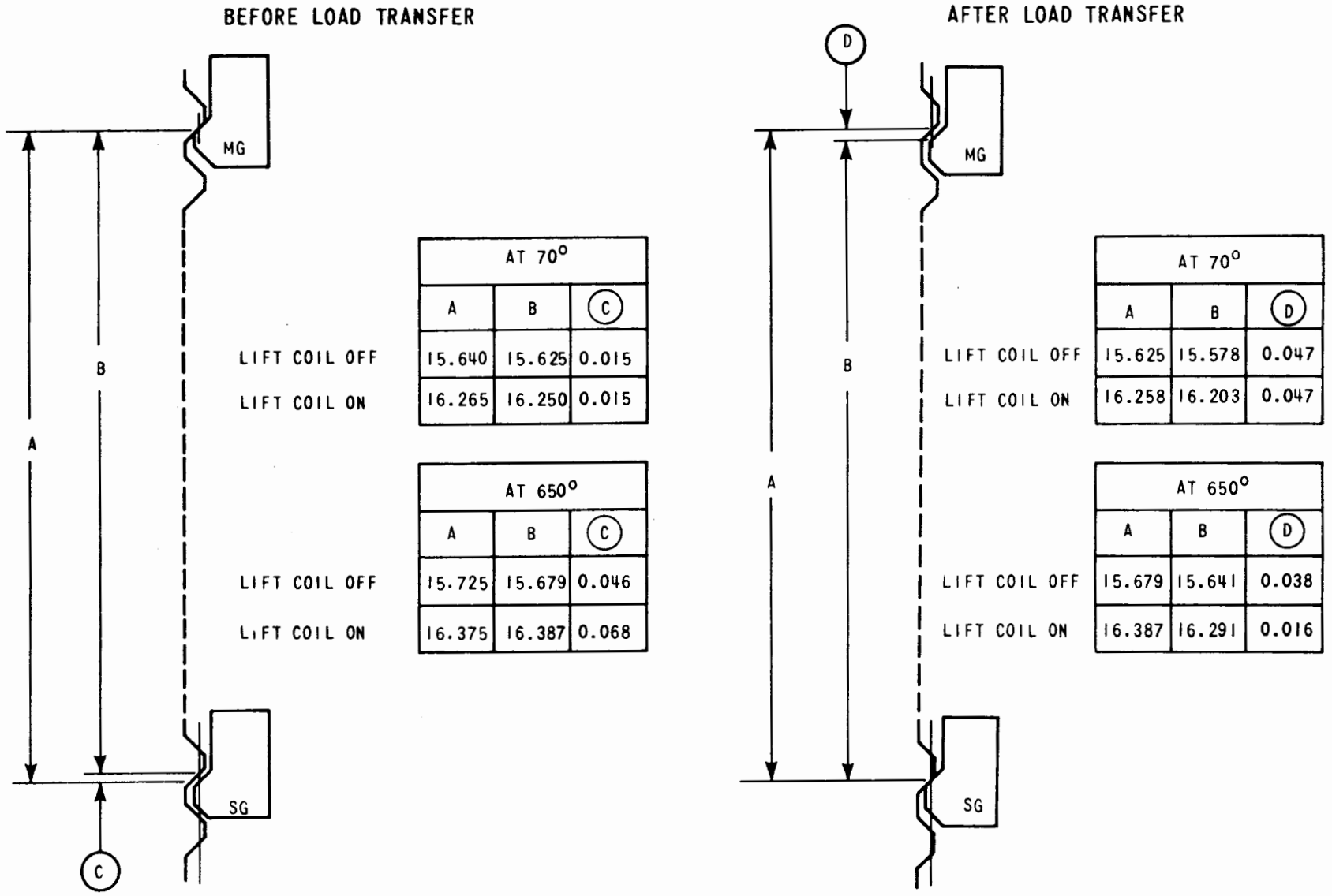

Figure 3.2-23 Nominal Latch Clearance at Minimum and Maximum Temperature

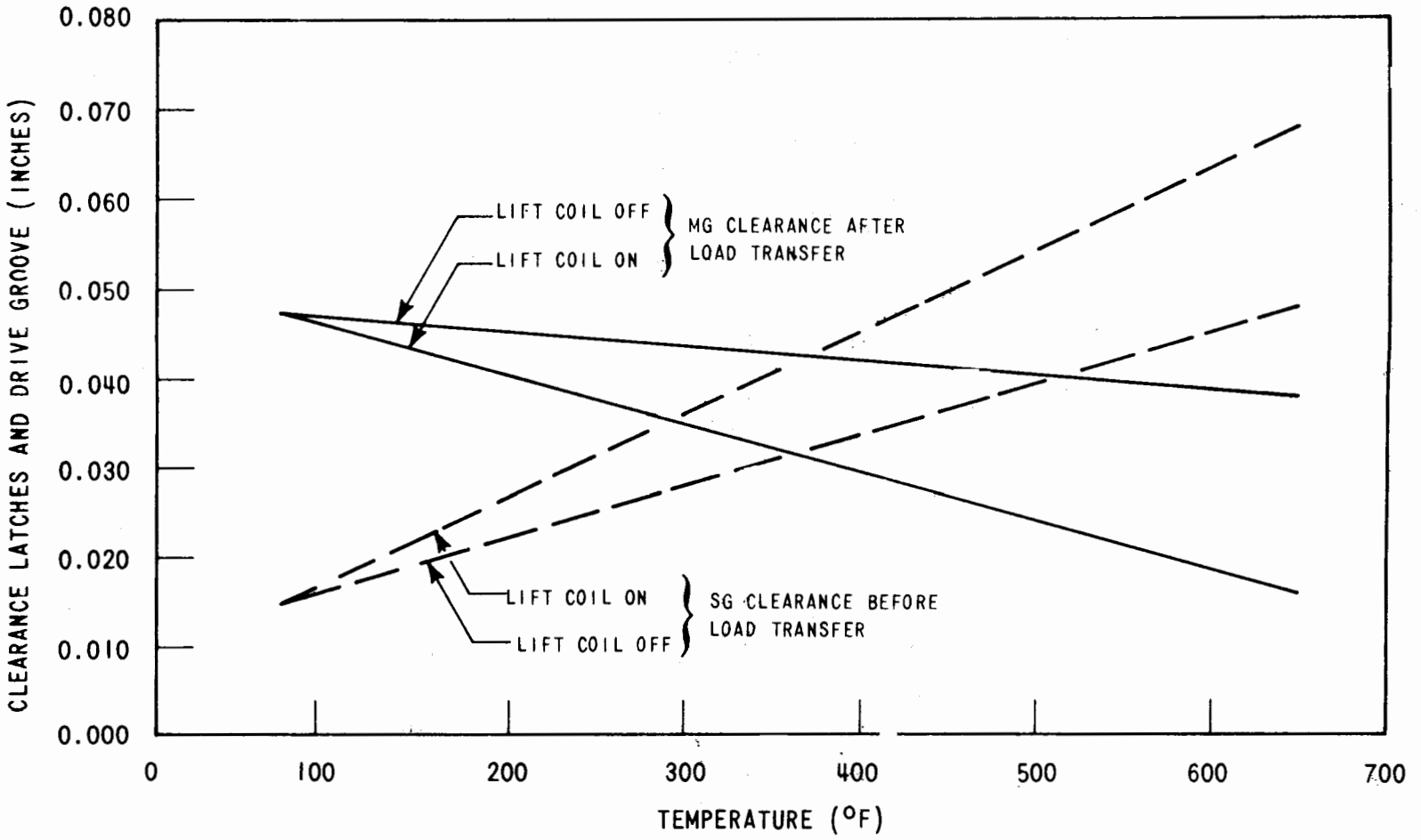

Figure 3.2-24 Control Rod Drive Mechanism Latch Clearance Thermal Effect

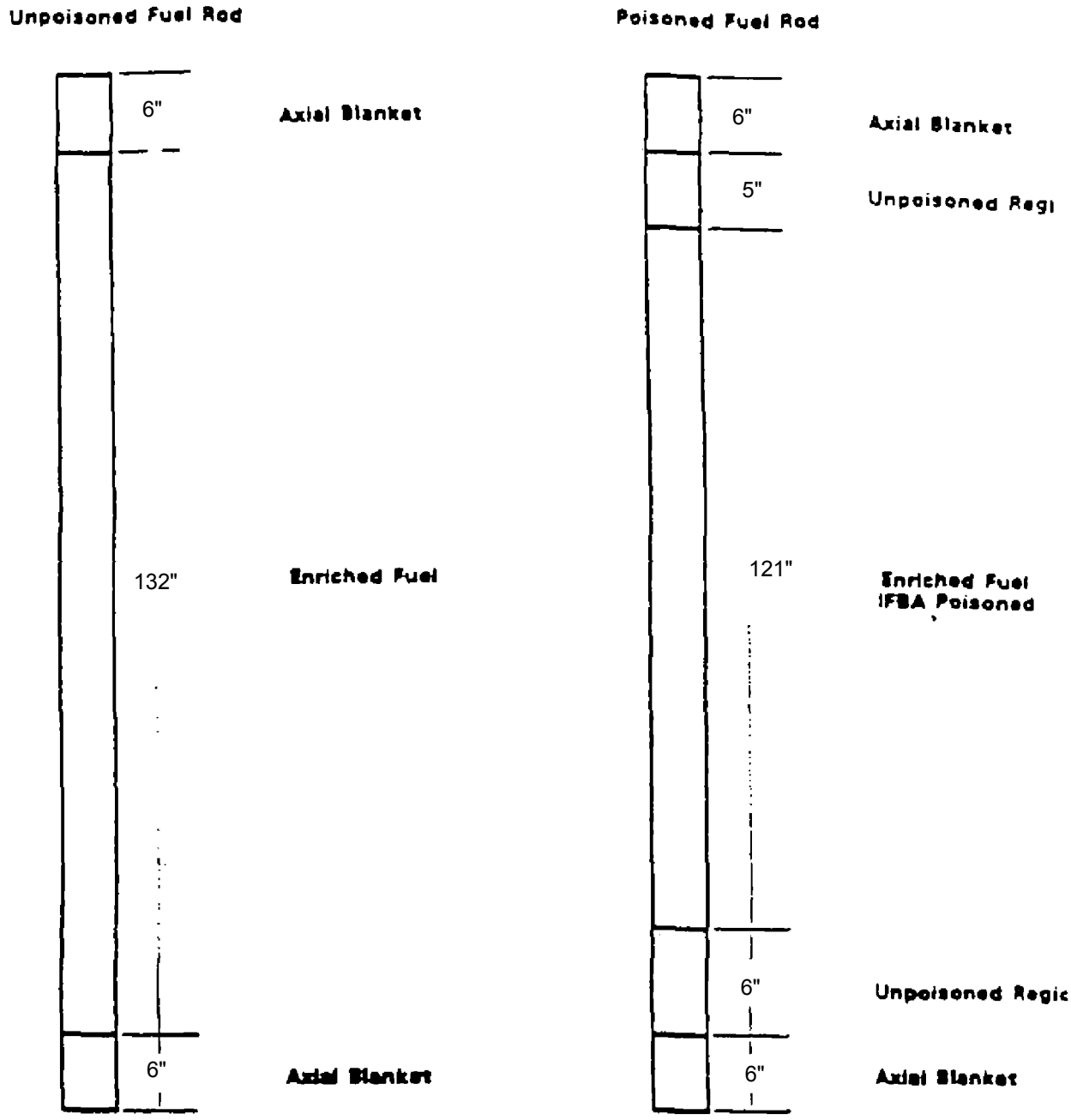

UNIT 2

16.4	REVISED PER 99-UFSAR-1242
REV. NO.	**DESCRIPTION**

REVISIONS

AMERICAN ELECTRIC POWER **COOK NUCLEAR PLANT** **NUCLEAR GENERATION GROUP** **BRIDGMAN, MICHIGAN**	**TITLE** **Typical Axial Zoning of Uranium Enrichment and IFBA Poisoning**	
	DWG. NO. **FSAR FIG. 3.3-1**	SH 1 of 1

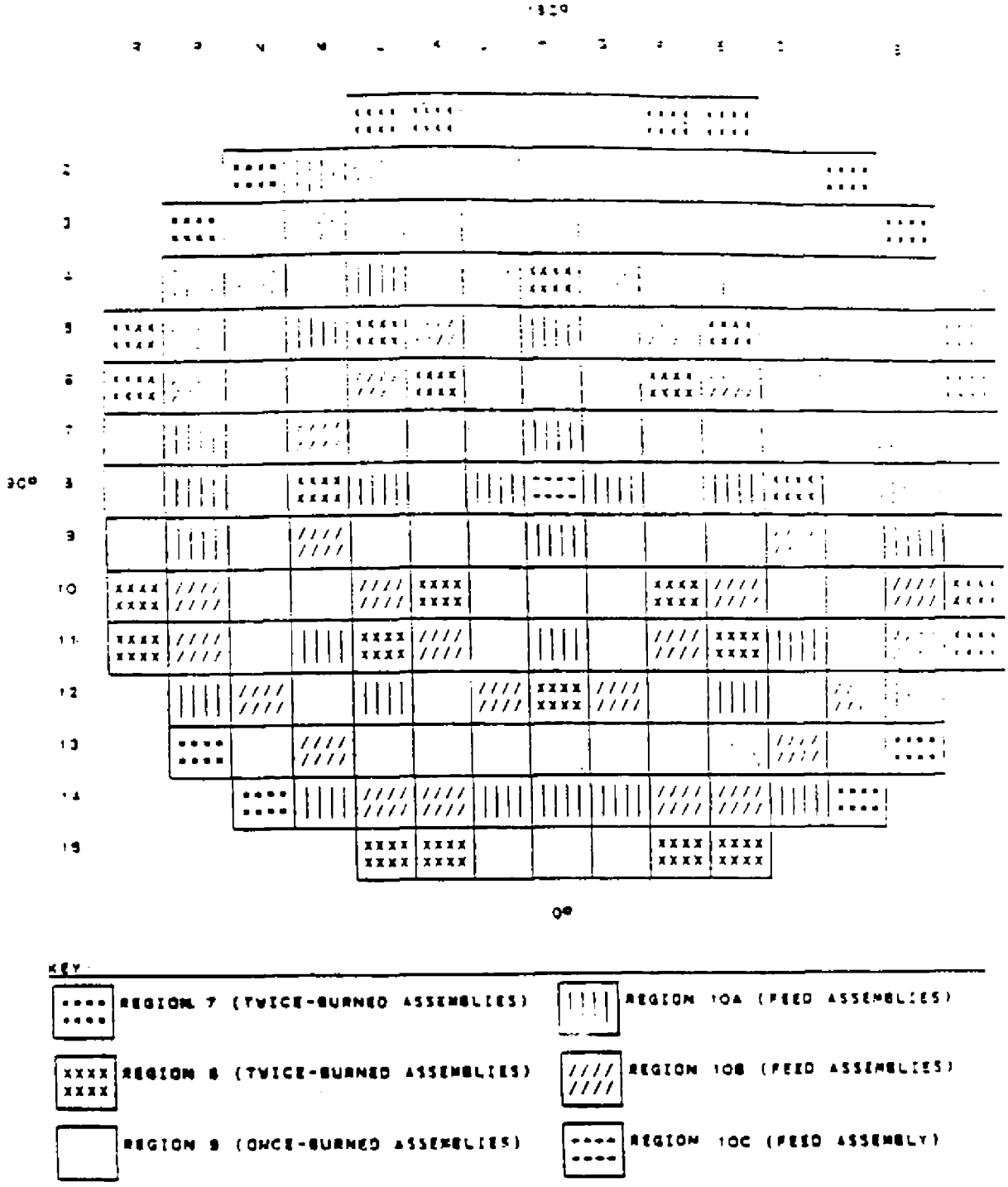

UNIT 2

16.4	REVISED PER 99-UFSAR-1242
REV. NO.	**DESCRIPTION**

REVISIONS

AMERICAN ELECTRIC POWER **COOK NUCLEAR PLANT** **NUCLEAR GENERATION GROUP** **BRIDGMAN, MICHIGAN**	**TITLE** **EXAMPLE LOW LEAKAGE FUEL LOADING ARRANGEMENT**	
	DWG. NO. **FSAR FIG. 3.3-2**	SH 1 of 1

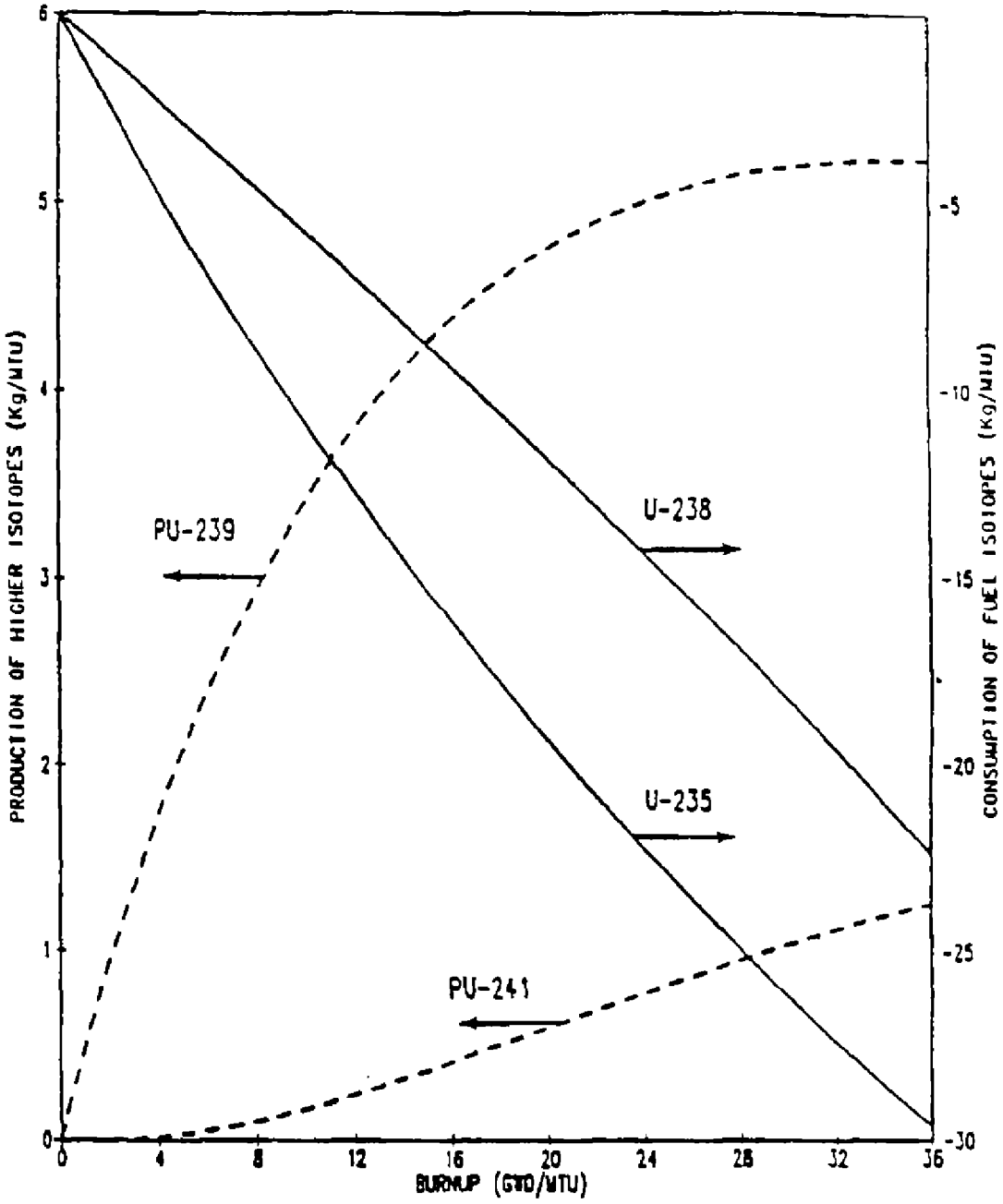

UNIT 2

16.4	REVISED PER 99-UFSAR-1242
REV. NO.	**DESCRIPTION**

REVISIONS

AMERICAN ELECTRIC POWER **COOK NUCLEAR PLANT** **NUCLEAR GENERATION GROUP** **BRIDGMAN, MICHIGAN**	**TITLE** **TYPICAL PRODUCTION AND CONSUMPTION OF HIGHER ISOTOPES**	
	DWG. NO. **FSAR FIG. 3.3 - 3**	SH 1 of 1

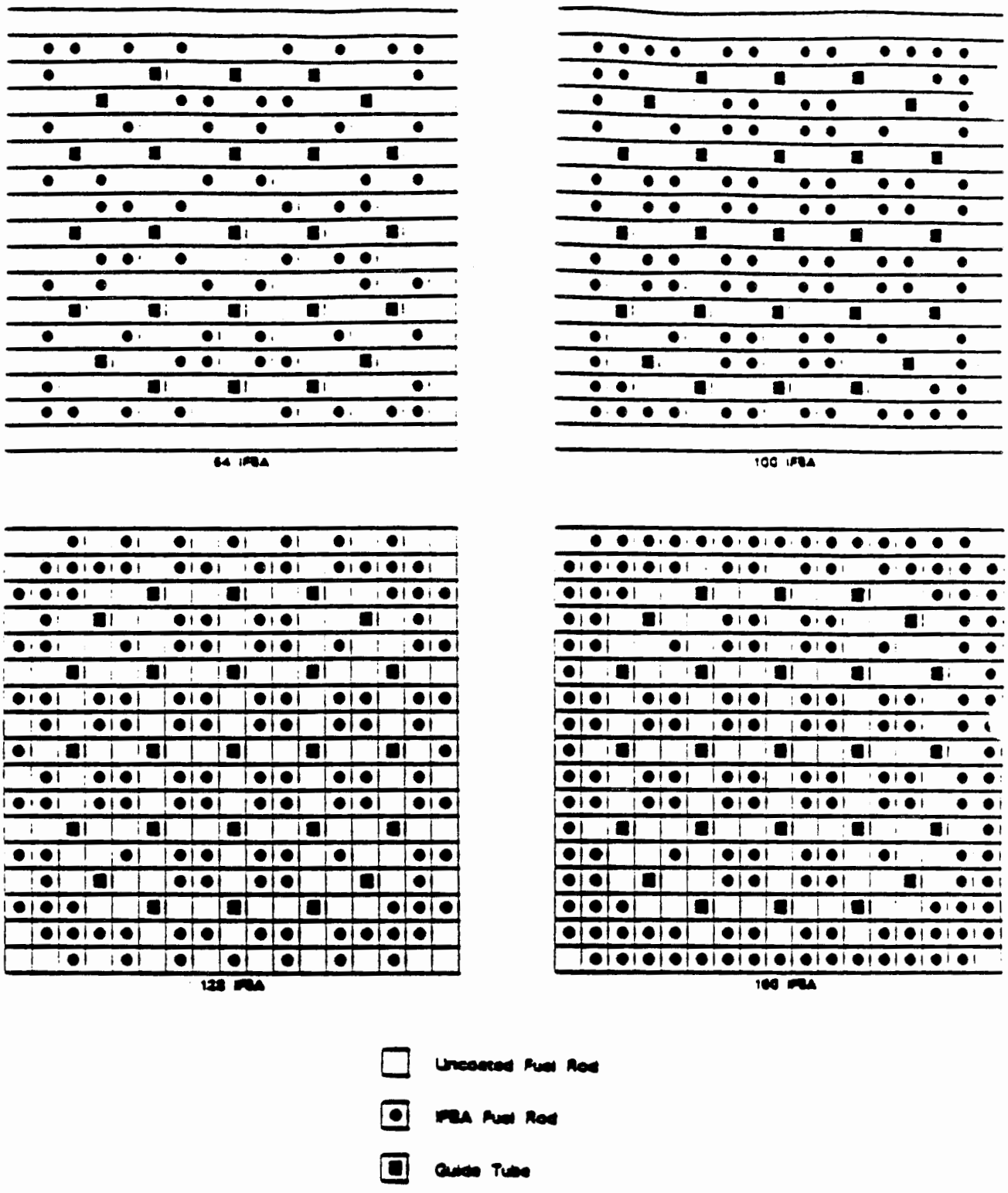

Figure 3.3-4 Example IFBA Arrangements Within an Assembly

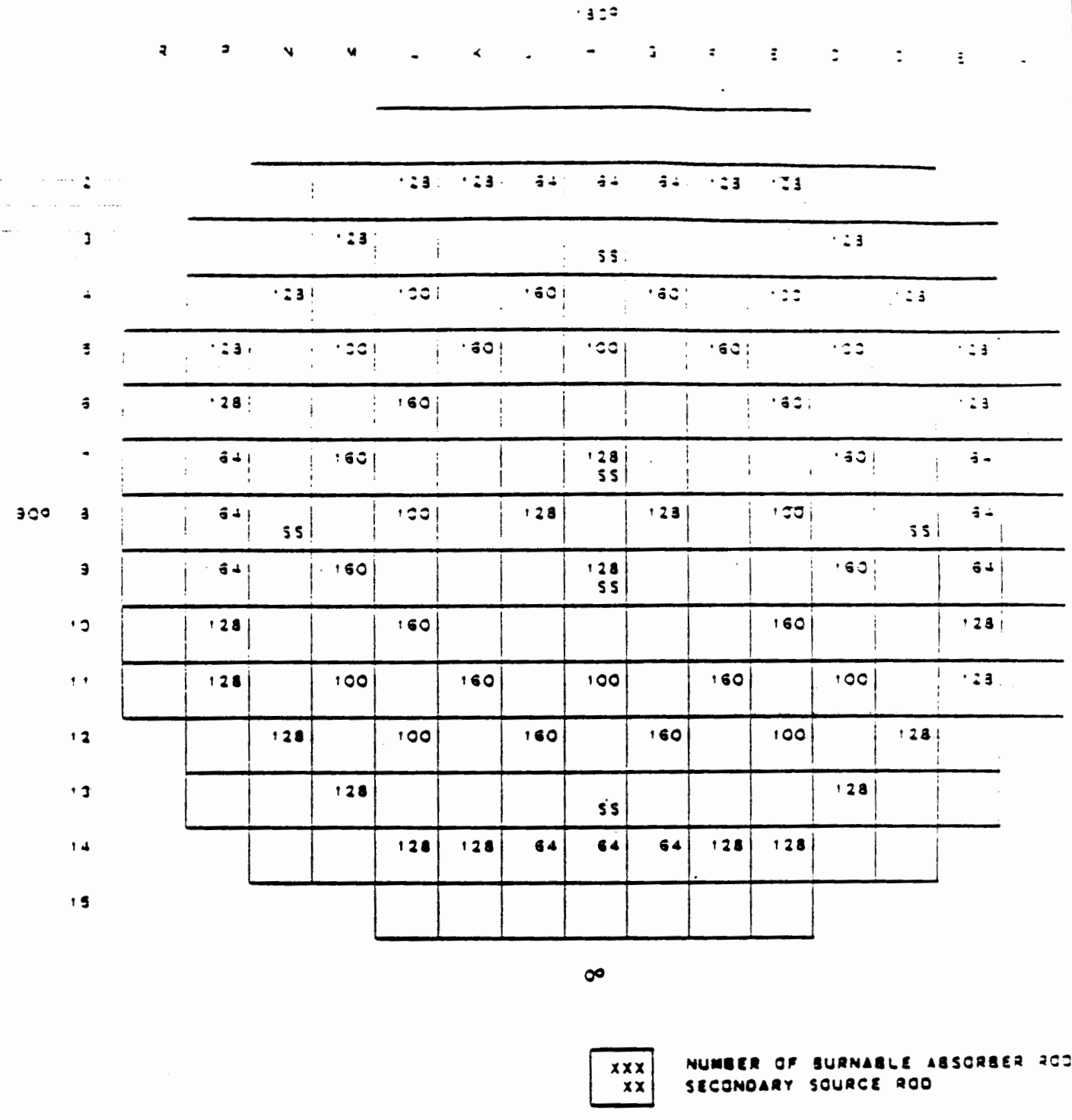

Figure 3.3-5 Example IFBA Loading Pattern

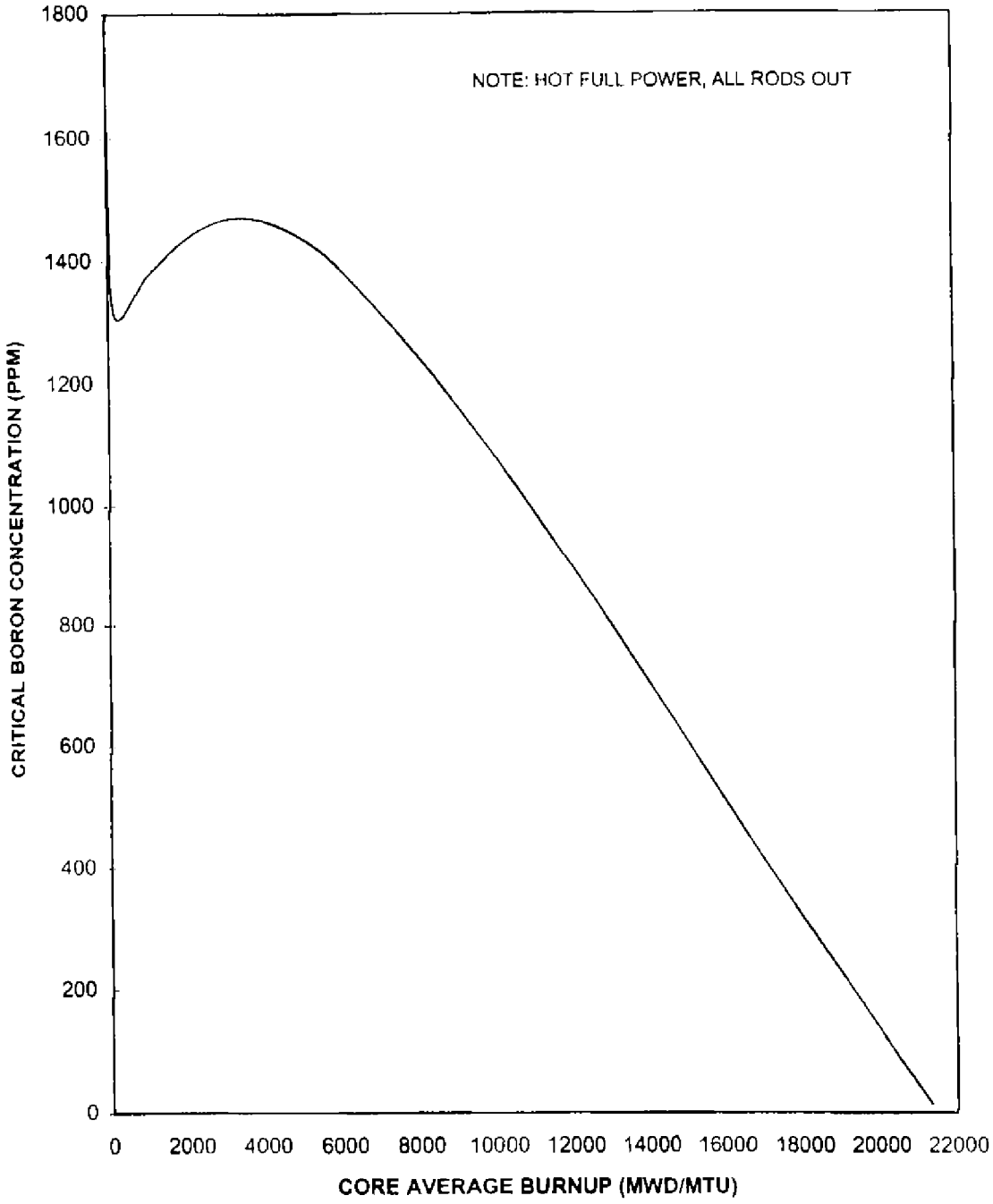

UNIT 2

16.4	REVISED PER 99-UFSAR-1242
REV. NO.	**DESCRIPTION**

REVISIONS

AMERICAN ELECTRIC POWER
COOK NUCLEAR PLANT
NUCLEAR GENERATION GROUP
BRIDGMAN, MICHIGAN

TITLE **EXAMPLE BORON CONCENTRATION OVER CYCLE LENGTH**

DWG. NO. **FSAR FIG. 3.3-6** SH 1 of 1

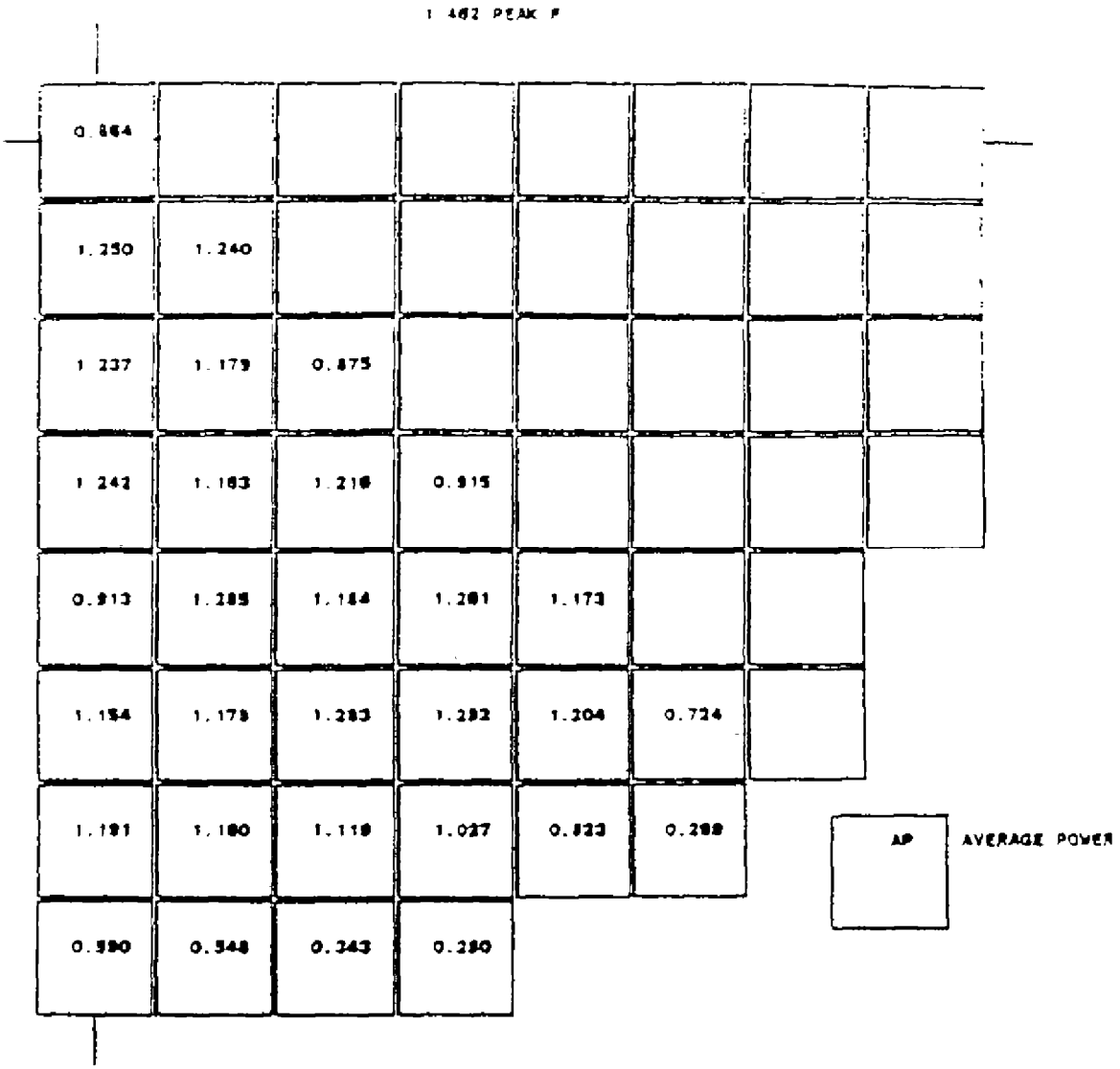

UNIT 2

16.4	REVISED PER 99-UFSAR-1242
REV. NO.	**DESCRIPTION**

REVISIONS

AMERICAN ELECTRIC POWER **COOK NUCLEAR PLANT** **NUCLEAR GENERATION GROUP** **BRIDGMAN, MICHIGAN**	**TITLE** **TYPICAL NORMALIZED POWER DENSITY DISTRIBUTION AT BEGINNING-OF-LIFE UNRODDED CORE, HOT FULL POWER, NO XENON**	
	DWG. NO. **FSAR FIG. 3.3-7**	SH 1 of 1

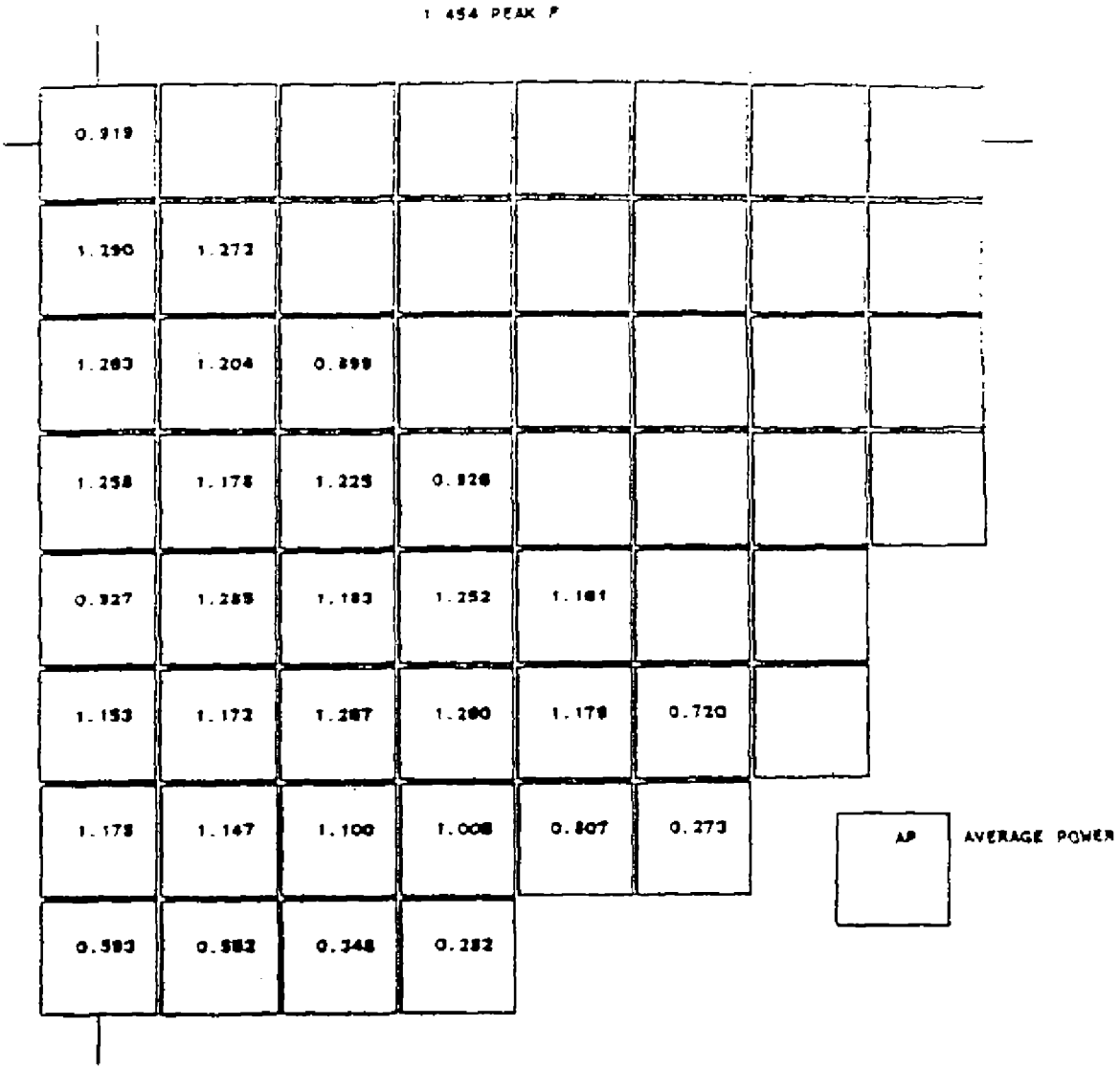

UNIT 2

16.4	REVISED PER 99-UFSAR-1242
REV. NO.	**DESCRIPTION**

REVISIONS

AMERICAN ELECTRIC POWER **COOK NUCLEAR PLANT** **NUCLEAR GENERATION GROUP** **BRIDGMAN, MICHIGAN**	**TITLE** **TYPICAL NORMALIZED POWER DENSITY DISTRIBUTION AT BEGINNING-OF-LIFE UNRODDED CORE, HOT FULL POWER, EQUILIBRIUM XENON**	
	DWG. NO. **FSAR FIG. 3.3-8**	SH 1 of 1

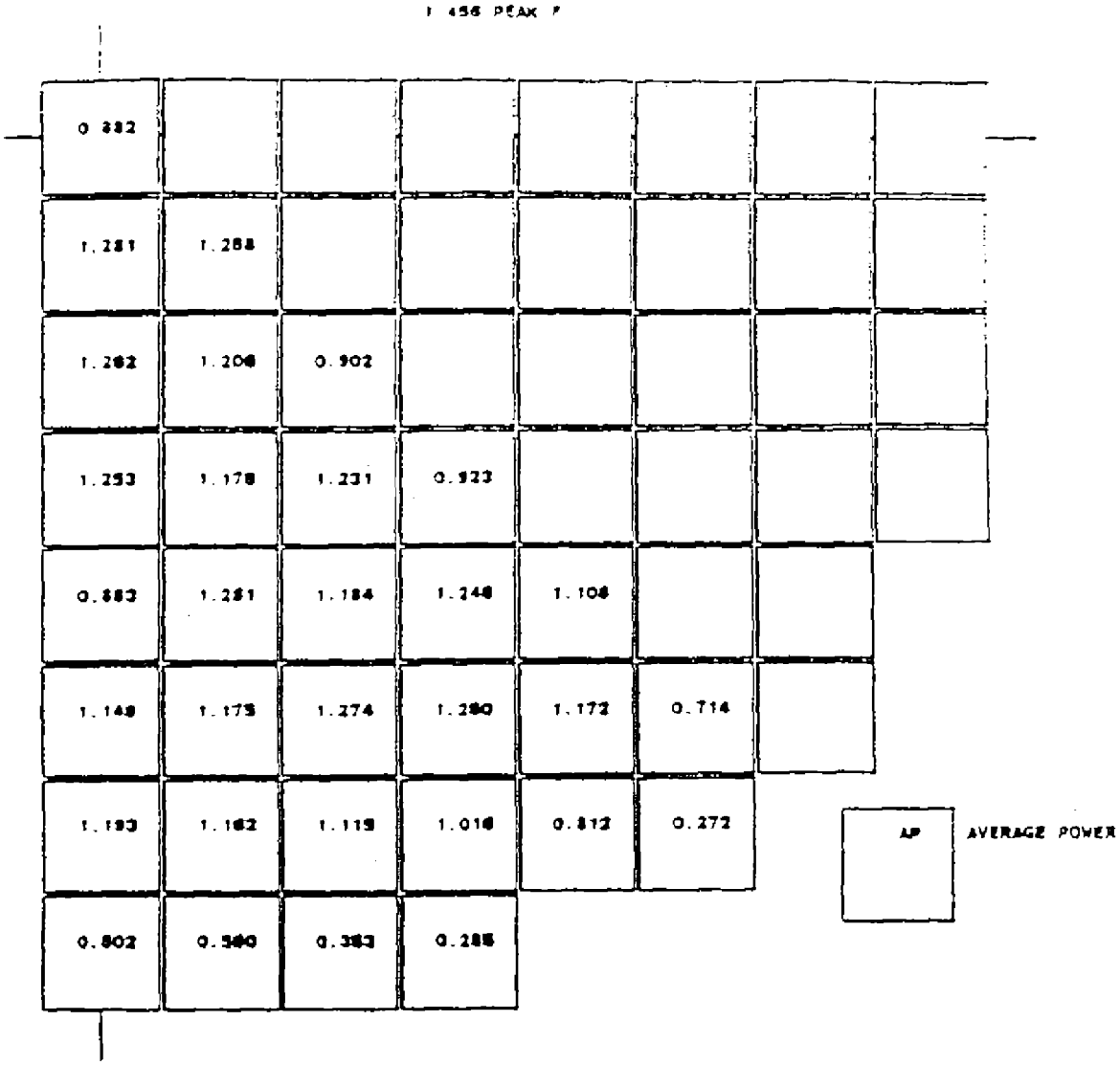

UNIT 2

16.4	REVISED PER 99-UFSAR-1242
REV. NO.	**DESCRIPTION**

REVISIONS

AMERICAN ELECTRIC POWER **COOK NUCLEAR PLANT** **NUCLEAR GENERATION GROUP** **BRIDGMAN, MICHIGAN**	**TITLE** **TYPICAL NORMALIZED POWER DENSITY DISTRIBUTION NEAR BEGINNING-OF-LIFE GROUP D AT INSERTION LIMIT, HOT FULL POWER, EQUILIBRIUM XENON**	
	DWG. NO. **FSAR FIG. 3.3-9**	SH 1 of 1

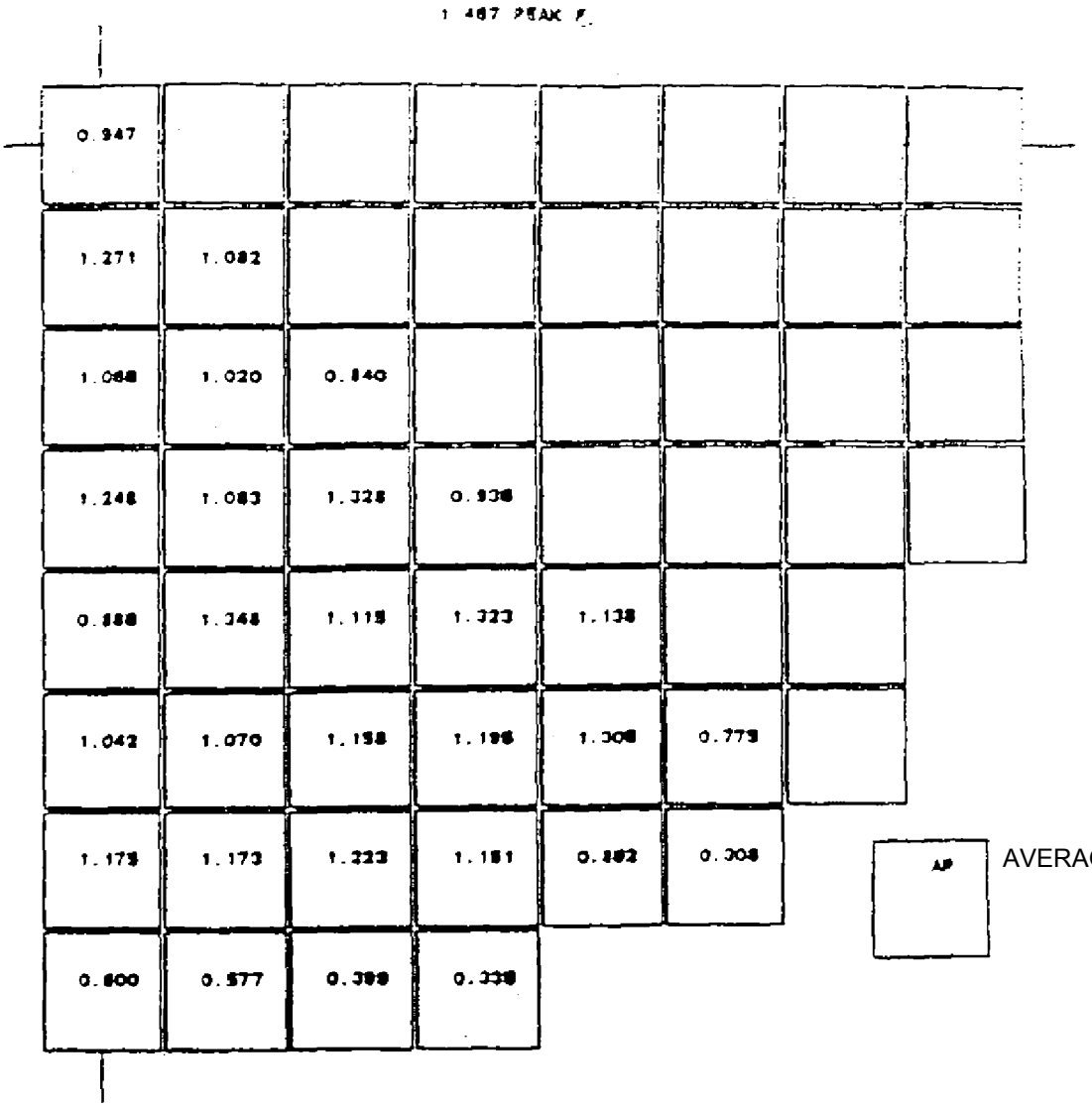

UNIT 2

16.4	REVISED PER 99-UFSAR-1242
REV. NO.	**DESCRIPTION**

REVISIONS

AMERICAN ELECTRIC POWER
COOK NUCLEAR PLANT
NUCLEAR GENERATION GROUP
BRIDGMAN, MICHIGAN

TITLE **TYPICAL NORMALIZED POWER DENSITY DISTRIBUTION AT MIDDLE-OF-LIFE UNRODDED CORE, HOT FULL POWER, EQUILIBRIUM XENON.**

DWG. NO. **FSAR FIG. 3.3-10** SH 1 of 1

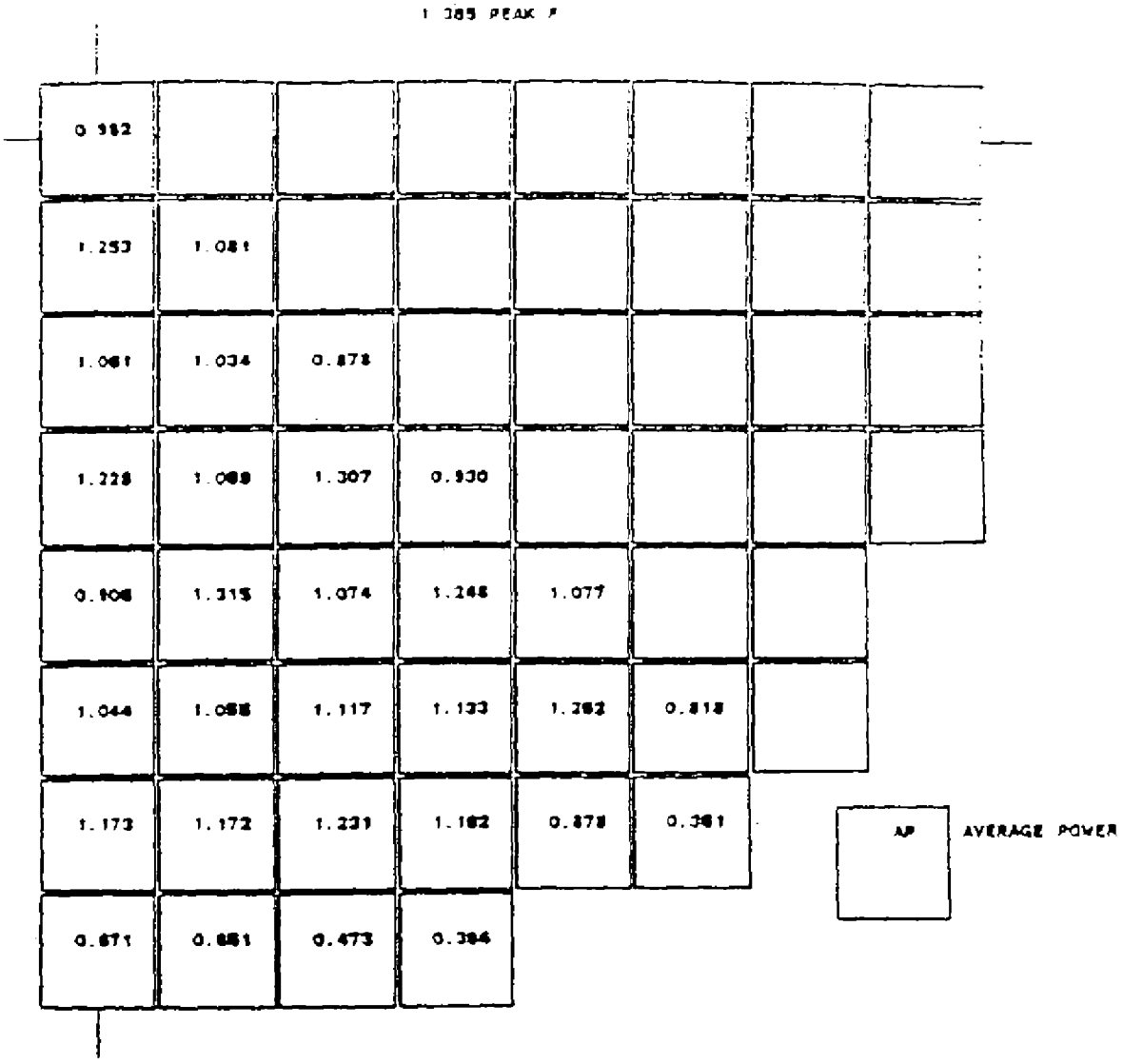

UNIT 2

16.4	REVISED PER 99-UFSAR-1242
REV. NO.	**DESCRIPTION**

REVISIONS

AMERICAN ELECTRIC POWER **COOK NUCLEAR PLANT** **NUCLEAR GENERATION GROUP** **BRIDGMAN, MICHIGAN**	**TITLE** **TYPICAL NORMALIZED POWER DENSITY DISTRIBUTION NEAR END-OF-LIFE UNRODDED CORE, HOT FULL POWER, EQUILIBRIUM XENON.**	
	DWG. NO. **FSAR FIG. 3.3-11**	SH 1 of 1

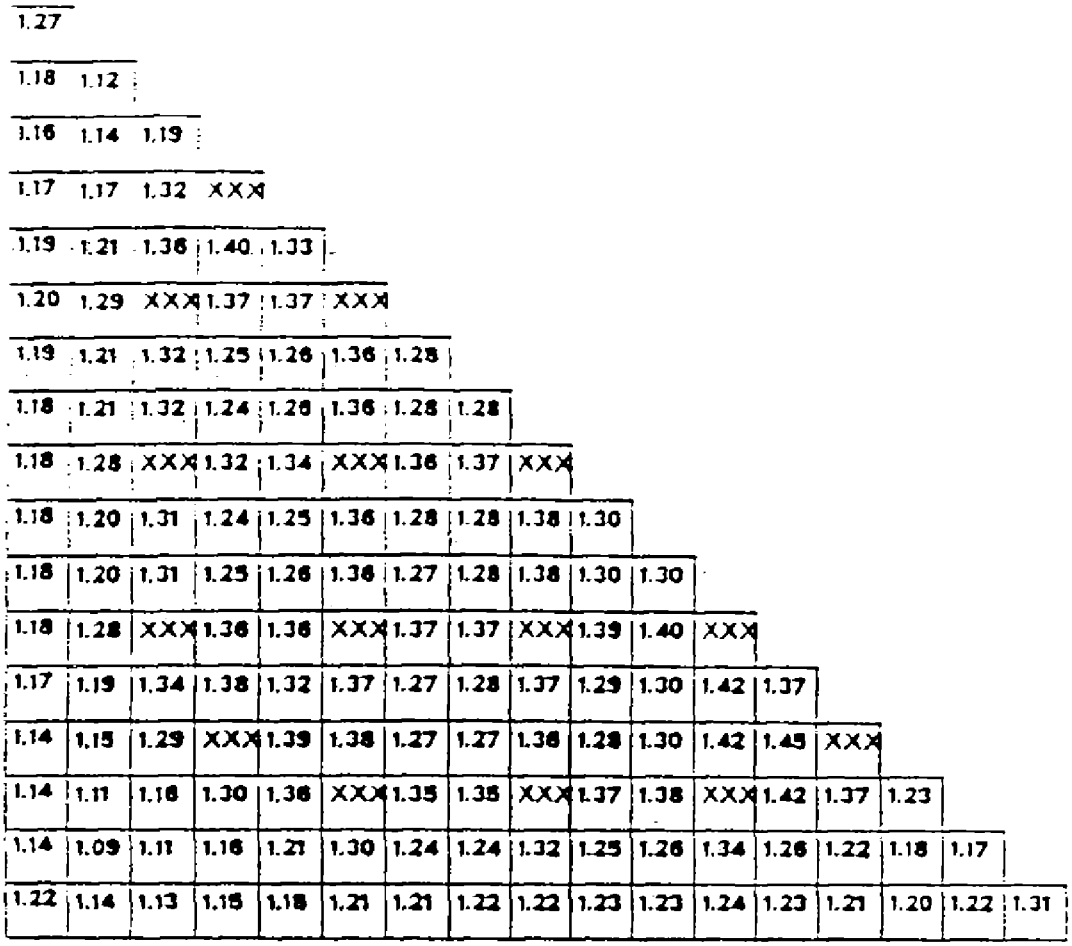

UNIT 2

16.4	REVISED PER 99-UFSAR-1242
REV. NO.	**DESCRIPTION**

REVISIONS

AMERICAN ELECTRIC POWER COOK NUCLEAR PLANT NUCLEAR GENERATION GROUP BRIDGMAN, MICHIGAN	**TITLE** **TYPICAL RODWISE POWER DISTRIBUTION IN A TYPICAL ASSEMBLY (ASSEMBLY G-12) NEAR BEGINNING-OF-LIFE, HOT FULL POWER, EQUILIBRIUM XENON, UNRODDED CORE.**	
	DWG. NO. FSAR FIG. 3.3-12	SH 1 of 1

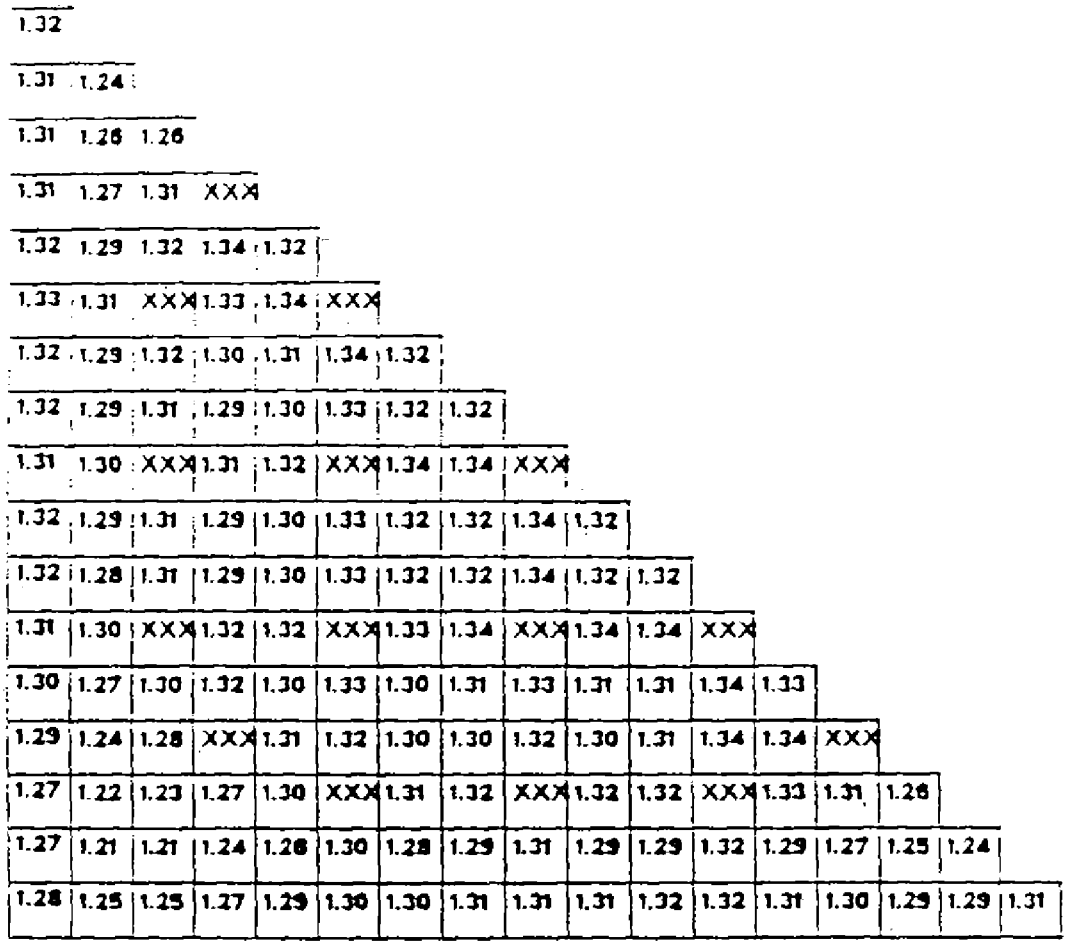

UNIT 2

16.4	REVISED PER 99-UFSAR-1242
REV. NO.	**DESCRIPTION**

REVISIONS

AMERICAN ELECTRIC POWER **COOK NUCLEAR PLANT** **NUCLEAR GENERATION GROUP** **BRIDGMAN, MICHIGAN**	**TITLE** **TYPICAL RODWISE POWER DISTRIBUTION IN A TYPICAL ASSEMBLY (ASSEMBLY G-12) NEAR END-OF-LIFE, HOT FULL POWER EQUILIBRIUM XENON, UNRODDED CORE.**	
	DWG. NO. **FSAR FIG. 3.3-13**	SH 1 of 1

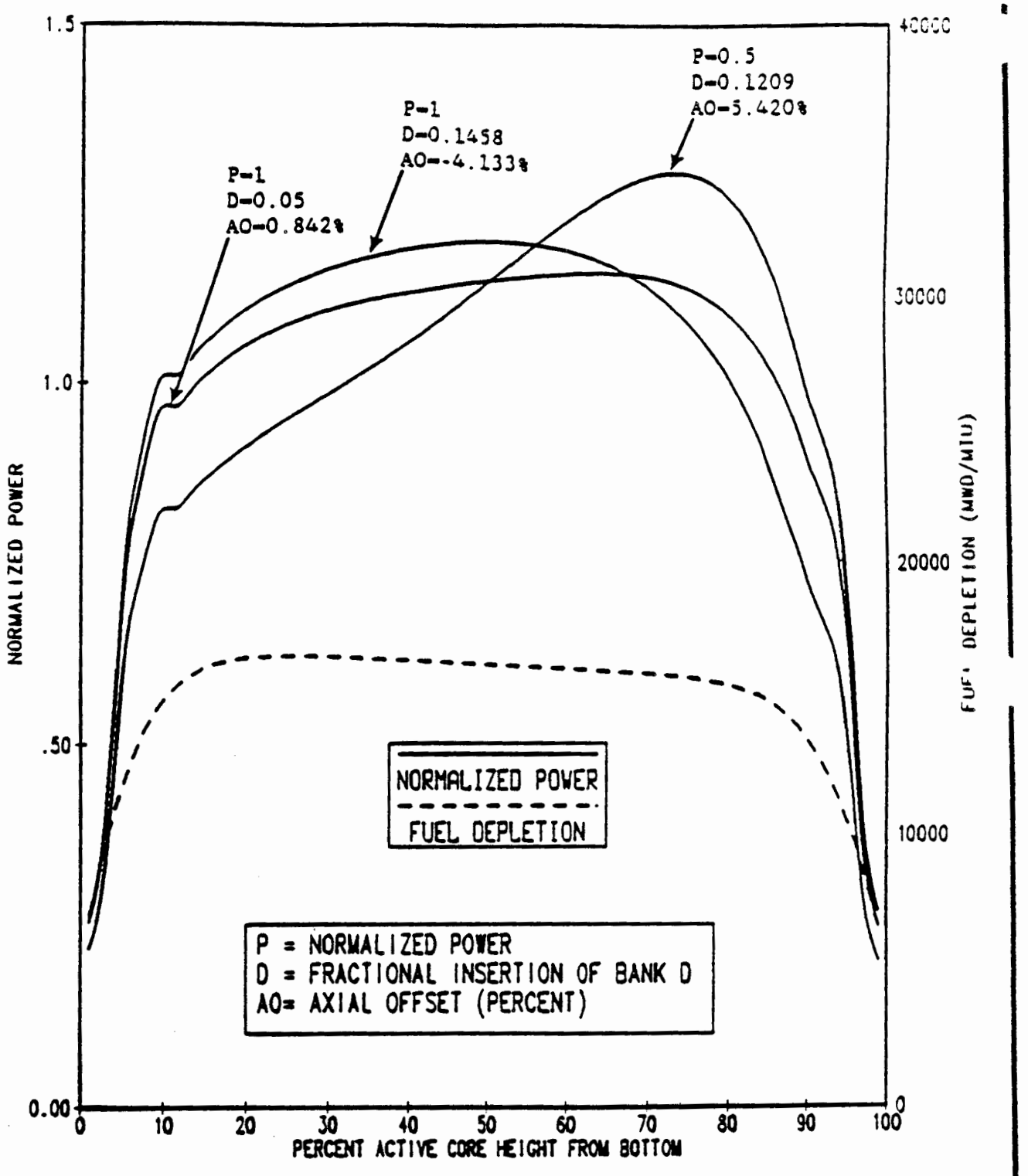

Figure 3.3-14 Example Axial Power Shapes Occurring at BOL

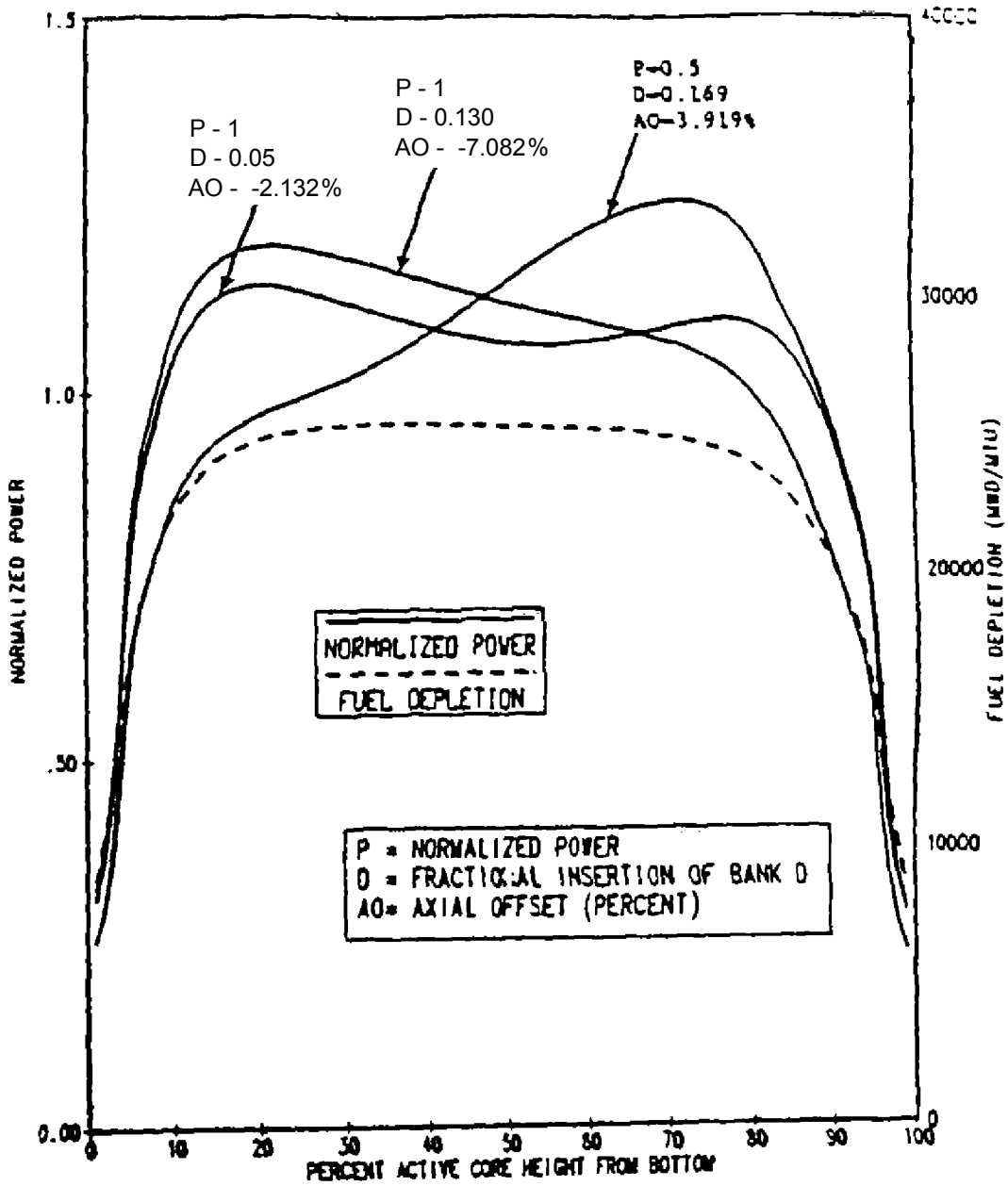

UNIT 2

16.4	REVISED PER 99-UFSAR-1242
REV. NO.	**DESCRIPTION**

REVISIONS

AMERICAN ELECTRIC POWER **COOK NUCLEAR PLANT** **NUCLEAR GENERATION GROUP** **BRIDGMAN, MICHIGAN**	**TITLE** **EXAMPLE AXIAL POWER SHAPES OCCURRING AT MOL**	
	DWG. NO. **FSAR FIG. 3.3-15**	SH 1 of 1

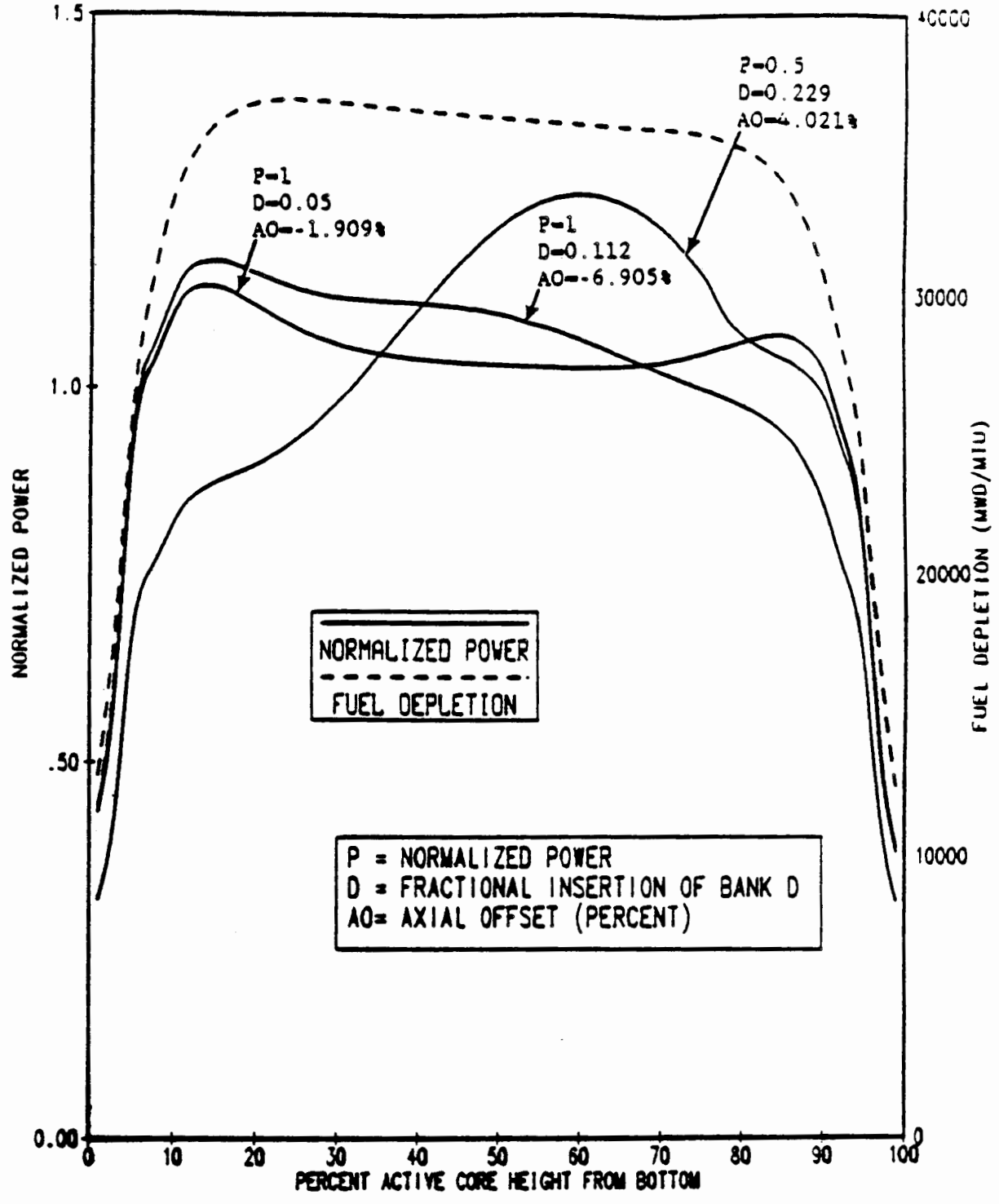

Figure 3.3-16 Example Axial Power Shapes Occurring at EOL

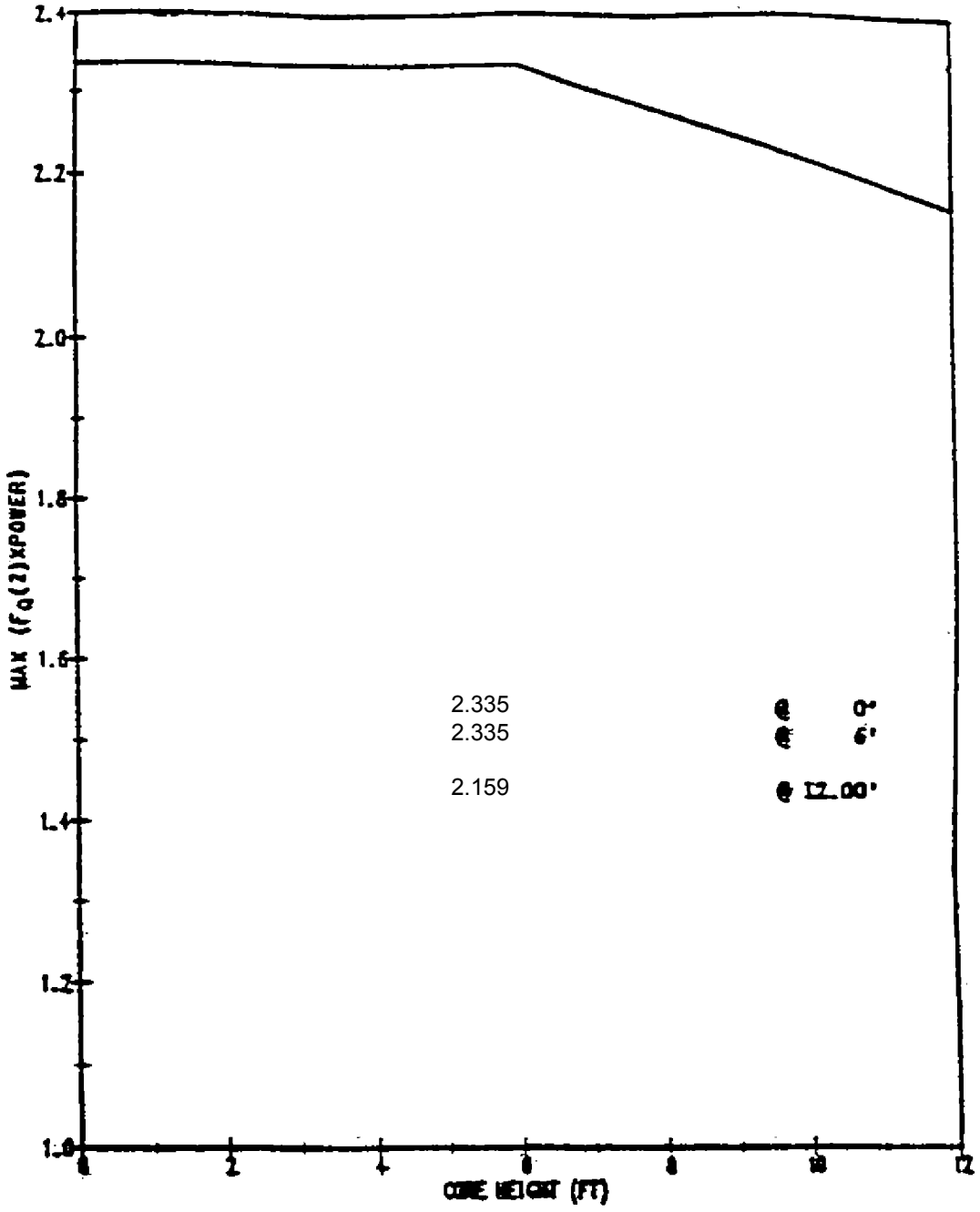

UNIT 2

16.4	REVISED PER 99-UFSAR-1242
REV. NO.	**DESCRIPTION**

REVISIONS

AMERICAN ELECTRIC POWER **COOK NUCLEAR PLANT** **NUCLEAR GENERATION GROUP** **BRIDGMAN, MICHIGAN**	**TITLE** **MAXIMUM $F_Q(Z)$ x POWER VERSUS AXIAL HEIGHT (Z) DURING NORMAL OPERATION**	
	DWG. NO. **FSAR FIG. 3.3-20**	SH 1 of 1

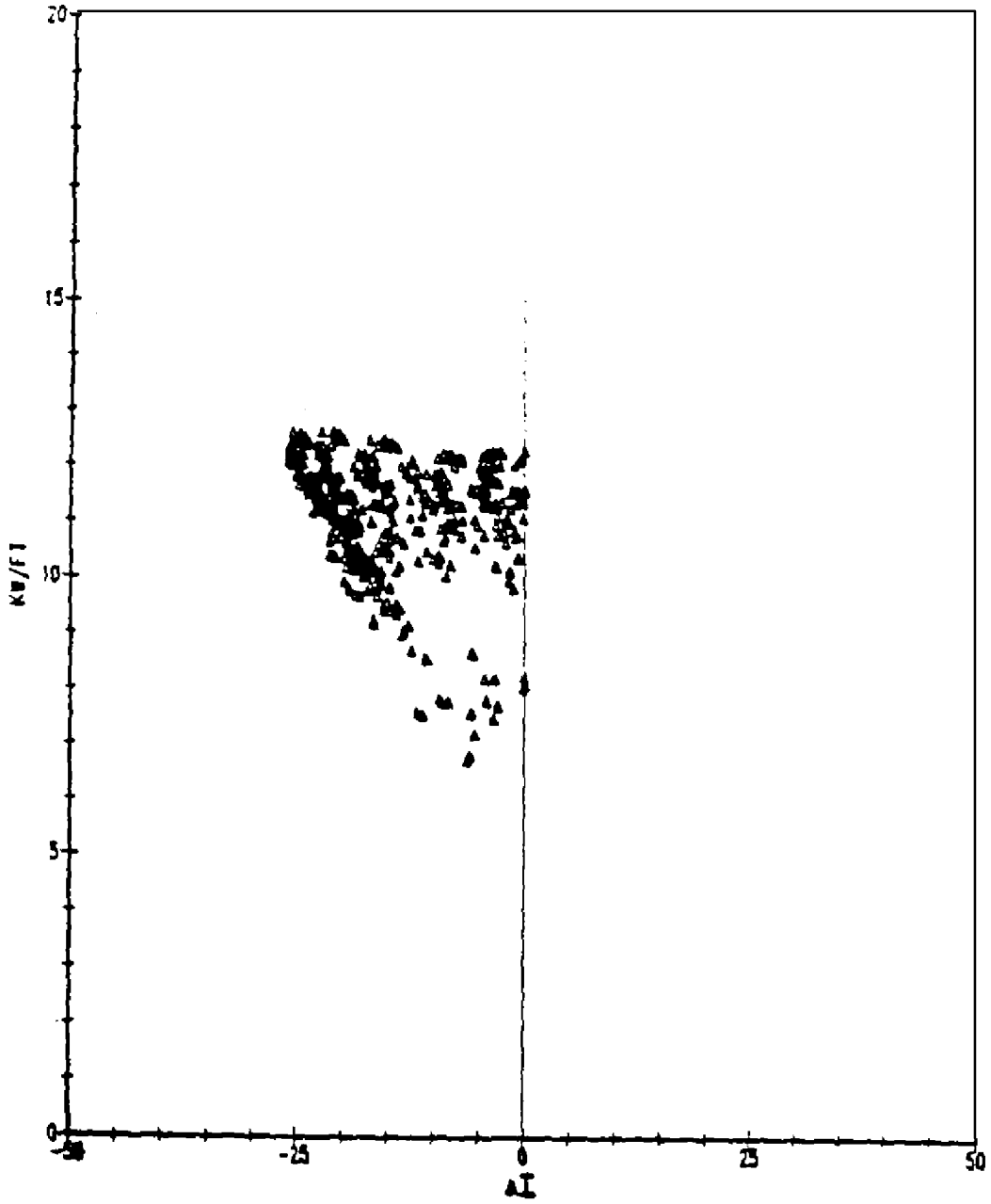

UNIT 2

16.4	REVISED PER 99-UFSAR-1242
REV. NO.	**DESCRIPTION**

REVISIONS

AMERICAN ELECTRIC POWER **COOK NUCLEAR PLANT** **NUCLEAR GENERATION GROUP** **BRIDGMAN, MICHIGAN**	**TITLE** **TYPICAL PEAK LINEAR POWER DURING CONTROL ROD MALFUNCTION OVERPOWER TRANSIENTS**	
	DWG. NO. **FSAR FIG. 3.3-21**	SH 1 of 1

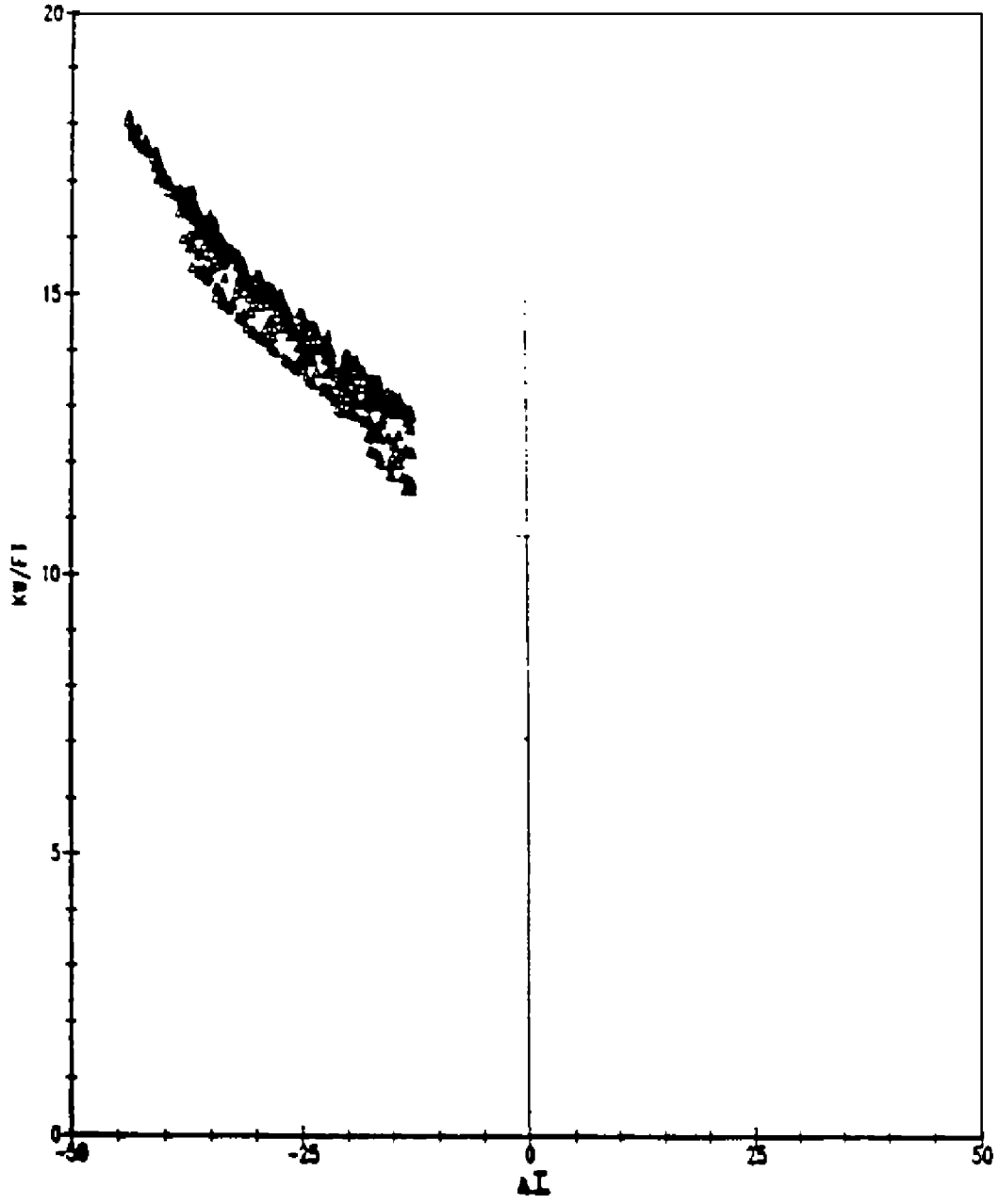

UNIT 2

16.4	REVISED PER 99-UFSAR-1242
REV. NO.	**DESCRIPTION**

REVISIONS

AMERICAN ELECTRIC POWER **COOK NUCLEAR PLANT** **NUCLEAR GENERATION GROUP** **BRIDGMAN, MICHIGAN**	**TITLE** **TYPICAL PEAK LINEAR POWER DURING BORATION/DILUTION OVERPOWER TRANSIENTS**	
	DWG. NO. **FSAR FIG. 3.3-22**	SH 1 of 1

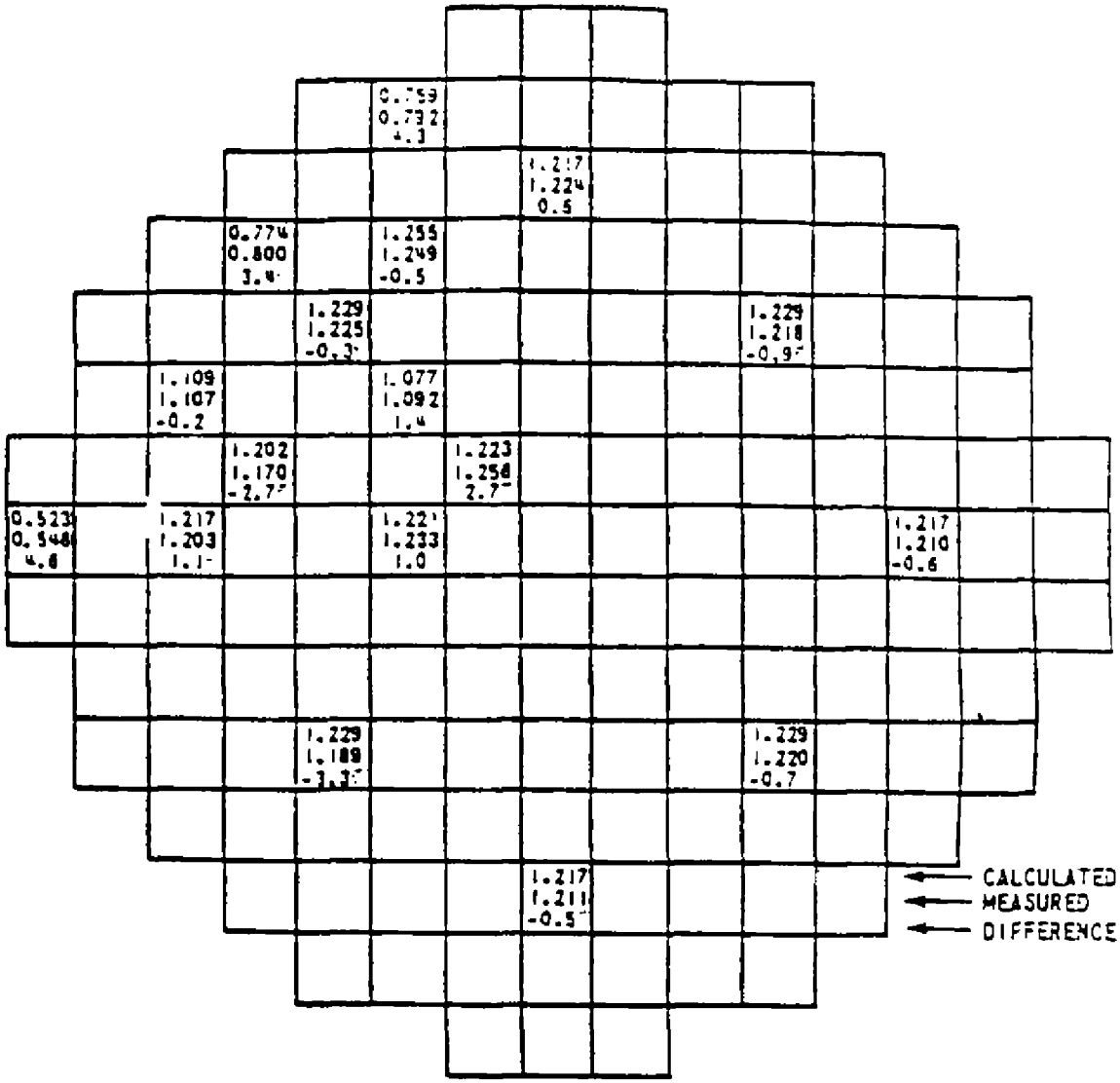

PEAKING FACTORS

$\bar{F}_z$ = 1.5

$F^R_{\Delta N}$ = 1.357

F^R_Q = 2.07 LOCATED AT M-8 SOUTH

UNIT 2

16.4	REVISED PER 99-UFSAR-1242
REV. NO.	**DESCRIPTION**

REVISIONS

AMERICAN ELECTRIC POWER **COOK NUCLEAR PLANT** **NUCLEAR GENERATION GROUP** **BRIDGMAN, MICHIGAN**	**TITLE** **ILLUSTRATION OF A COMPARISON BETWEEN CALCULATED AND MEASURED RELATIVE FUEL ASSEMBLY POWER DISTRIBUTION**	
	DWG. NO. **FSAR FIG. 3.3-23**	SH 1 of 1

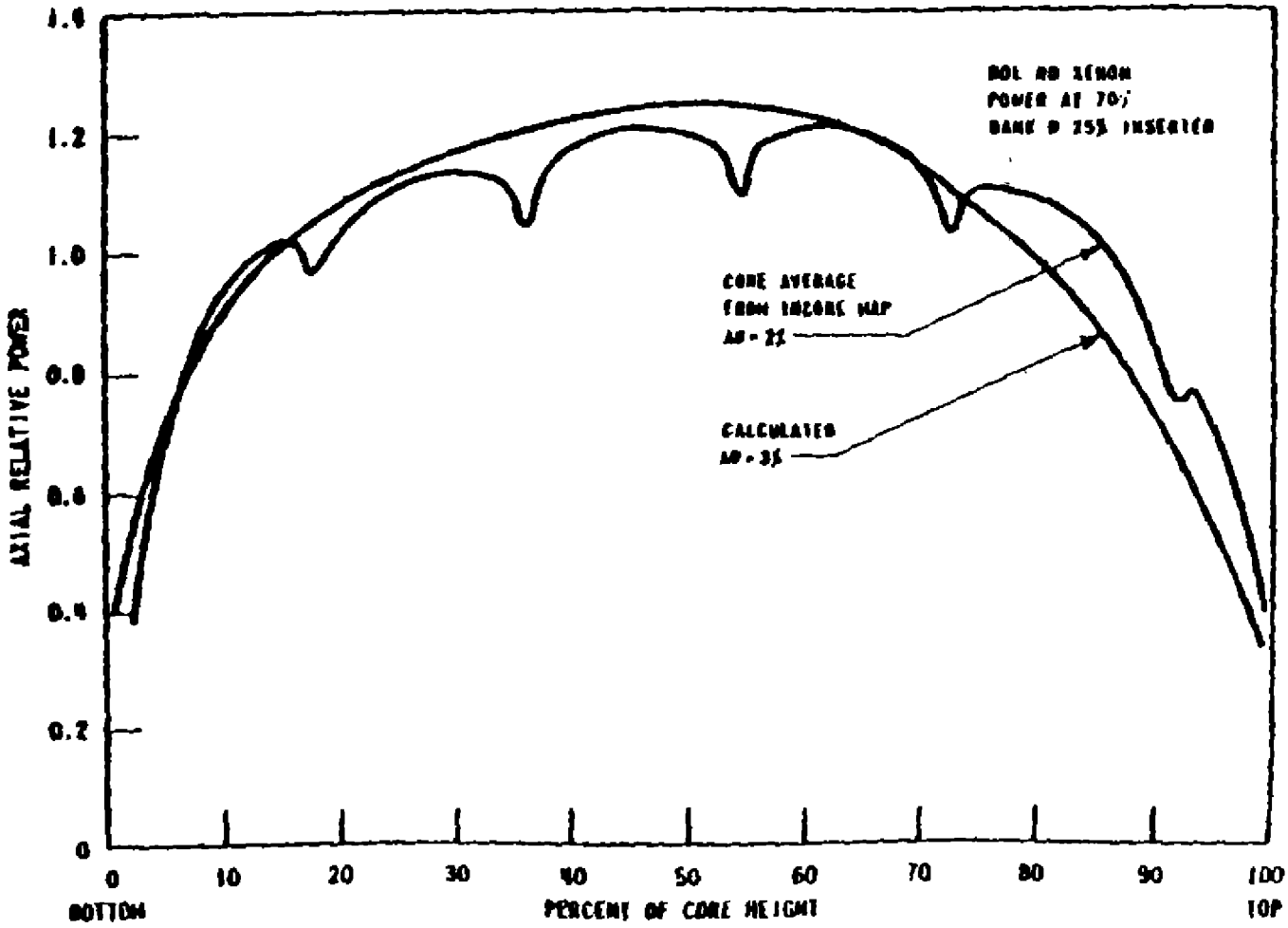

UNIT 2

16.4	REVISED PER 99-UFSAR-1242
REV. NO.	**DESCRIPTION**

REVISIONS

AMERICAN ELECTRIC POWER
COOK NUCLEAR PLANT
NUCLEAR GENERATION GROUP
BRIDGMAN, MICHIGAN

TITLE **COMPARISON OF TYPICAL CALCULATED AND MEASURED AXIAL SHAPE**

DWG. NO. **FSAR FIG. 3.3-24**

SH 1 of 1

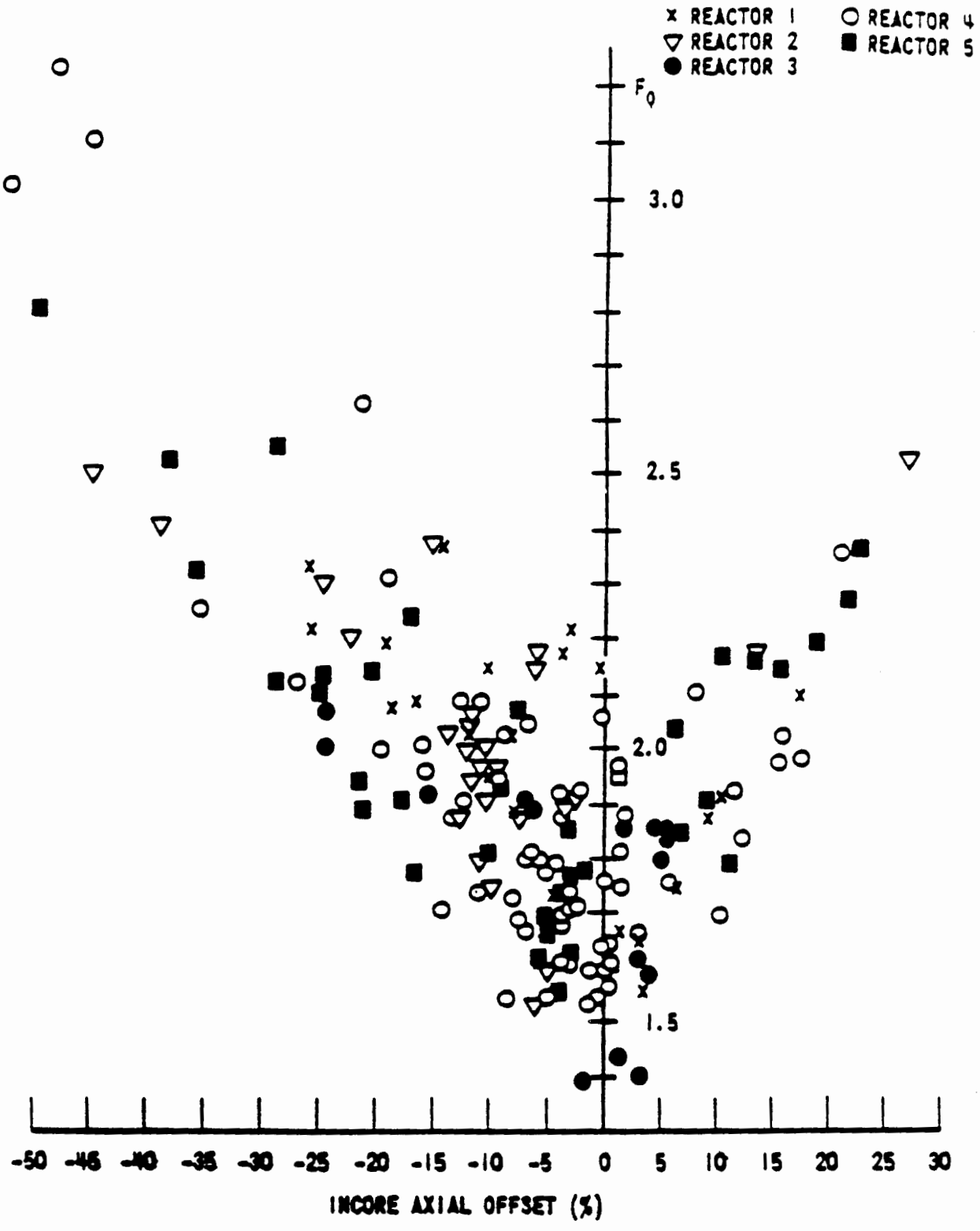

Figure 3.3-25 Measured Values of F_Q for Full Power Rod Configurations

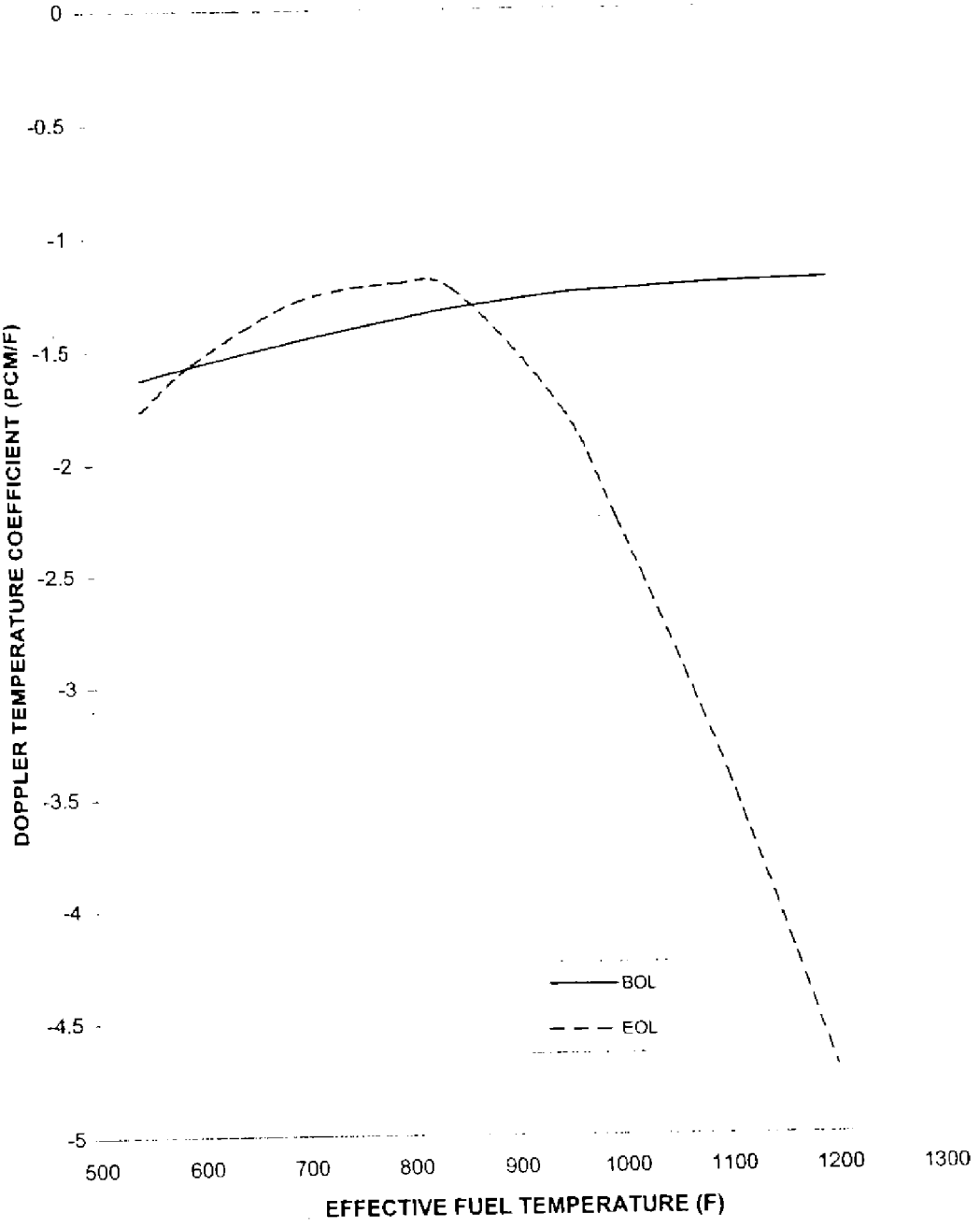

UNIT 2

16.4	REVISED PER 99-UFSAR-1242
REV. NO.	**DESCRIPTION**

REVISIONS

AMERICAN ELECTRIC POWER
COOK NUCLEAR PLANT
NUCLEAR GENERATION GROUP
BRIDGMAN, MICHIGAN

TITLE **EXAMPLE DOPPLER TEMPERATURE COEFFICIENT AT BOL AND EOL**

DWG. NO. **FSAR FIG. 3.3-26** SH 1 of 1

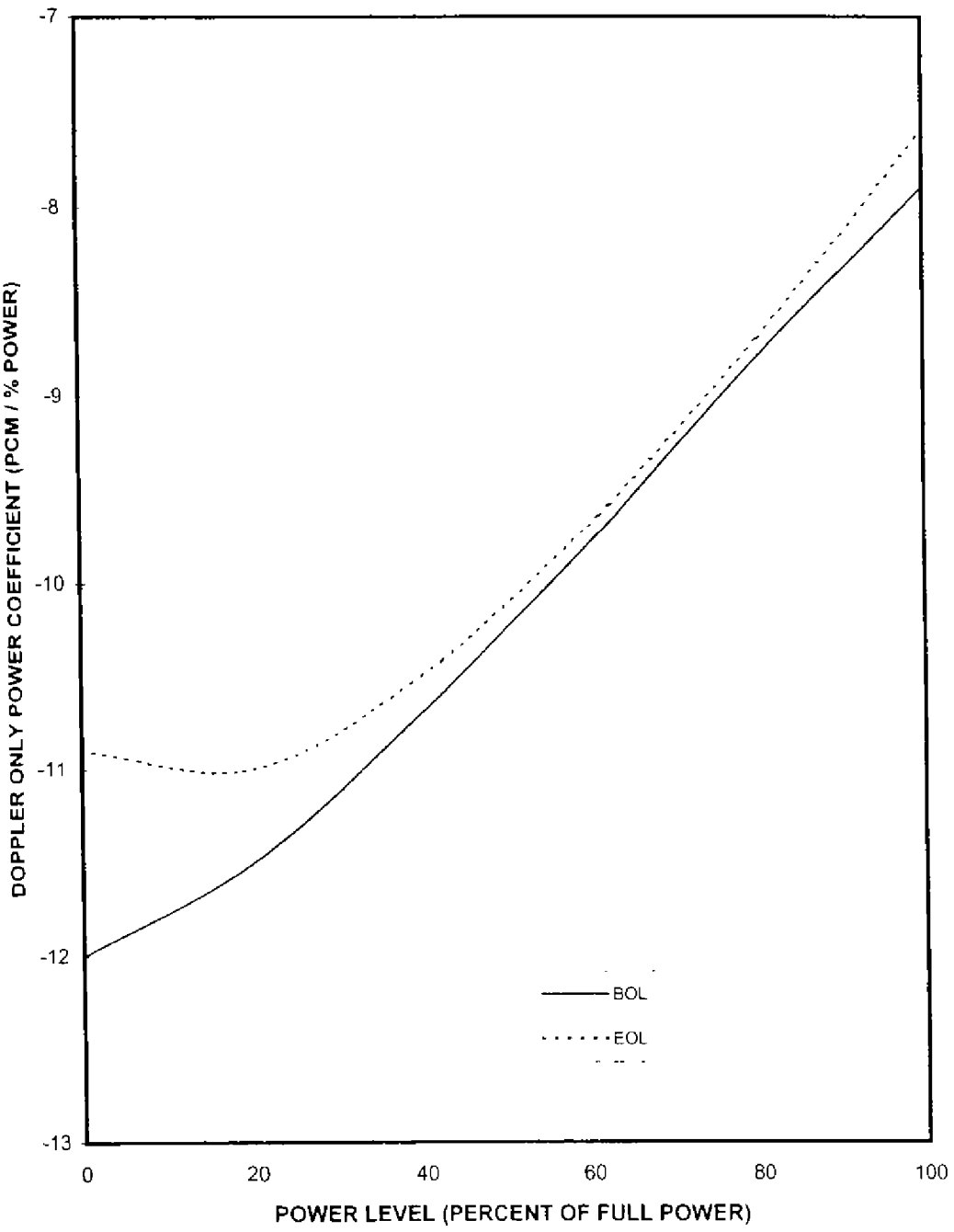

UNIT 2

16.4	REVISED PER 99-UFSAR-1242
REV. NO.	**DESCRIPTION**

REVISIONS

AMERICAN ELECTRIC POWER **COOK NUCLEAR PLANT** **NUCLEAR GENERATION GROUP** **BRIDGMAN, MICHIGAN**	**TITLE** **EXAMPLE DOPPLER ONLY POWER COEFFICIENT AT BOL AND EOL**
	DWG. NO. **FSAR FIG. 3.3-27** — SH 1 of 1

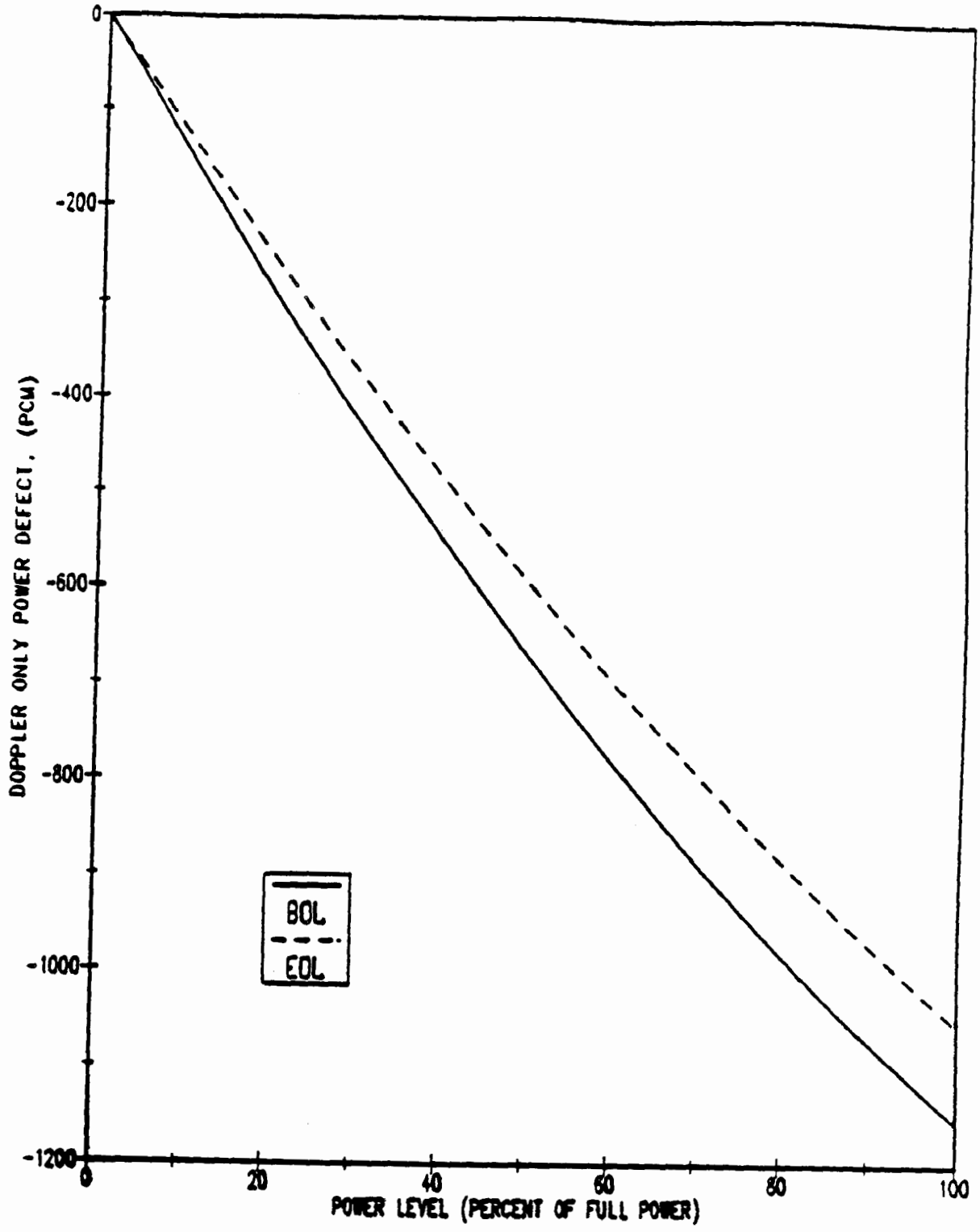

Figure 3.3-28 Example Doppler Only Power Defect - BOL, EOL

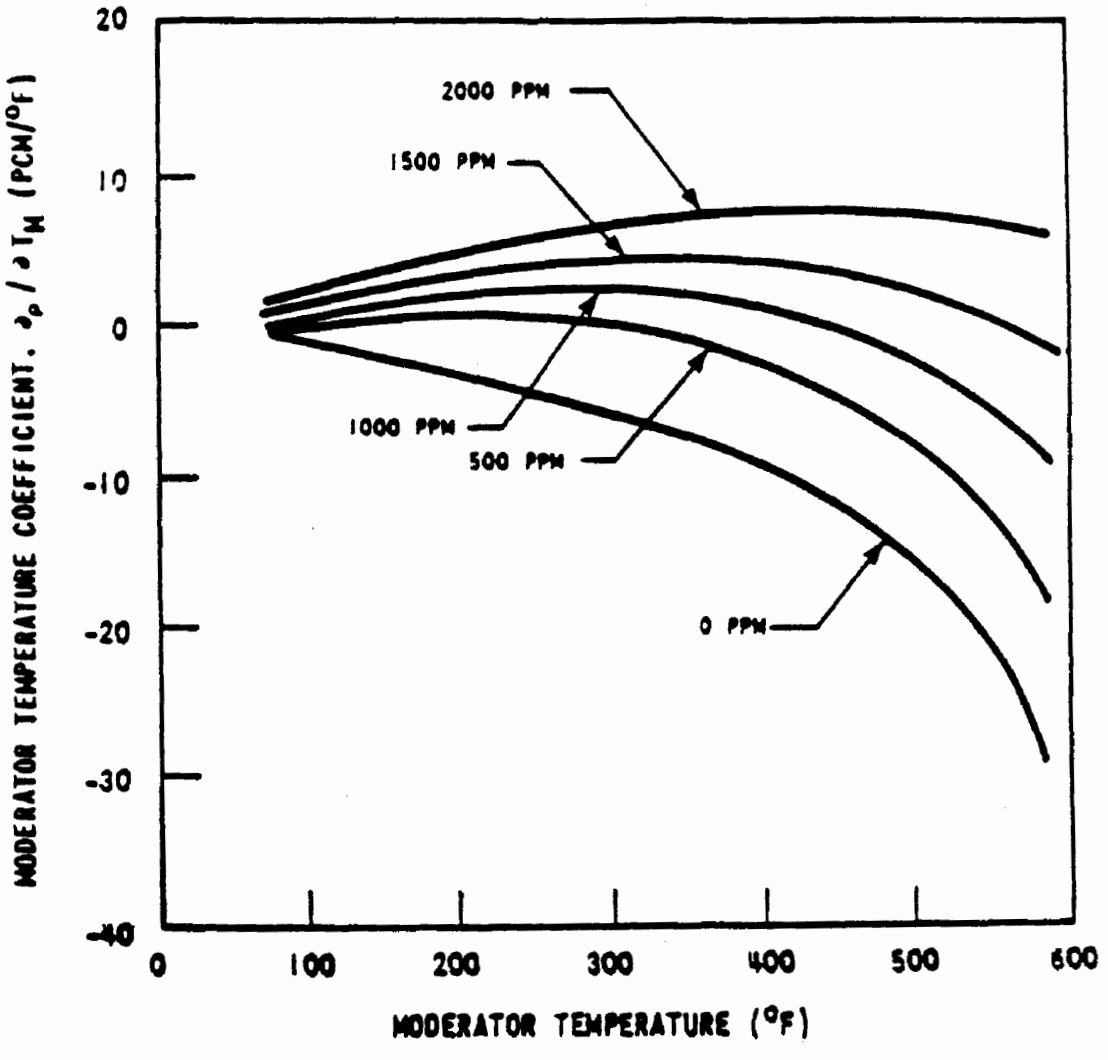

Figure 3.3-29 Example Moderator Temperature Coefficient - BOL, No Rods

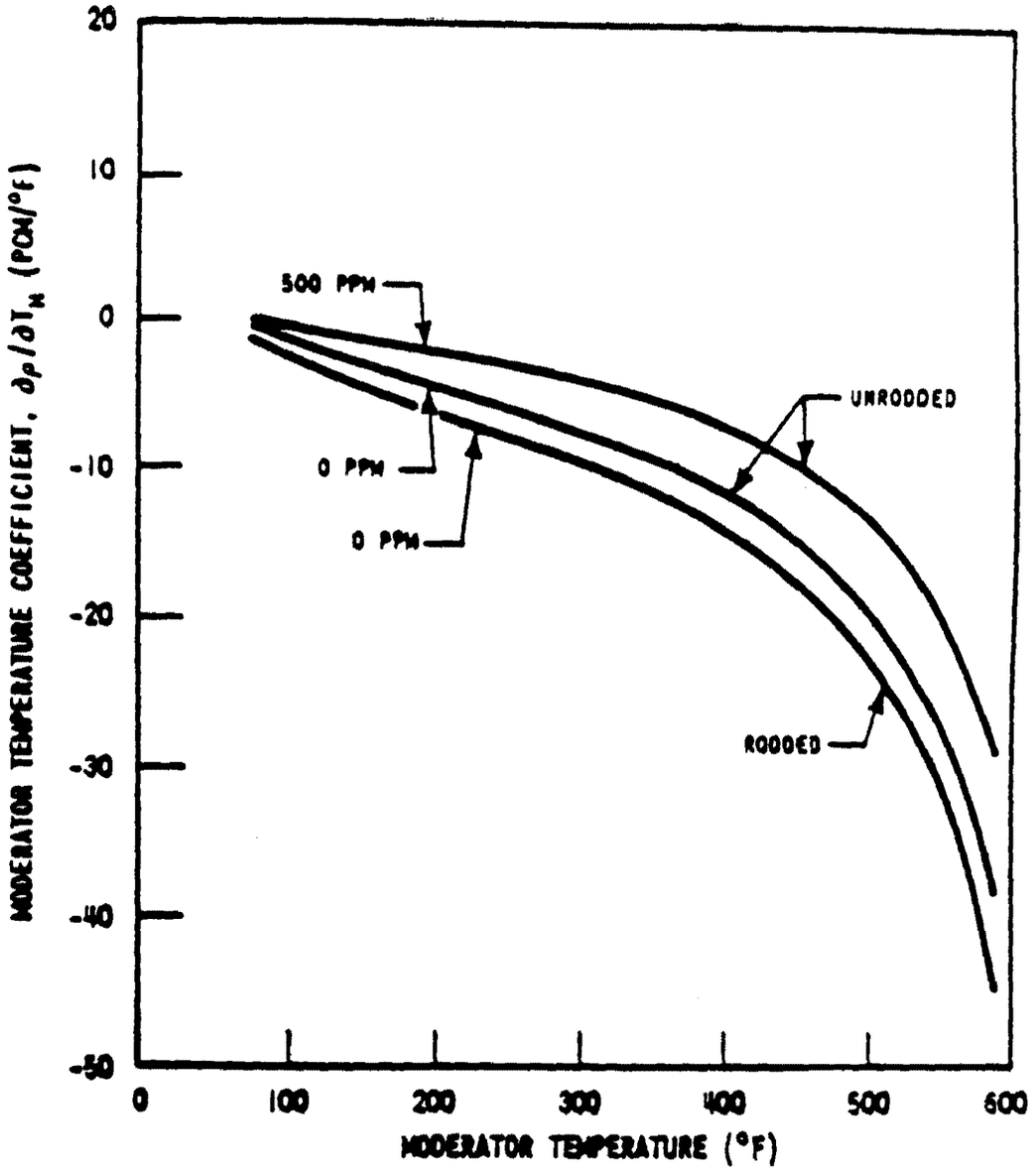

Figure 3.3-30 Example Moderator Temperature Coefficient - EOL

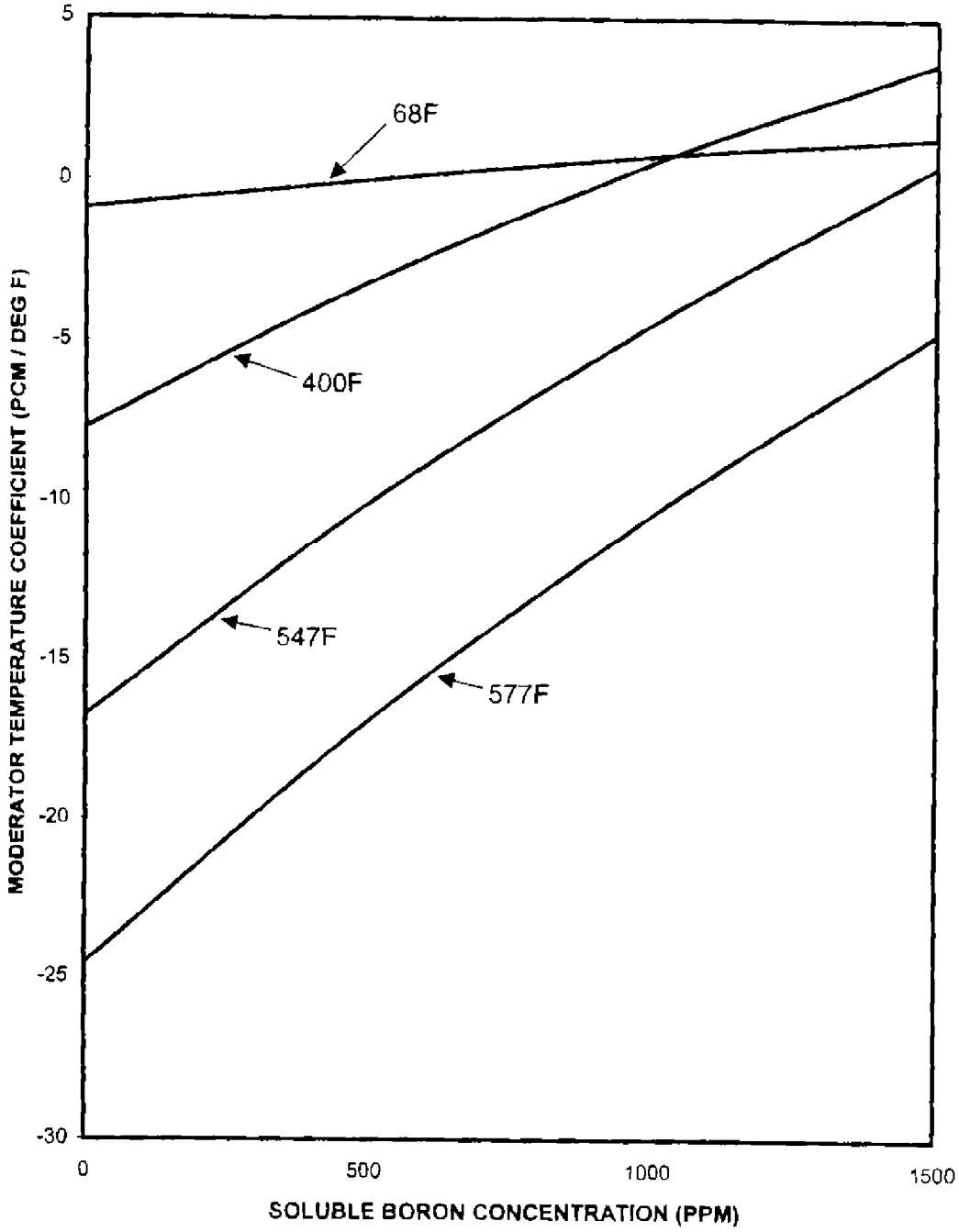

UNIT 2

16.4	REVISED PER 99-UFSAR-1242
REV. NO.	**DESCRIPTION**

REVISIONS

AMERICAN ELECTRIC POWER **COOK NUCLEAR PLANT** **NUCLEAR GENERATION GROUP** **BRIDGMAN, MICHIGAN**	**TITLE** **EXAMPLE MODERATOR TEMPERATURE COEFFICIENT AS A FUNCTION OF BORON CONCENTRATION - BOL, NO RODS**	
	DWG. NO. **FSAR FIG. 3.3-31**	SH 1 of 1

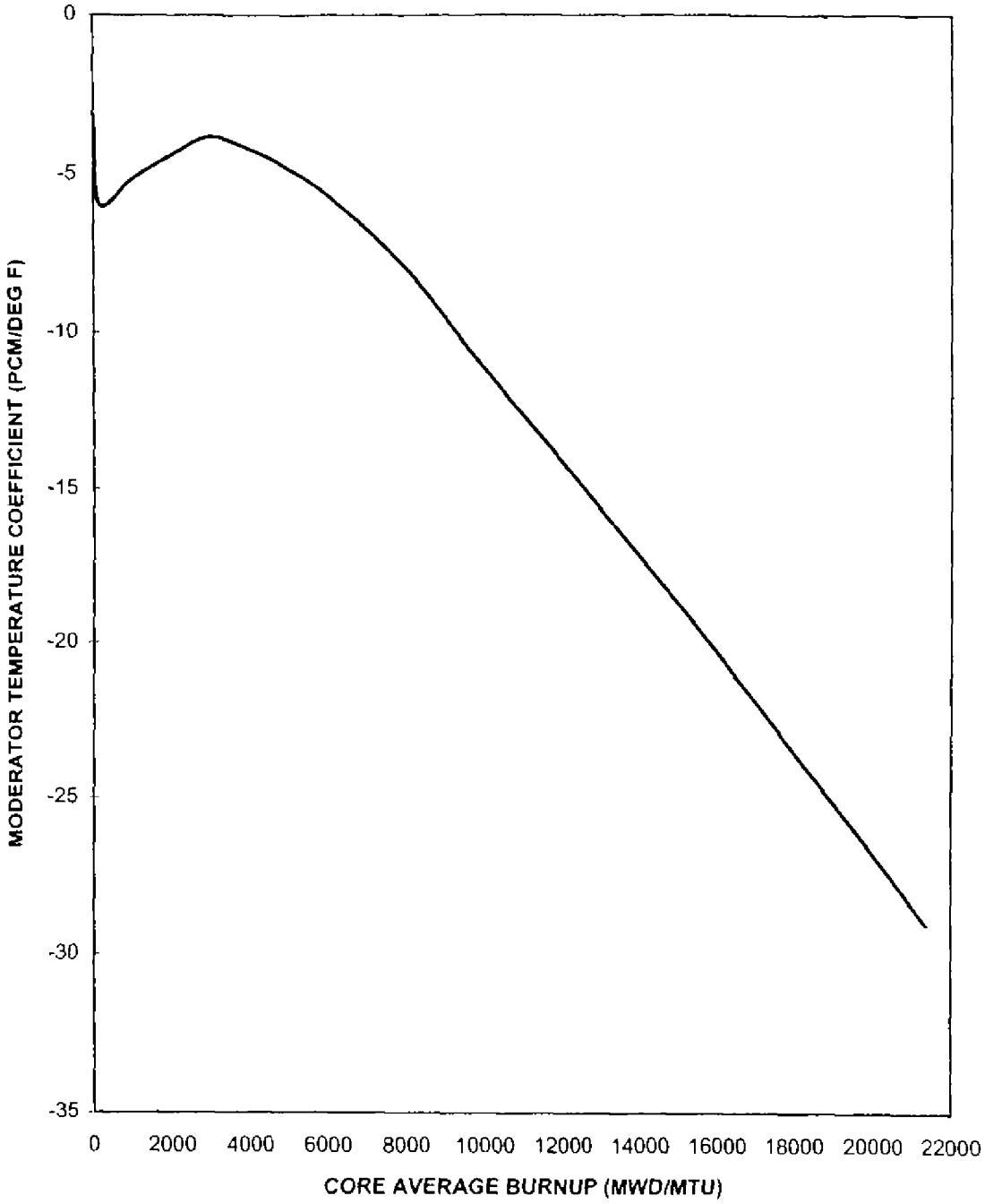

UNIT 2

16.4	REVISED PER 99-UFSAR-1242
REV. NO.	**DESCRIPTION**

REVISIONS

AMERICAN ELECTRIC POWER **COOK NUCLEAR PLANT** **NUCLEAR GENERATION GROUP** **BRIDGMAN, MICHIGAN**	**TITLE** **EXAMPLE HOT FULL POWER MODERATOR TEMPERATURE COEFFICIENT (AT THE CRITICAL BORON CONCENTRATION) VERSUS BURNUP**	
	DWG. NO. **FSAR FIG. 3.3-32**	SH 1 of 1

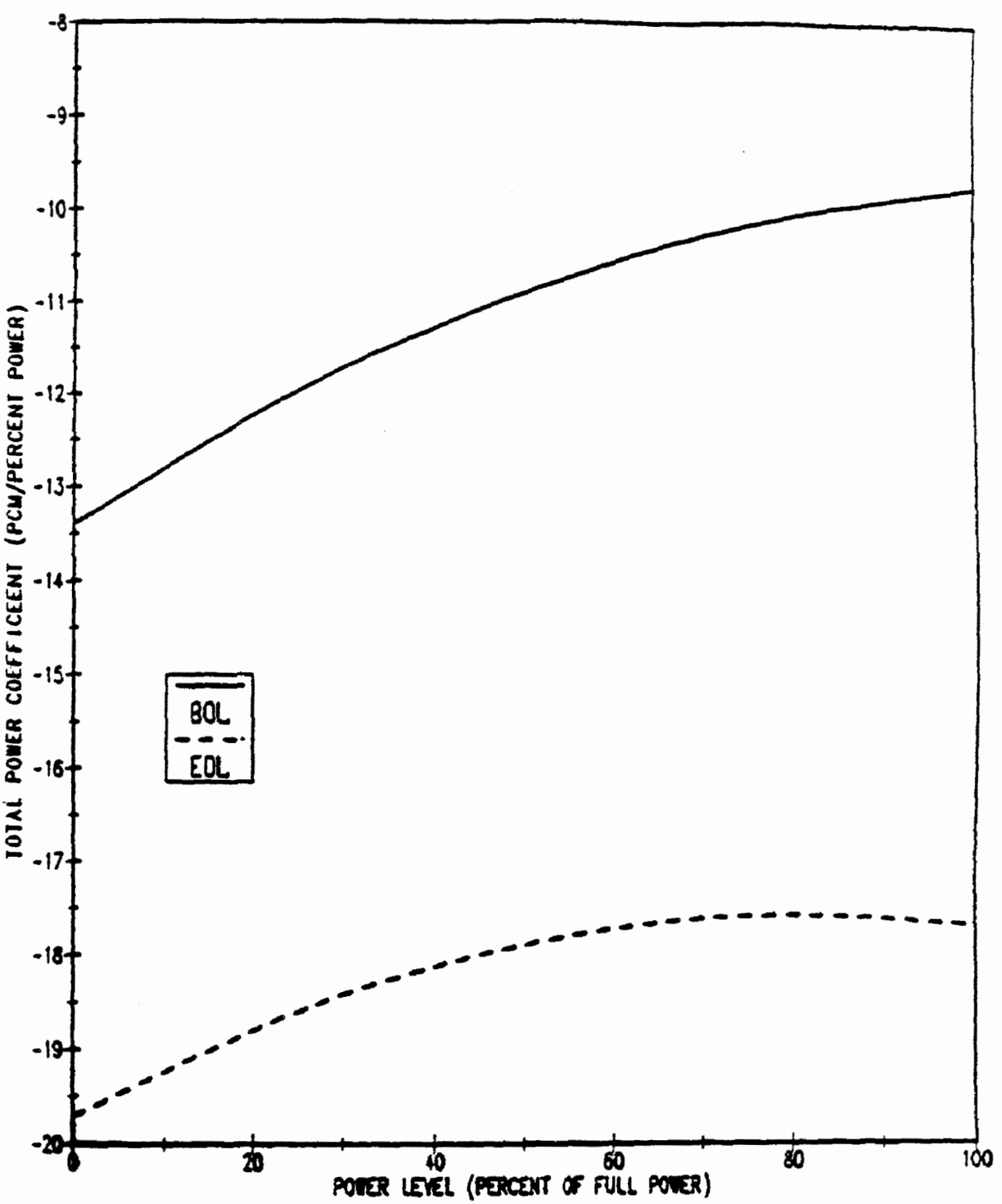

Figure 3.3-33 Example Total Power Coefficient at BOL and EOL

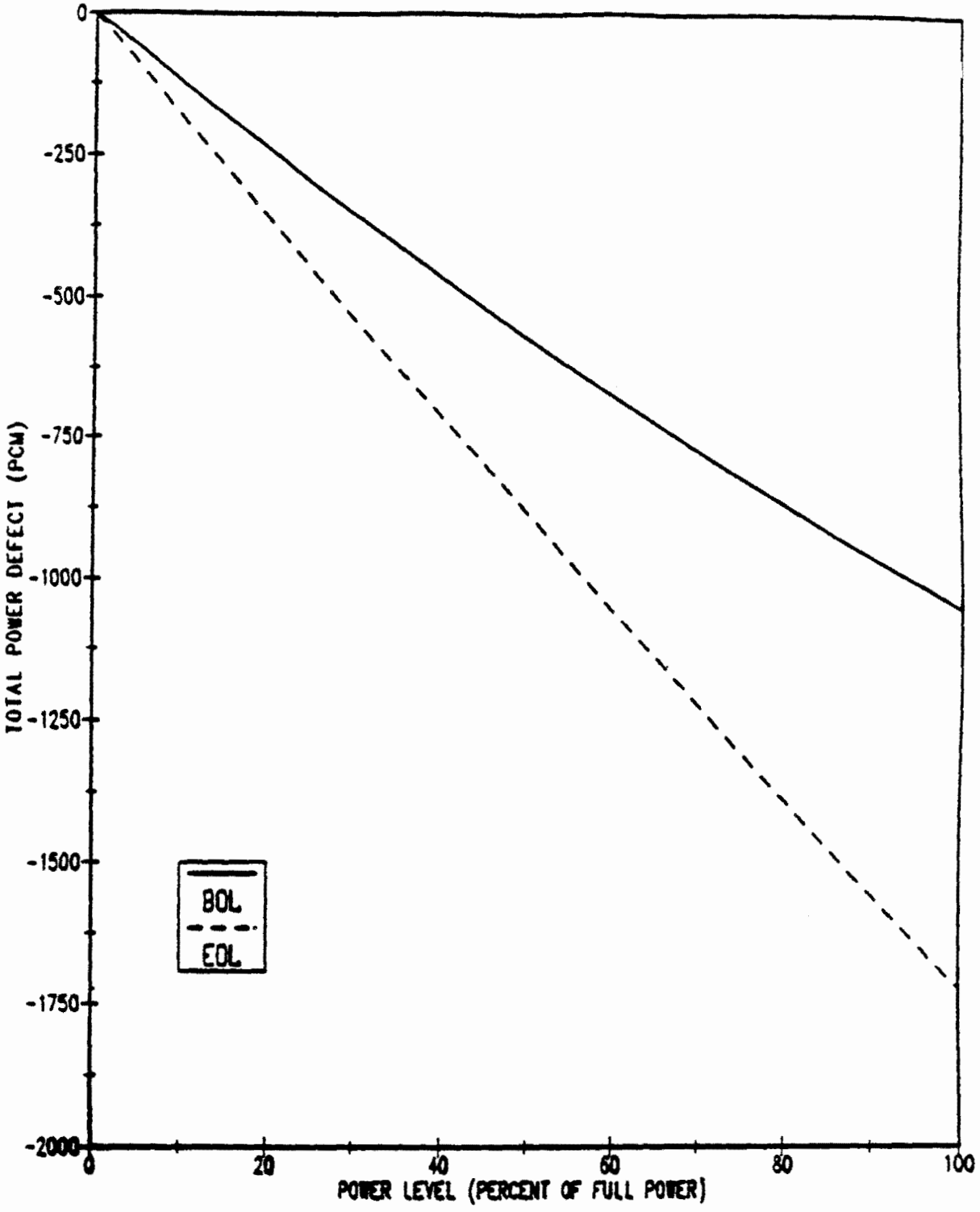

Figure 3.3-34 Example Total Power Defect at BOL and EOL

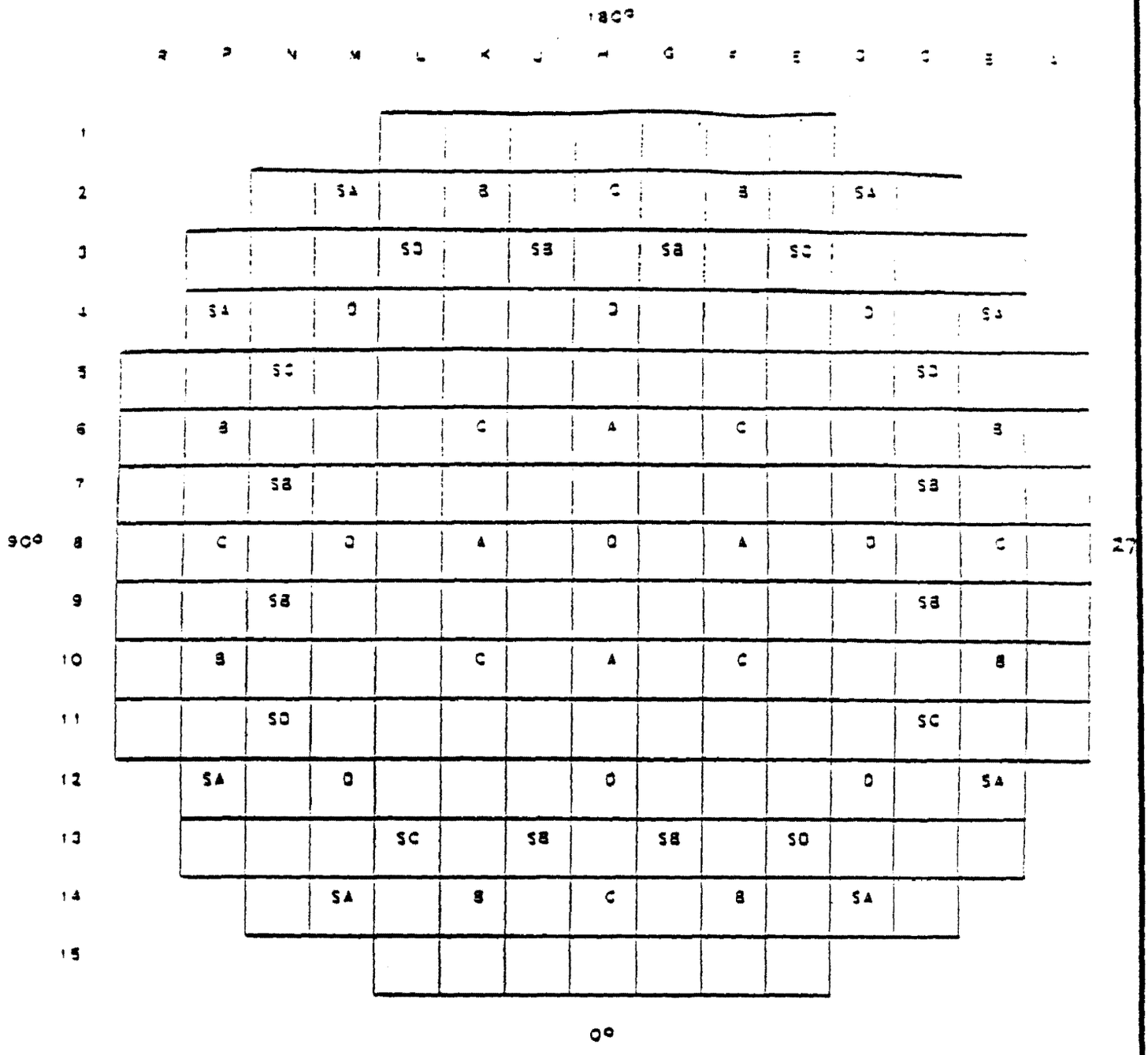

	FUNCTION	NUMBER OF ROD CLUSTERS
SHUTDOWN BANK	SA	8
SHUTDOWN BANK	SB	8
SHUTDOWN BANK	SC & SD	4 & 4
CONTROL BANK	A	4
CONTROL BANK	B	8
CONTROL BANK	C	8
CONTROL BANK	D	9

Figure 3.3-35 Rod Cluster Control Assembly Pattern

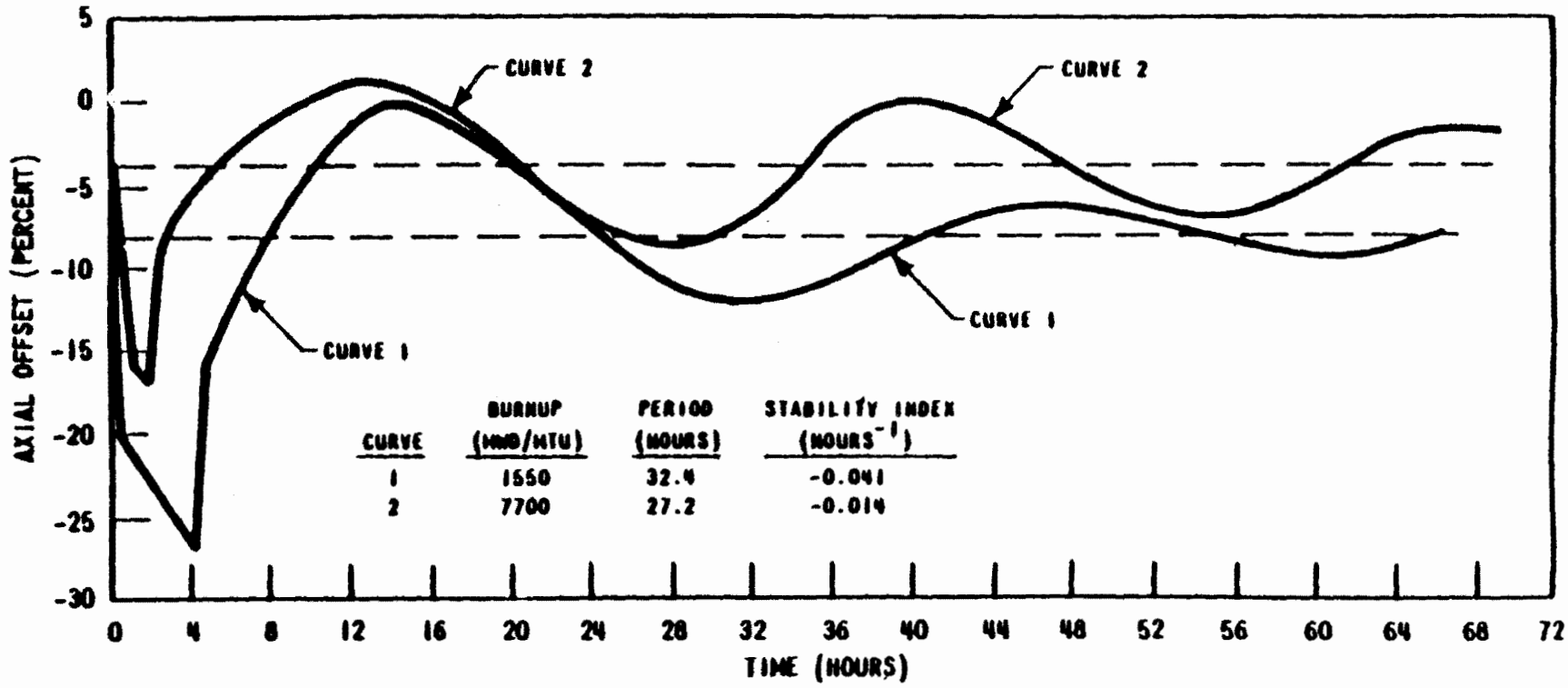

Figure 3.3-36 Axial Offset Versus Time PWR Core With a 12-Ft Height and 121 Assemblies

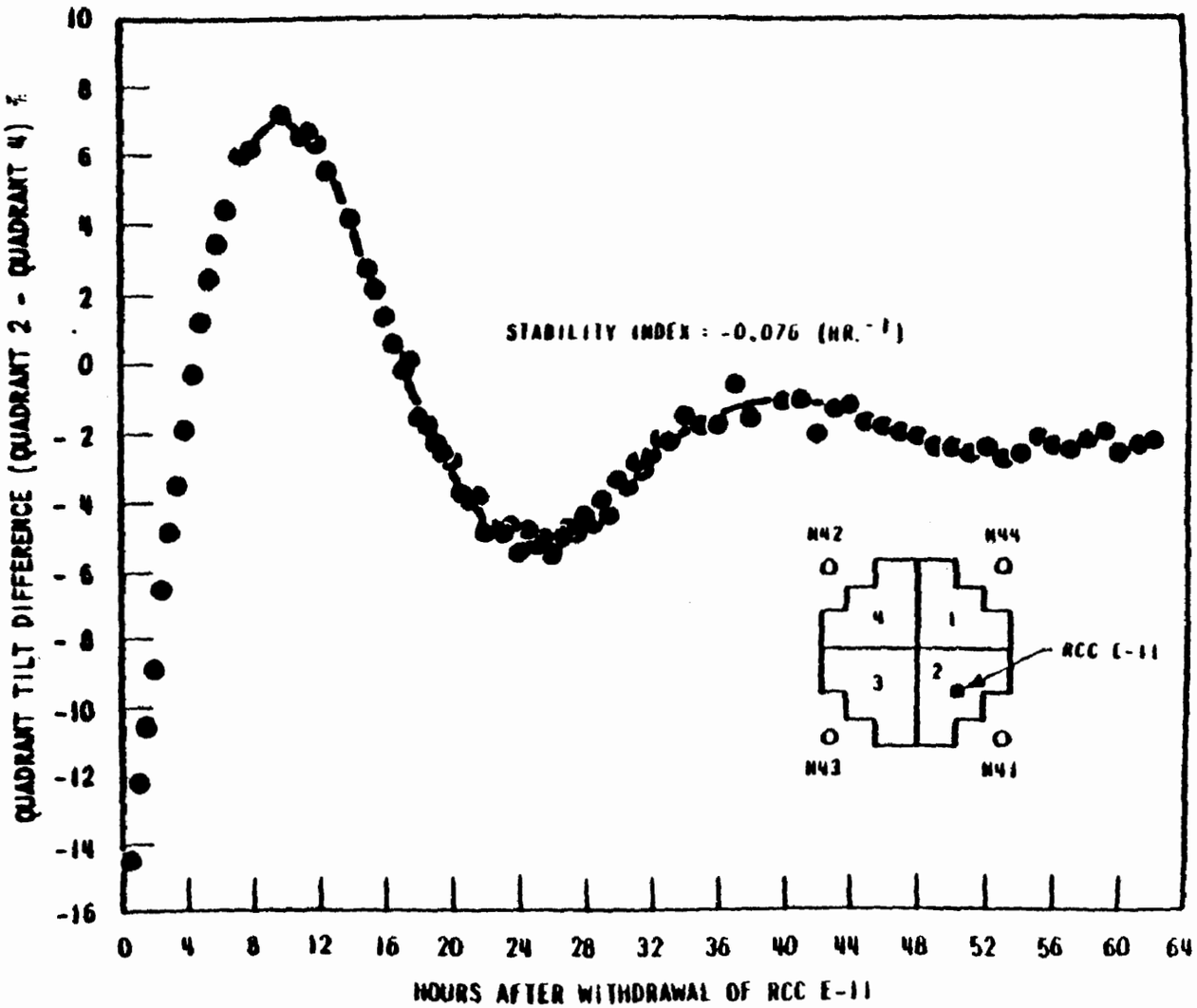

Figure 3.3-37 XY Xenon Test Thermocouple Response Quadrant Tilt Difference Versus Time

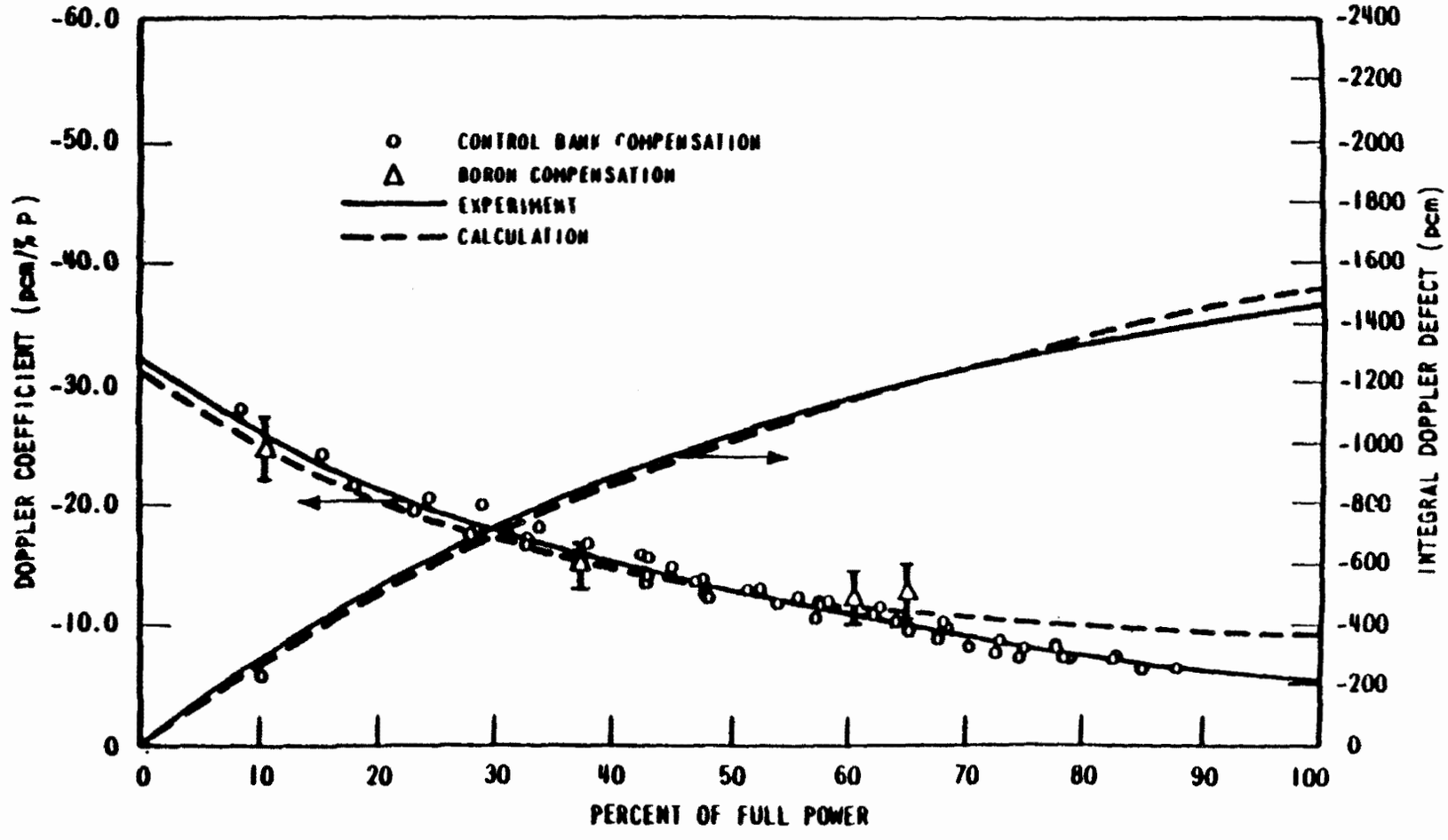

Figure 3.3-38 Calculated and Measured Doppler Defect and Coefficients at BOL Two-Loop Plant, 121 Assemblies, 12-Ft Core

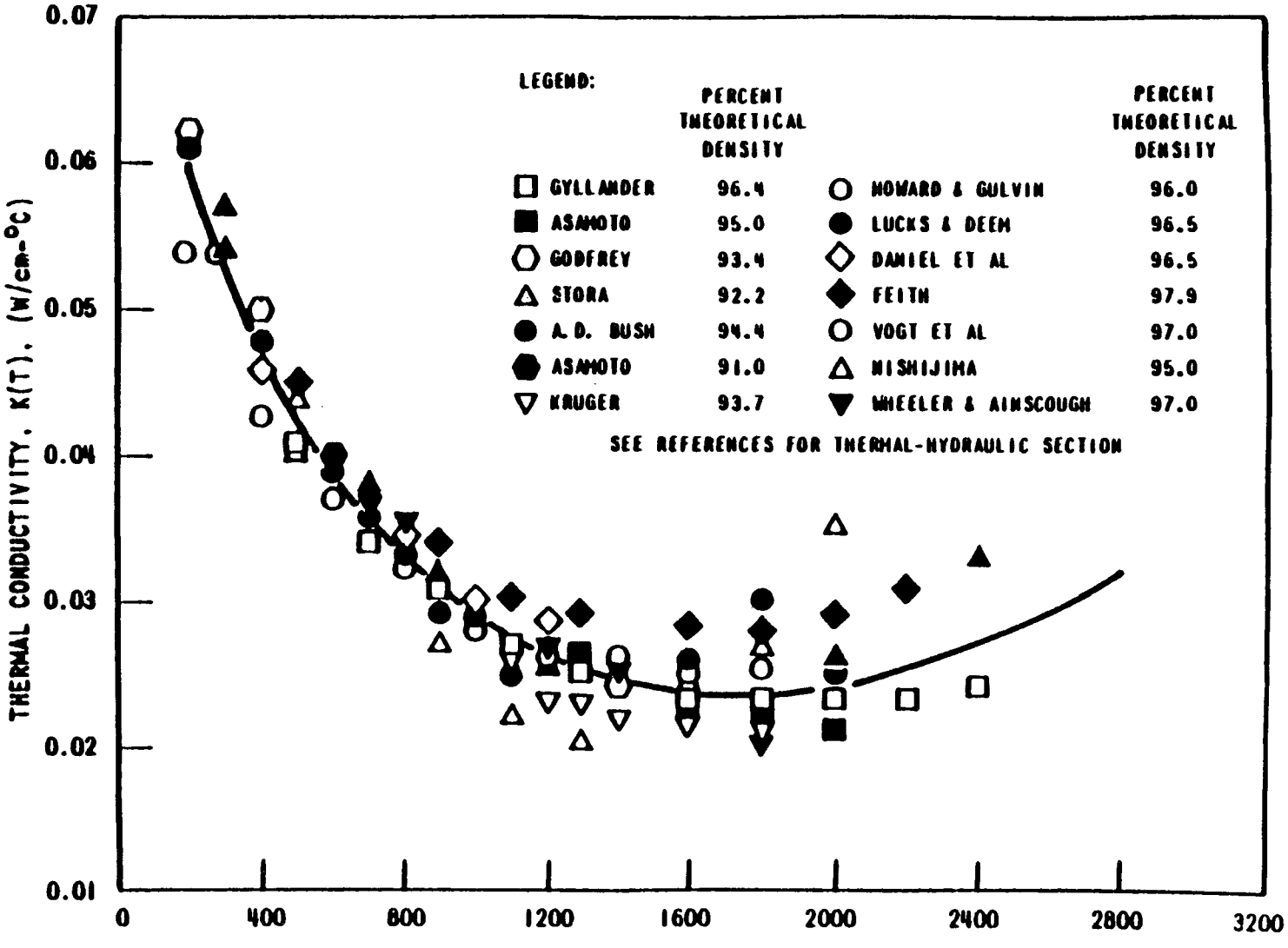

Figure 3.4-1 Thermal Conductivity of UO_2 (Data Corrected to 95% Theoretical Density)

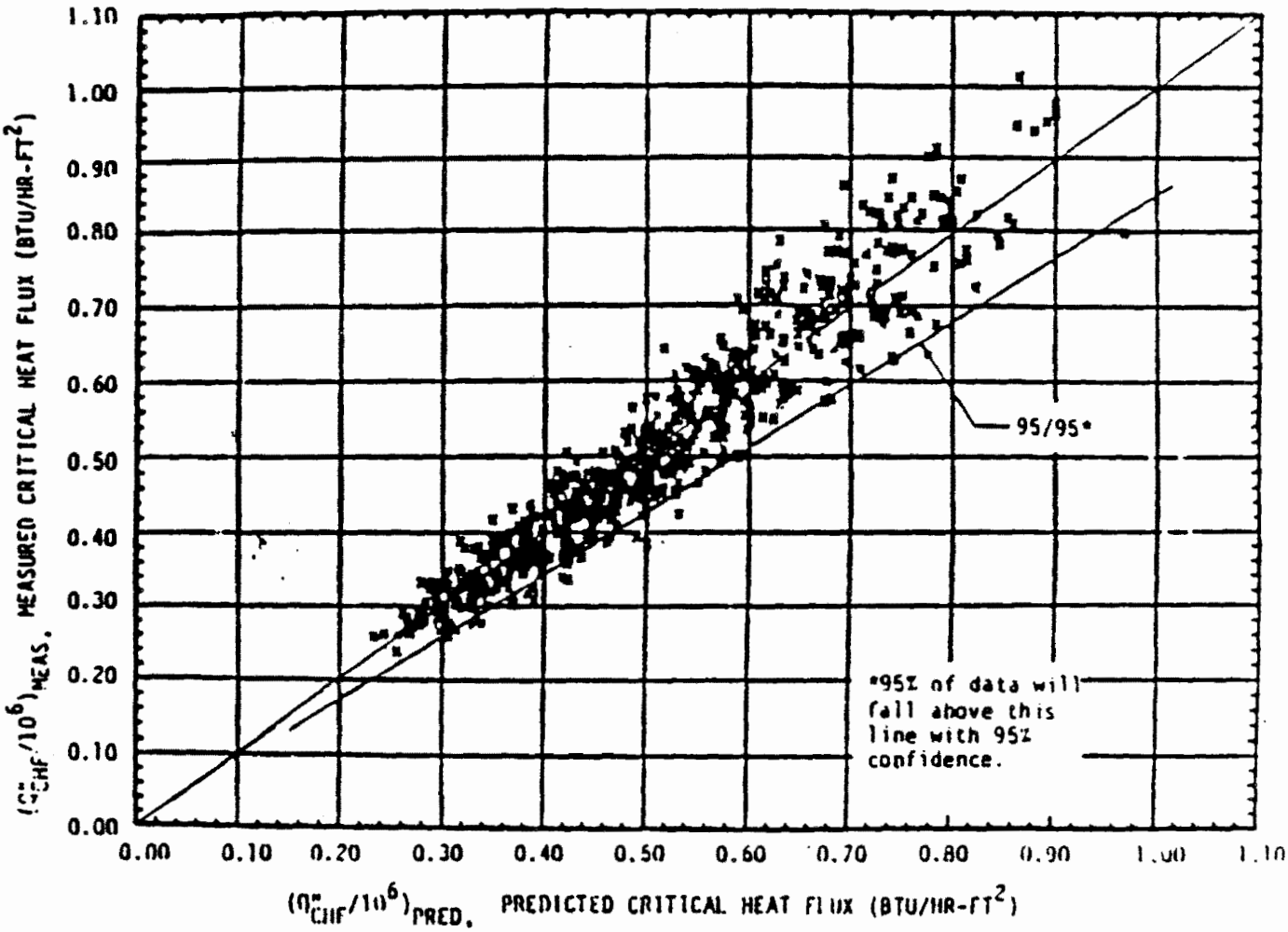

Figure 3.4-2 Measured Versus Predicted Critical Heat Flux - WRB2 Correlation

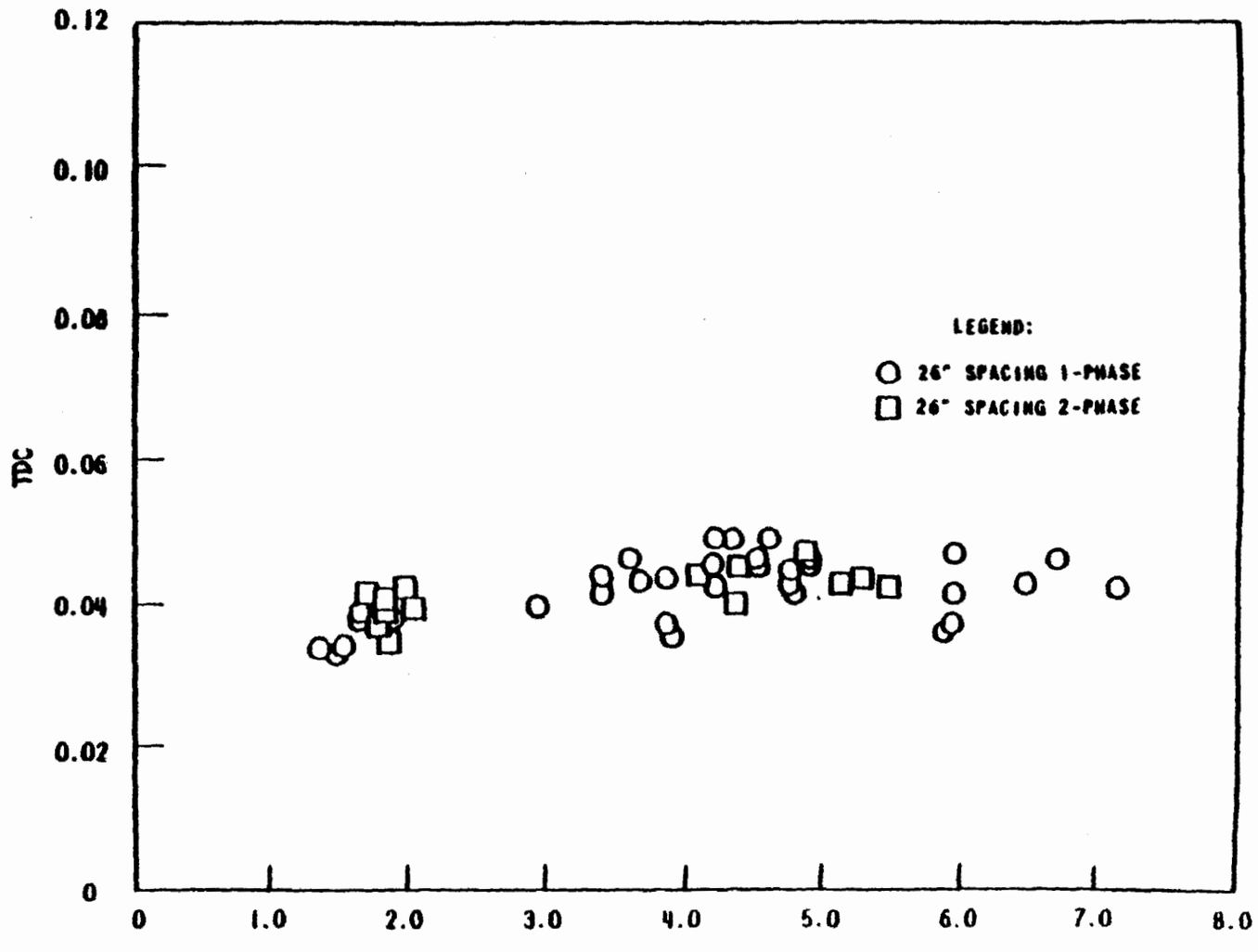

Figure 3.4-3 TDC Versus Reynolds Number for 26" Grid Spacing

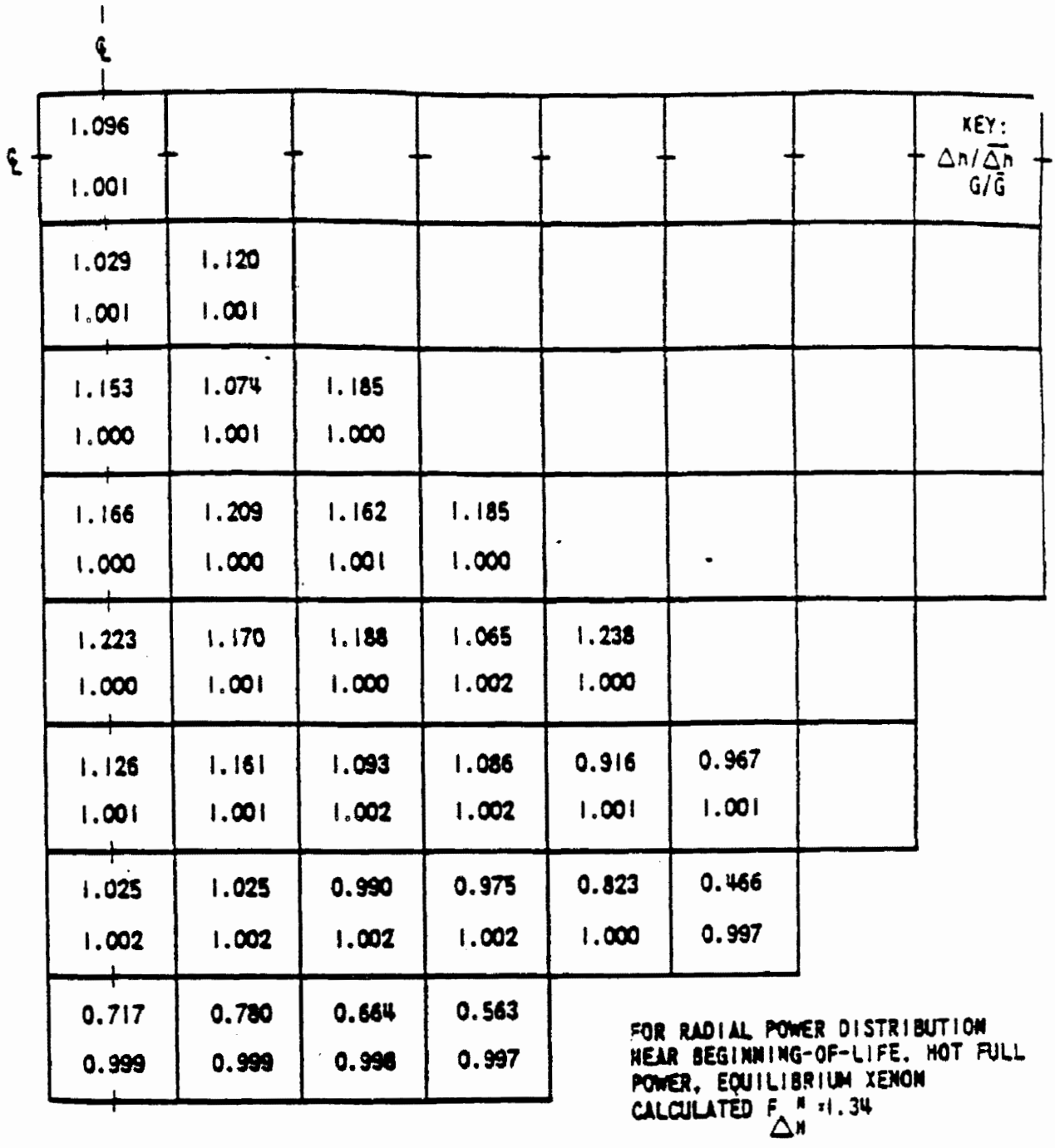

Figure 3.4-4 Normalized Radial Flow and Enthalpy Distribution at 4-Ft Elevation

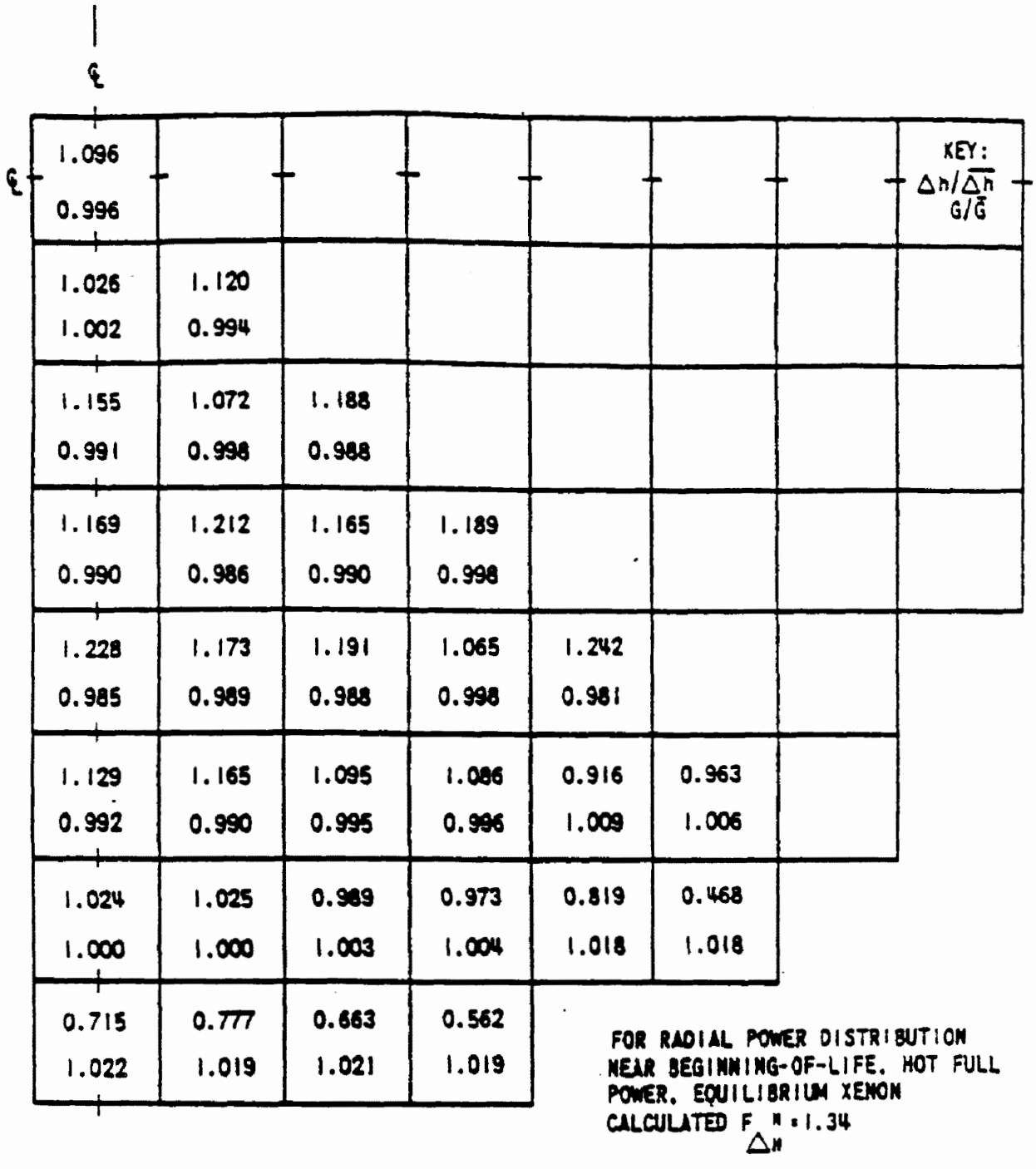

Figure 3.4-5 Normalized Radial Flow and Enthalpy Distribution at 8-Ft Elevation

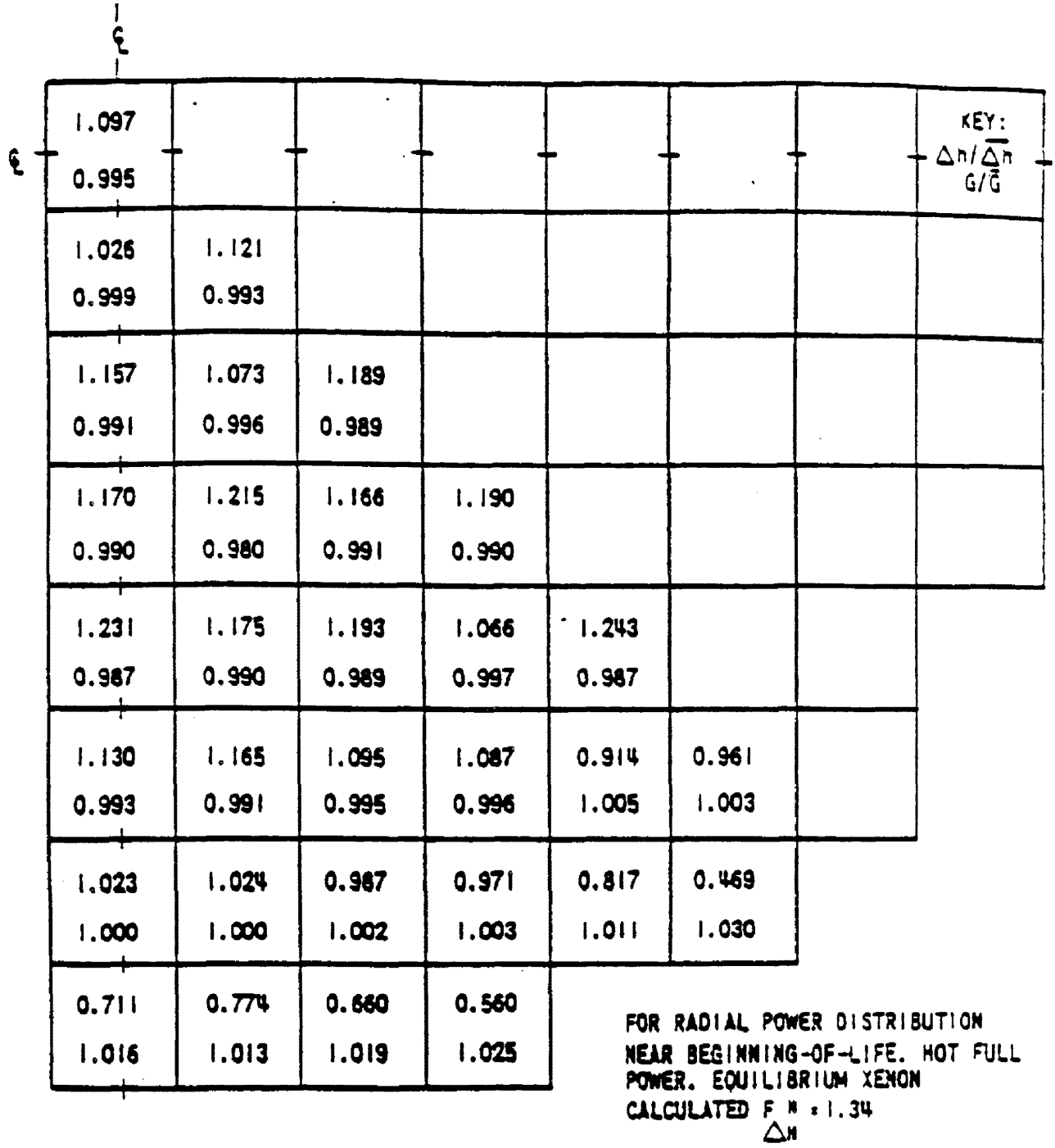

Figure 3.4-6 Normalized Radial Flow and Enthalpy Distribution at 12-Ft Elevation - Core Exit

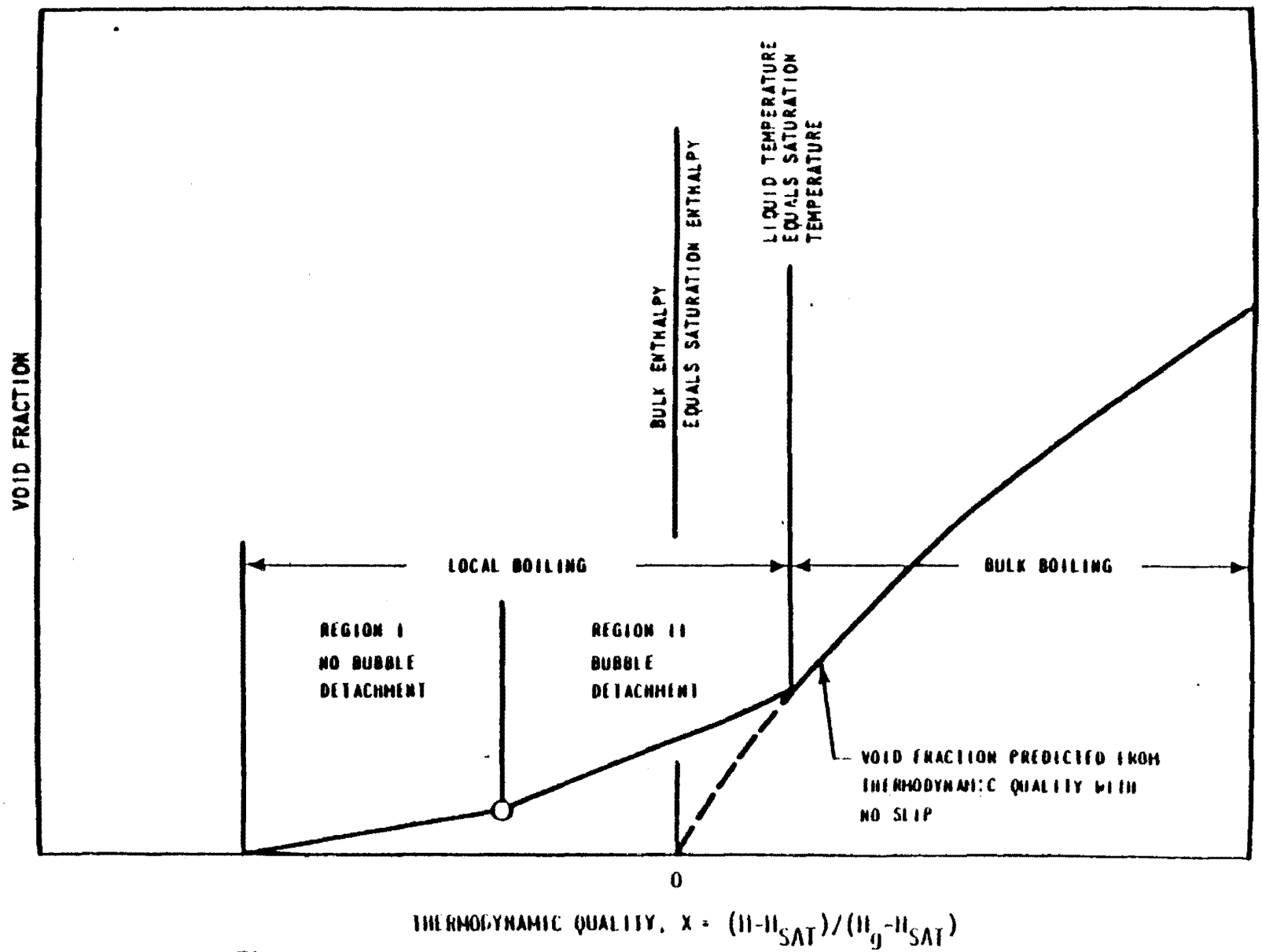

Figure 3.4-7 Void Fraction Versus Thermodynamic Quality $(H-H_{SAT})/(H_g-H_{SAT})$

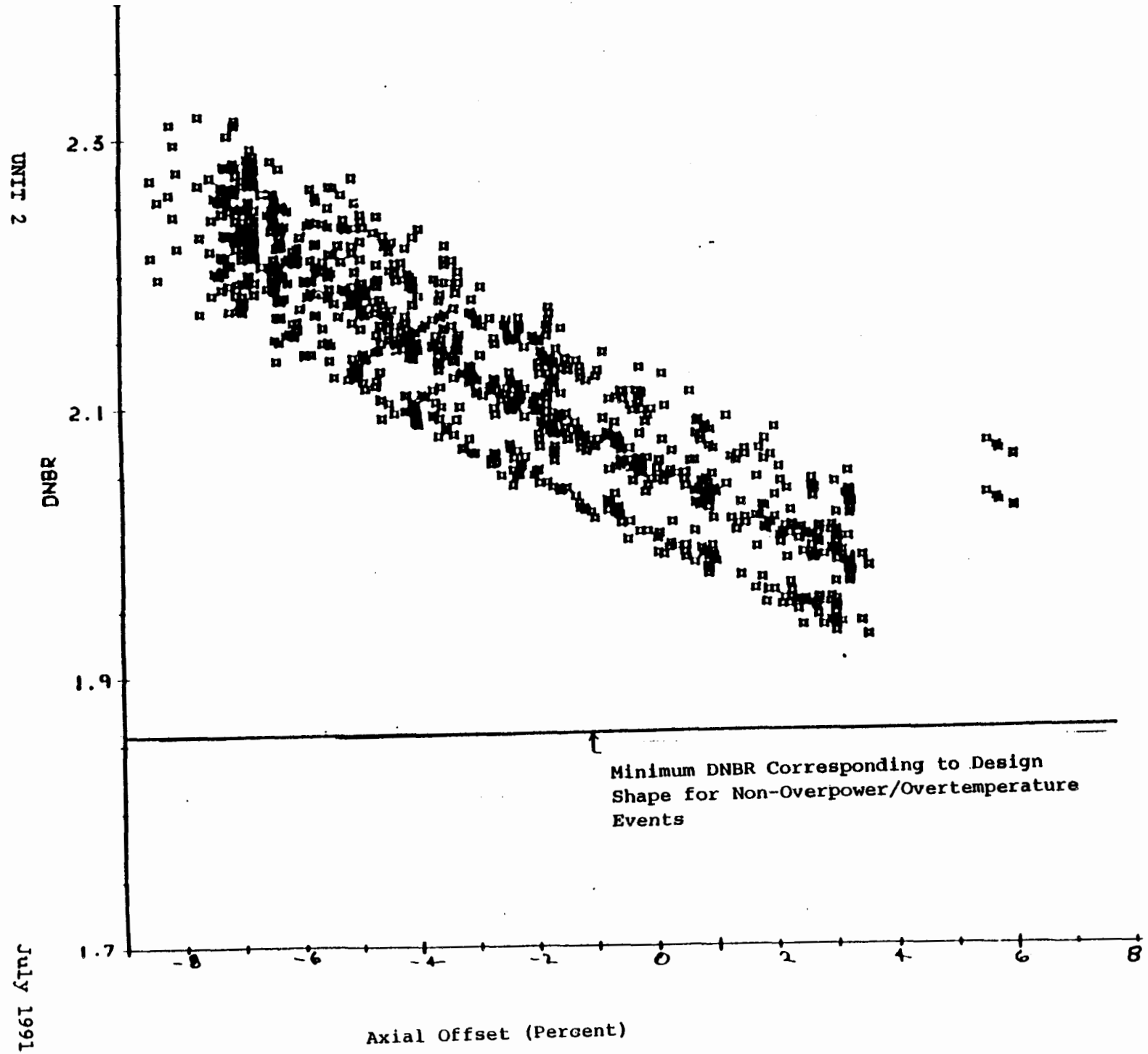

Figure 3.4-8 100% Power Shapes Evaluated at Conditions Representative of Loss of Flow: All Shapes Evaluated With $F^N_{\Delta H} = 1.59$

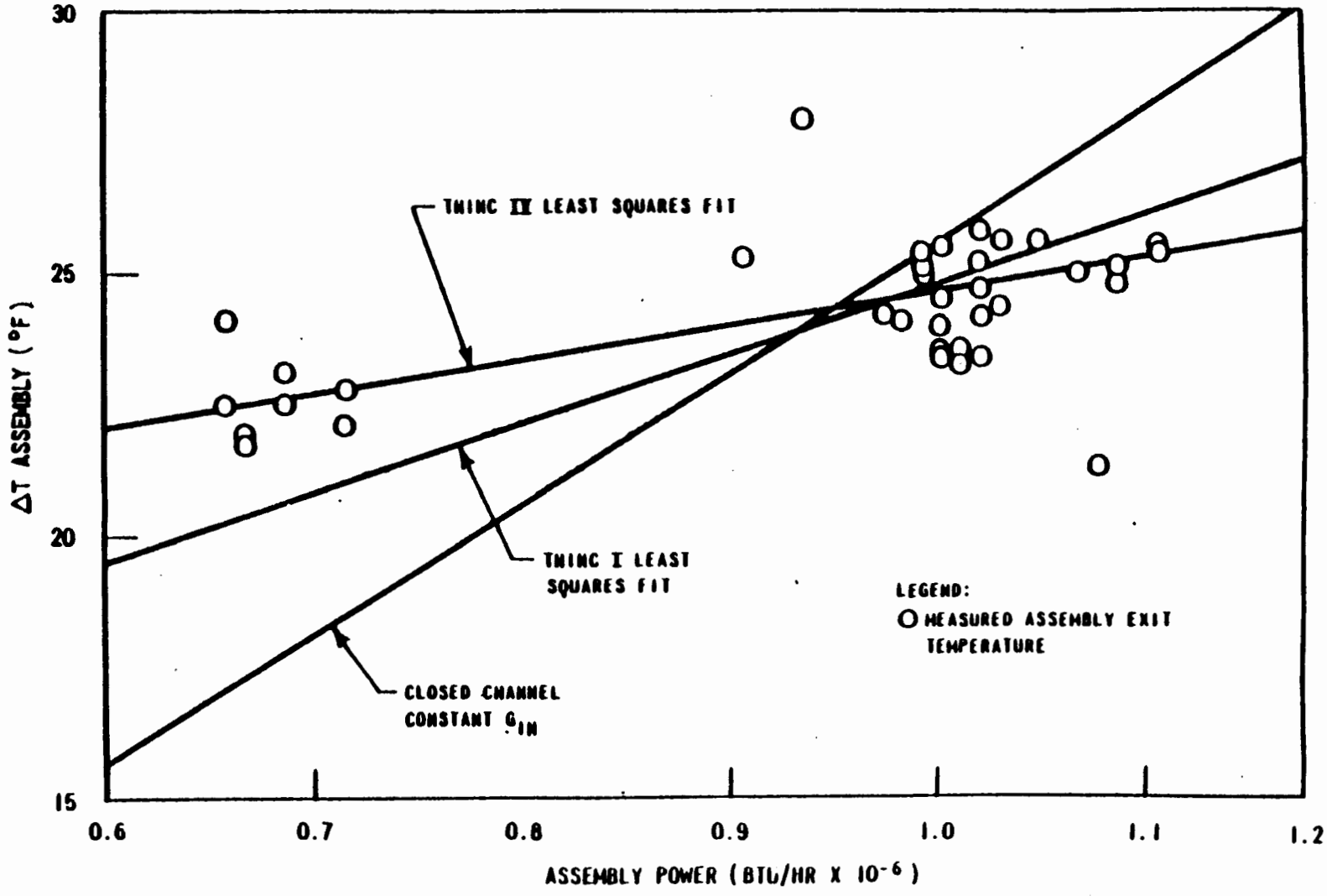

Figure 3.4-9 PWR Natural Circulation Test

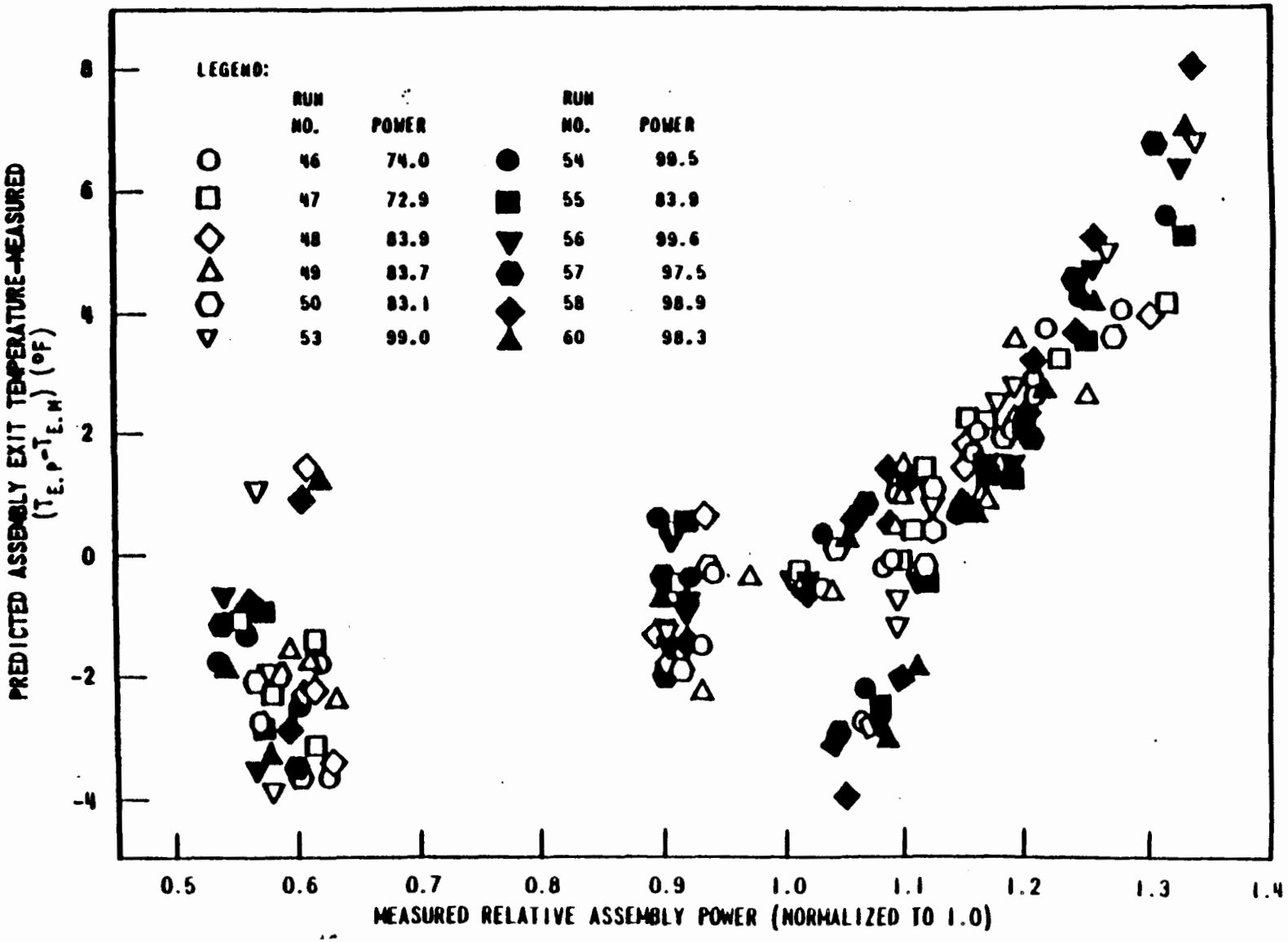

Figure 3.4-10 Comparison of a Representative W Two-Loop Reactor Incore Thermocouple Measurements with THINC-IV Predictions

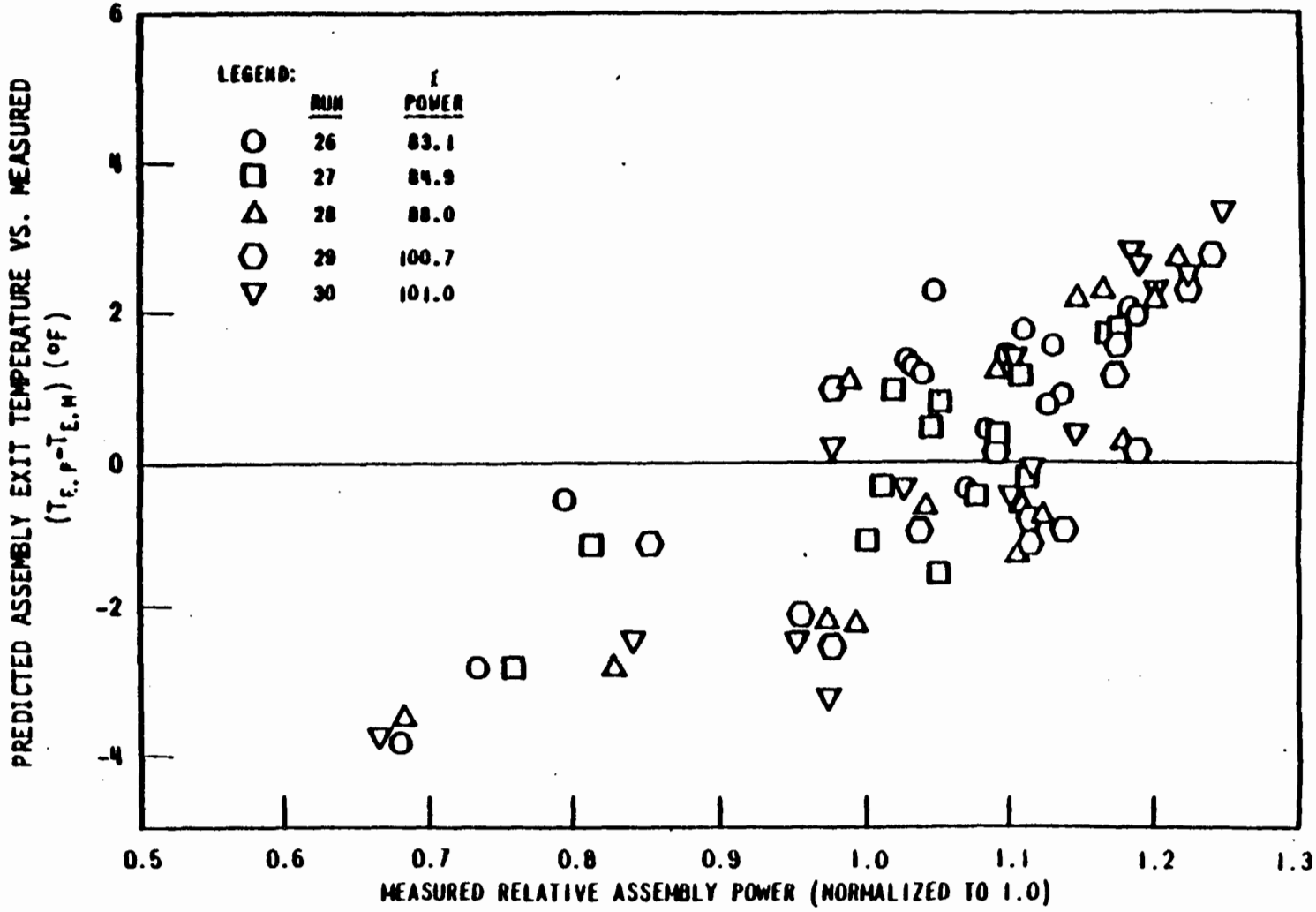

Figure 3.4-11 Comparison of a Representative W Three-Loop Reactor Incore Thermocouple Measurements with THINC-IV Predictions

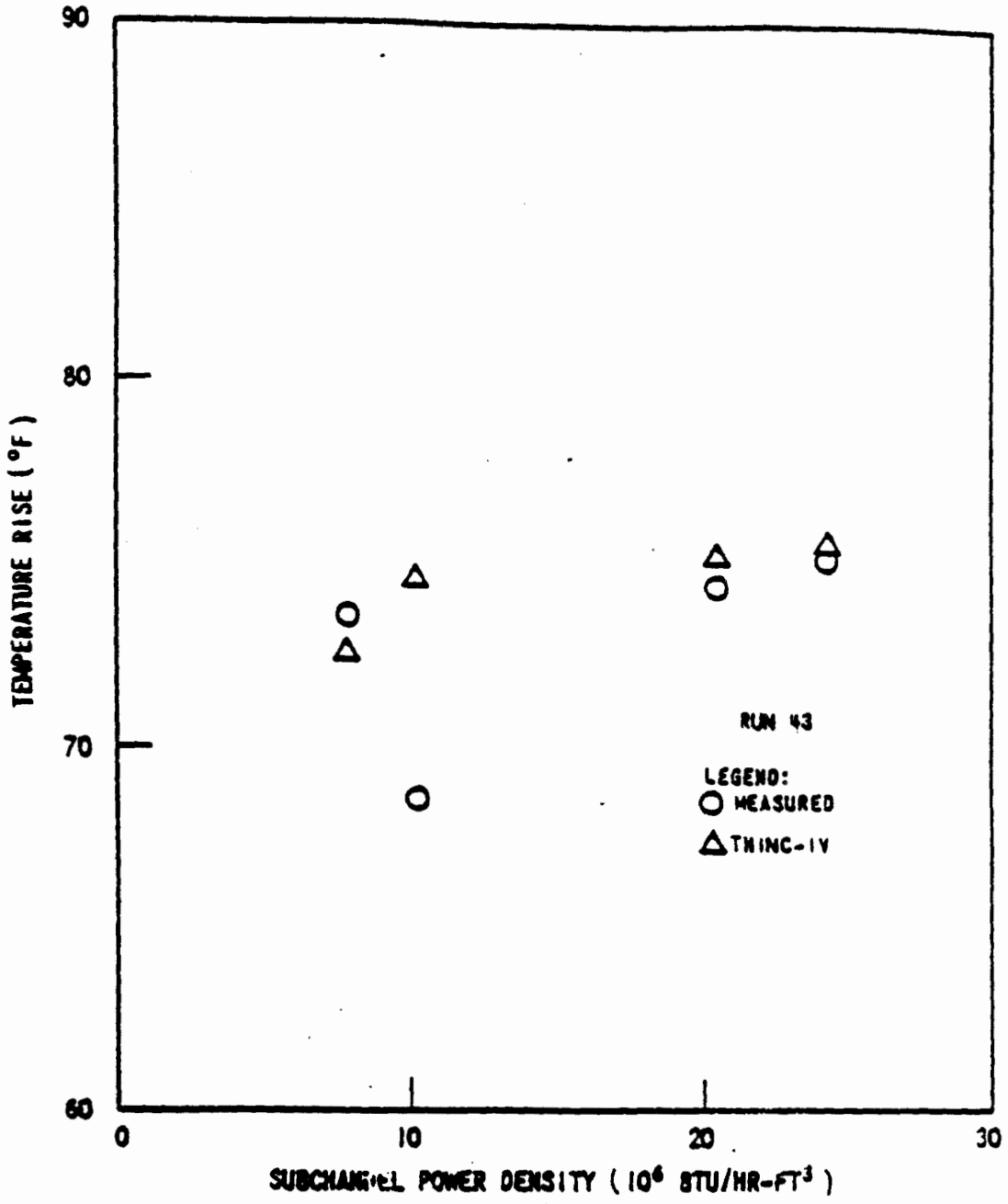

Figure 3.4-12 Hanford Subchannel Temperature Data Comparison with THINC-IV

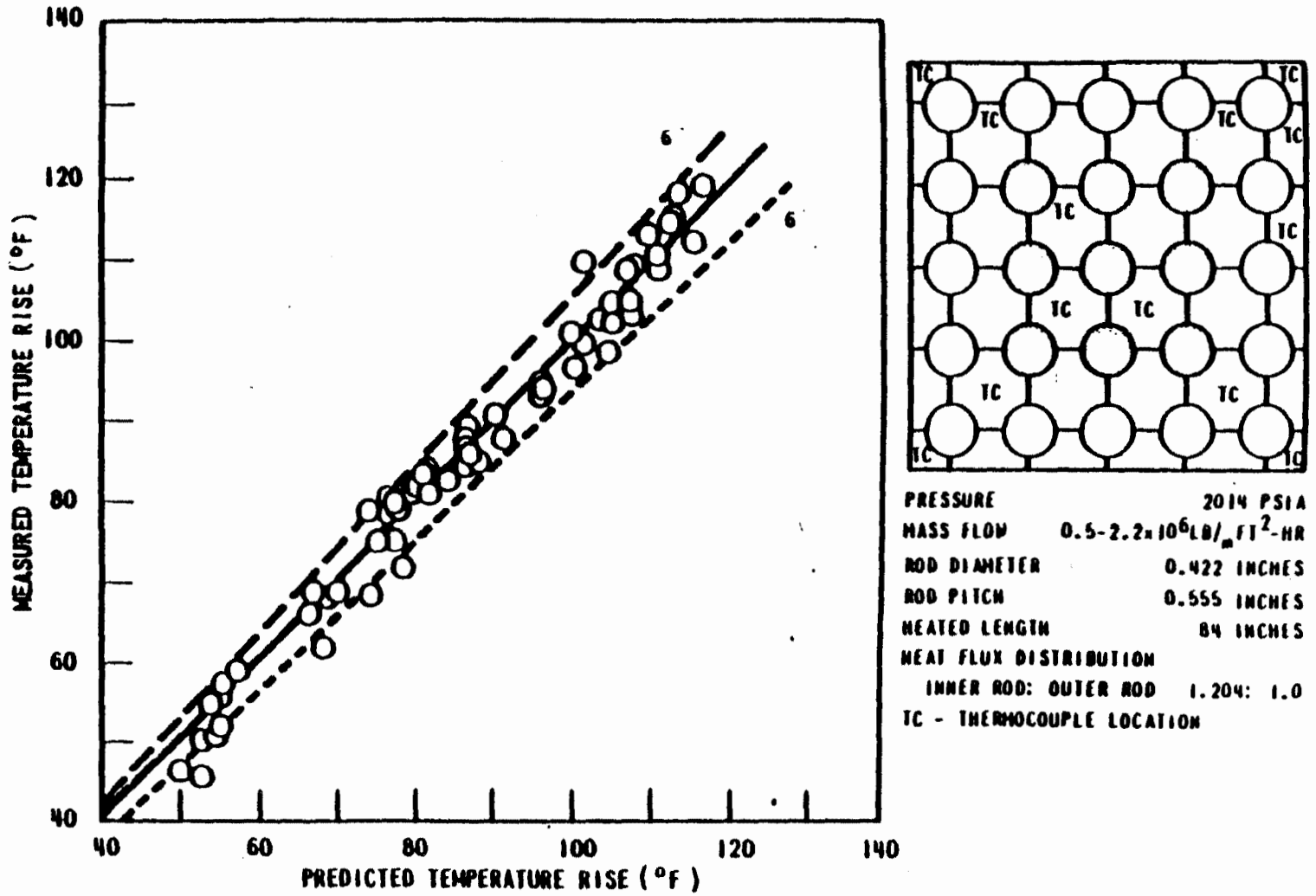

Figure 3.4-13 Hanford Subcritical Temperature Data Comparison with THING-IV

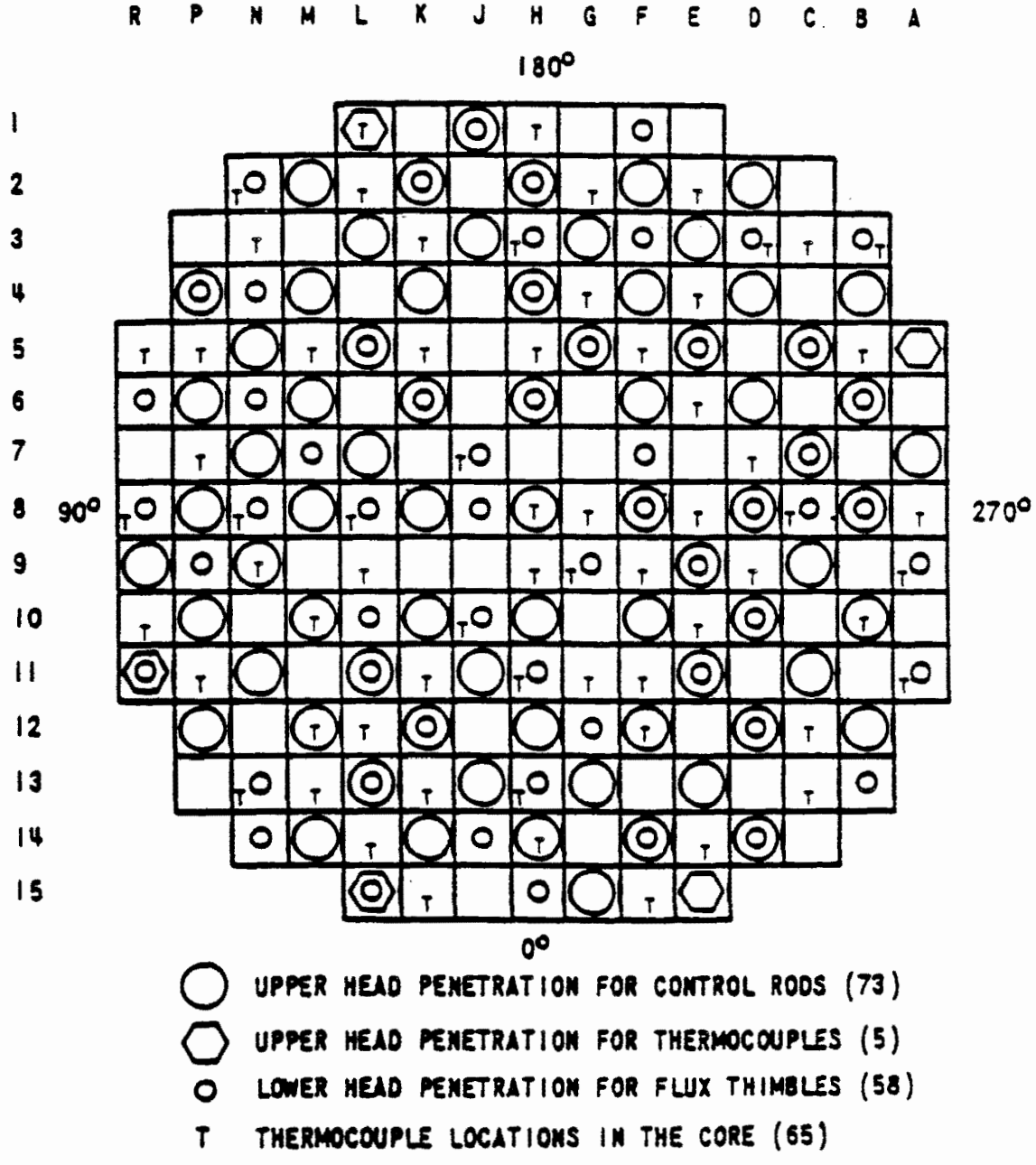

Figure 3.4-14 Distribution of Incore Instrumentation